DESIGN, SYNTHESIS, AND CHARACTERIZATION OF NOVEL, LOW DIELECTRIC, PHOTODEFINABLE POLYMERS

A Dissertation
Presented to
The Academic Faculty

by

Michael J. Romeo

In Partial Fulfillment
of the Requirements for the Degree
Doctor of Philosophy in the
School of Chemical and Biomolecular Engineering

Georgia Institute of Technology
August 2008

DESIGN, SYNTHESIS, AND CHARACTERIZATION OF NOVEL, LOW DIELECTRIC, PHOTODEFINABLE POLYMERS

Approved by:

Dr. Clifford L. Henderson, Advisor
School of Chemical and Biomolecular Engineering
Georgia Institute of Technology

Dr. Haskell W. Beckham
School of Polymer, Textile and Fiber Engineering
Georgia Institute of Technology

Dr. William J. Koros
School of Chemical and Biomolecular Engineering
Georgia Institute of Technology

Dr. Laren M. Tolbert
School of Chemistry and Biochemistry
Georgia Institute of Technology

Dr. Dennis W. Hess
School of Chemical and Biomolecular Engineering
Georgia Institute of Technology

Date Approved: June 19, 2008

To my family, for all of their love and support.

ACKNOWLEDGEMENTS

I would first like to thank my advisor Dr. Clifford L. Henderson for taking me under his wing and dramatically broadening my understanding and knowledge of how research should be conducted. I am especially thankful for his support when my results were less than desirable. It was this encouragement that motivated me through many long hours in the lab. I also would like to thank Dr. William J. Koros, Dr. Dennis W. Hess, Dr. Haskell W. Beckham, and Dr. Laren M. Tolbert for serving on my committee and providing valuable information during my work.

I also want to thank Central Glass Co., Ltd. for giving me the opportunity to work with their novel monomers during this research. In particular, I would like to thank Dr. Kazuhiro Yamanaka for his invaluable guidance throughout my research. Under his tutelage, I received the necessary synthetic knowledge to conduct my research. It was a true pleasure to work with him during his stay in Atlanta. Many thanks are also in order for Dr. Kazuhiko Maeda, Dr. Michio Ishida, and Dr. Roger Sinta for their numerous visits to Georgia Tech to help with this research.

I owe a great deal of gratitude to the past and present members of Dr. Henderson's research group. Dr. Lovejeet Singh and Dr. Cody Berger helped me to perform some of my initial characterization. Dr. Ashwini Sinha performed numerous tasks to aid me with film characterization as well as offering assistance with a variety of equipment issues. Dr. Benita Comeau helped with I-line exposure. Dr. Yueming Hua performed AFM tests on many of my films. Richard Lawson always made himself available to offer input with synthetic suggestions. In addition to Dr. Henderson's group,

many other students from different groups and departments helped with my film characterization. Marcus Foston from Dr. Beckham's group ran the GPC for all the polymers reported. Jiongxin Lu in Dr. Wong's group ran the TMA experiments for all of the polymers. Dr. Jason Hicks and Dr. Rebecca Shiels in Dr. Jones group as well as Dr. Pamela Pollet and Reagan Charney in Dr. Eckert's group helped me perform some of the synthetic steps. Dr. Janusz Kowalik in Dr. Tolbert's group was especially helpful with some of the more troubling synthetic issues encountered in this research.

TABLE OF CONTENTS

LIST OF TABLES

Page

LIST OF FIGURES

Page

LIST OF SYMBOLS AND ABBREVIATIONS

CTE – coefficient of thermal expansion

T_g – glass transition temperature

TMAH – tetramethylammonium hydroxide

DNQ – diazonaphthoquinone

PAC – photoactive compound

PAG – photoacid generator

PI – polyimide

BCB – benzocyclobutene

PBO – polybenzoxazole

NMR – nuclear magnetic resonance spectroscopy

ppm – parts per million

FTIR – Fourier transform infrared spectroscopy

GPC – gel permeation chromatography

TGA – thermogravimetric analysis

MS – mass spectroscopy

QCM – quartz crystal microbalance

SEM – scanning electron microscopy

PEB – post exposure bake

HFA – hexafluoroalcohol

TEA – triethylamine

6FDA – 2,2-bis(3,4-dicarboxyphenyl)hexafluoropropane dianhydride

NMP – N-methyl-2-pyrrolidone

DMAc – dimethylacetamide

THF – tetrhydrofuran

PGMEA – propylene glycol methyl ether acetate

GBL – γ-butyrolactone

DMF – dimethylformamide

DMSO – dimethyl sulfoxide

HFA-ODA – 3,3’-Bis(1-hydroxy-1-trifluoromethyl-2,2,2-trifluoroethyl)-4,4’oxydianiline

PBOX – polybenzoxazine

IPC – isophthaloyl chloride

BPDC – 4,4'-dibenzoyl chloride

6FDC – 4,4'-(hexafluoroisopropylidene)bis(benzoyl chloride)

6FBDC – 4-4’-Bi(3-(trifluoromethyl))benzoyl chloride

6FDIA – 2,2-bis[N-(4-carboxyphenyl)phthalimidyl]-hexafluoropropane

6FDIAC – 2,2-bis[N-(4-chlorocarboxyphenyl)phthalimidyl]-hexafluoropropane

SUMMARY

Polymers play an integral part in the semiconductor electronic industry. Due to the expanding diversity of a polymer's structural design and the resulting properties, different polymers serve as different components in the makeup and fabrication of the electronic package. The limiting factor in computer processing speed shifts from the transistors' gate delay to the interconnect delay below a circuit line width of 1.8 μm for interlayer dielectrics. Silicon dioxide has been used as the insulating layer between metal lines for many computer chip generations. Low dielectric constant polymers will need to supplant silicon dioxide as interlayer dielectrics in order to develop reliable circuits for future generations. Along with serving as interlayer dielectrics, low dielectric constant polymers are also incorporated in first and second level electronic packaging.

Deposition and patterning of these polymers can be significantly reduced by using photodefinable polymers. Most photodefinable polymers are in a precursor form for exposure and development in order to dissolve in industrial developers. Once developed, the polymer precursors are cured to produce the final polymer structure. This temperature is as high as 350 ^{o}C for many polymers. Thermal curing sets limitations on the use of the polymer in the electronics industry because of either the unwanted stress produced or the incompatibility of other electronic components that do not survive the thermal cure.

In addition to a low dielectric constant and photodefinability, many other properties are needed for successful implementation. Polymers must be soluble in organic solvents in order to spin coat films. Water absorption increases the dielectric constant of the patterned films and can lead to various adhesion problems and cause

delamination of the film. Mismatches between the coefficients of thermal expansion in adjacent layers can produce residual film stresses which leads to warping of the substrate or interfacial delamination. The glass transition temperature must be high because the thermal expansion is greatly increased when the glass transition temperature is exceeded. A high Young's modulus is also required to withstand external forces from thermal, electrical, and packaging stresses. When designing a polymer for low dielectric applications, all relevant properties must be simultaneously optimized.

The goal of this research was to develop novel, low dielectric, photodefinable polymers that can be processed at low temperatures. All polymers discussed will contain one of two monomers with hexafluoroalcohol (HFA) functional groups. Fluorine provides many properties that are advantageous for low dielectric applications whereas alcohols absorb water and increase the dielectric constant. Characterization of the polymers show the effect the fluorine has on the alcohol's high water absorption. All polymers will be synthesized by condensation polymerization of a diamine with a dianhydride or diacid chloride. One polymer design involves combining a polyimide with an HFA-substituted phenol to allow development. All other polymers will contain a novel HFA diamine. A new thermoplastic polymer structure based on the cyclization of an HFA situated ortho to an amide linkage produces a benzoxazine ring in the polymer backbone. Cyclization to form polybenzoxazines occurs at temperatures considerably lower than that needed to form polyimides. The lowest processing temperatures are achieved with protection of the HFA that can be cleaved with a photoacid generator.

CHAPTER 1

INTRODUCTION

1.1 Polymers in microelectronics

Polymers play a critical role in the microelectronics industry. They function as photoresists used in microlithography and as insulating dielectric materials in chip interconnect structures, chip packages, displays, and photonic devices [1]. The demand for devices capable of performing more complex and faster tasks in smaller packages requires producing semiconductor memory devices with higher memory densities and microprocessors with faster clock speeds. Figure 1.1 shows a schematic cross-section through a dynamic random access memory cell consisting of a capacitor and a transistor for storage of one data bit.

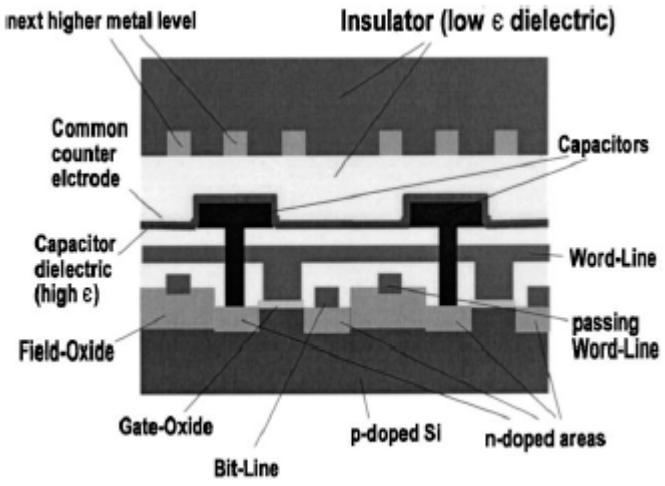

Figure 1.1 Schematic of dynamic random access memory cell [2]

As memory densities increase the dimensions of the metal interconnect lines and the insulation layers between them decrease. This closer spacing of adjacent metal lines results in capacitive coupling between the adjacent interconnects. A change of the electrical current in one line induces a current in neighboring lines through a change of the electrical field. Inductive cross-talk decreases the reliability of data transport. The signal delay is no longer dominated by the intrinsic gate delay of the transistor below a certain distance of the interconnecting lines, but by capacitive resistance of the interconnect array as shown in Figure 1.2.

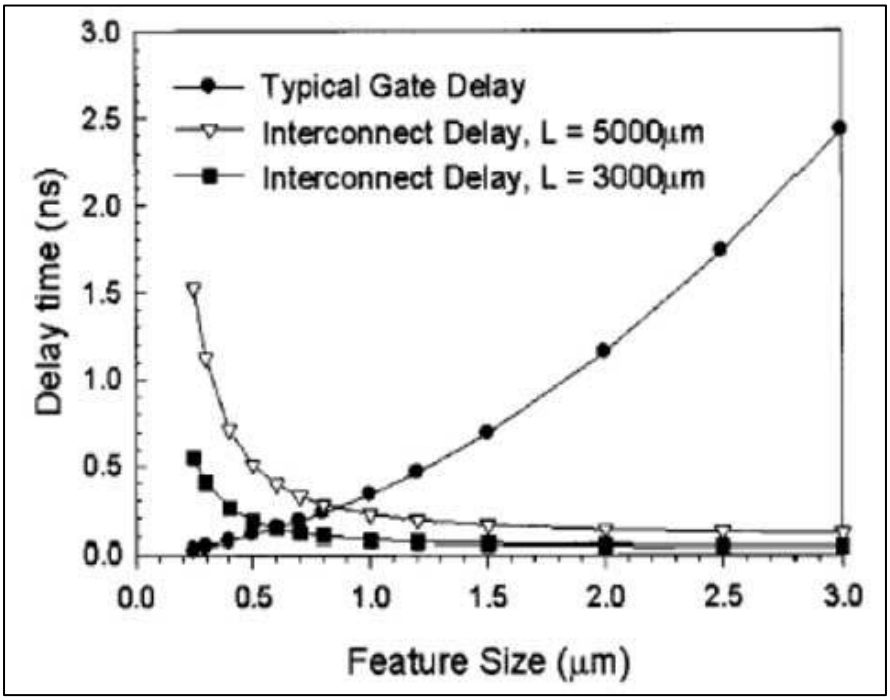

Figure 1.2 Dependence of signal delay on device size

This increased capacitive coupling increases the interconnect delay, also called RC time delay, in the device which limits the speed at which the device can operate.

Total RC delay is a combination of the total resistance of the line, the lateral line to line capacitance, and the vertical layer to layer capacitance as shown in Equation 1.1 [3]:

$$RC = 2\rho k\varepsilon_0 L^2\left(\frac{4}{P^2}+\frac{1}{T^2}\right) \qquad (1.1)$$

where R is the resistance, C is the capacitance, ρ is the resistance of the conductor, k is the dielectric constant of the insulator, ε_0 is the permittivity of vacuum, L is the line length, P is the line pitch, and T is the line thickness. There are two primary ways to fix this RC time delay problem: (1) decrease the resistance (ρ) of the metal interconnects and (2) decrease the capacitance (k) between adjacent interconnect lines. This first task of reducing interconnect resistance has been achieved by switching from higher resistance aluminum metal interconnects to lower resistance copper interconnects. In order to reduce the capacitive coupling, lower dielectric constant insulation layers or larger interconnect spacing needs to be used. Providing smaller pitch and interconnect densities increases interconnect line lengths which overwhelms any benefit due to increased resistances, and thus lower dielectric constant materials must be used.

One class of materials which has been and continues to be investigated for use in these interconnects and packaging insulation applications is polymers. Polymers offer several advantages over inorganic dielectrics including: (1) they can generally deposited over a wide range of thickness from solution using inexpensive equipment and low temperature processing methods such as spin casting, (2) they possess good mechanical properties such as resistance to brittle failure, can be tailored for an application through

molecular design, and (3) can in some cases be made directly photodefinable in order to eliminate separate costly lithography and plasma etching steps required for patterning other dielectrics. To be useful as a dielectric material, a polymer must possess a number of physical characteristics such as a low dielectric constant (*k*), low water absorption, low coefficient of thermal expansion (CTE), high thermal stability, and a high glass transition temperature (T_g). If the polymer is to be made photodefinable, it must possess an even longer list of required physical properties including solubility in an appropriate developer such as aqueous alkaline solutions and provide a mechanism for modulating that solubility through some radiation sensitive mechanism. The common aqueous alkaline developer used industrially is 0.26 N tetramethylammonium hydroxide (TMAH) due to its relatively low environmental waste impact. Although ddevelopers used historically have also included metal hydroxide solutions, such as sodium hydroxide, these types of developers are rarely used today due to factors such as potential metal ion contamination of the microelectronic device which can deteriorate their performance. Developing a polymer with such a combination of properties in a single compound is a significant challenge, but the payoff for developing such a material can be significant such as enabling a process for producing patterned dielectric films with extremely low cost and low complexity.

1.2 Review of Photodefinable Polymers

1.2.1 Photoresists

The earliest applications for photodefinable polymers in microelectronics were as photoresist materials used in microlithography (see Figure 1.3). A photoresist is a material that undergoes a change in its physical and/or chemical properties after exposure

to radiation, typically ultraviolet light, which allows for the development of a relief image in the material [4]. There are numerous ways in which to classify photoresists according to the manner in which they function. For example, photoresists can be classified as either positive-tone or negative-tone depending on their behavior in developer. Positive-tone photoresists dissolve in the areas exposed to radiation, while negative-tone photoresists dissolve in the areas unexposed to radiation.

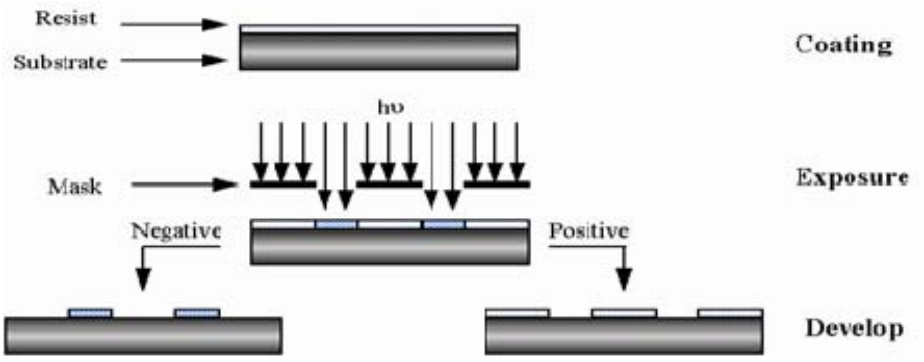

Figure 1.3 Positive and Negative Photoresists [5]

Negative tone polymers have typically been achieved by employing radiation activated cross-linking mechanisms. The disadvantage historically with these materials has been that they suffer from swelling problems that limit their resolution. However, there are a number of commercial photosensitive dielectric materials available which rely on such negative tone cross-linking mechanisms and which find use typically in applications with lower resolution requirements.

In contrast to negative-tone materials, positive-tone photoresists generally possess higher resolutions but also require the use of mechanisms which increase the polarity or solubility of the polymer in an aqueous developer solution. There are two prevalent classes of positive tone photoresists which function via different chemical mechanisms:

(1) diazonaphthoquinone (DNQ)-novolac photoresists and (2) chemically amplified photoresists (CARs).

DNQ-novolac resists are one of the oldest classes of photoresist materials used today. DNQ is often referred to as the photoactive compound (PAC) in DNQ-novolac resists because it is the component that responds to radiation exposure. Novolac is the polymer resin that provides high etch resistance, solubility in aqueous base developers, good film forming, and other desirable physical properties for the resist. DNQ reduces the dissolution rate of novolac polymers in aqueous base by forming hydrogen bonds with the hydroxyl sites on the polymer (see Figure 1.4), and thus is termed a "dissolution inhibitor" [6].

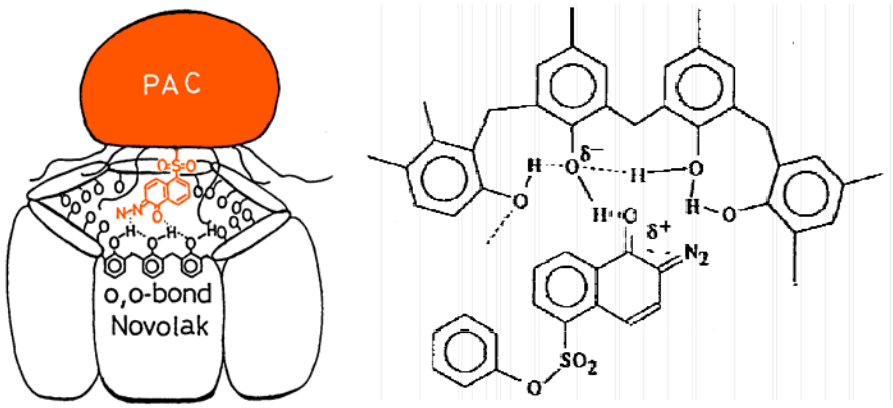

Figure 1.4 Schematic of one commonly proposed view of the interaction of DNQ with novolac is the "Octopus Pot" model which explains the strong inhibition power of DNQ through an inductive cluster polarization mechanism [7].

After exposure, the DNQ decomposes to form an aqueous alkaline soluble carboxylic acid photoproduct, thus disturbing the hydrogen bonding network (see Figure 1.5). This disruption of hydrogen bonding eliminates the inhibition effect while the

formation of the carboxylic acid often increases the overall dissolution rate of the film (see Figure 1.6) [8].

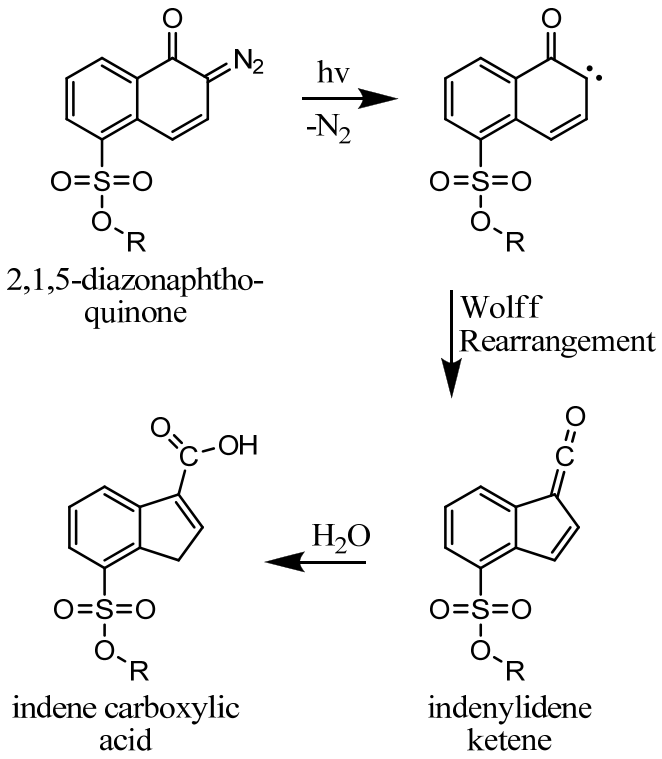

Figure 1.5 Decomposition of DNQ upon exposure to form a carboxylic acid

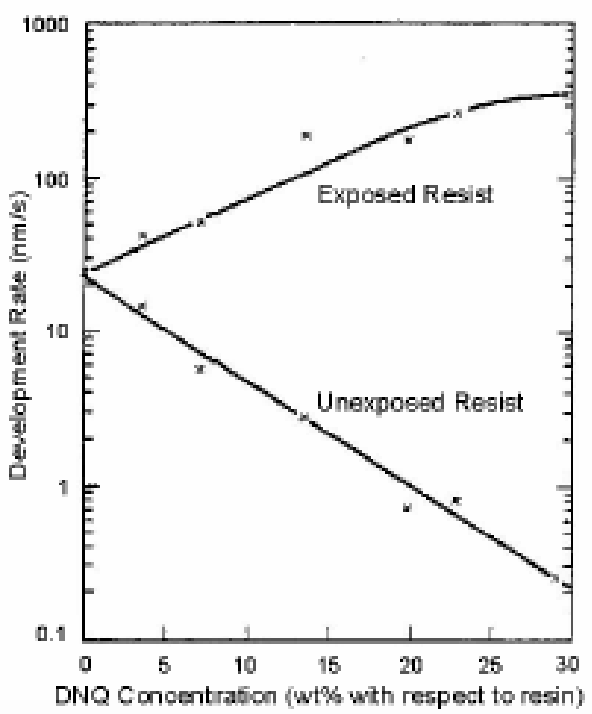

Figure 1.6 Meyerhofer plot showing the effect of addition of DNQ to novolac in both the unexposed and exposed state [9].

Chemically amplified photoresists (CAR) were developed to overcome problems associated with the relatively low sensitivity of DNQ-novolac resists. In their simplest form CARs are two component resist systems which consist of a protected polymer and a photoacid generator (see Figure 1.7). In the first step, exposure of the film triggers a photochemical reaction that produces an acid. The acid proton then reacts with the polymer protecting group to initiate removal or conversion of the protecting group to a different form, such as the protonation of the ester functional group shown in Figure 1.6. The protecting group decomposes in some manner to yield an ionizable group which increases the solubility of the polymer. In Figure 1.7, protonation of the ester results in formation of a carboxylic acid group on the polymer and a low molecular weight organic fragment from the protecting group. The transient carbocation formed when the

protecting group is removed from the polymer is unstable and undergoes a rearrangement to release a proton. In this way, the acid is regenerated in the reaction and the overall deprotection process is catalytic. This removal of a hydrophobic protecting group on the polymer and production of an ionizable hydrophilic group renders the exposed areas of the polymer soluble in aqueous alkaline developer and dramatically increases the sensitivity and contrast of the material due to the catalytic nature of the reaction triggered by the initial photoacid generator reaction event.

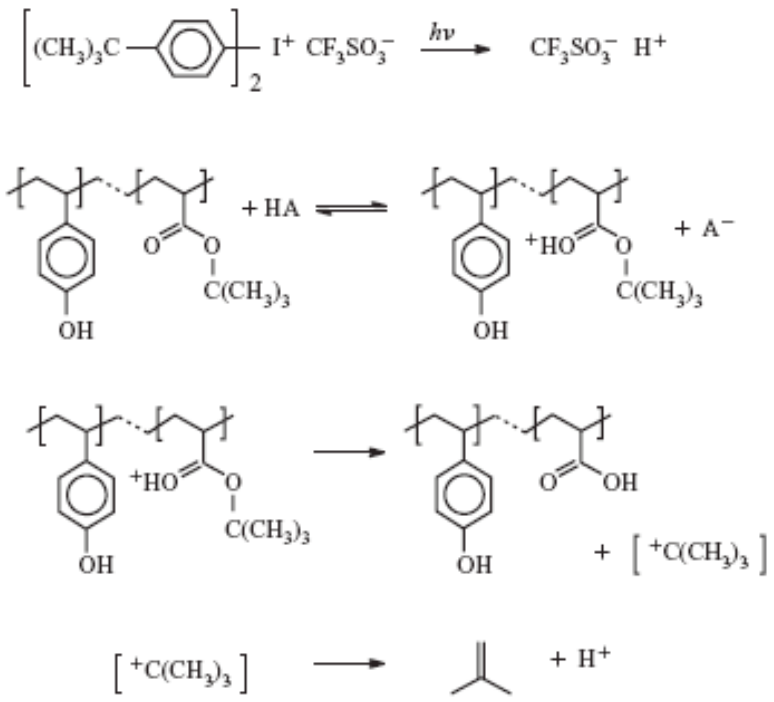

Figure 1.7 Imaging Chemistry of a Typical Positive-Tone CA Resist [10]

As mentioned earlier, it is in principle possible to utilize cross-linking, photoactive inhibitor mechanisms, and chemically amplified protection-deprotection mechanisms in developing photosensitive dielectric materials.

1.2.2 Photodefinable Dielectrics

The advantage of making a dielectric polymer photodefinable in terms of microelectronics processing is it requires half the processing steps of a non-photodefinable material [11]. A comparison of the processes required to pattern both types of materials are shown in Figure 1.8 which clearly demonstrates that a substantial number of steps and cost can be eliminated by the use of photodefinable materials.

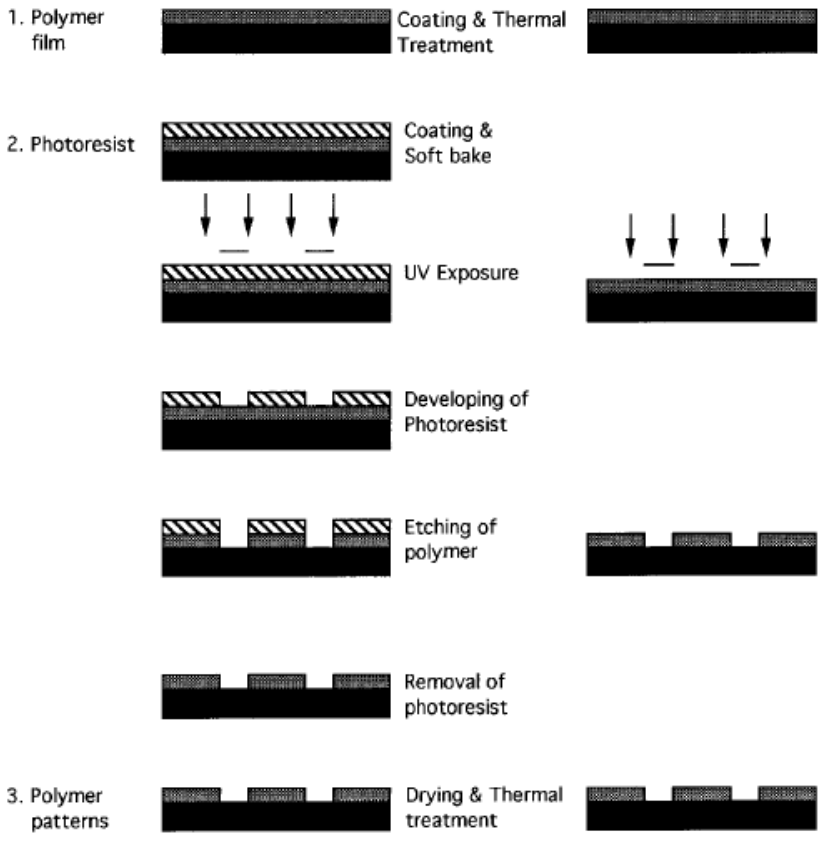

Figure 1.8 Processing Advantage of Photodefinable Materials

In terms of photosensitive dielectric polymers, polyimides have received the most attention. Photosensitive polyimides have been employed in a variety of configurations

[12, 13]. Photosensitive benzocyclobutenes and polybenzoxazoles have received less attention but have been reported in literature [14-16].

The exposure and development stage for most polymers typically occur when the polymer is in its precursor form. After development, the film is cured to complete cyclization to produce an insoluble product. This temperature exceeds 250 ^{o}C for many polymers and, as a result, sets limitations on the use of such polymers in the electronics industry. Due to the high curing temperature, the films are inherently stressed making them not ideal for dielectric applications [17]. In addition, alignment films in colored liquid crystal displays with thin film transistors must be cured below 200 ^{o}C because the color filters are decolorized and the thin film transistor loses its functional ability [18]. This also prevents incorporation into organic thin-film transistors as gate insulators because the curing temperature is higher than the T_g of the plastic substrate [19]. Also, the polymer curing at higher temperatures increases the oxidation rate of a metal substrate [20].

1.3 Review of Important Material Properties for Polymer Dielectrics in Microelectronics

The goal of this project is to design, synthesize, and characterize a series of new photodefinable, low dielectric constant polymers that can serve as advanced dielectric materials for microelectronics packaging and which possess processing and performance advantages relative to existing photodefinable dielectrics. In particular, polymers which possess lower dielectric constants and which can be processed at lower temperatures than other photodefinable polymers currently available are desired. To better understand the molecular design constraints and important physicochemical properties for such

materials, a discussion of the relevant important material properties as they apply to microelectronic applications is required.

1.3.1 Thermal Stability

Many steps utilized in fabricating microelectronic devices can require the use of elevated temperature processing. For example, copper metallization can be achieved by a variety of processes including electroplating, electroless plating, chemical vapor deposition, and physical vapor deposition. All of these processes can be performed at temperatures lower than 250 ^{o}C. Unfortunately, a thermal annealing step is generally required to ensure void free copper depositions. This annealing step can require temperatures as high as 400–450 °C [21]. This is an issue for some organic polymers, as they begin to decompose at lower temperatures. Obviously cracking, shrinking, and outgassing of materials in the device, such as the polymer dielectrics, must be completely avoided during such thermal processing.

1.3.2 Dielectric Constant

The next generation in microelectronic packaging requires the production of materials with lower dielectric constants while maintaining high thermal stability. Low dielectric materials are needed to support increased circuit densities [22]. High-density chips are approaching a minimum feature size with current materials. As feature sizes continue to decrease, interconnect delay time increases. An increased delay time reduces circuitry speed. Based on a survey of industrial customers by our collaborators in this project, Central Glass, it is felt that polymers with dielectric constants below 2.8 while maintaining thermal stability at temperatures below 350 ^{o}C would provide significant commercial opportunities.

Three mechanisms control dielectric polarization: electron density redistribution, bond stretching, and dipole orientation. Figure 1.9 provides a visual representation of the different forms of polarizability [23].

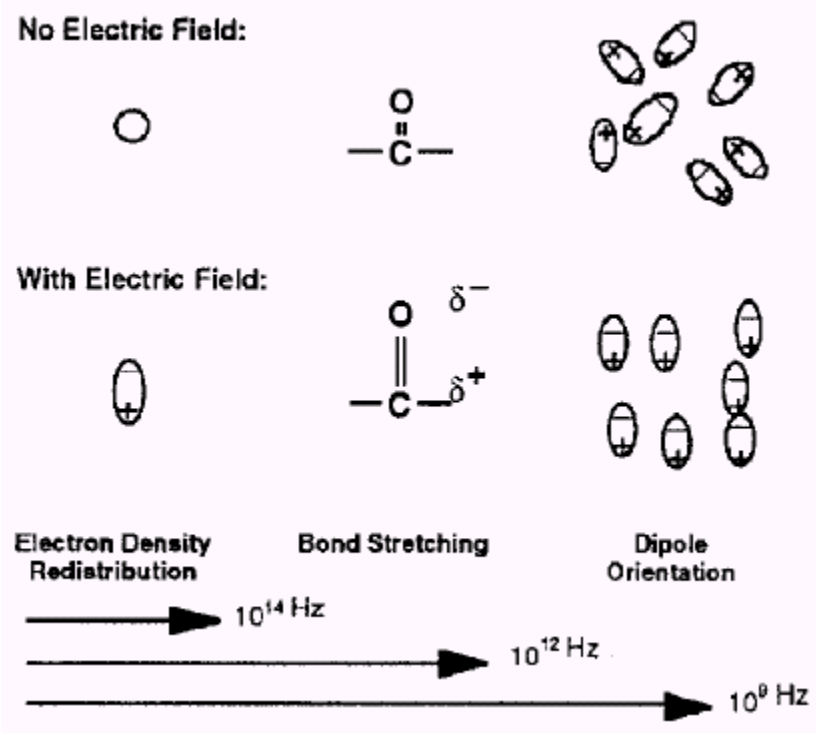

Figure 1.9 Forms of Polarization

Above a frequency of 10^{12} Hz (i.e. 1 GHz), dipole orientation is no longer possible. Above 10^{14} Hz (i.e. 100 GHz), bond stretching is no longer possible. Depending on the particular electronic application for the polymer insulator, all of these frequency ranges can be important. For example, currently printed wiring board signal frequencies are in the MHz range, computer microprocessor frequencies are in GHz range, and telecom devices are in the tens of GHz range.

The dielectric constant for a material is composed of contributions from the individual dielectric constants for the electron density redistribution, bond stretching, and dipole orientation. Dipole polarization is the strongest polarization in polymers with polar groups at reasonably low frequencies. At the highest frequencies, only electrons become polarized by electronic polarization since their low mass and ability to move spatially quickly allows them to respond to the alternating electric field. As the electric field oscillation frequency becomes progressively faster, dipole reorientation and then bond stretching can no longer occur quickly enough. This simple physical picture provides some insight as to how to design materials which possess low dielectric constant. By making it more difficult to relocalize electrons the electronic polarization contribution to the dielectric constant can be reduced. One way to achieve this is to make bonds in the material more electronegative. As a result, addition of electronegative fluorine into a polymer can in general reduce the dielectric constant contribution from electronic redistribution. Fluorine-containing polymers also often have other unique chemical and physical properties not observed with other organic polymers. They generally posses improved thermal stability, higher chemical stability, and lower refractive index as compared to their non-fluorinated analogs.

1.3.3 Moisture Content/Water Absorption

In many cases, unless extreme care is taken during processing and packaging, the dielectric polymer will be exposed to a humid environment. Water absorption must be minimized in order to maintain an acceptable dielectric constant in the polymer. Water is an extremely polar molecule with a dielectric constant in its pure form that is dependant on density, pressure and temperature as shown in Figure 1.10.

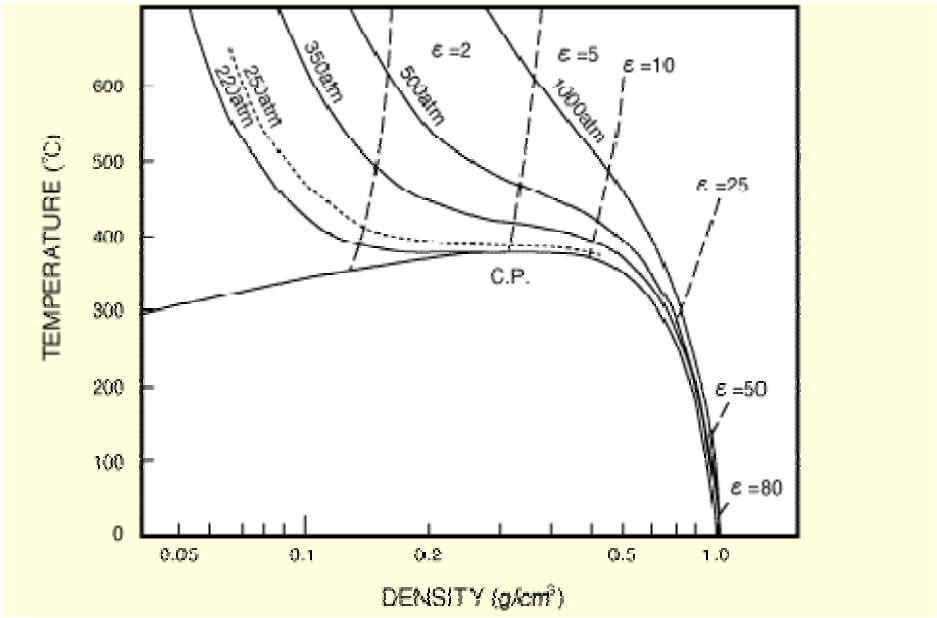

Figure 1.10 Temperature, Pressure, and Density Dependence of Dielectric Constant

At room temperature and atmospheric pressure, a dielectric constant of 83 for water is observed [24]. Furthermore, water absorption in polymer films can lead to interracial adhesion problems and delamination. In order to meet the demands of future generations in microelectronic packaging, the water absorption must be less than one percent.

1.3.4 Glass Transition Temperature

Most photodefinable polymers, such as photoresists, are amorphous glassy polymers. At temperatures above the glass transition temperature, polymers are "rubbery" and exhibit viscous flow with considerable motion of the polymer chain segments. At temperatures below the glass transition temperature (T_g), the motion of the chain segments is halted and the polymer behaves as a glass rather than a rubber. Heating above T_g enables a polymer film to anneal, relax out residual stress, and remove residual

solvent from spin cast films [8]. As temperature increases, the volume of the polymer increases. When the temperature exceeds the T_g, the volume increases at a much larger rate, corresponding to a much larger CTE above its T_g.

Glass transition temperature depends on many factors related to the chemistry and structure of a polymer. Each chain end has some free volume associated with it. A polymer with shorter chains, i.e. lower molecular weight, will have more chain ends per unit volume which will increase the free volume. Hence, the T_g for lower molecular weight polymers will generally be lower than the T_g for higher molecular weight polymers. Lower molecular weight polymers also have more free volume frozen in below T_g than higher molecular weight polymers. A polymer with a backbone that exhibits higher flexibility will also have a lower T_g. This is because the activation energy for conformational changes associated with T_g, i.e. the onset of "crank-shaft" rotations in the backbone, is lower and therefore these additional motions can take place at lower temperatures. Larger side groups can hinder bond rotation more than smaller ones, and therefore causes an increase in T_g. Groups which induce inter- and intramolecular interactions in the polymer can also increase the T_g. For example the addition of polar groups which can form hydrogen bonds or provide other similar interactions can increase the T_g of a polymer. Polar groups such as Cl, CN, or OH have the strongest effect. Polymers with more branching have more chain ends, resulting again in more free volume, which can reduce T_g. But the branches also hinder rotation, like large side groups, which can increase T_g. Which of these effects is greater depends on the polymer in question, and thus T_g may either rise or fall in branched materials. Cross-linking reduces chain mobility, and so T_g will generally be increased in cross-linked materials.

The desired T_g in polymer dielectrics is dependant on the processes and devices in question. Ideally, the polymer should not be exposed to temperatures substantially above its T_g for extended periods of time because the polymer's mechanical properties dramatically change above the transition [25]. This includes temperature increases during the deposition and etching of metal layers. However, polymers with extremely high glass transition temperatures can suffer from difficulty in the ability to coat and anneal films of desired quality.

1.3.5 Coefficient of Thermal Expansion

An important problem in microelectronics can be the difference in the coefficient of thermal expansion CTE between the various films and substrate that make up a device. CTE is defined as the fractional increase in length per unit rise in temperature [26]. Mismatches between the CTE in various device layers can produce stress effects in the films due to thermal processing or varying temperature during device operation. For example, residual film stresses can be developed during film deposition and processing which lead to warping of the substrate, or film stresses induced during processing or operation can lead to cracking or interfacial delamination. As a benchmark, the CTE for silicon is 2.9 ppm/^{o}C while that of a typical polymer can be in the range of 80-90 ppm/^{o}C.

1.3.6 Young's Modulus

Young's modulus (E) is a measure of the stiffness of a given material. It is defined as the ratio, for small strains, of the rate of change of stress with strain. Integration of a soft dielectric which deforms rather than cracks (such as a polymer) may seem a good choice for the low-k stack, but it may increase the risk of cracking for brittle layers in the structure (barriers, etch stops, hard masks, etc.) used in the Cu dual

damascene process [27]. Lower modules become very prone to process damages. Strong mechanical strength to have the ability to withstand external forces from thermal, electrical, and packaging stresses is a major challenge for the successful integration of the materials [28].

1.4 Review of Important Existing Classes of Polymer Dielectrics

1.4.1 Polyimides

Polyimides have already been used as intermetal dielectrics as early as the 1970's. PIs have –CO-N-CO- imido linkages in the backbone. Exclusions include polymers formed by additional polymerization of unsaturated imides with resulting pendant imido groups. Polyimides are normally formed from cyclization or ring closure of poly(amic acid) precursor polymers made by copolymerization of a diamine and a dianhydride (see Figure 1.11).

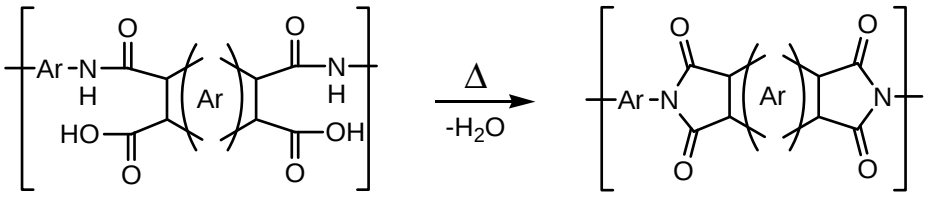

Figure 1.11 Polyimide Scheme

Polyimides contain polar carbonyl groups in the polymer backbone, generally leading to higher water absorption and a higher dielectric constant than other alternative dielectric polymers such as polybenzoxazoles [14]. The water uptake for most polyimides is between 1 – 4%, but it has been reported as high as 12%. Typical Polyimide dielectric constants range between 3.2 - 3.4 [29]. However, heavily

fluorinated PIs have shown dielectric constants as low as 2.3. PIs are commonly known to possess high thermal stability, high mechanical strength, and a high glass transition temperature. Some polyimides can display weight losses of less than 5% at 470 ^{o}C. The T_g for fluorinated polyimides reported in the literature ranges between 200 – 420 ^{o}C whereas the T_g for non-fluorinated polyimides ranges between 280 – 500 ^{o}C. Depending on the aromatic structure of the polyimide, the in plane CTE has been reported in the range from approximately -5 - 90 ppm/^{o}C. Using various additives and methods for functionalizing the polymer, photosensitive polyimides have been developed which are now used extensively in advanced microelectronics due to their excellent physical and chemical characteristics and ease of patterning [23, 26, 30-33].

Most polyimides are insoluble in aqueous alkaline solutions and many are insoluble in organic solvents. Therefore, most polyimides must be patterned using separate lithography and dry plasma etch processes and many can not be solution deposited at all. Therefore, many polyimides used commercially are processed via their poly(amic acid) precursor form. Such poly(amic acid) precursor polymers are generally soluble in a range of casting solvents and can often be developed in conventional aqueous alkaline developer solutions. After preparation and patterning of the precursor film, imidization must be completed, often thermally, in order to produce a polymer film with a high thermal stability, low water absorption, and low dielectric constant. Due to the inherent rigidity of the polyimide chains, high imidization temperatures, typically above 300 ^{o}C, are required.

In some cases, polyimides have been made into aqueous alkaline soluble forms by side group functionalization. Such materials can be made photodefinable in various ways

including both traditional schemes for making positive and negative-tone resists. For example, photodefinable polyimides can be made by attaching a photo-polymerizable moiety which can induce cross-linking of the polymer upon exposure, such as methacrylate type groups, onto the polyimide backbone using an ester or ionic linkage [34]. Processing these preimidized materials can obviously decrease the processing temperatures required for these materials, but the required addition of functional groups onto the PI to impart the photodefinable character and solubility can degrade the physiochemical properties of the material.

1.4.2 Benzocyclobutene

Benzocyclobutene (BCB) resins were developed by Dow in the 1980's [35]. The BCB group is a tautomer of the *ortho*-xylylidene group, which is believed to be the reactive species. This group can undergo many reactions. The *ortho*-xylylidene structure has a biradical character that is responsible for polymerization as shown in Figure 1.12.

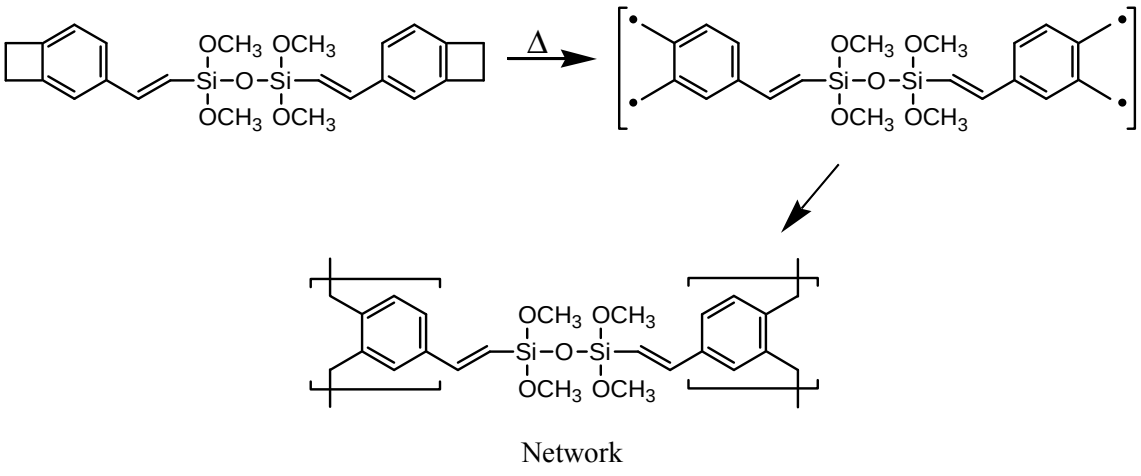

Figure 1.12 Benzocyclobutene Scheme

Curing is performed at 250 ^{o}C under an inert atmosphere because of the poor thermooxidative resistance of BCBs. BCBs can be reacted with each other, or with dienophiles such as imides. As a result, polymers produced from BCB can be modified to a great extent. With the addition of siloxane monomers, the dielectric constant can be as low as 2.6 with water uptake as low as 0.2% [29, 36]. BCB resins can also be thermally stable at temperatures as high as 350 ^{o}C with a coefficient of thermal expansion as low as 50 ppm/^{o}C.

1.4.3 Polbenzoxazoles

Polybenzoxazoles (PBO) have more recently received a great deal of attention and are known to possess a number of advantageous physical and chemical properties as compared to other polymer dielectrics [14, 37-42]. PBO polymers can be prepared by the reaction of terephthalic acid (TA) in poly(phosphoric acid) (PPA) with a diamino-dihydroxybenzene [43]. PBO polymers are often insoluble in essentially all casting solvents. In microelectronics, PBO materials are commonly processed by coating films using polyhydroxyamide solutions which are heated to remove solvent. Polyhydroxyamides are prepared by polymerizing a diamino-dihydroxy-containing molecule with a diacid chloride. Further heating cyclizes the *ortho*-hydroxyamide to the final desired benzoxazole group (see Figure 1.13).

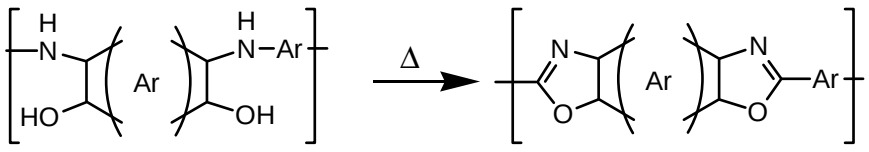

Figure 1.13 Polybenzoxazole scheme

Cyclization temperatures for PBOs can be as low as 250 ^{o}C [41, 44]. The lack of carbonyl groups in the backbone reduces water absorption and helps to reduce the dielectric constant of the materials as compared to PIs. Dielectric constants reported for PBO materials range from 2.0 – 3.2 with water uptakes below 1% [38]. Many PBOs degrade above 300 ^{o}C, but some have shown only 5% weight loss at 480 ^{o}C. By altering the aromatic group (Ar), the glass transition temperature of the polymer can be tailored to exceed 450 ^{o}C. Judicious choice of this aromatic group has also been shown to achieve polymers with CTE values in the 20 – 40 ppm/^{o}C range [45-47].

1.5 References

1. Tummala, R.R. *Fundamentals of microsystems packaging*. [Book; Internet Resource] 2001 [cited; vii, 967 p.: ill.; 25 cm.].

2. Maier, G., *Low dielectric constant polymers for microelectronics.* Progress in Polymer Science, 2001. **26**(1): p. 3-65.

3. Clarke, M.E., *Introducing Low-k Dielectrics into Semiconductor Processing*. 2001, Mykrolis. p. 1-20.

4. Thompson, L.F., C.G. Willson, and M.J. Bowden, *Introduction to microlithography*. 2nd ed. ACS professional reference book; 1994, Washington, DC: American Chemical Society. xiv, 527 p.

5. Barrett, C.R., *The Solid-State Century*, in *Scientific American, Special Issue*. 1997. p. 56-61.

6. Yan, Z. and A. Reiser, *Effect of Hydrogen Acceptors on pKa of Phenolic Resins: Link to Dissolution Inhibition.* Macromolecules, 1998. **31**(22): p. 7723-7727.

7. Dammel, R.R. *Diazonaphthoquinone-Based Resists*. in *SPIE Short Course SC104*.

8. Oyama, T., et al. *Novel Principle For Preparing Photosensitive Engineering Plastics: Reaction Development Patterning (RDP)*. in *RadTech Asia*. 2003.

9. Hoskins, T.P.J., *Characterization of Substituted Polynorbornenes for Advanced Lithography*. 2005, Georgia Institute of Technology. p. 223.

10. Hinsberg, W.D., et al., *Chemical and physical aspects of the post-exposure baking process used for positive-tone chemically amplified resists.* IBM Journal of Research and Development, 2001. **45**(5): p. 667-681.

11. Shi, F.F., L.A. Schneggenburger, and J. Economy, *New photoimageable dielectric insulating copolyester thin films: synthesis and characterization.* Journal of Applied Polymer Science, 1997. **63**(9): p. 1199-1211.

12. Choi, K.H., et al., *New base-soluble positive-working photosensitive polyimides having o-nitrobenzyl ester group.* Polymers for Advanced Technologies, 2005. **16**(5): p. 387-392.

13. Choi, S.M., et al., *Synthesis and characterization of negative-type photosensitive polyimides based on cyclobutane-1,2,3,4-tetracarboxylic dianhydride.* Journal of Applied Polymer Science, 2005. **96**(6): p. 2300-2308.

14. Hsu, S.L.-C. and W.-C. Chen, *A Novel Positive Photosensitive Polybenzoxazole Precursor for Microelectronic Applications.* Polymer, 2002. **43**(25): p. 6743-6750.

15. Robinson, J.D. and B. Humphreys, *Plasma etch optimization of a photo-sensitive benzocyclobutene (BCB) planarisation layer for photonic integrated circuit manufacturing.* Proceedings of SPIE-The International Society for Optical Engineering, 2003. **5260**(Applications of Photonic Technology 6): p. 411-417.

16. Yamaoka, T., et al., *A study of novel heat-resistant polymers: preparation of photosensitive fluorinated polybenzoxazole precursors and physical properties of polybenzoxazoles derived from the precursors.* Journal of Polymer Science, Part A: Polymer Chemistry, 1990. **28**(9): p. 2517-32.

17. Zhang, J.-Y. and I.W. Boyd, *UV light-induced deposition of low dielectric constant organic polymer for interlayer dielectrics.* Optical Materials (Amsterdam), 1998. **9**(1-4): p. 251-254.

18. Oba, M., *Effect of curing accelerators on thermal imidization of polyamic acids at low temperature.* Journal of Polymer Science, Part A: Polymer Chemistry, 1996. **34**(4): p. 651-58.

19. Pyo, S., et al., *Low-temperature processable inherently photosensitive polyimide as a gate insulator for organic thin-film transistors.* Applied Physics Letters, 2005. **86**(13): p. 133508/1-133508/3.

20. Wang, T.H., et al., *Temperature effect on polyimide/copper interface.* Journal of Applied Polymer Science, 1993. **47**(6): p. 1057-64.

21. Shamiryan, D., et al., *Low-k dielectric materials.* Materials Today (Oxford, United Kingdom), 2004. **7**(1): p. 34-39.

22. Dang, T.D., et al. *Low Dielectric Constant Polymers Developed for High-Speed Integrated Circuits*. 2001 [cited; Available from: http://www.afrlhorizons.com/Briefs/June01/ML0016.html. Accessed June 3, 2004.

23. Simpson, J.O. and A.K. St. Clair, *Fundamental insight on developing low dielectric constant polyimides.* Thin Solid Films, 1997. **308-309**: p. 480-485.

24. Treichel, H., et al., *Low dielectric constant materials for interlayer dielectric.* Microelectronic Engineering, 1998. **40**(1): p. 1-19.

25. Bai, Y., et al., *Photosensitive polynorbornene based dielectric. I. Structure-property relationships.* Journal of Applied Polymer Science, 2004. **91**(5): p. 3023-3030.

26. Ando, S. and M. Yoshida. *Synthesis and Optical Properties of Rod-Like Fluorinated Polyimides Having High Charge-Transfer Interactions*. in *Proc. 6th European Conf. Polyimides & High Performance Polymers*. 2003.

27. Moore, T.M., et al., *Mechanical characterization of low-K dielectric materials.* AIP Conf. Proc. FIELD Full Journal Title:AIP Conference Proceedings, 2001. **550**(Characterization and Metrology for ULSI Technology): p. 431-439.

28. Hsia, C.C., *The quest of porous ELK materials for high performance logic technologies.* Microelectron. Eng. FIELD Full Journal Title:Microelectronic Engineering, 2006. **83**(11-12): p. 2055-2058.

29. Foster, R., *Photoimageable BCB technology lowers costs for MCMs.* Solid State Technology, 1995. **38**(6): p. 125-6,128,130.

30. Hsu, S.L.-C., et al., *Synthesis and characterization of a positive-working, aqueous-base-developable photosensitive polyimide precursor.* Journal of Applied Polymer Science, 2002. **86**(2): p. 352-358.

31. Oishi, Y., et al., *Synthesis of fluorine-containing wholly alicyclic polyimides by in situ silylation method.* Journal of Photopolymer Science and Technology, 2003. **16**(2): p. 263-266.

32. Qian, Z.G., et al., *Photoimageable polyimides derived from a,a-(4-amino-3,5-dimethylphenyl)phenylmethane and aromatic dianhydride.* Journal of Polymer Science, Part A: Polymer Chemistry, 2002. **40**(17): p. 3012-3020.

33. Simpson, J., Z. Ounaies, and C. Fay, *Polarization and piezoelectric properties of a nitrile substituted polyimide.* Materials Research Society Symposium Proceedings, 1997. **459**(Materials for Smart Systems II): p. 59-64.

34. Hall, S. and C.C. Schuckert, *Single mask wafer overcoat process using photodefinable polyimide.* Solid State Technology, 1999. **42**(10): p. 95-96.

35. Kirchhoff, R.A. and K.J. Bruza, *Polymers from benzocyclobutenes.* Advances in Polymer Science, 1994. **117**(High Performance Polymers): p. 1-66.

36. Farona, M.F., *Benzocyclobutenes in polymer chemistry.* Progress in Polymer Science, 1996. **21**(3): p. 505-555.

37. Chang, J.-H., D.-K. Park, and K.J. Ihn, *Montmorillonite-based nanocomposites of polybenzoxazole: synthesis and characterization (Part 1).* Journal of Polymer Science, Part B: Polymer Physics, 2001. **39**(5): p. 471-476.

38. Dang, T.D., et al., *Synthesis and characterization of fluorinated benzoxazole polymers with high Tg and low dielectric constant.* Journal of Polymer Science, Part A: Polymer Chemistry, 2000. **38**(11): p. 1991-2003.

39. Ebara, K., Y. Shibasaki, and M. Ueda. *New synthetic route for positive photoresist based on poly(benzoxazole) precursor from diphenyl isophthalate and bis(o-aminophenol).* in *RadTech Asia*. 2003.

40. Hsu, S.L.-C., W.-C. Chen, and P.-I. Lee, *A novel positive photosensitive polybenzoxazole based on a tetrahydropyranyl (THP) protected polyhydroxyamide.* Polymer Bulletin (Berlin, Germany), 2003. **50**(5-6): p. 295-302.

41. Kim, J.-H. and J.K. Lee, *Hydroxy-substituted polyenaminonitrile as a soluble precursor for rigid-rod polybenzoxazole.* Bulletin of the Korean Chemical Society, 2001. **22**(9): p. 999-1004.

42. Lee, J.K., J.-H. Kim, and Y.J. Kim, *Synthesis and characterization of fluorine-containing polybenzoxazoles by high-temperature direct polycondensation.* Bulletin of the Korean Chemical Society, 2003. **24**(7): p. 1029-1031.

43. So, Y.-H., J.P. Heeschen, and C.L. Murlick, *A mechanistic study of polybenzoxazole formation with model compounds.* Macromolecules, 1995. **28**(21): p. 7289-90.

44. Toyokawa, F., Y. Shibasaki, and M. Ueda, *A novel low temperature curable photosensitive polybenzoxazole.* Polymer Journal (Tokyo, Japan), 2005. **37**(7): p. 517-521.

45. Fujita, Y. and M. Tomikawa, *Positive photoimaging polybenzoxazole precursor compositions containing o-quinonediazide derivatives*. 2001, (Toray Industries, Inc., Japan). Application: JP. p. 12 pp.

46. Hasegawa, T. and K. Maeda, *Polybenzoxazoles with low linear thermal expansion coefficient, their precursors, coating solutions containing them, their films, and their manufacture*. 2005, (Central Glass Co., Ltd., Japan). Application: JP. p. 14 pp.

47. Maeda, K., et al., *Fluorinated polybenzoxazoles with low dielectric constant and thermal expansion, and their precursors*. 2000, (Central Glass Co., Ltd., Japan). Application: JP. p. 8 pp.

CHAPTER 2

EXPERIMENTAL METHODS

2.1 Introduction

The different experimental techniques used to evaluate the materials are summarized in this chapter. As mentioned previously, polymer dielectrics must possess a variety of different physical and chemical properties to be commercially useful. Analysis of the different structures and properties between the various polymers, as well as the evaluation of the lithographic performance requires numerous analytical techniques. The methods summarized in this chapter include nuclear magnetic resonance spectroscopy (NMR), Fourier transform infrared spectroscopy (FTIR), gel permeation chromatography (GPC), thermogravimetric analysis (TGA) and mass spectroscopy (MS). In addition, a variety of techniques were used to measure the physiochemical properties and evaluate the lithographic performance of the polymers under evaluation.

2.2 Chemical Structure and Properties

2.2.1 Nuclear Magnetic Resonance Spectroscopy

Nuclear magnetic resonance (NMR) spectroscopy has become one of the most powerful tools for clarifying chemical structures of organic and inorganic compounds. NMR spectrometers are of two general types, continuous wave and pulsed, or Fourier transform (FT-NMR) [1]. Continuous wave instruments are largely limited to special routine applications such as quality assurance of industrial processes, while FT-NMR dominates the NMR market.

The theory of NMR is based on the fact that when a compound is placed in a strong magnetic field and irradiated with a radio-frequency signal, energy absorption of certain nuclei occurs at discrete frequencies, thus a macroscopic magnetization develops. In addition to mass, electrons, neutrons, and protons have spin. Spin is a quantum mechanical property with no classical counterpart, equivalent to internal angular momentum. Spin comes in multiples of ½ and can be positive or negative. Since spins can be paired and canceled, it is the net spin, or the spin quantum number, that is important.

In the absence of a magnetic field, the magnetic moment vector is randomly oriented with no net magnetization and all nuclei have the same energy. When placed in a magnetic field, the magnetic moment vectors are aligned with orientations according to their magnetic quantum numbers, and a net magnetization can be detected. The vector sum of the magnetic moment vectors is the net equilibrium magnetization that rotates about the applied magnetic field direction [2].

When radio-frequency energy is absorbed by a nucleus, the angle of precession must change. In FT-NMR, nuclei in a strong magnetic field are subjected periodically to very brief pulses, typically less than 10μs, of intense radio-frequency radiation. The interval between pulses usually ranges from one to several seconds. During that interval, a time-domain, radio-frequency signal, called the free induction decay (FID) signal, is emitted as nuclei return to their original state. FID can be detected with a radio-receiver coil that is perpendicular to the static magnetic field. This same coil is generally used to pulse the sample. The FID signal is then digitized and stored in a computer for data processing. In order to improve the signal-to-noise ratio, the time-domain decay signals

from numerous successive pulses are added together. The resultant is then converted to a frequency-domain signal by a Fourier transform. The resulting output is the familiar spectrum used to describe NMR results.

Two environmental effects that can be used in proton spectral analysis are chemical shift and spin-spin splitting. Small differences in the absorption frequency of a given hydrogen atom depend upon the group to which the hydrogen atom is bonded. Small magnetic fields that generally oppose the applied magnetic field are generated by electrons as they circulate around nuclei. As a consequence, each hydrogen atom experiences a characteristic effective field that is somewhat smaller or larger than the applied field. This leads to a shift in the frequency absorbed by the different hydrogen atoms relative to one another, and is seen in an NMR spectrum as a shift along the x-axis. NMR spectra are typically given as Intensity versus parts per million (ppm) plots. Since spectroscopy is the measurement of some interaction as a function of energy, the use of a concentration unit (ppm) as a unit of energy is not immediately apparent. The ppm refers to the number of frequency units that the NMR signal is shifted with respect to a reference material. This shift occurs in the Hz regime and is normalized by the operating frequency of the spectrometer, which is in MHz. To avoid using very small numbers, this normalized frequency is reported as ppm, but are directly related to energy.

Spin-spin splitting is put on top of the chemical shift and sometimes causes absorption peaks to be split into multiple peaks. The splitting of a chemical shift can be explained by assuming that the magnetic moment of a nucleus interacts with the magnetic moments of all other nuclei surrounding it, thus causing splitting of energy levels and hence multiple transitions. This coupling interaction is believed to arise through a

polarization of spins that is transmitted by the bonding electrons. In ^{1}H-NMR, the number of peaks present for a particular hydrogen atom is directly related to the number of hydrogen atoms attached to adjacent nuclei. For example, a methyl group connected to a carbonyl group would experience no splitting since there are no hydrogen atoms on the adjacent carbon. For this case, a single peak would be observed at the characteristic frequency. On the other hand, if the methyl group were instead attached to a –CH– functional group, the peak for the methyl hydrogen atoms would become a doublet. The multiplicity of the splitting becomes more complex as more and more hydrogen atoms are present on adjacent atoms. The combination of the chemical shift and spin-spin splitting provide very distinct NMR spectra for each compound examined.

In addition to ^{1}H-NMR, examining the carbon atoms in a molecule with ^{19}F-NMR, can be an extremely valuable tool set for confirming desired reaction products. Both ^{1}H-NMR and ^{19}F-NMR were used to determine the structures of the reaction products in this work. Spectra were measured with a Varian Mercury-Vx 400 (400 MHz) spectrometer.

2.2.2 Fourier Transform Infrared Spectroscopy

Fourier transform infrared spectroscopy (FTIR) is the study of the interaction of infrared light with matter [3]. Light is composed of electric and magnetic waves in plane perpendicular to each other. Light waves move through space in a plane perpendicular to the electric and magnetic planes. The electric vector interacts with molecules. The amplitude of the electric vector has the form of a sine wave. The wavelength is the distance between adjacent crests or troughs. The wavenumber of light is the inverse of the wavelength. The wavenumber is a measure of the number of waves there are in a

centimeter. Wavenumbers are the units typically used in FTIR to denote different kinds of light. The wavenumber is directly proportional to the energy as follows:

$$Energy = hcW \qquad (2.1)$$

where c is the speed of light, h is Planck's constant, and W is the wavenumber (cm^{-1}).

High wavenumber light has more energy than low wavenumber light. The majority of FTIRs operate with mid-infrared radiation (4000-400 cm^{-1}). Infrared radiation is another name for heat. All objects above absolute zero give of infrared radiation. When infrared radiation interacts with matter it can be absorbed which causes the chemical bonds to vibrate. Chemical structures tend to absorb infrared radiation in the same wavenumber range regardless of the surrounding chemical structure. Table 2.1 lists some common chemical bonds and their corresponding frequency range. FTIR spectra of pure compounds are generally so unique that they are like a molecular "fingerprint". While organic compounds have very rich, detailed spectra, inorganic compounds are usually much simpler. For most common materials, the spectrum of an unknown can be identified by comparison to a library of known compounds. This correlation allows the structure of unknown molecules to be identified from the infrared spectrum.

Table 2.1 Common Bond Energies

Bond	Compound Type	Frequency range, cm^{-1}
C-H	Alkanes	2960-2850(s) stretch
		1470-1350(v) scissoring and bending
	CH_3 Umbrella Deformation	1380(m-w) - Doublet - isopropyl, *t*-butyl
C-H	Alkenes	3080-3020(m) stretch
		1000-675(s) bend
C-H	Aromatic Rings	3100-3000(m) stretch
	Phenyl Ring Substitution Bands	870-675(s) bend
	Phenyl Ring Substitution Overtones	2000-1600(w) - fingerprint region
C-H	Alkynes	3333-3267(s) stretch
		700-610(b) bend
C=C	Alkenes	1680-1640(m,w)) stretch
C≡C	Alkynes	2260-2100(w,sh) stretch
C=C	Aromatic Rings	1600, 1500(w) stretch
C-O	Alcohols, Ethers, Carboxylic acids, Esters	1260-1000(s) stretch
C=O	Aldehydes, Ketones, Carboxylic acids, Esters	1760-1670(s) stretch
O-H	Monomeric -- Alcohols, Phenols	3640-3160(s,br) stretch
	Hydrogen-bonded -- Alcohols, Phenols	3600-3200(b) stretch
	Carboxylic acids	3000-2500(b) stretch
N-H	Amines	3500-3300(m) stretch
		1650-1580 (m) bend
C-N	Amines	1340-1020(m) stretch
C≡N	Nitriles	2260-2220(v) stretch
NO_2	Nitro Compounds	1660-1500(s) asymmetrical stretch
		1390-1260(s) symmetrical stretch

v - variable, m - medium, s - strong, br - broad, w – weak

An FTIR is a Michelson interferometer with a movable mirror. By scanning the movable mirror over some distance, an interference pattern is produced that encodes the spectrum of the source. In its simplest form, a Fourier transform spectrometer consists of two mirrors located at a right angle to each other and oriented perpendicularly, with a beamsplitter placed at the vertex of the right angle and oriented at a 45° angle relative to the two mirrors as shown in Figure 2.1.

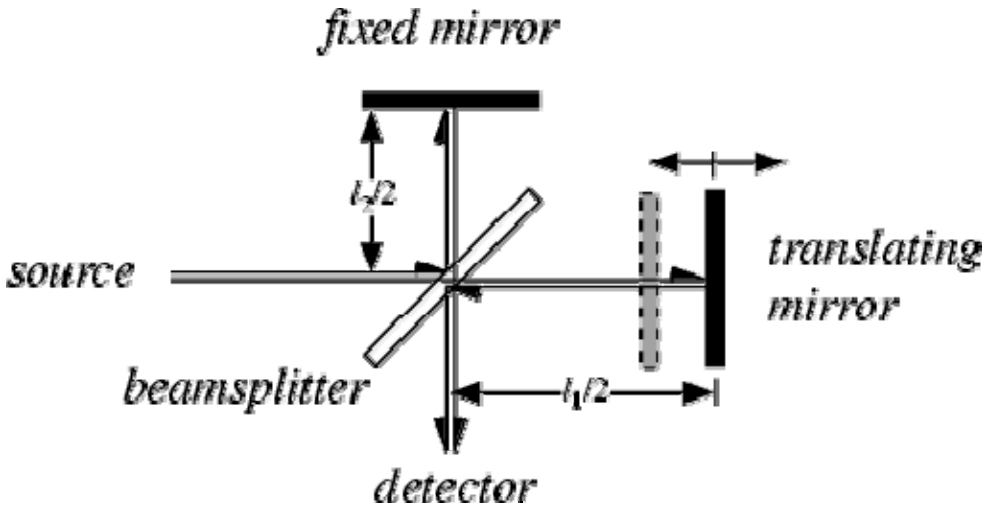

Figure 2.1 FTIR Setup

Radiation incident on the beamsplitter from one of the two "ports" is then divided into two parts, each of which propagates down one of the two arms and is reflected off one of the mirrors. The two beams are then recombined and transmitted out the other port. When the position of one mirror is continuously varied along the axis of the corresponding arm, an interference pattern is swept out as the two phase-shifted beams interfere with each other. Spectra were measured with a Bruker KLS/088 FTIR.

2.2.3 Gel Permeation Chromatography

Molecular weight (MW) determination is an important characterization procedure when studying polymers. One of the most widely used MW determination techniques is gel permeation chromatography (GPC). GPC makes use of a column, or series of columns, packed with particles of a porous substrate. The column is maintained at a constant temperature, and solvent is passed through at a constant rate. Figure 2.2 shows a schematic of how particles of different sizes are separated in a GPC [4]. First, a small amount of polymer solution is injected just ahead of the column at the start of a run. The polymer is then carried through the column by the solvent flow. Smaller molecules in the sample diffuse in and out of the pores, while larger molecules are swept more directly through the voids between the packing particles since they cannot fit into the pores. A separation is therefore obtained with larger molecules passing through the column first, followed by successively smaller molecules.

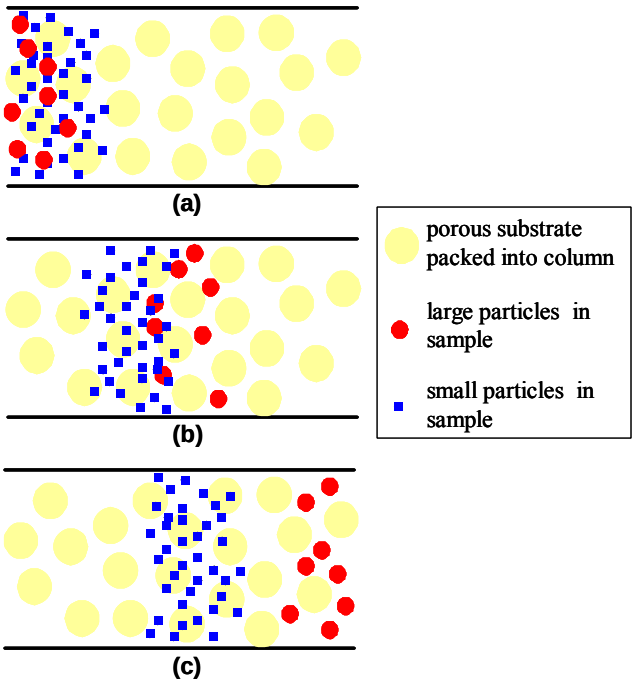

Figure 2.2 Schematic representation of separation by gel permeation chromatography. (a) A sample is injected into a column of porous beads. (b) The sample is carried through the column by solvent flow where smaller molecules diffuse in and out of the pores, while larger molecules are swept more directly through the voids between the packing particles. (c) Separation is obtained with larger molecules passing through the column first, followed by the smaller molecules.

A detector is placed at the outlet of the column that is concentration sensitive. The most common detector is a differential refractometer. This detector measures differences in refractive index between pure solvent and the polymer solution leaving the column. This is a sensitive measure of the concentration of the solution passing through the detector according to Equation 2.2.

$$Q = kc \qquad (2.2)$$

where Q is the detector readout, k is a proportionality constant, and c is the mass concentration of polymer (g/cm^3). Conventional GPC is a relative method; a calibration curve is needed to provide quantitative results. Calibration with monodisperse polymer standards provides a relationship between the retention time and the molecular weight of the sample polymer. The calibration curve, strictly speaking, applies only to the particular polymer, solvent, temperature, flow rate, and column for which it is established.

Molecular weights may be approximated directly from the sample and calibration curves by breaking the curves into arbitrary volume increments Δv. If the molecular weight of polymer in the ith volume increment, M_i, is considered constant over small Δv, the number of moles of polymer in a volume increment is n_i:

$$n_i = \frac{c_i \Delta v}{M_i} = \frac{Q_i \Delta v}{k M_i} \tag{2.3}$$

the number-average molecular weight (M_n) and weight-average molecular weight (M_w), can then be calculated by Equations 2.4 and 2.5, respectively.

$$\overline{M}_n = \frac{\sum_i n_i M_i}{\sum_i n_i} = \frac{\sum_i Q_i}{\sum_i (Q_i / M_i)} \tag{2.4}$$

$$\overline{M}_w = \frac{\sum_i n_i M_i^2}{\sum_i n_i M_i} = \frac{\sum_i Q_i M_i}{\sum_i (Q_i)} \tag{2.5}$$

Finally, a measure of the breadth of the distribution of molecular weights, or the polydispersity index (PDI), can be determined according to Equation 2.6. Comparison of the sample curve to the calibration curve determines the molecular weight distribution of the unknown sample with respect to the standards used.

$$PDI = \overline{M}_w \Big/ \overline{M}_n \qquad (2.6)$$

GPC analyses were carried out using a Waters 1525 binary pump coupled to a Waters 2414 refractive index detector with tetrahydrofuran as an eluant on two 10-micron particle size, linear mixed bed packing columns (American Polymer Standards) in series. The pore sizes of the packing material were 10,000 and 500 Å. Although using this "column set" increases the time required for a sample to traverse the system, it also increases the molecular weight range and resolution of the system. All chromatograms were calibrated using polystyrene standards. Since the polymers studied in this work are not structurally similar to polystyrene, GPC results cannot be viewed as absolute molecular weight measurements, but the relative trends are accurate.

2.2.4 Ellipsometry

Ellipsometry is a very sensitive technique for measuring the thickness of thin films. When linearly polarized light encounters a thin film or surface, a polarization change occurs. The basic theory behind ellipsometry is to measure this change. The fundamentals of ellipsometry are described by the solutions to Maxwell's equations for the electromagnetic plane wave. Since ellipsometry directly measures changes in

polarization and does not rely solely on the accurate measurement of relative changes in reflected intensity, ellipsometry is far superior to simple reflectance measurement, in accuracy and sensitivity, as a thin film measurement technique.

The ideal film thicknesses for ellipsometry analysis are those that are not too much smaller or larger than the wavelength of light used for the analysis. This gives a range of thickness from a few nanometers to several microns when visible light is used. This range covers a majority of the values one would typically encounter when working with thin-films in the microelectronics industry. Single-wavelength instruments (typically 632.5nm, red light) have been used for decades, but these instruments are very limited in the types of samples that can be accurately analyzed. Not only must the sample be very uniform, both in terms of thickness and optical properties, but refractive index and thickness become strongly correlated, especially for thinner films. Obtaining unique solutions for film thickness and optical properties is therefore difficult unless the refractive index of the material is known. Another drawback is that only materials that are transparent at the analysis wavelength of the ellipsometer can be measured accurately.

More advanced ellipsometry systems have recently become available, which allow the user to vary the angle of light incidence and to collect data over a wide spectroscopic range. Variable angle spectroscopic ellipsometry (VASE) enables the collection of a large amount of data from a given sample. This ability helps to overcome many of the limitations described above for single-wavelength instruments. It is also possible to characterize a wide range of sample types, including strongly absorbing materials and samples with physical non-idealities such as thickness non-uniformity, optical constant anisotropy, and surface roughness. Another benefit to such a system lies

in the flexibility to control the data acquisition parameters in order to optimize data acquisition for any particular sample type. VASE is a powerful technique for determining film thicknesses and optical constants in thin film samples.

Film thickness and optical constants for films were determined using a V-VASE and W-VASE variable angle spectroscopic ellipsometer (J.A. Woollam Co., Inc). The ellipsometer measurements were made over the spectral range from 400 nm to 1000 nm at three different angles (65°, 70 and 75° from normal incidence) with a 5 nm sampling interval. The films were modeled using a Cauchy dispersion model for determination of film thickness and optical constants.

Optical models are required to simulate the response of light when it encounters a particular material or film stack in order to properly analyze the data collected using a VASE tool. An optical model for a particular film typically consists of a thickness value, optical constants, and any additional non-idealities that exist in the material. In analyzing ellipsometry data, different parameters of the optical model are adjusted and used to fit the model to the experimental data. As long as a unique solution is determined, and there is not significant correlation between any of the model fit parameters, the results are very accurate. A good fit to the experimental data, however, does not guarantee the accuracy of results, and it is often necessary to determine if a particular result is physically realistic. In most cases, is a straightforward determination and can be based on the fundamental properties of the interaction of electromagnetic radiation with solids. This is especially true for simple optical models such as the Cauchy model, which is a parametric dispersion model for transparent materials.

Materials like dielectrics, polymers, and some semiconductors, where the index of refraction and extinction coefficient vary smoothly as a function of wavelength, can usually be described using the Cauchy model. In general, a Cauchy model can describe any material that is transparent in the wavelength range of interest. The materials studied in this work are transparent ($k = 0$) over the visible and near-IR wavelength range, but that have some absorption ($k \neq 0$) in the ultraviolet (UV). In the Cauchy layer model, the material optical constants are described by the following equations:

$$n(\lambda) = A_n + \frac{B_n}{\lambda^2} + \frac{C_n}{\lambda^4} \tag{2.7}$$

A, *B*, and *C* are referred to as Cauchy parameters and are arbitrary constants that are used to specify the refractive index profile for the material as a function of wavelength. This model can be modified to account for simple absorption by adding a model for the extinction coefficient of the material (Equation 2.8) if the wavelength range in which the model is used extends near an absorption band edge.

$$k(\lambda) = \alpha^{\beta\left(12400\left(\frac{1}{\lambda}-\frac{1}{\gamma}\right)\right)} \tag{2.8}$$

Here α, β, and γ correspond to the amplitude of the absorption edge, the exponential factor, and the band edge (central wavelength position of the absorption edge), respectively. When fitting a Cauchy model to VASE data, the thickness and Cauchy parameters (Equation 2.7) are set as parameters and are fit to experimental data measured

over a wavelength range where the film is known to be transparent. After accurately determining the film thickness, the thickness parameter is removed as a fit parameter and the remaining optical constants may be determined without worrying about correlations, even if wavelength ranges where the material is absorbing are included at the edge of the data set being analyzed. In this work, materials were studied over the range 400-1200 nm, where the residue films do not possess appreciable absorbance. In this case, a simple Cauchy model with no absorption ($k = 0$) may be used.

2.2.5 Thermogravimetric Analysis

Thermogravimetric analysis (TGA) is a relatively simple analytical technique that records the mass of a sample as a function of temperature or time as the temperature of the sample is increased (usually linear with time) in a controlled atmosphere [1]. Results are typically plotted as mass or mass percent as a function of time or temperature. Modern commercial TGA instruments consist of four components: (1) a sensitive analytical balance, (2) a furnace, (3) a purge gas system for providing an inert (or sometimes reactive) atmosphere, and (4) a microcomputer or microprocessor for instrument control and data acquisition and display. Figure 2.2 shows a general schematic of the furnace casing. TG methods are largely limited to decomposition and oxidation reactions and to such physical processes as vaporization, sublimation, and desorption since temperature variations must produce a change in mass.

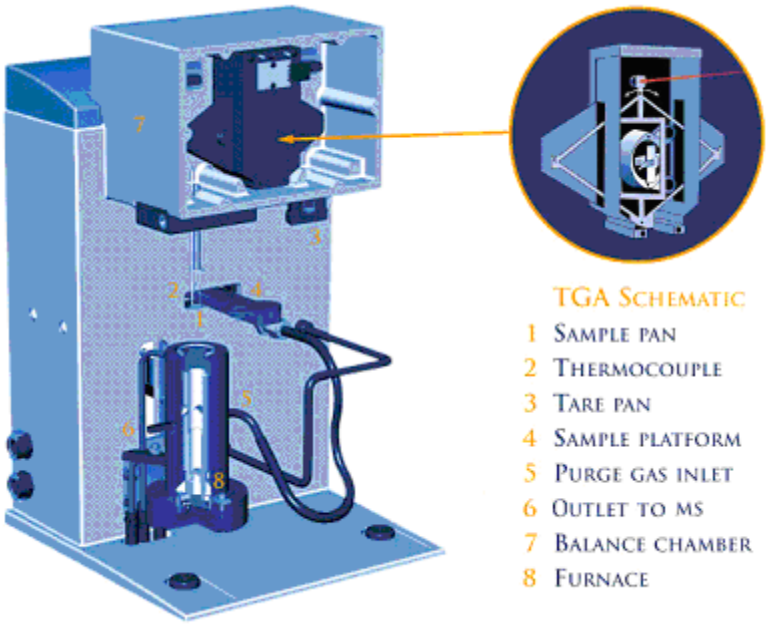

Figure 2.3 Schematic of Thermogravimetric Analysis (TGA) instrument

While the information provided by TGA is much more limited than that obtained by other thermal methods, it provides crucial information in the evaluation of polymers for use as low-k dielectrics. Not only does it give the decomposition temperature of the polymer and provide information on the complexity of the decomposition mechanism, it also identifies when polymer cyclization begins.

A TA Instruments Q500 thermal gravimetric analysis (TGA) instrument was used to determine the polymer's thermal stability. The films were heated at a rate of 10 ^{o}C/min.

2.2.6 Mass Spectroscopy

Attached to the TGA, a Pfeiffer Vacuum OmniStar Mass Spectrometer (MS) was used to analyze the molecules that leave the TGA. In order to measure the molecular weight of individual molecules, the MS them to ions so that they can be manipulated by

external electric and magnetic fields. Ions are very reactive and short-lived; therefore, their formation and manipulation must be conducted in a vacuum. Ions must be handled in an atmosphere less than a billionth of an atmosphere.

A small compound is ionized, usually to cations, by loss of an electron. The ions are then sorted and separated according to their mass and charge. The separated ions are finally detected and tallied. A mass spectrum will usually be presented as a vertical bar graph, where each bar represents an ion having a specific mass-to-charge ratio (m/z) and the length of the bar indicates the abundance of the ion. Most ions formed in the MS have a single charge, so the m/z value is equivalent to the mass of the compound. The highest-mass ion in a spectrum is normally considered to be the molecular ion, and the lower-mass ions are fragments from the molecular ion, assuming the sample is a single pure compound.

In a typical procedure, molecules of the sample are bombarded by electrons issuing from a heated filament. Cations formed by the electron bombardment are pushed away by a charged repellor plate that attracts anions. The cations are then accelerated toward other electrodes, having slits through which the ions pass as a beam. When the ion beam experiences a strong magnetic field perpendicular to its direction of motion, the ions are deflected in an arc whose radius is inversely proportional to the mass of the ion. Lighter ions are deflected more easily than heavier ions. By varying the strength of the magnetic field, ions of different mass can be focused progressively on a detector fixed at the end of a curved tube under high vacuum.

When a high energy electron collides with a molecule it often ionizes it by knocking away one of the molecular electrons. This leaves behind a molecular ion.

Residual energy from the collision may cause the molecular ion to fragment into neutral pieces and smaller fragment ions. The molecular ion is a radical cation, but the fragment ions may either be radical cations or carbocations, depending on the nature of the neutral fragment.

2.2.7 Dielectric Constant

Parallel plate capacitors were employed to generate through plane dielectric constants for the polymers under investigation. The corresponding equations are shown below:

$$1/C_{meas} = 1/C + 1/C \qquad (2.9)$$

$$k = 2C_{meas}\delta/\varepsilon_o A \qquad (2.10)$$

where C_{meas} is the capacitance measured on the probe station in Farads (F), C is the capacitance between the top and bottom electrodes in F, k is the dielectric constant, δ is the film thickness in meters (m), A is the capacitor area in m, and ε_o is the permittivity of air ($8.854*10^{-12}$ F/m). Figure 2.4 shows The Micromanipulator Co. Model 6000 probe station used to measure the capacitance. Capacitance was measured with a Solartron 1260 Impedance/Gain-Phase Analyzer.

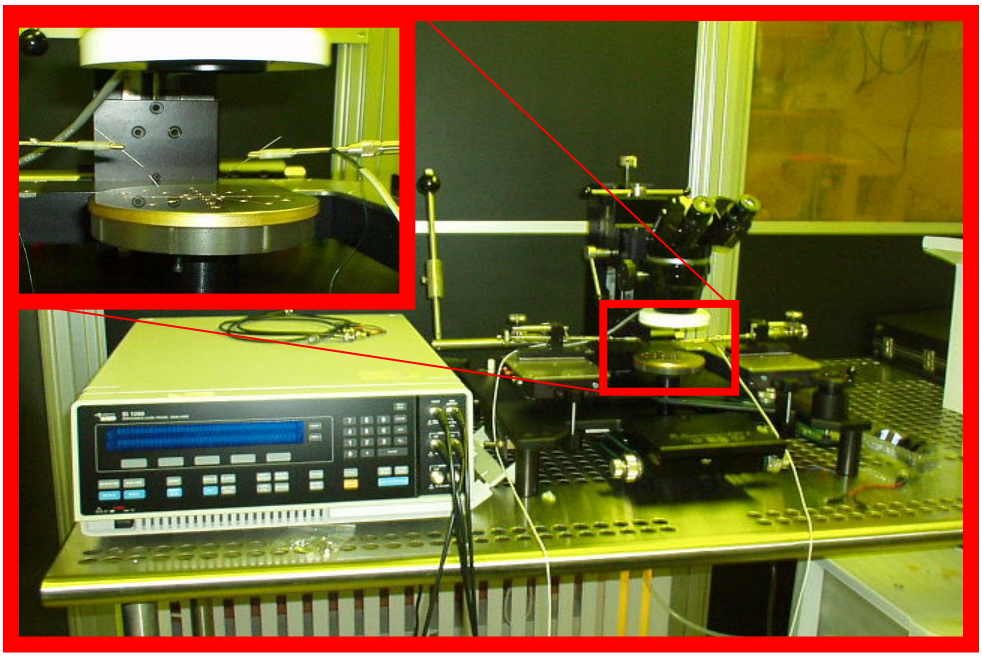

Figure 2.4 The Micromanipulator Co. Model 6000 probe station and Solartron 1260 Impedance/Gain-Phase Analyzer.

The bottom electrode is 300 Å Ti/3000 Å Pt for films on a silicon wafer. Free-standing films have 3000 Å Al as the bottom electrode. Both metals were sputtered on using a CVC DC Sputterer. The top layer is 300 Å Ti/3000 Å Au with 2 mm diameter circles with 3 mm spacing for all polymers. The top layer was deposited with a CVC E-Beam Evaporator.

2.2.8 Moisture Content/Water Absorption

Water absorption was performed on a Quartz Crystal Microbalance (QCM). A QCM utilizes oscillating quartz crystals as a means for mass measurement. When an electric potential is applied to the uncoated quartz crystal, the piezoelectric nature of quartz will cause the crystal to oscillate at a baseline resonant frequency. The result is the formation of a standing wave within the quartz known as a shear wave that is centered along the center line of the quartz slice. As mass is added to the crystal's surface, the

effective thickness of the quartz increases which increases the wavelength of the shear wave effectively lowering the oscillation frequency.

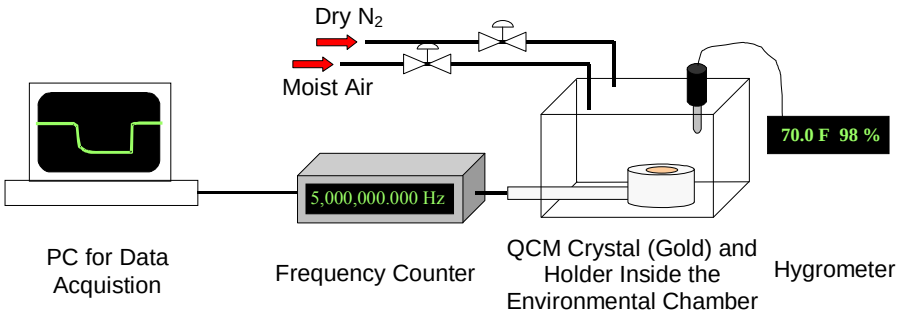

Figure 2.5 Setup for quartz crystal microbalance

QCM measurements were performed with a Maxtek quartz crystal microbalance (PLO-10 Phase Lock Oscillator, 5 MHz gold plated quartz crystals model # SC-501-1, 1.227 cm^2 active area). Frequency data was collected with an Agilent Universal Frequency Counter, with the data analyzed by Agilent Intuilink software within Microsoft Excel. From the Sauerbrey equation, the change in frequency is proportional to the change in mass [5]. By monitoring the changes in the oscillation frequency of the resist coated quartz crystal, it is possible to monitor the absorption and desorption of water from the film. Changes in the frequency between a dry and wet film are made by alternating the quartz between a dry chamber and a chamber effectively saturated with water vapor.

2.2.9 Coefficient of Thermal Expansion and Glass Transition Temperature

The through-plane coefficient of thermal expansion (CTE) was determined using an Omega CN76000 temperature controller attached to a JA Woollam VASE

Ellipsometer to analyze the thickness at varying temperatures. Figure 2.6 shows the laboratory setup.

From the graph, a dThickness/dT slope can be used to generate a CTE value in ppm/K by the following equations [6]:

$$CTE_{constrained} = (dThickness/dT)/(average\ thickness) \quad (2.11)$$

$$CTE_{unconstrained} = CTE_{constrained}*((1-\nu)/(1+\nu)) \quad (2.12)$$

where ν is the Poisson's ratio relating expansion in the z direction to expansion in the x direction and will be assumed to be equal to 0.33 for all polymers. This term converts the expansion constrained by the wafer to an unconstrained CTE value.

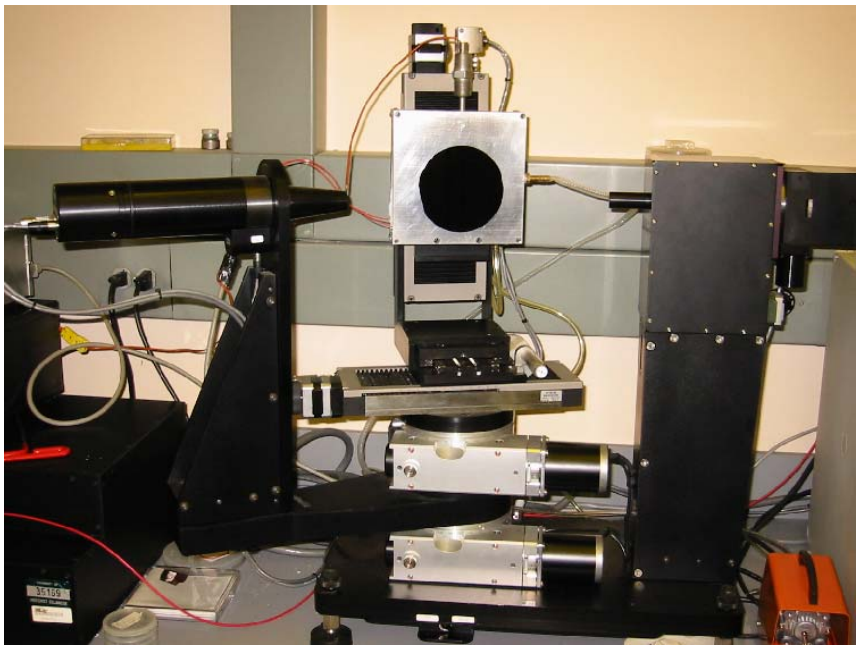

Figure 2.6 Spectroscopic Ellipsometry using hot stage. Scan performed at constant temperature.

Thermal mechanical analysis was performed on a polymer free standing film with a Perkin Elmer TMA 7 to determine the T_g and in-plane CTE. As with CTE measurements on an ellipsometer, multiple heating steps were employed to relieve any thermo-mechanical history in the film. The films were heated at a rate of 10 ^oC/min.

Another method to determine T_g is by the use of a differential scanning calorimeter (DSC). DSC is a technique in which the difference in the amount of heat required to increase the temperature of a sample and reference are measured as a function of temperature. Although no formal phase change is observed, T_g can be detected because of the change in heat capacity between the glass and rubbery states which appears as a step in the baseline of the recorded signal.

2.2.10 Young's Modulus

Indentation tests are commonly applied means of testing the mechanical properties of materials. Two methods of indentation were employed to determine the Young's modulus of the film. The first method uses an atomic force microscope (AFM) [7]. AFM cantilevers are small elastic beams 100–400 mm in length and a few mm in thickness. They often have an almost rectangular or triangular shape. One end of the beam is fixed to a chip; the other free end holds the sensor tip. Force curves are taken by compressing the sample with an indenting AFM tip and analyzing the elastic response of the sample under this loading force. The slope of a force curve already describes the elastic properties of a sample in a qualitative way. On an infinitely stiff sample, the deflection, *d*, of the cantilever is identical to the movement of the piezo in the *z* direction: $d = z$. In the case of a soft sample, the cantilever tip will indent the sample. This indentation δ leads to a smaller deflection $d = z - \delta$, resulting in a flatter force curve with

a smaller slope. Hooke's law connects the deflection of the cantilever and the applied loading force via the force constant, *k*, of the cantilever as shown in Equation 2.13. The Hertz model gives the following relation between the indentation and the loading force *F* as shown in Equation 2.14.

$$F = kd = k(z - \delta) \tag{2.13}$$

$$F = (2 / \pi)[E/(1 - \nu^2)]\delta^2 \tan(\alpha) \tag{2.14}$$

In Equation 2.14, *E* is the elastic or Young's modulus, ν is the Poisson ratio of the sample, and α is the half opening angle of the indenting cone. To calculate the Young's modulus, we apply a fit of the Hertz model to the curve that is calculated as the average value of the approach and the retract trace of each force curve. Combining the equations yields the following:

$$z - z_0 = d - d_0 + \sqrt{\frac{k(d - d_0)}{(2/\pi)[E(1 - \nu^2)]\tan(\alpha)}} \tag{2.15}$$

The zero deflection, d_0, has to be determined before the contact part of the force curve. In Equation 2.15, two quantities are unknown: the contact point, z_0, and the Young's modulus *E*. These quantities can be determined independently by taking two different deflection values and their corresponding *z* values from a force curve, as shown in Figure 2.7. These two data points then define the range of deflection values, corresponding to the range of loading force, in which the Hertz model is applied.

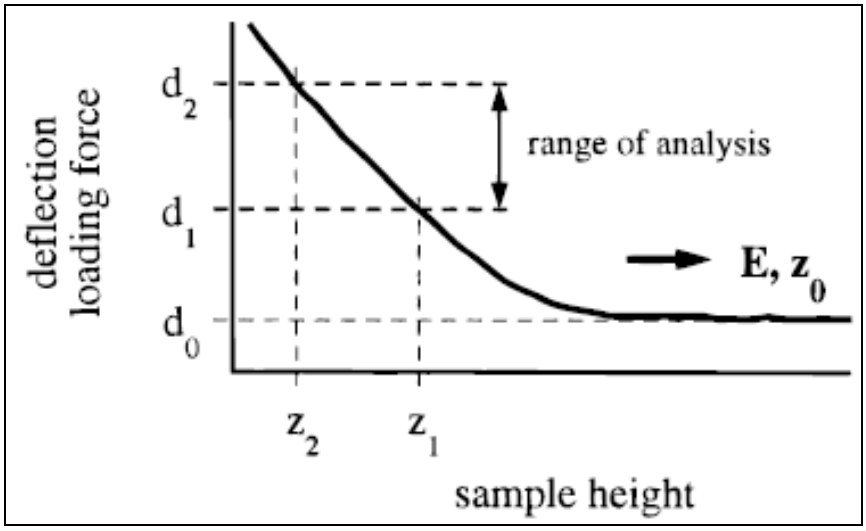

Figure 2.7 Force curve for a polymer film

A force constant of 60 mN/m and a half-opening angle of 10° was used. In this study, a Molecular Imaging PicoPlus Atomic Force Microscope was used. In addition to AFM indentation, nanoindentation was used. Nanoindentation is depth-sensing indentation testing in the sub-micrometer range [8]. In nanoindentation, an arbitrarily small volume of material can be tested if a very sharp tip is used. In such a test, a hard tip, typically a diamond, is pressed into the sample with a known load. After some time, the load is removed. The area of the indentation in the sample is measured and the hardness, H, is defined as the maximum load, P, divided by the residual area, A_r. One problem with nanoindentation is determining the indentation area. To solve this problem, the load and displacement of the indenter are recorded to obtain the contact area.

Indentation load-displacement curves consist of three parts; load, hold, and unload. The initial slope of the unloading curve can measure the elastic properties by using the following equations:

$$E_r = (\pi/4)^{1/2}(1/A_c)^{1/2}(dP/dh) \quad (2.16)$$

$$E/(1-\nu^2) = \{(1/E_r) - [(1-\nu_i^2)/E_i]\}^{-1} \quad (2.17)$$

where E_r is the reduced modulus of the sample, A_c is the contact area, dP/dh is the initial slope of the unloading curve (Figure 2.8), E and ν are the Young's modulus and Poisson's ratio for the sample, and E_i and ν_i are the same parameters for the indenter (E_i = 1140 GPa, ν_i = 0.07).

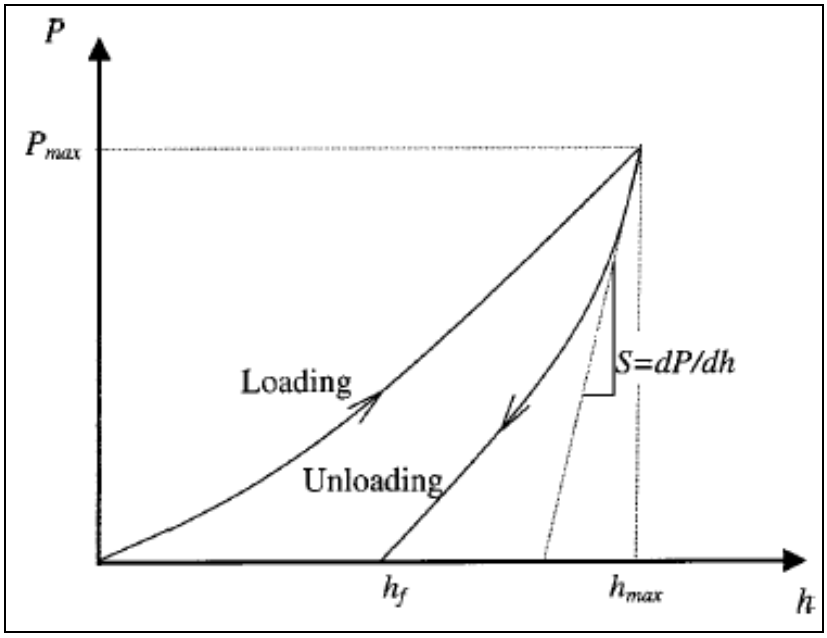

Figure 2.8 Schematic diagram of load-displacement curve

As with values calculated for the through-plane CTE, the Poisson's ratio will be assumed to be equal to 0.33 for all polymers. Measurements were performed using a Hysitron TriboIndenter with a Berkovich indenter tip.

2.3 Measuring Lithographic Performance

2.3.1 Ultraviolet Energy Sources

Successful evaluation of the lithographic performance of any material is dependent on the ability to accurately characterize the radiation source used to carry out optical patterning. The type of radiation being used must be accurately described in terms of both spectral character and intensity. The number and type of wavelengths being used are important, as they directly impact the chemistry that occurs in the photosensitive material and the maximum resolution that can be achieved. While the materials studied in this work behave in a different manner than traditional photoresist materials, it is generally accepted that the minimum feature size possible in a photodefinable material decreases with decreasing wavelength of the radiation used for patterning.

UV exposure of the polymer films in this work was performed using an ACCUDOSE 9000 i-line exposure tool (Oriel Instruments), with a 500W Hg short arc lamp source. The unfiltered spectral output of this tool covers the entire emission spectrum of Hg arc lamp sources (250-460 nm). Band-pass filters with center wavelengths of 436 nm (g-line) or 365 nm (i-line) can be used when specific exposure wavelengths are desired. Exposure dose was controlled by programming the software to open and close the shutter at specific space increments and time intervals.

2.3.2 Dose quantification

In order to properly characterize the radiation sensitivity of the materials used in this work, accurate quantification of exposure doses are necessary. Processing time can be one of the most important factors in determining overall process cost.

Dose measurements were performed using a Molectron EPM2000e power/energy meter and a PM3 power probe. The EPM200e, is a dual-band meter that is capable of measuring power (W) and energy (J) for both continuous and pulsed energy sources over a wide range (30 pJ-300 J and 3 mW-10 kW), with high resolution (10 fJ and 10 μW).

2.3.3 Sensitivity and Contrast

The two common lithographic characteristics of sensitivity and contrast were quantified. In order to evaluate these characteristics, contrast curves, which plot normalized film thickness remaining after development (defined here as the ratio of remaining film thickness after development to the film thickness before development) as a function of the log of the exposure dose, were measured. The contrast data was generated in the following manner:

(1) Polymer system is deposited on a silicon wafer by spin-coating

(2) Initial film thickness is measured via ellipsometry or profilometry

(3) Sample is exposed to varying doses of energy at 365 nm

(4) Sample is placed on hotplate for post exposure bake (PEB)

(5) Sample is developed by placing wafer in developing solution

(6) Sample is washed with water

(7) Sample is dried with nitrogen for 15 seconds

(8) Final film thickness is measured by ellipsometry or profilometry

The lithographically useful sensitivity has been defined as the dose per unit area that results in dimensional equality of clear and opaque features that are nominally equal

in pattern design [9]. This dose is sometimes referred to as the Dose-to-Clear (E_o), and is more generally defined as the sensitivity of a given photosensitive system. For a positive tone system, the sensitivity is represented by the dose required for complete development of the exposed polymer. Contrast (γ), or the resolving power of the resist system, defines how the resist responds to changes in exposure dose. Both of these properties can be determined by generating a plot of normalized thickness loss as a function of log dose, also called a contrast curve. On this curve, the x-intercept of this curve is E_o, and the slope is γ.

2.4 Evaluation of Lithographic Performance

2.4.1 Scanning Electron Microscopy

In evaluating structures patterned and fabricated in this work, it was important to be able to characterize the size and shape of those structures. In addition to feature width and height, the profile of these structures (i.e. encapsulated air channels) were crucial to the determining the success of the experiments. One method used to evaluate these attributes was scanning electron microscopy (SEM). A Hitachi 3500H Scanning Electron Microscope was utilized for these evaluations.

In obtaining an electron microscope image, a finely focused beam of electrons sweep the surface of a solid sample in a raster pattern. A raster is a scanning pattern in which an electron beam is (1) swept across a surface in a straight line, (2) returned to its starting position, and (3) shifted downward by a standard increment. This process is then repeated across until the desired area of the surface has been scanned. When a surface is scanned with an energetic beam of electrons, several types of signals are produced from

the surface. These include backscattered, secondary, and Auger electrons, X-ray fluorescence, and other photons of various energies. Only the backscattered and secondary electrons serve as the basis for SEM.

Scanning electron microscopes typically consist of an electron source, electron optics, the sample and sample holder, and a detector. From the source, such as an electron gun, energetic electrons are injected into the system. This beam of electrons is then focused by the optics of the system, which also control the raster scanning of the sample. Since low pressures are needed to produce the electron beam, the sample chamber must be pumped to pressure of 10^{-4} torr or less before scanning. The sample holder, or stage, of most instruments has the ability to hold various sample sizes, and can be moved in the X, Y, and Z directions in addition to being rotated about each axis. Therefore, samples can be viewed from almost any perspective. The detector is used to collect and measure the backscattered and secondary electrons emitted from the sample surface. This results in a three-dimensional picture of the sample surface.

One drawback of SEM is that conductive samples are best to study since the unimpeded flow of electrons to ground minimizes artifacts associated with the buildup of charge. Electrically conductive samples are also usually good conductors of heat, thus, minimizing the possibility of thermal degradation of the sample. Unfortunately, most polymeric materials are not conductive; therefore, some sample preparation is needed in these cases. For this work, a thin film of gold (~ 200Å) was sputtered onto the surface in order to improve the SEM studies.

2.4.2 Optical Profilometry

While SEM is a powerful tool for viewing the structures developed in this work, gold coating of the sample is not always desirable, particularly if further processing is required. In these cases, optical profilometry was a useful alternative since most non-conductive surfaces can also be examined. An optical profilometer has several advantages over the more widely used profilometers utilizing stylus probes. For elastomeric samples such as polymers, the stylus tends to dig into the surface and the results do not truly represent the microtopography. Other disadvantages include their sensitivity to vibrations, uncertainty in point of contact of stylus on rough surfaces, and the delicate nature of the stylus and its mechanism [10]. Optical profilometry is a noncontact technique that gives a direct measure of the sample height.

Optical profilometers, similar to the SEM described above, consist of an illumination source, relatively complex optics (including the microscope objectives and field of view lenses), a sample and sample holder, and a detector. For profilometers based on a two-beam interferometer like the one used in this work, light from the illuminator is reflected down to an objective by a beamsplitter. Once the light reaches the objective, another beamsplitter splits the light into two beams: one (the reference beam) reflects from a super smooth mirror in the objective; one (the test beam) reflects from the surface of the sample and back to the objective. If the surface of the sample is in *focus*, the two light beams will recombine and form an interference pattern of light and dark bands called fringes. The interference pattern can then be received by the detector, and the signal can be transferred to a computer that then produces a graphical representation of the sample surface.

For these experiments, a Wyko® NT3300 Optical Profilometer (Veeco Instruments) with 5x and 50x objectives, as well as 0.5x, 1x, and 2x field of view lenses, was used. This instrument has two modes of operation: phase shifting interferometry (PSI) and vertical scanning interferometry (VSI), but only the VSI mode was used. VSI uses the interference of light to map the surface of the sample. In VSI, an internal translator scans downward during the measurement. A CCD camera takes snapshots, called frames. As each point on the surface comes into focus, the modulation on that point reaches a maximum and then tapers off as the translator passes through focus. By recording the height of the translator at maximum modulation, the system can determine the height of each pixel and these measurements are used to reconstruct a map of the surface of the sample.

2.5 References

1. Skoog, D.A. and J.J. Leary, *Principles of Instrumental Analysis*. 4th ed. 1992, San Diego, CA: Saunders College Publishing, A Harcourt Brace Javanovich College Publisher.

2. Beckham, H.W., *Spectroscopy*. 2000, Atlanta, GA: Georgia Institute of Technology.

3. Smith, B.C., *Fundamentals of Fourier Transform Infrared Spectroscopy*. 1996: CRC Press. 224.

4. Rosen, S.L., *Fundamental Principles of Polymeric Materials*. 2nd ed. 1993, New York, NY: John Wiley & Sons, Inc.

5. Vogt, B.D., et al., *Effect of Film Thickness on the Validity of the Sauerbrey Equation for Hydrated Polyelectrolyte Films.* Journal of Physical Chemistry B, 2004. **108**(34): p. 12685-12690.

6. Kahle, O., et al., *Glass transition temperature and thermal expansion behavior of polymer films investigated by variable temperature spectroscopic ellipsometry.* Thin Solid Films, 1998. **313-314**: p. 803-807.

7. Domke, J. and M. Radmacher, *Measuring the Elastic Properties of Thin Polymer Films with the Atomic Force Microscope.* Langmuir, 1998. **14**(12): p. 3320-3325.

8. Huang, X. and A.A. Pelegri, *Nanoindentation Measurements on Low- k Porous Silica Thin Films Spin Coated on Silicon Substrates.* Journal of Engineering Materials and Technology, 2003. **125**: p. 361-367.

9. Thompson, L.F., C.G. Willson, and M.J. Bowden, *Introduction to microlithography*. 2nd ed. ACS professional reference book;. 1994, Washington, DC: American Chemical Society. xiv, 527 p.

10. Bhushan, B., J.C. Wyant, and C.L. Koliopoulos, *Measurement of surface topography of magnetic tapes by Mirau interferometry.* Applied Optics, 1985. **24**(10): p. 1489-1497.

CHAPTER 3

PHOTODEFINABLE POLYIMIDE WITH CLEAVABLE ESTER LINKAGE

3.1 Introduction

Aromatic polyimides have been widely exploited as high performance polymeric materials in a variety of applications because of their excellent thermal stability, chemical resistance, and good dielectric performance. These outstanding properties have resulted in numerous applications for aromatic polyimides in microelectronics, such as films for protection and insulation layers for ULSI and multi-chip modules. In particular, photosensitive polyimides have received significant attention due to the reduced processing effort and cost that can be realized from using such directly photodefinable materials. There are generally two approaches to producing photosensitive polyimide compositions: (1) formulations based on the use of poly(amic-acid) precursors which are coated, imaged, and then thermally converted to their imide form and (2) formulations based on the use of soluble polyimides. There are several disadvantages to using formulations based on poly(amic-acid) precursors including the high curing temperatures required for final ring closure and conversion to their polyimide form, the build-up of film stress during such high temperature curing, and difficulty with swelling and control of the dissolution rate of the poly(amic-acid) precursors during development in aqueous alkaline solutions. In contrast, formulations based on soluble polyimides generally allow for lower processing temperatures since formation of the imide ring has been

accomplished in advance. In order to make polyimides soluble in both casting solvents and aqueous alkaline developers, polar functional groups which increase solubility of the polymer in polar organic solvents and which can ionize and impart solubility in aqueous alkaline solutions are generally added to the polyimide structures. For example, polyimides containing phenolic hydroxyl groups have been widely studied [1, 2]. Unfortunately, the introduction of such polar functional groups produces several problems including higher dielectric constants and higher water uptakes as compared to the native polymer. This degradation in the physical and electrical performance is undesirable for dielectric materials application in microelectronic devices.

Recently, alternate functional groups have been introduced and applied as replacements for phenolic hydroxyl moieties in the development of polymers for 193 nm and 157 nm photoresists. In particular, the hexafluoroisopropanol (HFA, bis-trifluoromethyl carbinol) functional group has been widely investigated for such applications [3-7]. As compared to the phenolic hydroxyl group, use of an HFA group instead of a phenolic hydroxyl group can serve to lower the dielectric constant, moisture uptake, and low wavelength ultraviolet absorbance of the polymer while retaining similar solubility characteristics in alkaline developer. So far, many kinds of polymer backbones containing the HFA group have been studied including styrenes [8], norbornenes [9-12], methacrylates [13], acrylates [14], and vinyl ethers [15]. In this paper, the preparation and characterization of a novel HFA-substituted polyimide that can be cast from common organic solvents and developed in standard 0.26 N TMAH developer is reported.

3.2 Monomer Synthesis

As shown in Figure 3.1, an HFA-substituted diamine monomer **3.3** was prepared by a condensation reaction of the HFA-substituted phenol **3.1** and 3,5-dinitrobenzoyl chloride followed by subsequent hydrogenation.

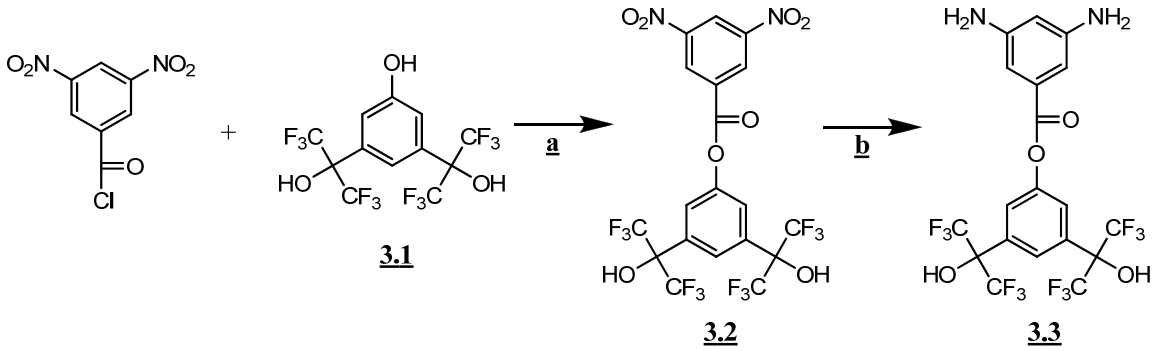

Figure 3.1 Monomer **3.3** synthesis (a) pyridine, CH_2Cl_2, r.t., 5 hrs; (b) 10 % Pd/C, H_2, methanol, r.t., 1 atm., 6 hrs.

Synthesis of precursor compound **3.2**, which possesses nitro groups that are later used for forming the desired diamine, was investigated in some detail to obtain selectivity for the condensation reaction at the desired phenolic site. When triethylamine (TEA) was used as an organic base in the condensation reaction, undesired side-products were obtained by forming ester linkages at the HFA hydroxyl site. On the other hand, the use of pyridine resulted in the desired reaction at only the phenolic hydroxyl site without observable production of the HFA esterified side products. After pouring 0.6 N HCl aq. into the reaction mixture, a white powdery precipitate was obtained in 73 % yield. The structure of the resulting precipitate was characterized by ^{1}H- and ^{19}F-NMR measurements. All peaks in the ^{1}H-NMR spectrum of the precipitate were successfully assigned to protons in **3.2**. On the other hand, NMR analysis of a resulting filtrate

showed that the filtrate contained both **3.1** and 3,5-dinitrobenzoic acid in addition to the desired product **3.2**.

Without further purification, hydrogenation of **3.2** was carried out at atmospheric pressure in the presence of 10 % Pd/C as shown in step **b** in Scheme 3.1. After the reaction, the reaction mixture was filtered using celite and then evaporated. Recrystallization of the resulting crude product in a mixture of methanol and water produced a white powdery product **3.3** which was recovered in 57 % yield.

3.3 Polymer Synthesis and Characterization

As shown in Figure 3.2, the polymerization of diamine monomer **3.3** with 2,2-bis(3,4-dicarboxyphenyl)hexafluoropropane dianhydride (6FDA) was performed in NMP. The polymerization reaction proceeded in homogeneous solution. After pouring the solution into a mixture of methanol and water to precipitate the polymer product, a white fibrous polymer **3.4** was obtained in 95 % yield. An inherent viscosity (η_{inh}) of the resulting polymer **3.4** was 0.20 dL/g (measured in NMP at a concentration of 0.5 g/dL at 25 ^{o}C). The structure of **3.4** was characterized by NMR, IR, and thermogravimetric analysis (TGA). In the ^{1}H-NMR spectrum, a broad peak assigned to the amide is located at approximately 10.8 ppm, while the peak assigned to the HFA proton is found at 9.2 ppm (Appendix A). The integration ratio of these peaks is essentially consistent with the expected ratio. Also, in the ^{19}F-NMR spectrum, peaks attributed to hexafluoroisopropylidene and HFA were observed at –62.5 ppm and –73.5 ppm with a reasonable integration ratio (Appendix B). In the IR spectrum, the peak characteristic of the amide carbonyl group was observed at approximately 1650 cm^{-1}. Figure 3.3 shows the TGA curve for polymer **3.4**, respectively. TGA analysis of **3.4** showed weight loss

due to the thermal conversion into the polyimide in the range of 180-250 ^{o}C (curve A in Figure 3.3). All of these analyses support the formation of the desired poly(amic-acid) polymer **3.4**.

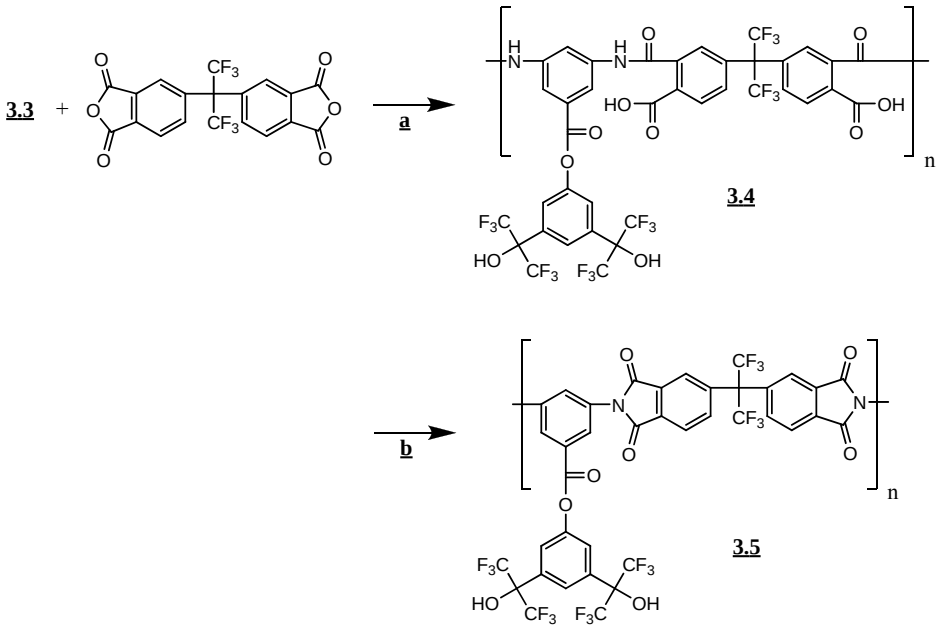

Figure 3.2 Polymer **3.5** synthesis (a) 400 wt% DMAc, N_2, r.t.; (b) Ac_2O, pyridine, DMF, N_2, 100 ^{o}C.

Thermal imidization of **3.4** was examined by curing the poly(amic acid) precursor polymer over a range of temperatures at 250 ^{o}C, 300 ^{o}C, and 350 ^{o}C. From the IR analysis, two peaks characteristic of imide carbonyl group formation were clearly observed at 1734 cm^{-1} and 1788 cm^{-1} with a corresponding decrease and ultimate disappearance in the amide carbonyl group peak at 1650 cm^{-1} after thermal treatment of the poly(amic acid) polymer at temperatures as low as 250 ^{o}C (see Figure 3.4). It was also observed from the IR data that after thermal treatment at 350 ^{o}C, the peaks assigned to C-F bonds in the range of 1200-1300 cm^{-1} were also obviously decreased. Consistent

with this observation, thermogravimetric analysis of **3.4** showed multiple weight loss steps at temperatures above 280 ^{o}C. Both the TGA and FTIR data suggested that some form of thermal degradation and removal of the HFA substituent groups on the polymer occurred at temperatures above approximately 280 ^{o}C. This issue will be discussed later based on mass spectrometry data.

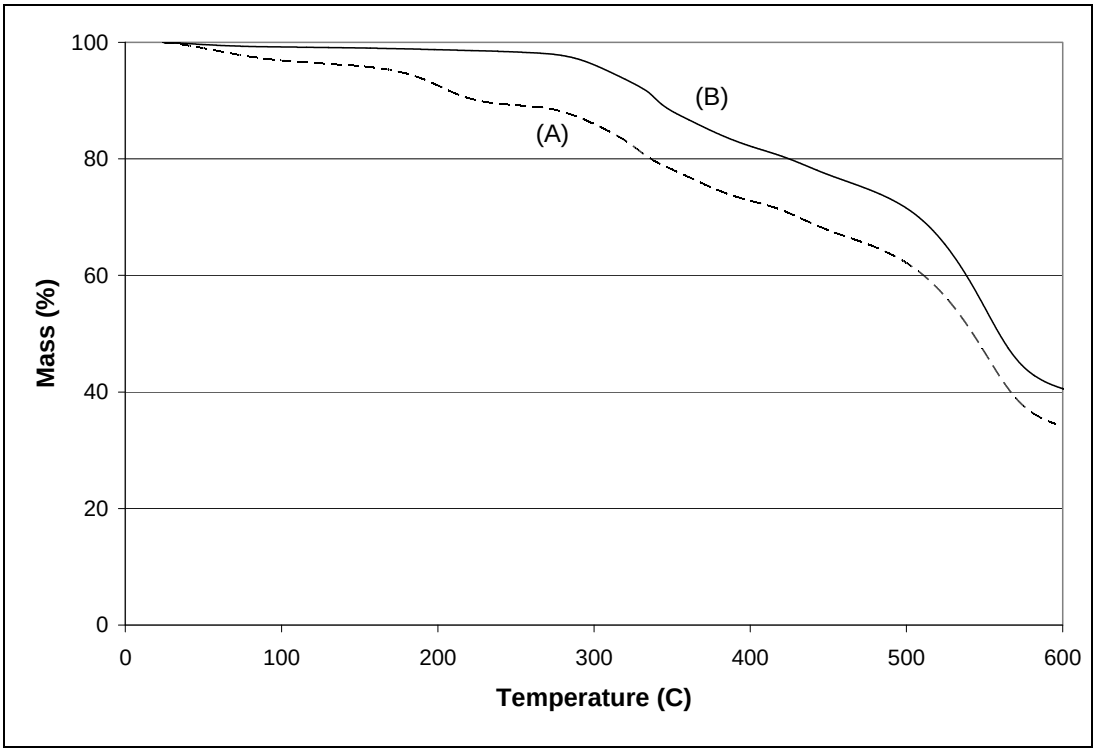

Figure 3.3 TGA curves of (A) polymer **3.4** and (B) polymer **3.5** in nitrogen at a heating rate of 10 ^{o}C/min.

Chemical imidization of **3.4** in the presence of pyridine and acetic anhydride was also examined. A light yellow powdery product **3.5** was obtained in 90 % yield from the chemical imidization treatment. The inherent viscosity (η_{inh}) of the resulting polymer **3.5** was 0.18 dL/g. In the IR spectrum of **3.5**, two peaks assigned to the imide carbonyl groups were detected at 1731 cm^{-1} and 1788 cm^{-1} while no amide carbonyl group peak at

1650 cm^{-1} can be seen (see Figure 3.4). The TGA curve for **3.5** is shown as curve B in Figure 3.3. This TGA data shows that no significant weight loss is detected in polymer **3.5** below approximately 280 ^{o}C. All of these observations are consistent with the formation of polyimide **3.5** from the poly(amic acid) precursor polymer using the chemical imidization treatment. Polyimide **3.5** exhibited good solubility in acetone, methanol, tetrhydrofuran (THF), propylene glycol methyl ether acetate (PGMEA), γ-butyrolactone (GBL), and 0.26 N TMAH. For a thin film of polymer **3.5** cast onto a silicon wafer using a solution of **3.5** in PGMEA, a dissolution rate (DR) of 3.4 nm/s was measured in 0.26 N TMAH developer using a multi-wavelength dissolution rate monitor [16, 17]. The absorption spectrum of the cast film of **3.5** also showed very good transparency (0.04 μm^{-1}) at 365 nm (Hg lamp I-line).

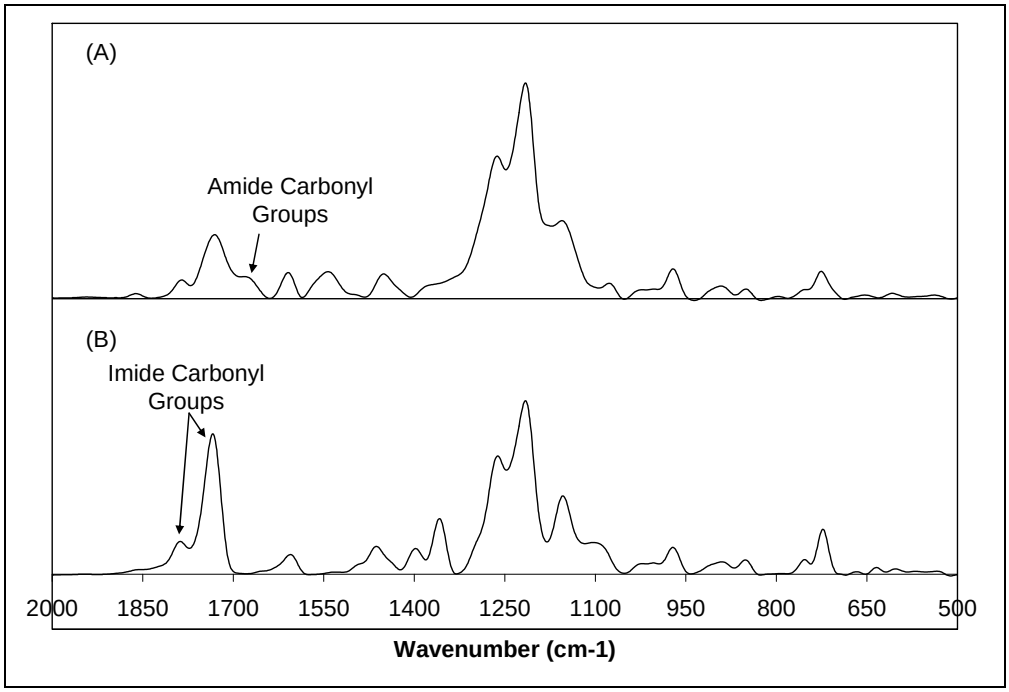

Figure 3.4 FTIR for polymers (A) **3.4** and (B) **3.5**.

Due to the complex decomposition behavior observed in the TGA analysis of polymers **3.4** and **3.5**, additional thermogravimetric studies were performed. Both polymers **3.4** and **3.5** exhibited similar multiple weight losses at temperatures above 280 ^{o}C. To understand the exact nature of the decomposition, the volatile products produced from the thermal decomposition of polymer **3.5** were investigated and identified using a combined TGA-mass spectrometry system. Mass spectra of the fragments produced from the polymer were measured while holding the polymer sample at 250 ^{o}C, 300 ^{o}C, 350 ^{o}C, and 400 ^{o}C for 10 min each. Mass spectra collected at both 350 ^{o}C and 400 ^{o}C were almost identical, with a parent fragment peak being detected at an M/z of 425.9 (Figure 3.5). This resulting M/z number was found to be consistent with the mass expected for 3,5-HFA-phenoxide ($C_{12}H_5F_{12}O_3$), i.e. the result of thermal cleavage and removal of the HFA functionalized phenyl substituent group on the polyimide. The mass spectrometry data also showed evidence of the successive elimination of CF_3 groups from the 3,5-HFA-phenoxide group which could be the result of either thermal cleavage in the polymer or energetic cleavage from the phenoxide parent ion in the mass spectrometer. As for the dissolution rate into 0.26 N TMAH for polymer **3.5** cured at 350 ^{o}C, it was found to be insoluble and showed no swelling in developer. All these findings indicate that the heat treatment of polyimide **3.5** above 280 ^{o}C causes thermal degradation of the HFA-substituted side-group at the ester linkage, resulting in conversion of the polymer to a rigid structure with little or no remaining hydrophilic groups.

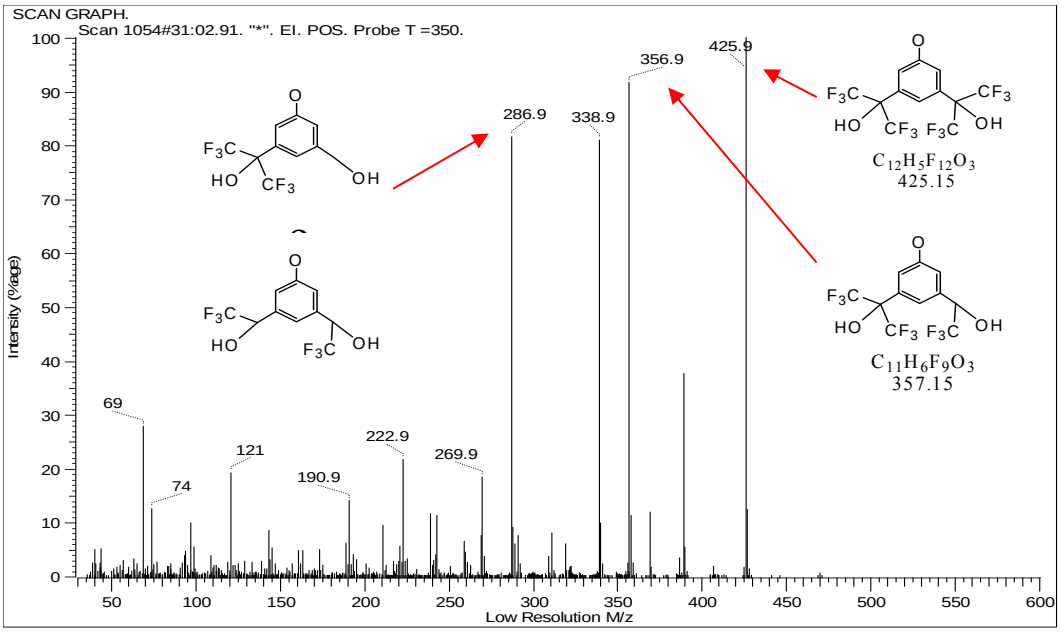

Figure 3.5 Mass spectrum of gas evolved from **3.5** at 350 °C.

It was anticipated that this ability to thermally remove the HFA containing substituent groups from the polymer at relatively low temperatures (i.e. below the normal temperatures required to cause complete imidization in poly(amic acid) precursor polymers) could prove to be very useful for formulating useful low dielectric constant polymers since removal of the hydrophilic groups added to the polymer for providing lithographic imaging could be removed thermally in a post-lithographic thermal bake which should in turn reduce the final dielectric constant of the polymer. In other words, it was hoped that polymer **3.5** could be shown to possess a low dielectric constant similar to or lower than materials made from poly(amic acid) precursor films while maintaining the ability to be processed at lower temperatures due to the solubility enhancement and imaging ability provided by the hydrophilic HFA substituent groups. The dielectric constant of polymer **3.5** produced by both thermal and chemical imidization treatments was measured using parallel plate capacitor structures to be 3.2 at a frequency of 1 MHz.

After thermal treatment of polymer **3.5** at 350 °C for 30 minutes to remove the HFA substituent groups, the dielectric constant of the resulting film was again measured using parallel plate capacitor structures to be 2.6 at 1 MHz. This result confirms that removal of the hydrophilic and polarizable HFA substituent groups is effective in substantially reducing the dielectric constant of the resulting polymer film.

3.4 Polymer Film Properties

Polymer film properties including dielectric constant, thermal expansion coefficient (CTE), water absorption, and Young's modulus were examined. The dielectric constants were measured to be 3.30 (3.20) and 2.60 (2.60) at 100 kHz (1 MHz) for polyimide films of **3.4** treated with thermal cures at 250 °C and 350 °C for 30 minutes, respectively. The dielectric constants were similarly measured to be 3.30 (3.20) at 100 kHz (1 MHz) for polyimide films of **3.5**. A substantial reduction in the polymer dielectric constant was observed for the material cured at 350 °C. This result is most likely due to cleavage and removal of the HFA-substituted side group since this removes the polar alcohol moieties from the polymer. It was believed that the heavy fluorination surrounding the alcohol might serve to reduce the negative effects that arise from having polar alcohols present. Based on the dielectric results, the removal of two alcohols from the polymer diamine better serves to lower the dielectric constant than the addition of twelve fluorines.

Using a thermoplastic Poisson's ratio of 0.33, the through plane CTE for the polyimide film of **3.4** cured at 250 °C was calculated to be 79.8 ppm/K by ellipsometry upon initial heating with almost identical values exhibited during repeated heating cycles (30-150 °C). After curing at 350 °C, the polymer film exhibited an initial through plane

CTE of only 36.8 ppm/K upon first heating but displayed a higher CTE of 59.6 ppm/K during repeated heating cycles as shown in Figure 3.6. It is believed that this difference is due to the fact that the first heating and cooling cycle, which are conducted at slow ramp rates, allow free volume introduced by cleavage of the HFA-substituted side groups in the polymer to be relaxed out resulting in a more dense film.

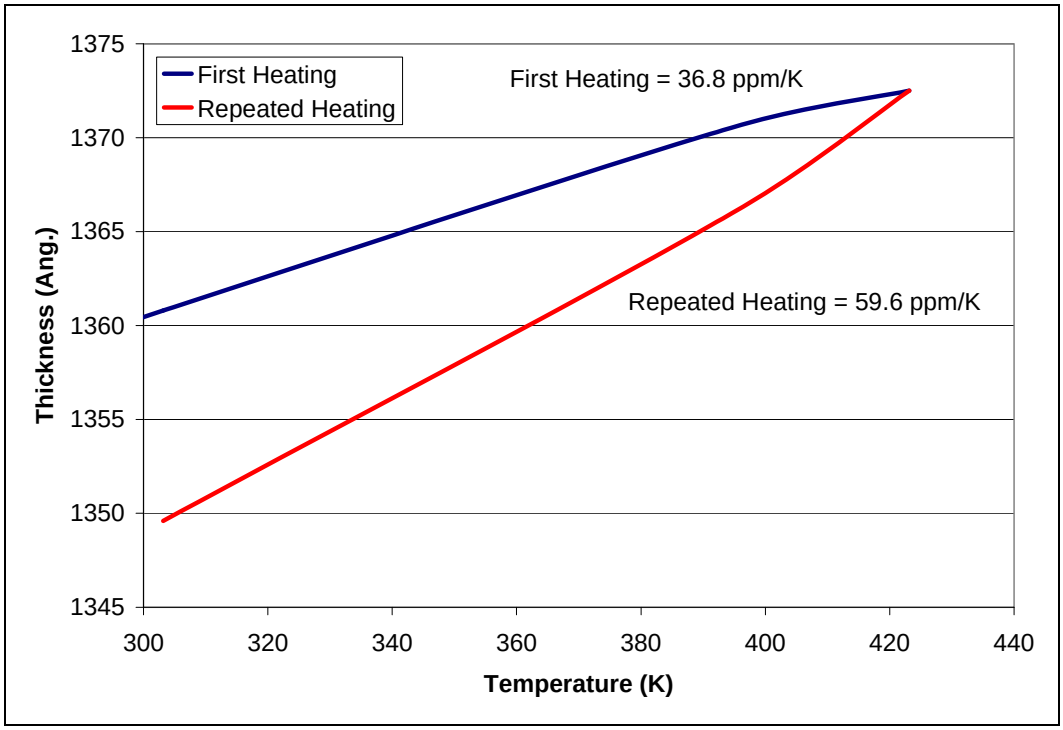

Figure 3.6 Ellipsometry data for polymer **3.4** cured at 350 °C for 30 min.

Water absorption for polyimide **3.5** was found to be 4.1% as shown in Figure 3.7. The high water absorption explains the increased dielectric constant before side group cleavage. No value was found for polyimide **3.4** or **3.5** after side group cleavage because the quartz crystal resonator was unable to produce a measurable frequency after heating at 350 °C for 30 minutes. It is expected the water absorption will be lower because of the removal of the polar alcohol moieties as well as the decreased dielectric constant.

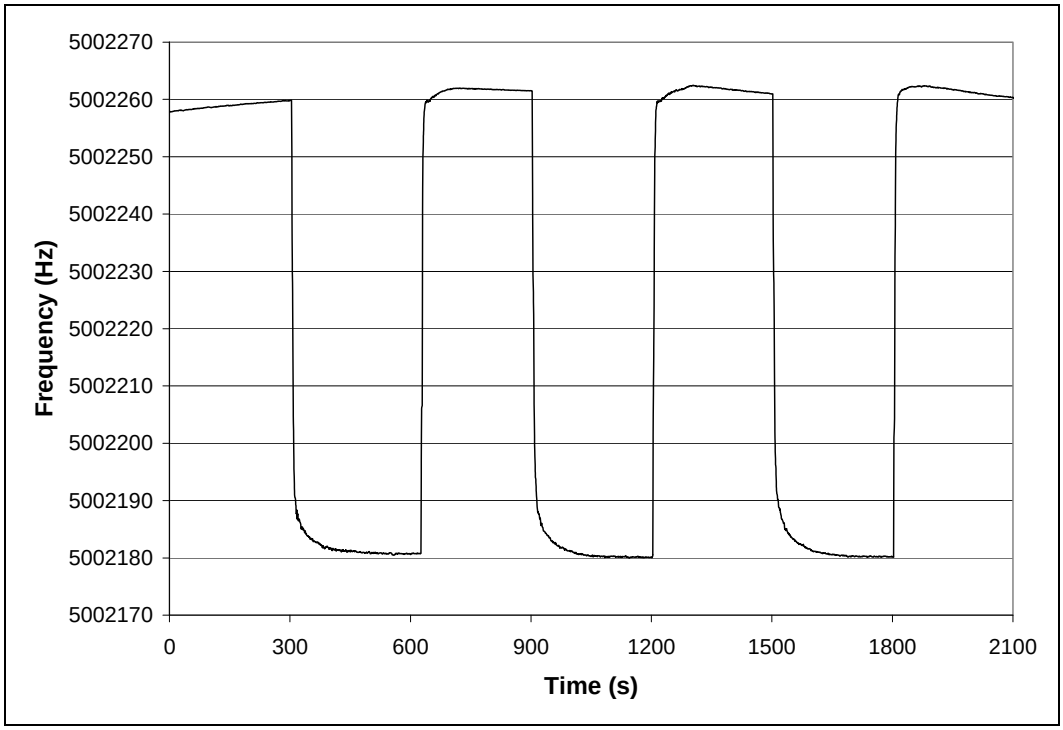

Figure 3.7 Water absorption for polymer **3.5**

The Young's modulus was measured to be 23.3 GPa for polymer **3.5**. A substantial reduction in the polymer's Young's modulus was observed to be 5.9 GPa for the material cured at 350 ^{o}C. This result is not consistent with the effect of fluorine on other polymer's Young's modulus. The addition of fluorine is typically known to lower a polymer's mechanical properties. However, Young's modulus is also dependant on the density of the polymer in question. High density polyethylene has a higher Young's modulus than low density polyethylene. A suitable explanation can be that because the polymer removes such a large side group, the decrease in polymer density outweighs the decrease in fluorine content.

3.5 Formulation of a Photodefinable Polyimide

The properties of photodefinable polyimide formulations made by loading a trifunctional DNQ inhibitor (see Figure 3.8) into polymer **3.5** were examined. Figure 3.6 shows a Meyerhofer plot for various loadings of the DNQ in polymer **3.5**. It is observed the difference between the dissolution rate (DR) of the unexposed and exposed formulation in 0.26N TMAH is a factor of ~45 at a loading of 20 wt% DNQ. This DR contrast is sufficient for photo-patterning experiments. It may also be noted in Figure 3.5 that a slight increase in DR was observed for the unexposed 15 wt% DNQ-loaded **3.5** (4.2 nm/sec) as compared to the DR for the pure polyimide **3.5** (3.4 nm/sec). This increase in dissolution rate with added inhibitor is somewhat surprising. However, polyimide **3.5** was found to exhibit almost complete hydrogen bonding of the hydroxyl sites in the HFA groups by IR analysis. It is hypothesized that the addition of small amounts of inhibitor can actually serve to disrupt this intra- and intermolecular hydrogen bonding and thus result in some increase in the polymer dissolution rate. The presence of such strong hydrogen bonding in the pure polymer is also likely to be responsible for the failure of the DNQ to produce substantial reductions in the unexposed dissolution rate since there are few hydroxyl sites for the DNQ to interact with which do not already participate in a strong hydrogen bond. A dramatic acceleration effect is observed though in the case of the exposed materials. The conventional contrast curve of the 20 wt% DNQ-loaded **3.5** resulted in a sensitivity of 170 mJ/cm^2 and a contrast of 1.32.

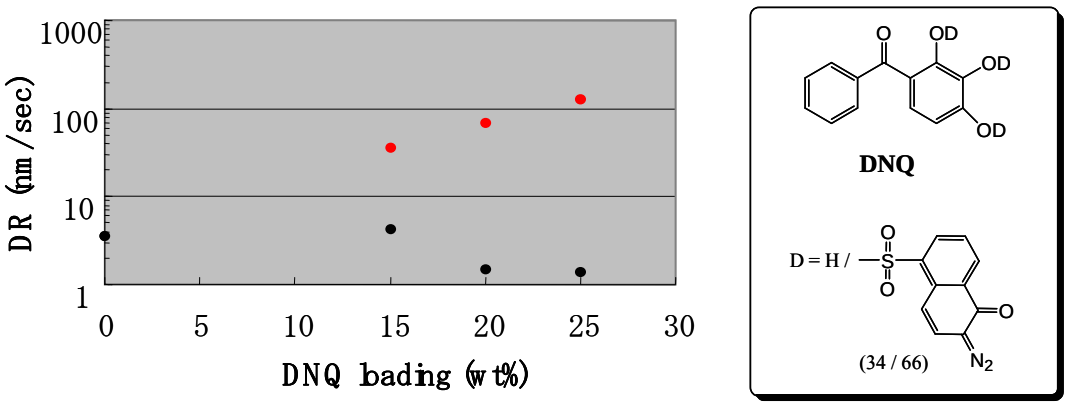

Figure 3.8 Dependence of unexposed (black) and exposed (red, I-line at 2 J/cm^2) DRs onto DNQ loading for polymer **3.5**

As described earlier, polyimide **3.5** has been shown to exhibit thermal cleavage of its side-group at temperatures above 280 ^{o}C. In order to get a suitable cure temperature after development, FT dependence on cure temperature was investigated using profilometry measurements (Figure 3.9). An initial FT (IFT) of 1.65 μm changed clearly down to 1.05 μm (61 % of IFT) by heating up to 350 ^{o}C. After the treatment at 250 ^{o}C for 30 min, a 19 % of IFT was lost (Figure 3.9B). The value was almost consistent with a loading amount (20 wt%) of DNQ. The cure temperature was determined to be 250 ^{o}C for further experiments. Also it was found the pattern did not show any collapse even at 350 ^{o}C.

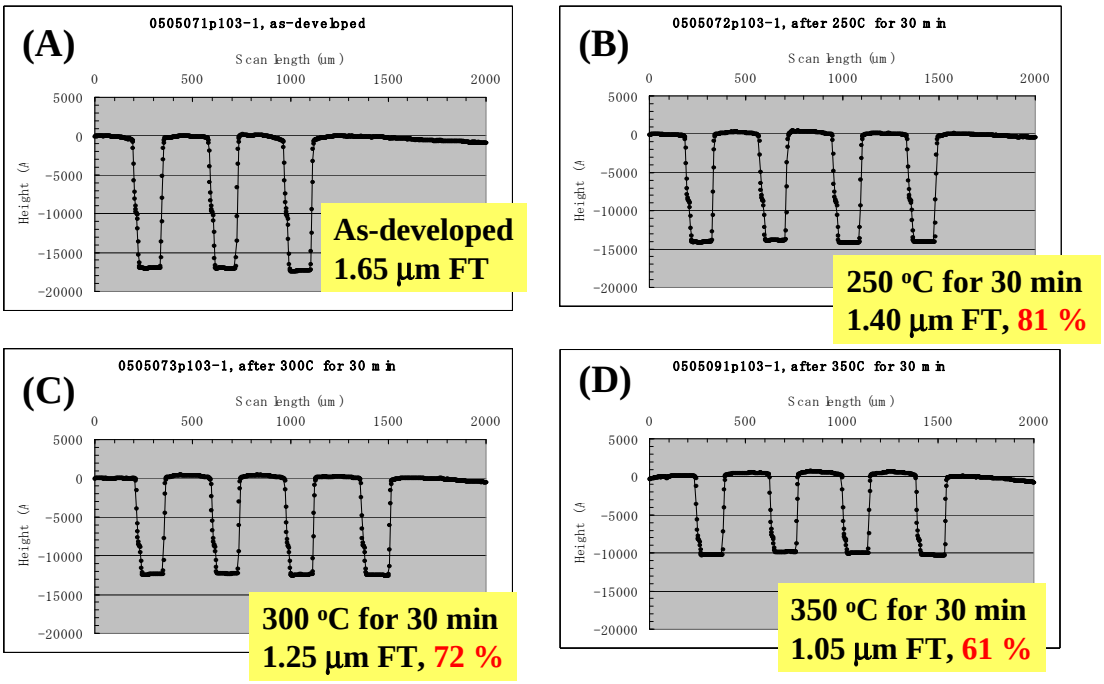

Figure 3.9 Film thickness (FT) dependence of photo-patterned polymer **3.5** on cure temperature: (A) as-developed, (B) 250 °C for 30 min., (C) 300 °C for 30 min., and (D) 350 °C for 30 min.

The lithographic imaging performance of photodefinable polyimides based on polymer **3.5** was tested. Figure 3.10 shows SEM pictures of contact-printed images obtained from dark and bright field masks which produce dense space and line arrays, respectively. The SEM pictures used I-line exposure at 210 mJ/cm^2 with a photosensitive composition based on **3.5**, which was prepared by loading 20 wt% relative to polymer solids of DNQ inhibitor (THBP) into a 20 wt% solution of polymer **3.5** in PGMEA.

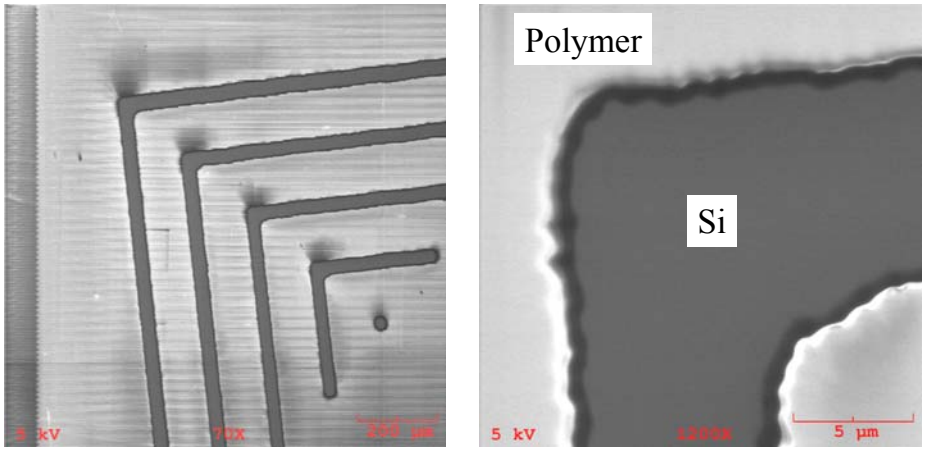

Mask size (L/S): 130/40 (µm/µm)

(A)

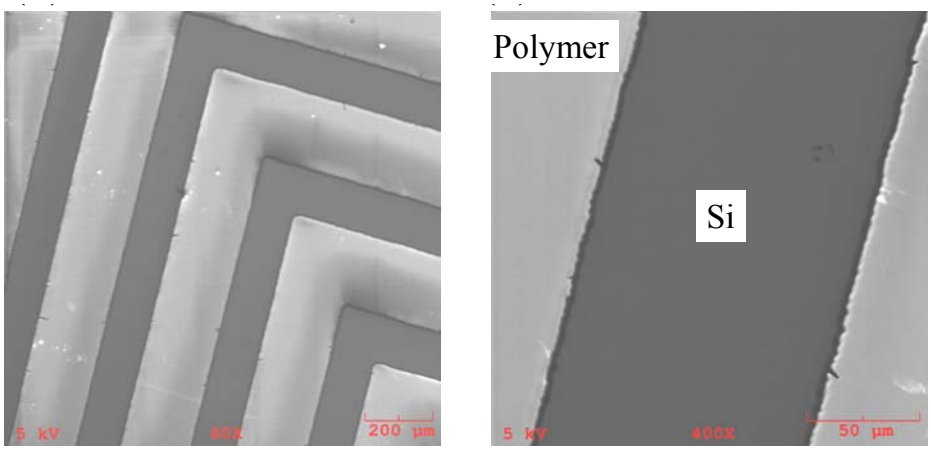

Mask size (L/S): 150/220 (µm/µm)

(B)

Figure 3.10 SEM pictures of 20 wt% **DNQ**-loaded polyimide **3.5** obtained by using a (A) dark and (B) bright field mask: exposed at 210 mJ/cm^2, developed with 0.26 N TMAH for 1 min., and then cured at 250 ^{o}C for 30min.

Both resulting images have feature sizes that are similar to that of the mask used for imaging. As can be seen in Figure 3.9A, the 10-µm space feature was observed to possess a wavy edge that suggests that the material swells during development. This tendency implies that the swelling is a combination of the fact that polyimide **3.5** is very hydrophilic and yet is not extremely soluble and develops slowly. It may be possible to

improve this imaging performance by reducing the polymer swelling by replacing some portion of the current HFA-diamine **3.3** with another conventional diamine (4,4'-oxydianiline, 4,4'-diaminobiphenyl etc.) to reduce the polymer hydrophilicity. Also in terms of the contrast, such a diamine replacement is also expected to be helpful.

3.6 Negative-Tone Imaging

Based on the attractive dielectric constant of the polymer after thermal cleavage of the side group, further work was done to develop a photodefinable version of this material. Formulation of polymer **3.5** with DNQ inhibitors was successfully shown to produce a photodefinable material with good resolution [18]. However, achieving the most desirable final physical properties still requires cleavage of the HFA groups after imaging.

Although the results were promising, the temperature required for cleavage of the side group containing HFA was still high to achieve the desired sub-250 ^{o}C process. Therefore, it was decided to investigate the possibility of catalyzing the cleavage of the side group at lower temperatures using acid as is done in chemically amplified resists. In fact, if a photoacid can be used to induce low temperature cleavage of the side group, a negative tone form of **3.5** could be made simply by addition of the appropriate photoacid generator (PAG).

Figure 3.11 shows the results of TGA experiments designed to see if strong acids can be used to catalyze side group cleavage in polymer **3.5**. In one experiment, camphor-10-sulfonic acid (CSA) was mixed in a 2:3 molar ratio with polymer **3.5**. The purpose was to determine if an acid could cleave the side group thermally at a temperature lower than 250 ^{o}C. CSA was selected because it has an acceptable thermal stability for this

experiment. The theoretical line is generated by combining the products of the percent weight loss of each chemical with the total weight of the chemical in the experimental mixture. From Figure 3.11, it can be seen that the experimental weight loss path did not deviate from the theoretical line to a great extent. This suggests that the acid has not successfully cleaved the HFA side group.

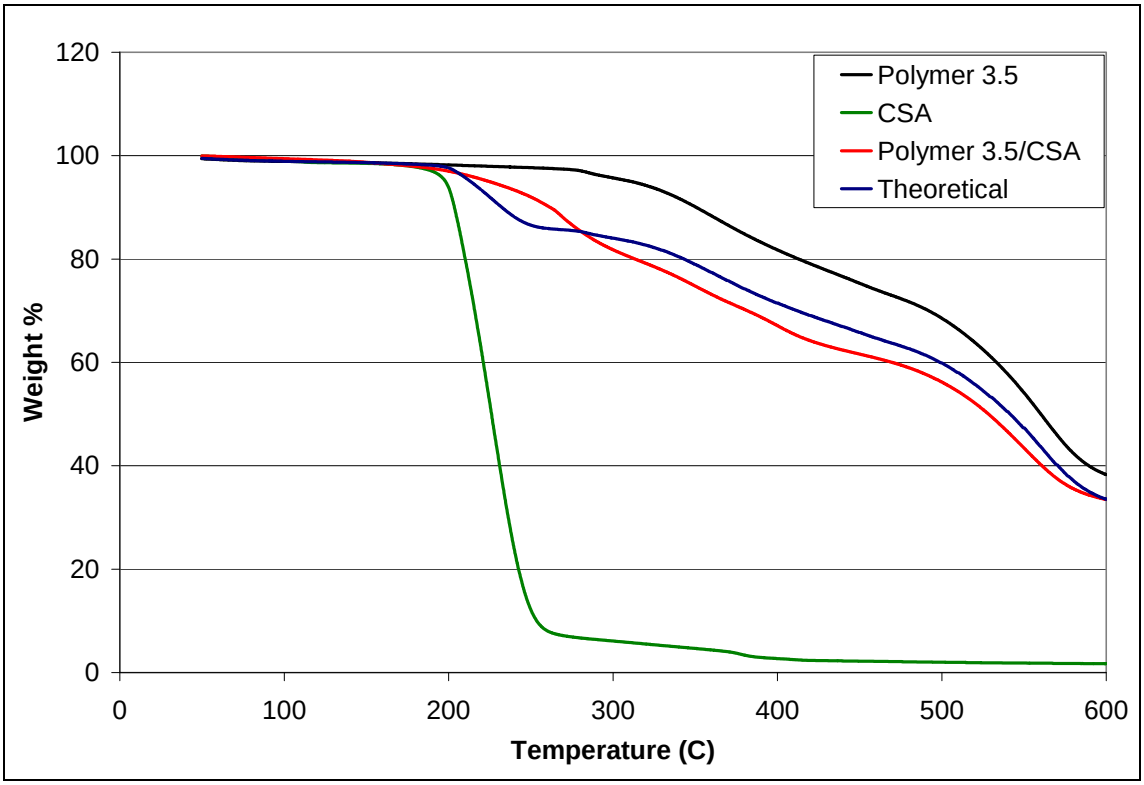

Figure 3.11 TGA runs for polymer **3.5** with CSA.

Another experiment mixed triphenylsulfonium hexafluoroantimonate, photosensitizer 9-anthracenemethanol, and **3.5** in a 1:2:4 molar ratio (see Figure 3.12). The sample was exposed to an Oriel 87000 series DUV Hg-Xe flood exposure tool for 3 minutes before the TGA run.

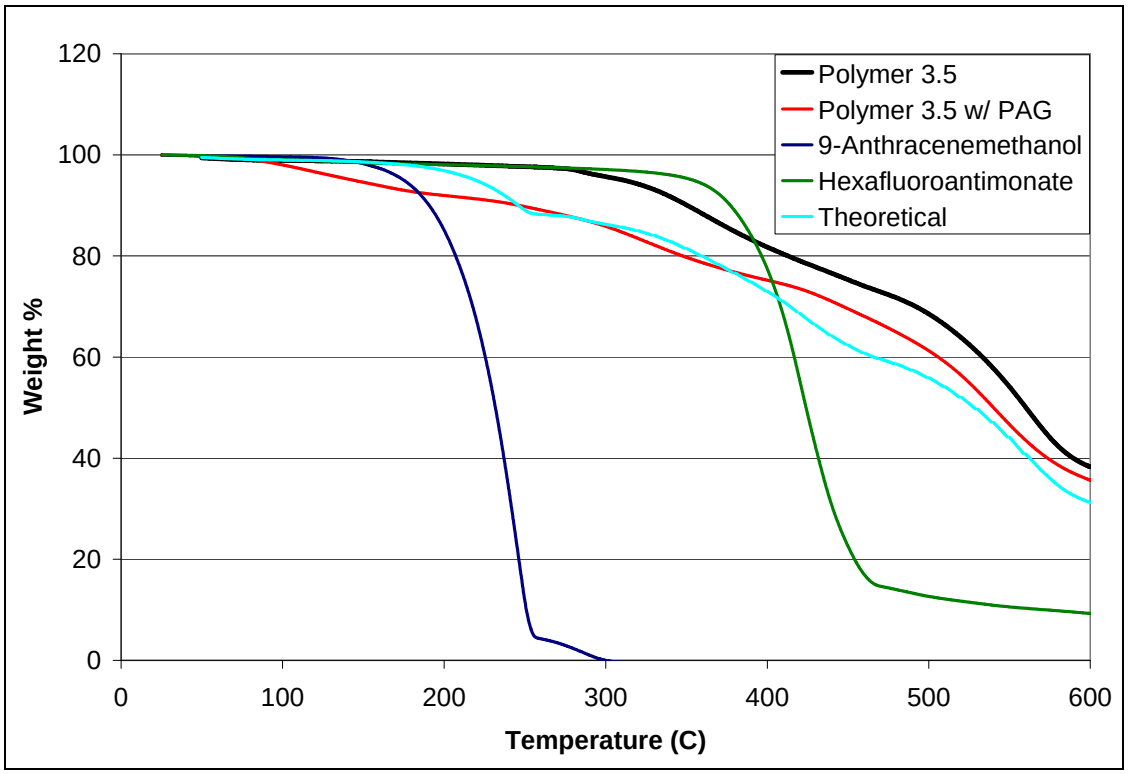

Figure 3.12 TGA runs for polymer **3.5** with PAG.

From the graph, the experimental line deviates from the theoretical line at the beginning. A 1:4 mole ratio of acid to side group correlates to 25% removal of the side group. The side group constitutes 40% of the total polymer weight. As a result, 25% removal of the side group will appear as a 10% weight loss due to the non-catalytic nature of the cleavage. The experimental path in fact does deviate from the theoretical path by about 10% in the beginning. For this experiment, the PAG was 10% and the sensitizer was 10% of the total weight. If the weight loss is due to side group cleavage, then the final mixture must contain 40% PAG as well as 10% or more sensitizer leaving polymer **3.5** to undesirably represent less than 50% of the total film. Unfortunately, the small decrease in the experimental path from the theoretical path is not considered to be a result of polymer side group cleavage.

3.7 Experimental Section

3.7.1 Chemicals

An HFA-substituted phenol **3.1** and 6FDA were provided by Central Glass. Co., Ltd. The DNQ inhibitor used in this work (THBP) was provided by St-Jean Photochemicals Inc. The TMAH developer solution used in this work was AZ 300 MIF (0.26 N) which was provided by AZ Electronic Materials. Other solvents and reagents were purchased from Aldrich and used as-received.

3.7.2 Preparation of 3.3

In a 300-mL three-neck flask, 20.0 g (46.9 mmol) of **3.1**, 10.8 g (46.9 mmol) of 3,5-dinitrobenzoyl chloride, 4.6 ml of pyridine and 150 ml of dichloromethane were added and stirred under nitrogen at 40 ^{o}C for 3 hrs. The reaction mixture was poured into 0.6 N HCl aq. for work-up and precipitation. The white powdery product **3.2** was obtained by filtration, giving 21.0 g after drying overnight under vacuum at room temperature: yield 72 %; ^{1}H-NMR (Appendix A.3, Acetone-d_6) δ 9.31-9.32 (d, 2H, Ar-H), 9.25-9.26 (d, 1H, Ar-H), 8.25 (s, 1H, Ar-H), 8.07-8.08 (d, 2H, Ar-H), 8.04 (s, 2H, HFA-OH) ppm.

In a 300-mL three-neck flask, 9.90 g (16.0 mmol) of **3.2**, 0.97g of 10% palladium carbon and 75ml of methanol were stirred under hydrogen balloon at r.t. for 12 hrs. The reaction liquid was treated with celite filtration, and the resulting filtrate was evaporated. The resulting solid was purified by recrystallization from a mixture of water and methanol to obtain white powdery product **3.3**, giving 5.13 g: yield 57 %; ^{1}H-NMR

(Appendix A.4, Acetone-d_6) δ 9.19 (s, 2H, HFA-OH), 7.93 (s, 1H, Ar-H), 7.66 (s, 2H, Ar-H), 6.68-6.69 (d, 2H, Ar-H), 6.10-6.12 (t, 2H, Ar-H), 5.12 (s, 4H, amine-H) ppm.

3.7.3 Preparation of Poly(amic-acid) 3.4 and Polyimide 3.5

In a 100-mL three-neck flask, 1.50 g (2.7 mmol) of **3.3**, 1.19 g (2.7 mmol) of 6FDA (2,2-bis(3,4-dicarboxyphenyl) hexafluoro propanoic acid dianhydride) and 10.8 ml of N,N-dimethylacetamide (DMAc) were stirred under nitrogen at r.t. for 5 hours. The reaction solution was poured into a mixture of methanol and water, precipitating a polymer. The polymer **3.4** was collected by filtration, and then dried under vacuum drying overnight at 50 ^{o}C. The yield was 95 % (2.50g). An inherent viscosity (η_{inh}) was 0.20 dL/g at a concentration of 0.5 g/dL in NMP at 25 ^{o}C; ^{1}H-NMR (Appendix A.6, DMSO-d_6) δ 10.89 (br, 2H, amide-H), 9.20 (s, 2H, HFA-OH), 7.49-8.46 (br, 14H, Ar-H) ppm; ^{19}F-NMR (Appendix B.1, DMSO-d_6) δ -63.50 (d, 6F, hexafluoroisopropylidene-F), -74.41 (s, 12F, HFA-F) ppm; IR (KBr) 1650 (amide C=O) cm^{-1}.

In a 100-mL three-neck flask, 0.50 g (0.50 mmol) of **3.4**, 0.09 g (1.10 mmol) of pyridine, 0.10 g (1.0 mmol) of acetic anhydride and 4.5 g of dimethylformamide (DMF) were added and stirred at 110 ^{o}C for 12 hrs in nitrogen. The reaction solution was poured into a mixture of methanol and water to precipitate. The polymer **3.5** was collected by filtration, and then dried under vacuum overnight at 100 ^{o}C. The yield was 90% (0.43g). The inherent viscosity (η_{inh}) was 0.19 dL/g at a concentration of 0.5 g/dL in NMP at 25 ^{o}C; ^{1}H-NMR (Appendix A.7, DMSO-d_6) δ 9.17 (s, 2H, HFA-OH), 7.78-8.37 (br, 12H, Ar-H) ppm; ^{19}F-NMR (Appendix B.2, DMSO-d_6) δ -63.37 (br, 6F, hexafluoroisopropylidene-F), -74.47 (s, 12F, HFA-F) ppm; IR (KBr) 1734, 1788 (imide C=O) cm^{-1}.

3.7.4 Lithographic Characterization

For patterned materials, a photosensitive solution was created by adding 20 wt% (relative to polymer solids) THBP into a 20 wt% solution of polymer **3.5** in PGMEA. Silicon wafers were primed with hexamethyldisilazane (HMDS) to improve adhesion of the polymer film onto the substrate. The photosensitive polyimide solutions were spin coated onto the HMDS-treated Si wafers at 1500 rpm for 30 sec, then soft baked 80 ^{o}C for 3 min. The films were exposed using a chrome-on-quartz mask in contact mode using an Oriel Instruments exposure tool containing an I-line bandpass filter. After I-line exposure and post-exposure baking at 80 ^{o}C for 1 min, films were developed in 0.26 N TMAH for 60 sec, rinsed with deionized water, and then cured at 250 ^{o}C for 30 min.

3.8 Summary

A novel HFA-substituted aromatic polyimide was successfully prepared. The resulting polyimide showed good solubility in common organic solvents including PGMEA, γ-GBL, THF, methanol, and 0.26 N TMAH. It was shown that the HFA-containing side-group can be cleaved thermally and removed to produce final materials which do not contain polar hygroscopic groups and which are insoluble in TMAH. The final polyimide with the thermally cleaved side-group is shown to have a lower dielectric constant and CTE. A photosensitive composition of the polyimide loaded with a DNQ inhibitor was shown to serve as a positive-type photodefinable polyimide using I-line exposure. This ability to remove these polar groups, which provide improved solubility characteristics when compared to the pre-imidized polymer as well as the ability to develop these materials in common aqueous developers, is viewed as a distinct and unique advantage to produce a final polymer with a lower dielectric constant and lower

water uptake over other previously reported polyimides that have been functionalized with hydrophilic groups such as phenols. This general design strategy is currently being explored in polyimides and other related materials to produce photodefinable polymers for electronics and optoelectronics applications with improved final film properties and lower processing temperatures.

3.9 References

1. Akimoto, S., M. Jikei, and M.-A. Kakimoto, *A novel photosensitive polyimide: a polyimide containing the hydroxytriphenylamine structure with diazonaphthoquinone.* High Perform. Polym. FIELD Full Journal Title:High Performance Polymers, 2000. **12**(1): p. 177-184.

2. Nakayama, T., A. Mochizuki, and M. Ueda, *New positive-type photosensitive polyimide: poly(hydroxyimide) with diazonaphthoquinone.* React. Funct. Polym. FIELD Full Journal Title:Reactive & Functional Polymers, 1996. **30**(1-3): p. 109-115.

3. Dammel, R.R., et al., *New resin systems for 157 nm lithography.* J. Photopolym. Sci. Technol. FIELD Full Journal Title:Journal of Photopolymer Science and Technology, 2001. **14**(4): p. 603-612.

4. Ito, H., et al., *Polymer design for 157-nm chemically amplified resists.* Proc. SPIE-Int. Soc. Opt. Eng. FIELD Full Journal Title:Proceedings of SPIE-The International Society for Optical Engineering, 2001. **4345**(Pt. 1, Advances in Resist Technology and Processing XVIII): p. 273-284.

5. Li, W., et al., *Rational design in cyclic olefin resists for sub-100-nm lithography.* Proc. SPIE-Int. Soc. Opt. Eng. FIELD Full Journal Title:Proceedings of SPIE-The International Society for Optical Engineering, 2003. **5039**(Pt. 1, Advances in Resist Technology and Processing XX): p. 61-69.

6. Sasaki, T., et al., *A new monocyclic fluoropolymer for 157-nm photoresists.* J. Photopolym. Sci. Technol. FIELD Full Journal Title:Journal of Photopolymer Science and Technology, 2004. **17**(4): p. 639-644.

7. Yamashita, T., et al., *Synthesis of fluorinated materials for 193 nm immersion lithography and 157 nm lithography.* J. Photopolym. Sci. Technol. FIELD Full Journal Title:Journal of Photopolymer Science and Technology, 2005. **18**(5): p. 631-639.

8. Przybilla, K.J., H. Roeschert, and G. Pawlowski, *Hexafluoroacetone in resist chemistry.* Adv. Mater. (Weinheim, Fed. Repub. Ger.) FIELD Full Journal Title:Advanced Materials (Weinheim, Germany), 1992. **4**(3): p. 239-42.

9. Chiba, T., et al., *Resist (157 nm) materials: a progress report.* J. Photopolym. Sci. Technol. FIELD Full Journal Title:Journal of Photopolymer Science and Technology, 2000. **13**(4): p. 657-664.

10. Ito, H., N. Seehof, and R. Sato, *Synthesis and preliminary evaluation of substituted poly(norbornene sulfones) for 193 nm lithography.* Polym. Mater. Sci. Eng. FIELD Full Journal Title:Polymeric Materials Science and Engineering, 1997. **77**: p. 449-450.

11. Ito, H., et al., *Development of 157 nm positive resists.* J. Vac. Sci. Technol., B FIELD Full Journal Title:Journal of Vacuum Science & Technology, B: Microelectronics and Nanometer Structures, 2001. **19**(6): p. 2678-2684.

12. Ogata, T., et al., *Effects of protecting group of fluoroalcohol on lithographic performance.* J. Photopolym. Sci. Technol. FIELD Full Journal Title:Journal of Photopolymer Science and Technology, 2003. **16**(5): p. 707-712.

13. Jakubek, V., et al., *Strategies for high transparency acrylate resists for 157 nm lithography.* J. Photopolym. Sci. Technol. FIELD Full Journal Title:Journal of Photopolymer Science and Technology, 2003. **16**(4): p. 573-580.

14. Bae, Y.C., et al., *Tailoring transparency of imageable fluoropolymers at 157 nm by incorporation of hexafluoroisopropyl alcohol to photoresist backbones.* Chem. Mater. FIELD Full Journal Title:Chemistry of Materials, 2002. **14**(3): p. 1306-1313.

15. Ito, H., et al., *Fluoropolymer resists: Fundamentals and lithographic evaluation.* J. Photopolym. Sci. Technol. FIELD Full Journal Title:Journal of Photopolymer Science and Technology, 2004. **17**(4): p. 609-620.

16. Agrawal, A. and C.L. Henderson, *Investigation of surface inhibition and its effects on the lithographic performance of polysulfone-novolak electron-beam resists.* Proc. SPIE-Int. Soc. Opt. Eng. FIELD Full Journal Title:Proceedings of SPIE-The International Society for Optical Engineering, 2003. **5039**(Pt. 2, Advances in Resist Technology and Processing XX): p. 1019-1030.

17. Henderson, C.L., *Advances in Photoresist Characterization and Lithography Simulation*. 1998, University of Texas at Austin.

18. Yamanaka, K., et al., *Novel low-dielectric constant photodefinable polyimides for low-temperature polymer processing.* Proc. SPIE-Int. Soc. Opt. Eng. FIELD Full Journal Title:Proceedings of SPIE-The International Society for Optical Engineering, 2006. **6153**(Pt. 1, Advances in Resist Technology and Processing XXIII): p. 61531H/1-61531H/11.

CHAPTER 4

POLYMERS BASED ON POLYBENZOXAZINES

4.1 Introduction

As the feature sizes in microelectronic devices continue to diminish and as devices continue to operate at higher frequencies, there continues to be a growing need for lower dielectric constant insulator materials that can be used in both device fabrication and packaging applications. Insulating polymers with low dielectric constants (low-k), such as polyimides, are certainly one important class of materials used today in both device fabrication and packaging. However, essentially all current polymer dielectrics used in microelectronics processing suffer from one or more problems that limit their utility including: (1) requiring high temperature processing (e.g. > 300 ºC for polyimides made from poly(amic acid) precursor films), (2) possessing large coefficients of thermal expansion (CTE) that cause stress build-up during temperature cycling in device manufacturing and operation, (3) requiring separate lithographic patterning and etching to form patterned polymer layers, and (4) exhibiting undesirable water absorption or other physiochemical properties due to modifications made to the material so that they are solution processable.

Polybenzoxazoles have received significant attention in the microelectronics industry as a photosensitive dielectric and alternative to polyimide materials [1, 2]. Polybenzoxazoles form rings from the dehydration of an alcohol situated ortho to an amide. However, formation of the polybenoxazole ring requires relatively high temperatures (~350 ^{o}C). In searching for alternative polymers that can be formulated into

photosensitive compositions and which offer low dielectric constants, excellent thermal stability, and relatively low processing temperatures, a method for producing a new class of polymers referred to here as polybenzoxazines was developed. The term polybenzoxazine is traditionally used to refer to a class of thermosetting polymer resins where the actual polymer itself is the product of benzoxazine polymerizing via a thermally induced ring-opening reaction to form a phenolic-like structure via a Mannich base bridge [3-7]. These polymers are not the material of interest in this work. Instead, polybenzoxazine in this work is used to refer to polymers that contain a benzoxazine ring directly in the polymer backbone. In a manner similar to that of polybenzoxazoles, the benzoxazine rings in the polymer backbone described in this work are formed by the dehydration of a hexafluoroalcohol (HFA) group situated ortho to an amide.

In this chapter, the use of a combination of a novel HFA-substituted diamine monomer with various acid chloride monomers to synthesize novel thermoplastic polybenzoxazine amide alcohol precursor polymers is reported. Dehydration of the hexafluoroisopropanol moiety situated ortho to the amide forms the six membered benzoxazine ring structure rather than the five membered ring seen in polybenzoxazoles. In contrast to polybenzoxazoles which are known to cyclize at temperatures well above 280 ^{o}C, the new polymers reported here can be cyclized at temperatures as low as 210 ^{o}C. This characteristic of polybenzoxazines is due to the ease of atomic bonds angles forming a six membered ring. This substantially lower thermal cyclization temperature reduces problems such as thermal stress build-up during curing and allows for integration of these polymers with a wider variety of materials. The polybenzoxazine amide alcohol precursor polymers have exhibited good solubility in a variety of different casting

solvents including methanol, THF, PGMEA, GBL, DMF, and have also shown solubility in 0.26 N TMAH. Characterization of the physiochemical properties of these polybenzoxazine materials are presented including polymer structures, dielectric constants, coefficients of thermal expansion, and lithographic characteristics.

4.2 Polymer Synthesis

As shown in Figure 4.1, polymerization of the HFA-containing diamine, 3,3'-bis(1-hydroxy-1-trifluoromethyl-2,2,2-trifluoroethyl)-4,4'oxydianiline (HFA-ODA), with various acid chloride monomers (Figure 4.2) to form polybenzoxazine was carried out in DMAc for 24 hours. All polybenzoxazines (PBOX) will be identified by the acid chloride because HFA-ODA is the only diamine used. The reactions proceeded in homogeneous solution. The solutions were poured into a mixture of methanol and water to precipitate the product.

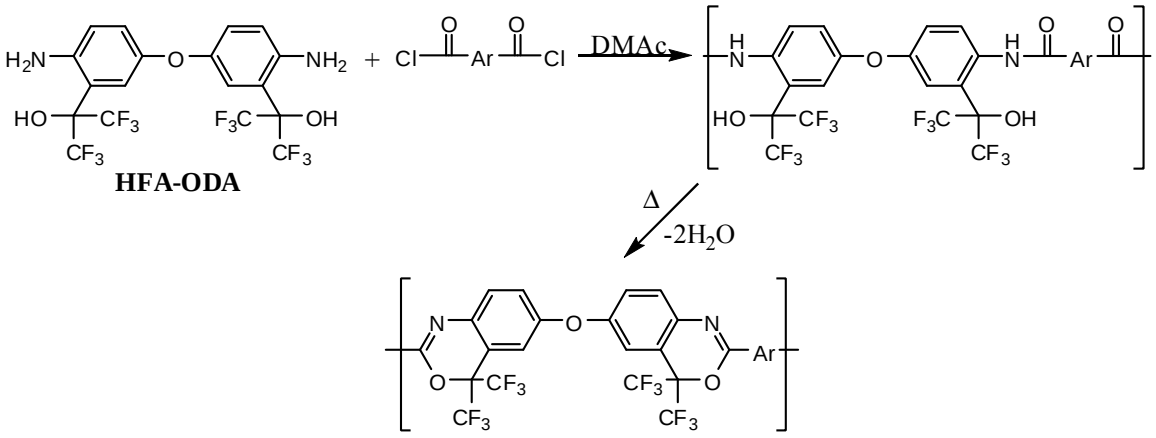

Figure 4.1 Polymerization and thermal formation of polybenzoxazines

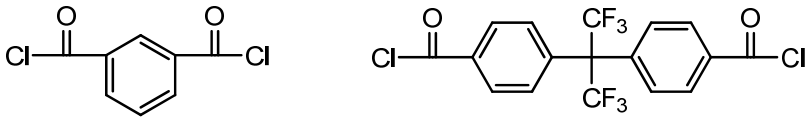

IPC

6FDC

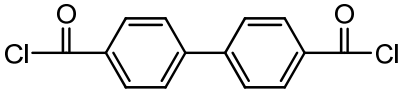

BPDC

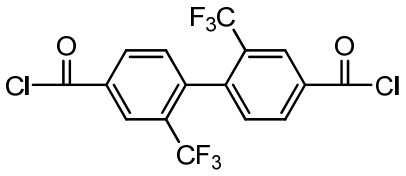

6FBDC

Figure 4.2 Acid chloride monomers

4.3 Polymer Characterization

The polymer structures were characterized by NMR, IR, and thermogravimetric analysis (TGA) measurements. The ^{1}H-NMR and ^{19}F-NMR spectra of the resulting compounds show the desired structures (Appendices A and B). Continuous ramp TGA curves (10 ºC/min ramp rate) are shown in Figure 4.3. Weight loss from cyclization can be seen below 250 ^{o}C for all polybenzoxazines. Below 200 ^{o}C, there is weight loss that cannot be explained by the removal of water. From the Mass Spectrometer, a large peak at 87 g/mol appears. This corresponds to residual DMAc that has been trapped by the polymer during precipitation. From Figure 4.3, the polymer appears to have very little degradation at temperatures below 450 ^{o}C.

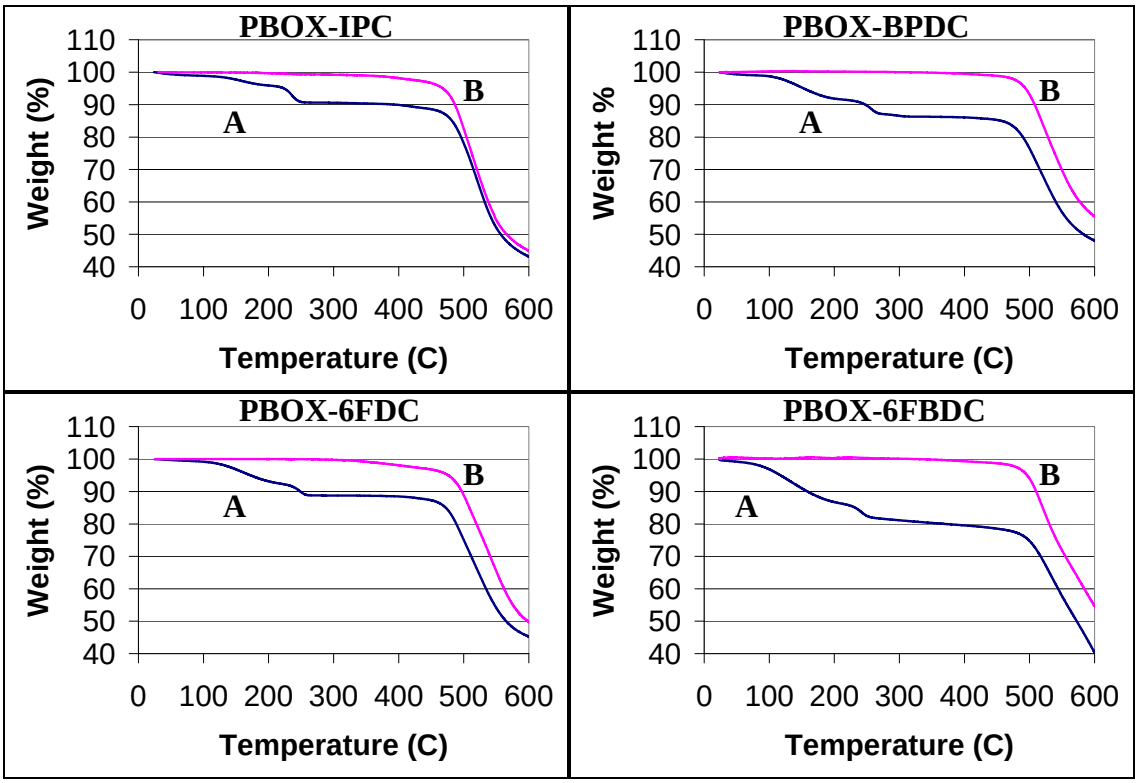

Figure 4.3 TGA curves in nitrogen at a heating rate of 10 ^{o}C/min for: (**A**) the amide alcohol polymer precursor and (**B**) the polymer cured at specified cyclization temperature.

Thermal cyclization was then examined further by curing at varying constant temperature conditions. From IR analyses, disappearance of the OH peak between 3000 cm^{-1} and 3650 cm^{-1} confirmed cyclization (Figure 4.4). Benzoxazole ring formation is confirmed by the presence of medium-intensity absorption bands at 1600 and 1460 cm^{-1} [8, 9]. The band at 1640 cm^{-1} is due to the formation of the carbon nitrogen double bond present in benzoxazine rings. Table 4.1 lists the solubility properties of the four polybenzoxazines.

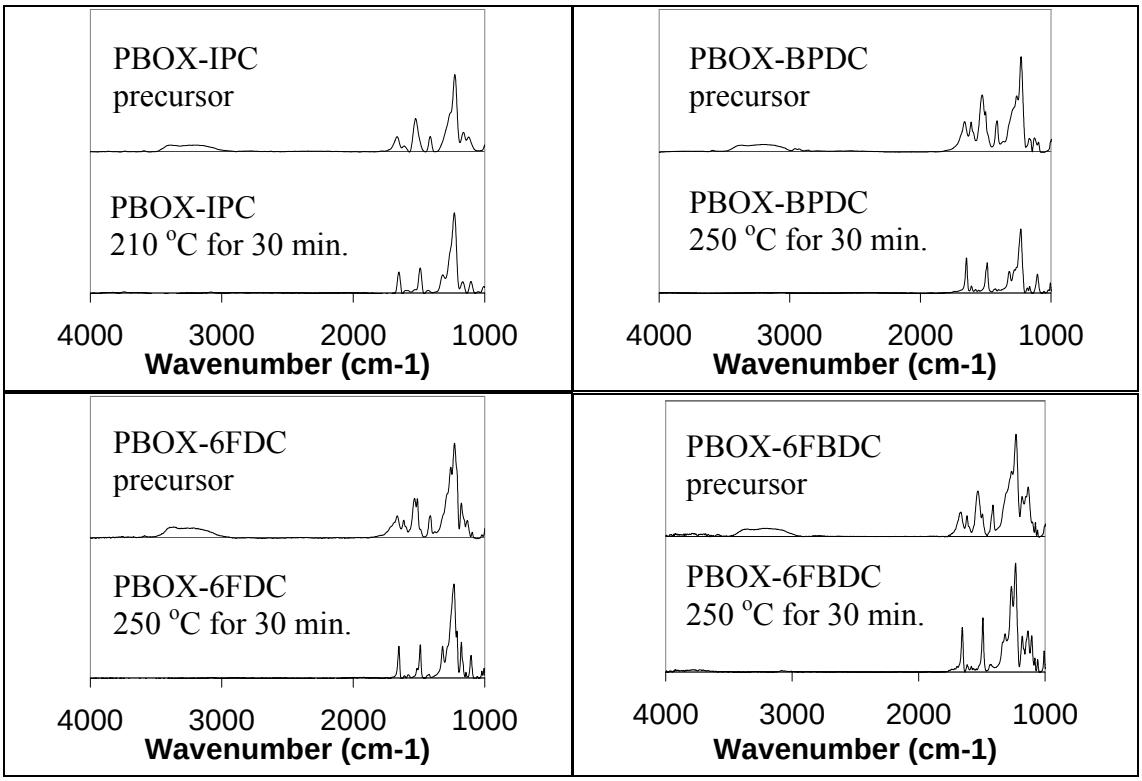

Figure 4.4 FTIR of Polybenzoxazines

Table 4.1 Solubility of the various polybenzoxazines in different solvents.

Polymer PBOX-	Acetone	Methanol	DMF	GBL	PGMEA	THF	0.26N TMAH
IPC	√	√	√	X	X	√	√
BPDC	√	√	√	X	X	√	√
6FDC	√	√	√	√	√	√	√
6FBDC	√	√	√	√	√	√	√

4.4 Polymer film properties

Polymer film properties including precursor viscosity, dielectric constant, CTE, T_g, cure temperature, Young's modulus, degradation temperature, and water absorption were examined. All film properties are shown in Table 4.2.

Table 4.2 Polymer properties

Polymer PBOX-	IPC	BPDC	6FDC	6FBDC
Precursor η_{inh} (dL/g)	0.26	1.20	0.27	0.67
M_n / M_w (kg/mol)	9.8/20.1	29.6/73.5	22.8/46.4	33.8/78.3
Cure Temperature (^oC)	210	250	250	250
Dielectric Constant	2.5	2.6	2.0	2.2
Water Absorption (wt%)	0.38	0.42	0.09	0.12
CTE (ppm/^oC)	85.7	89.9	81.5	84.3
T_g (^oC)	178	226	230	211
T_5/T_{10} (^oC)	468/486	494/508	476/497	496/510
Young's Modulus (GPa)	6.0	4.3	17.6	23.0

As shown in Figure 4.4, all polybenzoxazines cyclize at or below 250 ^oC. The large presence of fluorine in the diamine led the belief that the polymers would have a lower dielectric constant. Experimental results conclude that all polybenzoxazines do have a low dielectric constant. As expected, a reduction in the polymer dielectric constant was observed for the presence of fluorine in the acid chloride.

Figure 4.5 shows an example of a QCM (Quartz Crystal Microbalance) measurement for water absorption and desorption in a film of PBOX-6FDC cured at 250 ^oC for 30 min. The measured difference in QCM frequency between the dry and wet (i.e., exposed to a ~95 % humidity atmosphere) films corresponds to a water absorption value of 0.09 wt%. This value is very desirable for polymer dielectrics and considerably lower than the observed range of water absorption values for polyimides in general which typically range from approximately 1 wt% to 5 wt%. The low dielectric constant of PBOX-6FDC helps to justify the low water absorption observed, but PBOX-IPC displayed a similar water absorption value of 0.4 wt% yet has a much higher dielectric constant than PBOX-6FDC.

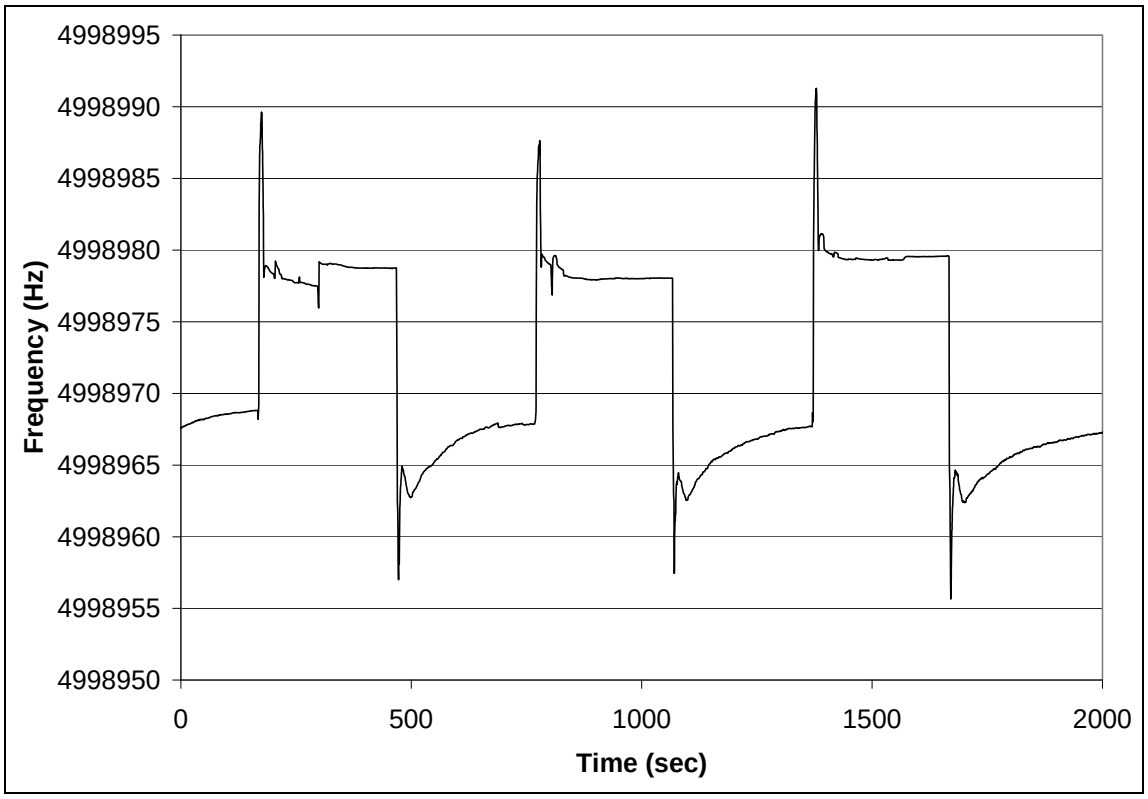

Figure 4.5 QCM measurement of PBOX-6FDC cured at 250 ^{o}C for 30 min.

The in-plane CTE and T_g were determined by TMA using free standing films. From Figure 4.6, PBOX-6FDC is shown to have the most desirable combination of glass transition and low CTE with a value of 81.5 ppm/^{o}C and a T_g of 230 ^{o}C. Later chapters will cover attempts to lower the CTE and increase the T_g.

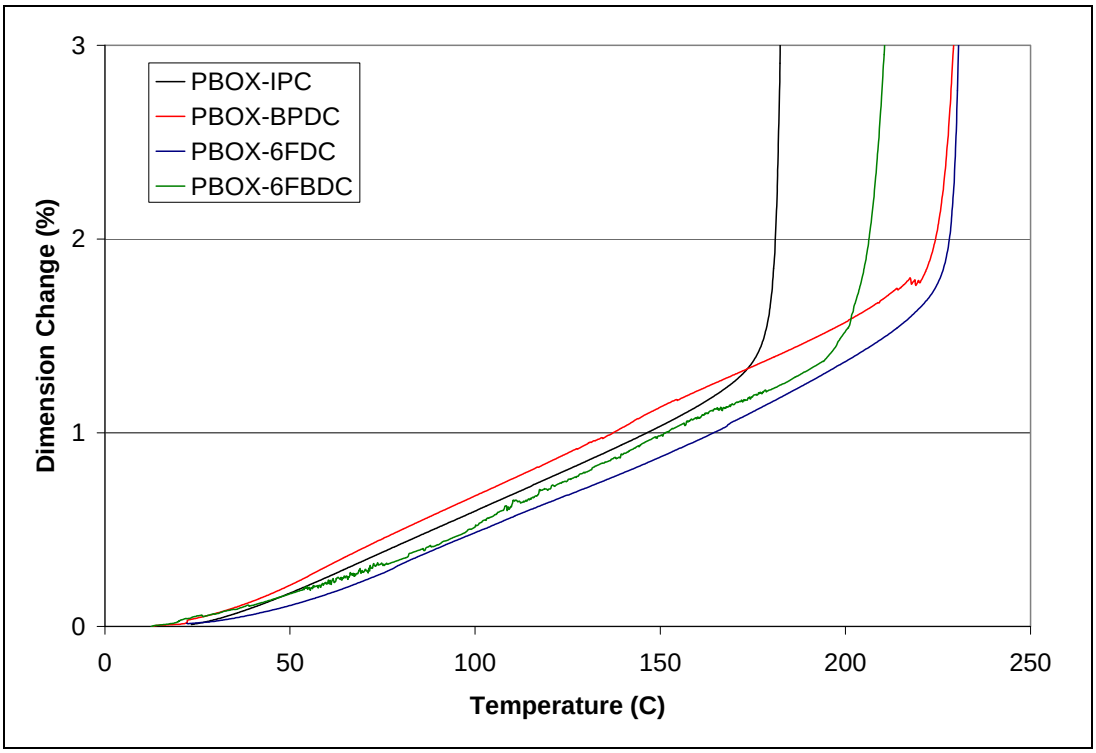

Figure 4.6 TMA data for PBOX at a heating rate of 10 ^{o}C/min.

The polybenzoxazines under investigation can avoid decomposition during a thermal annealing step required in industry to ensure void free copper depositions at temperatures as high as 400–450 °C. In addition to the dielectric constant, the Young's modulus of polybenzoxazines appears to be dependant on the fluorine content in the acid chloride. All polybenzoxazines investigated have a high enough Young's modulus to be used as an insulating dielectric.

4.5 Formulation of a Photodefinable Polybenzoxazine

Photodefinable polybenzoxazine formulations were made by loading a trifunctional DNQ inhibitor into the polymers. Figure 4.7 shows a Meyerhofer plot for various loadings of the DNQ in PBOX-IPC. It is observed the difference between the dissolution rate (DR) of the unexposed and exposed formulation in 0.26N TMAH is a

factor of ~10 at a loading of 15 wt% DNQ and a factor of ~50 at a loading of 25 wt% DNQ. This DR contrast is sufficient for photo-patterning experiments.

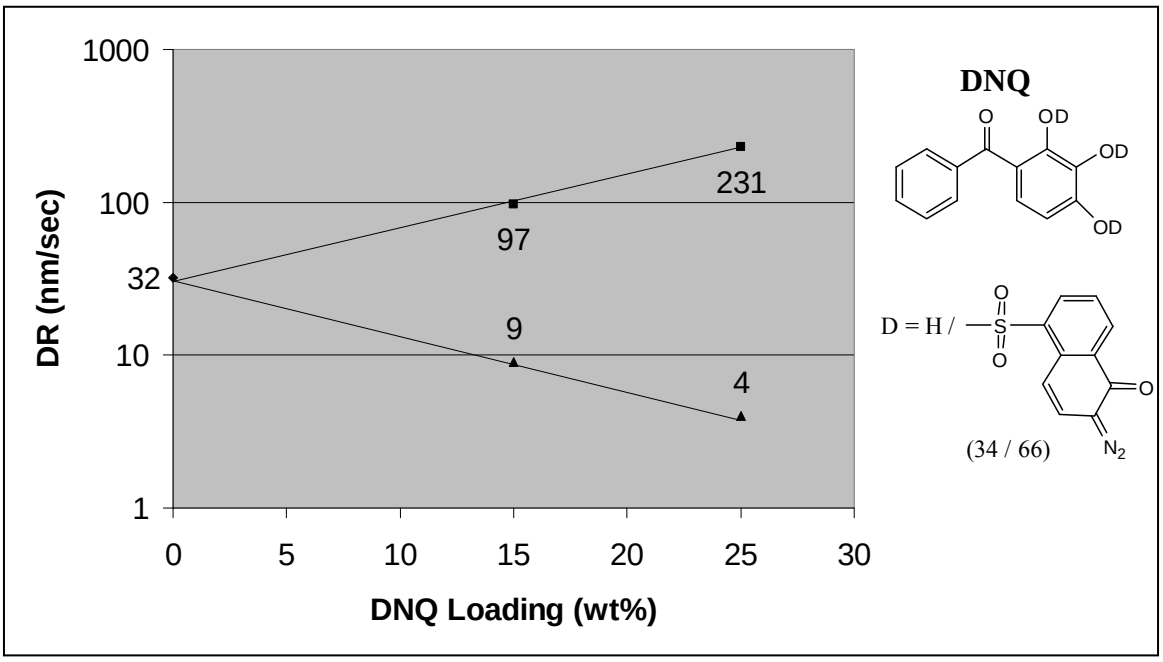

Figure 4.7 Dependence of unexposed (▲) and exposed (■, I-line at 2000 mJ/cm^2) DRs onto DNQ loading for PBOX-IPC

Figures 4.8 and 4.9 show optical microscope pictures of contact-printed images for a 0.5 micron thick film of PBOX-IPC obtained from dark and bright field masks which produce dense space and line arrays, respectively. Both resulting images agreed well with mask feature sizes. Figure 4.9b shows representative images of some of the small scale patterns printed in the 25 wt% DNQ loaded PBOX-IPC (here a 130-μm feature is shown).

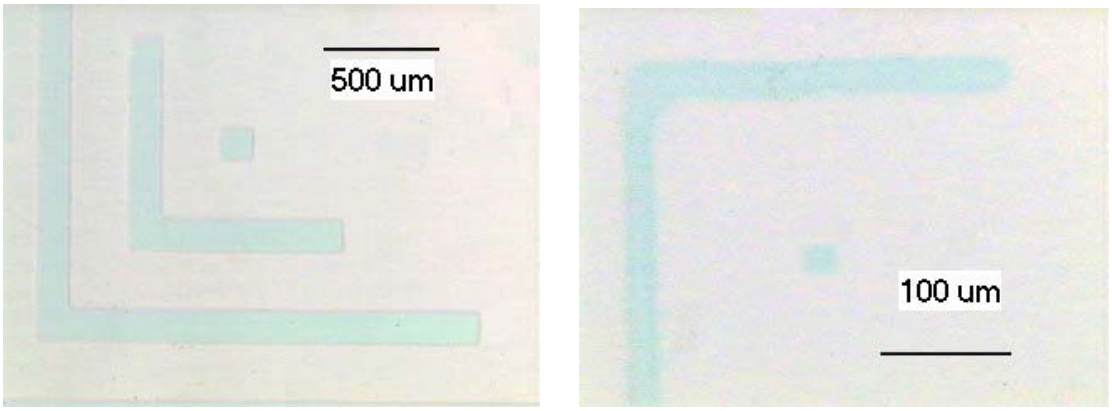

(a) (b)

Figure 4.8 Optical microscope pictures of 25 wt% DNQ-loaded PBOX-IPC at x10 magnification obtained by using a dark field mask: exposed at 2 J/cm^2, developed with 0.26 N TMAH for 60 sec., and then cured at 210 ^{o}C for 30 min.

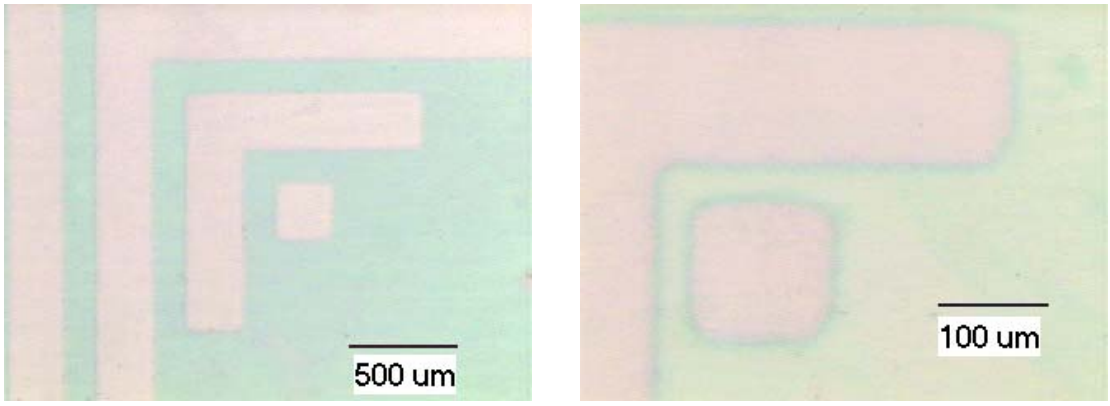

(a) (b)

Figure 4.9 Optical microscope pictures of 25 wt% DNQ-loaded PBOX-IPC at x10 magnification obtained by using a bright field mask: exposed at 2 J/cm^2, developed with 0.26 N TMAH for 60 sec., and then cured at 210 ^{o}C for 30 min.

From Figure 4.9b, there appears to be some swelling as a result of development. These pictures agree with results from the DRM. During development, the polybenzoxazine film swelled by 34 % of the initial polymer film thickness. This undesirable property will limit the types of features that can be imaged.

4.5 Experimental Section

4.5.1 Chemicals

3,3'-Bis(1-hydroxy-1-trifluoromethyl-2,2,2-trifluoroethyl)-4,4'oxydianiline, 4,4'-(hexafluoroisopropylidene)bis(benzoic acid), and 4-4'-Bi(3-(trifluoromethyl))benzoic acid were provided by Central Glass. Co., Ltd. The DNQ inhibitor used in this work was provided by St-Jean Photochemicals Inc. The TMAH developer solution used in this work was AZ 300 MIF which was provided by AZ Electronic Materials. Other solvents and reagents were purchased from Aldrich and used as-received.

4.5.2 Preparation of 4,4'-(hexafluoroisopropylidene)bis(benzoyl chloride) (6FDC)

In a 100 mL flask, 10.012 g (25.5 mmol) of 4,4'-(hexafluoroisopropylidene) bis(benzoic acid), 5 drops of DMF and 30mL of thionyl chloride were added and stirred under nitrogen at 95 ^{o}C for 12 hrs. The thionyl chloride was removed by vacuum. The product was recrystallized in n-hexane, giving 10.138 g: yield 92.6 %; ^{1}H-NMR (Appendix A.9, Acetone-d_6) δ 8.27-8.29 (d, 4H, Ar-H), 7.72-7.74 (d, 4H, Ar-H) ppm.

4.5.3 Preparation of 4-4'-Bi(3-(trifluoromethyl))benzoyl chloride (6FBDC)

In a 100-mL flask, 10.179 g (26.9 mmol) of 4-4'-Bi(3-(trifluoromethyl))benzoic acid, 3 drops of DMF and 30 mL of thionyl chloride were added and stirred under nitrogen at 85 ^{o}C for 12 hrs. The product was recrystallized in n-hexane, giving 7.911 g:

yield 70.8 %; ^{1}H-NMR (Appendix A.10, Acetone-d_6) δ 8.54 (s, 2H, Ar-H), 8.52-8.53 (d, 2H, Ar-H), 7.81-7.84 (d, 2H, Ar-H) ppm.

4.5.4 Preparation of PBOX-IPC

In a 100-mL three-neck flask, 1.503 g (2.8 mmol) of HFA-ODA and 6mL of N,N-dimethylacetamide (DMAc) were stirred under nitrogen at r.t. When a solution was reached, the flask was lowered into an ice water bath. After the solution was cooled, 0.873 g (2.8 mmol) of IPC and 2.2mL of DMAc were added. The solution was stirred for 24 hrs and slowly warmed to r.t. The reaction solution was poured into a mixture (1:1, v/v) of methanol and water, precipitating a polymer. The polymer was collected by filtration, and then dried under vacuum drying overnight at 90 ^{o}C. The yield was 96.2% (1.799g). An inherent viscosity (η_{inh}) was 0.26 dL/g at a concentration of 0.5 g/dL in NMP at 25 ^{o}C; ^{1}H-NMR (Appendix A.11, DMSO-d_6) δ 10.68 (br, 2H, amide-H), 10.47 (s, 2H, HFA-OH), 8.46-8.47 (d, 2H, Ar-H), 8.45 (s, 1H, Ar-H), 8.08-8.11 (d, 2H, Ar-H), 7.79-7.83 (t, 1H, Ar-H), 7.38-7.41 (d, 2H, Ar-H), 7.13 (s, 2H, Ar-H) ppm.

4.5.5 Preparation of PBOX-BPDC

In a 100-mL three-neck flask, 1.502 g (2.8 mmol) of HFA-ODA and 6 mL of N,N-dimethylacetamide (DMAc) were stirred under nitrogen at r.t. When a solution was reached, the flask was lowered into an ice water bath. After the solution was cooled, 0.789 g (2.8 mmol) of BPDC and 3 mL of DMAc were added. The solution was stirred for 24 hrs and slowly warmed to r.t. The reaction solution was poured into a mixture (1:1, v/v) of methanol and water, precipitating a polymer. The polymer was collected by filtration, and then dried under vacuum drying overnight at 85 ^{o}C. The yield was 99.8 %

(2.08 g). An inherent viscosity (η_{inh}) was 1.20 dL/g at a concentration of 0.5 g/dL in NMP at 25 ^{o}C; ^{1}H-NMR (Appendix A.12, DMSO-d_6) δ 10.69 (br, 2H, amide-H), 10.59 (s, 2H, HFA-OH), 8.50 (d, 2H, Ar-H), 7.99 (d, 8H, Ar-H), 7.36-7.39 (d, 2H, Ar-H), 7.11 (s, 2H, Ar-H) ppm.

4.5.6 Preparation of PBOX-6FDC

In a 100-mL three-neck flask, 1.500 g (2.8 mmol) of HFA-ODA and 7mL of DMAc were stirred under nitrogen at r.t. When a solution was reached, the flask was lowered into an ice water bath. After the solution was cooled, 1.211 g (2.8 mmol) of 6FDC and 4mL of DMAc were added. The solution was stirred for 24 hrs and slowly warmed to r.t. The reaction solution was poured into a mixture (1:1, v/v) of methanol and water, precipitating a polymer. The polymer was collected by filtration, and then dried under vacuum drying overnight at 90 ^{o}C. The yield was 98.7% (2.520g). An inherent viscosity (η_{inh}) was 0.27 dL/g at a concentration of 0.5 g/dL in NMP at 25 ^{o}C; ^{1}H-NMR (Appendix A.13, DMSO-d_6) δ 10.65 (br, 2H, amide-H), 10.39 (s, 2H, HFA-OH), 8.38-8.41 (d, 2H, Ar-H), 7.98-8.00 (d, 4H, Ar-H), 7.54-7.56 (d, 4H, Ar-H), 7.34-7.36 (d, 2H, Ar-H), 7.09 (s, 2H, Ar-H) ppm; ^{19}F-NMR (Appendix B.3, DMSO-d_6) δ -63.37 (s, 6F, hexafluoroisopropylidene-F), -73.41 (s, 12F, HFA-F) ppm.

4.5.7 Preparation of PBOX-6FBDC

In a 100-mL three-neck flask, 1.499 g (2.8 mmol) of HFA-ODA and 7 mL of DMAc were stirred under nitrogen at r.t. When a solution was reached, the flask was lowered into an ice water bath. After the solution was cooled, 1.168 g (2.8 mmol) of 6FBDC and 3.7 mL of DMAc were added. The solution was stirred for 24 hrs. The

reaction solution was poured into a mixture (1:1, v/v) of methanol and water, precipitating a polymer. The polymer was collected by filtration, and then dried under vacuum drying overnight at 85 ^{o}C. The yield was 99.7 % (2.454 g). An inherent viscosity (η_{inh}) was 0.67 dL/g at a concentration of 0.5 g/dL in NMP at 25 ^{o}C; ^{1}H-NMR (Appendix A.14, DMSO-d_6) δ 10.65 (br, 2H, amide-H), 10.28 (s, 2H, HFA-OH), 8.35 (s, 2H, Ar-H), 8.27-8.30 (d, 2H, Ar-H), 8.19-8.21 (d, 2H, Ar-H), 7.68-7.72 (d, 2H, Ar-H), 7.39-7.42 (d, 2H, Ar-H), 7.17 (s, 2H, Ar-H) ppm; ^{19}F-NMR (Appendix B.4, DMSO-d_6) δ -57.51 (s, 6F, hexafluoroisopropylidene-F), -73.28 (s, 12F, HFA-F) ppm.

4.5.8 Lithographic Characterization

For generation of the Meyerhofer plot (see Figure 4.7) and patterned materials (see Figures 4.8 and 4.9), solutions of DNQ loaded in the polymers were made in DMF at 20 wt% total solids. Silicon wafers were primed with polyimide to improve adhesion of the polymer film onto the substrate. Photosensitive polybenzoxazine solutions were spin coated onto the treated Si wafers at 1000 rpm for 30 sec, then soft baked at 80 ^{o}C for 3 min. After exposure and post-exposure baking at 80 ^{o}C for 3 min, films were developed in 0.26 N TMAH for 60 sec, rinsed with water, and then cured at 210 ^{o}C for 30 min.

4.6 Summary

A novel, low dielectric photodefinable polymer was successfully prepared. The resulting polybenzoxazine amid alcohol precursors showed good solubility in common organic solvents including acetone, methanol, THF, PGMEA, GBL, DMF and 0.26 N TMAH. All polybenzoxazines have shown acceptably low dielectric constants and water absorptions. A photosensitive composition based on the polybenzoxazine precursor

loaded with a trifunctional DNQ inhibitor was found to serve as a positive-tone photodefinable polybenzoxazine using standard 0.26N TMAH developer. During development, it was shown that there is swelling that might limit the implementation of this material. Unlike traditional dielectric polymer precursors, thermal curing is shown to be achievable in polybenzoxazines at temperatures as low as 210 ^{o}C. Thermal curing renders the polymer insoluble in aqueous developers and produces a polymer with a low dielectric constant and low water absorption.

4.7 References

1. Hsu, S.L.-C. and W.-C. Chen, *A Novel Positive Photosensitive Polybenzoxazole Precursor for Microelectronic Applications.* Polymer, 2002. **43**(25): p. 6743-6750.

2. Yamaoka, T., et al., *A study of novel heat-resistant polymers: preparation of photosensitive fluorinated polybenzoxazole precursors and physical properties of polybenzoxazoles derived from the precursors.* Journal of Polymer Science, Part A: Polymer Chemistry, 1990. **28**(9): p. 2517-32.

3. Tsutomu Takeichi, T.A., Rachib Zeidam, *Preparation and Properties of Polybenzoxazine/Poly(imidesiloxane) Alloys: In Situ Ring-Opening Polymerization of Benzoxazine in the Presence of Soluble Poly(imide-siloxane)s.* Journal of Polymer Science: Part A: Polymer Chemistry, 2001. **29**: p. 2633-2641.

4. Tsutomu Takeichia, Y.G., Sarawut Rimdusit, *Performance improvement of polybenzoxazine by alloying with polyimide: effect of preparation method on the properties.* Polymer, 2005. **46**: p. 4909–4916.

5. Yi-Che Su, F.-C.C., *Synthesis and characterization of fluorinated polybenzoxazine material with low dielectric constant.* Polymer, 2003. **44**: p. 7989–7996.

6. Yi-Che Su, W.-C.C., Feng-Chih Chang, *Investigation of the Thermal Properties of Novel Adamantane-Modified Polybenzoxazine.* Journal of Applied Polymer Science, 2004. **94**: p. 932-940.

7. Ying-Ling Liu, J.-M.Y., Ching-I Chou, *Preparation and Properties of Novel Benzoxazine and Polybenzoxazine with Maleimide Groups.* Journal of Polymer Science: Part A: Polymer Chemistry, 2004. **42**: p. 5954-5963.

8. Chang, J.-H., et al., *Two-step thermal conversion from poly(amic acid) to polybenzoxazole via polyimide: their thermal and mechanical properties.* Journal of Polymer Science, Part B: Polymer Physics, 2000. **38**(19): p. 2537-2545.

9. Chen, X., M. Anthamatten, and D.R. Harding, *Vapor deposition and curing of polybenzoxazole precursors.* Macromolecules, 2006. **39**(22): p. 7561-7565.

CHAPTER 5

BENZOXAZINE/IMIDE COPOLYMER

5.1 Introduction

From the previous chapter and literature, it appears that polyimides possess some of the desired properties (low CTE and high T_g) while polybenzoxazines possess other desired properties (lower dielectric constant and low water absorption). Unfortunately, neither polymer platform is perfect in terms of possessing the ideal combination of all the desired properties. One possible way to produce a material with a better blend of physical properties would be to form a copolymer containing both imide and benzoxazine units. Theoretically, the property under investigation for a copolymer should lie between that of the pure polyimide and polybenzoxazine. Properties of copolymers as well as copolyimides have been reported in the literature that fall between the properties of the pure polymers [1, 2].

In this chapter, the use of a combination of the HFA-substituted diamine monomer with an acid chloride containing an imide monomer to synthesize a novel thermoplastic polybenzoxazine/imide amide alcohol precursor polymer is reported. In contrast to polybenzoxazoles and polyimides which are known to cyclize at temperatures as high as 350 ^{o}C, the new polymers reported here can be cyclized at 265 ^{o}C. This substantially lower thermal cyclization temperature reduces problems such as thermal stress build-up during curing and allows for integration of these polymers with a wider variety of materials. The polybenzoxazine/imide amide alcohol precursor polymer exhibited good solubility in a variety of different casting solvents including acetone,

THF, PGMEA, GBL, DMF, and have also shown solubility in 0.26 N tetramethyl ammonium hydroxide (TMAH). Characterization of the physiochemical properties of these polybenzoxazine materials are presented including polymer structures, dielectric constants, coefficients of thermal expansion, and lithographic characteristics.

5.2 Monomer Synthesis

As shown in Figure 5.1, 6FDA was combined with 4-aminobenzoic acid in refluxing glacial acetic acid. A white precipitate was obtained in 93.3 % yield. To produce the acid chloride, 6FDIA was added to refluxing thionyl chloride with a small amount of pyridine. The white powdery product was obtained in 79.9 % yield. Monomers 6FDIA and 6FDIAC have been reported in literature [3-10].

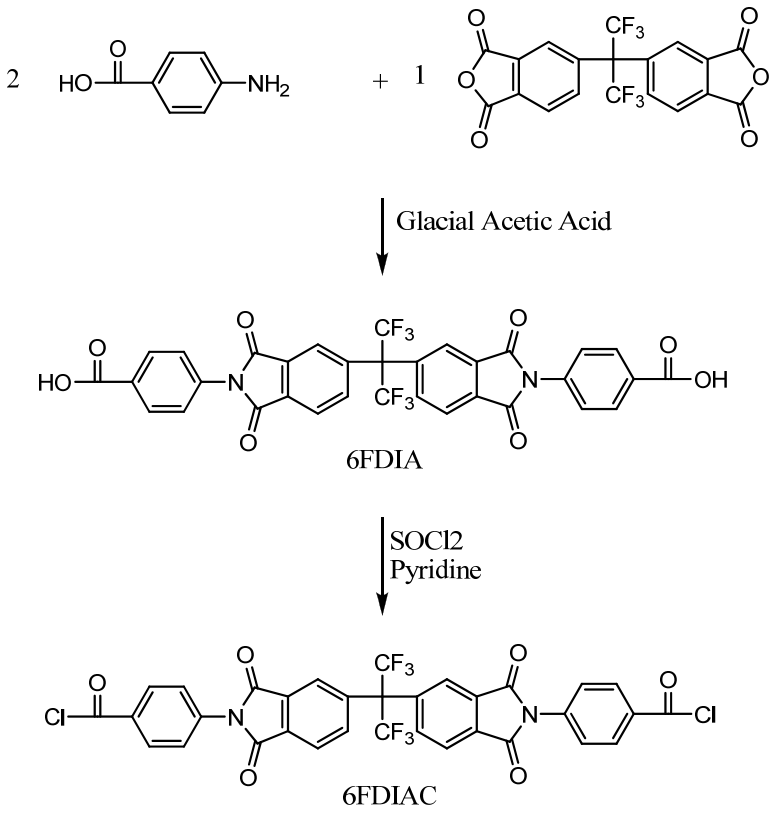

Figure 5.1 6FDIAC synthesis

5.3 Polymer Synthesis

As shown in Figure 5.2, polymerization of 3,3'-bis(1-hydroxy-1-trifluoromethyl-2,2,2-trifluoroethyl)-4,4'oxydianiline (HFA-ODA) with the acid chloride to form the benzoxazine/imide copolymer (PBOX-6FDIAC) was carried out in DMAc for 24 hours. The reactions proceeded in a homogeneous solution. The solution was poured into methanol to precipitate the product.

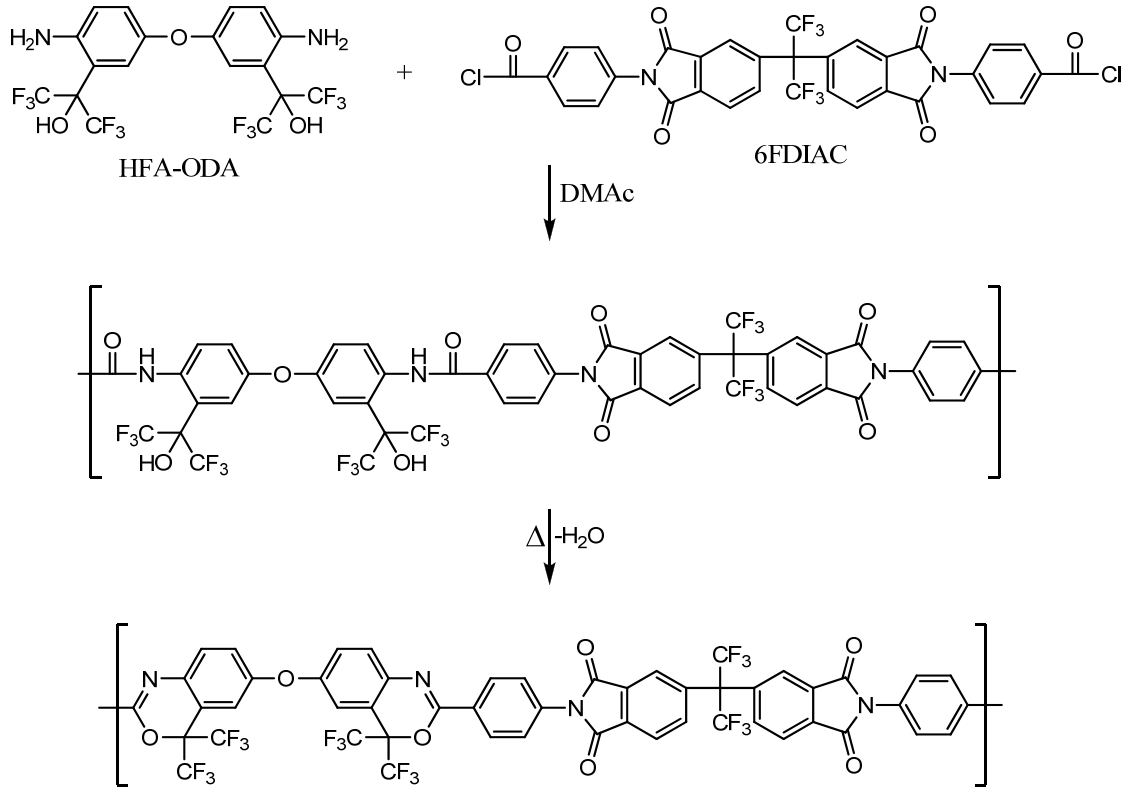

Figure 5.2 PBOX-6FDIAC synthesis

5.4 Polymer Characterization

The polymer structure was characterized by NMR, IR, and TGA measurements. The ^{1}H-NMR and ^{19}F-NMR spectra of the resulting compounds show the desired

structure (Appendices A and B). Continuous ramp TGA curves (10 ºC/min ramp rate) are shown in Figure 5.3. For PBOX-6FDIAC, a more gradual decline between 100-300 ^{o}C is observed. By analyzing the mass spectrum during the cure (Figure 5.4), cyclization appears to begin above approximately 250 ^{o}C. Thermal cyclization was then examined further by curing at varying constant temperature conditions. From IR analyses, disappearance of the OH peak between 3200 cm^{-1} and 3650 cm^{-1} confirmed cyclization (Figure 5.5). Benzoxazine ring formation is confirmed by the presence of medium-intensity absorption band at 1650 cm^{-1} [11, 12]. The band at 1650 cm^{-1} is most likely due to the formation of the carbon nitrogen double bond. Table 5.1 lists the solubility properties of PBOX-6FDIAC.

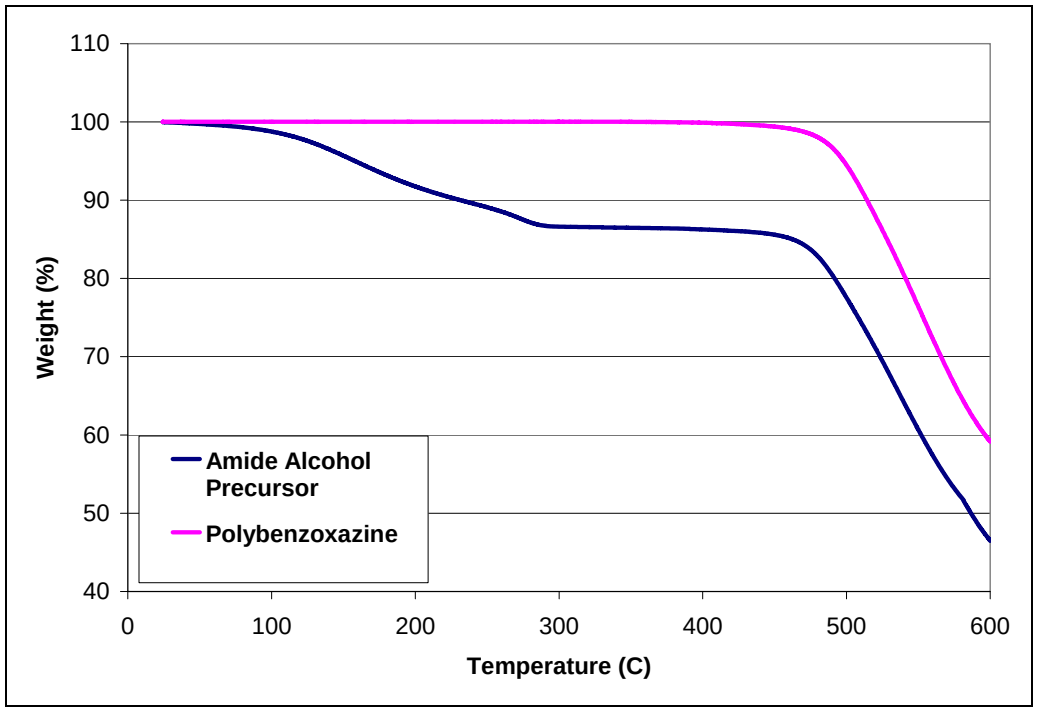

Figure 5.3 TGA curve of PBOX-6FDIAC in nitrogen at a heating rate of 10 ^{o}C/min.

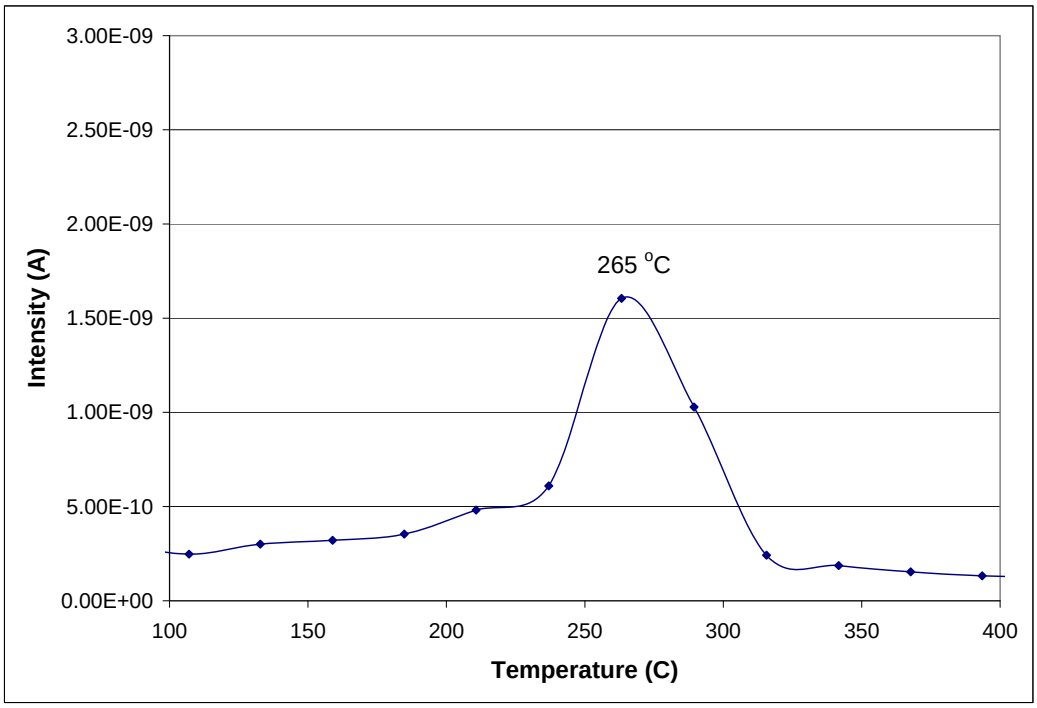

Figure 5.4 TGA-MS of water removed from PBOZ-6FDIAC.

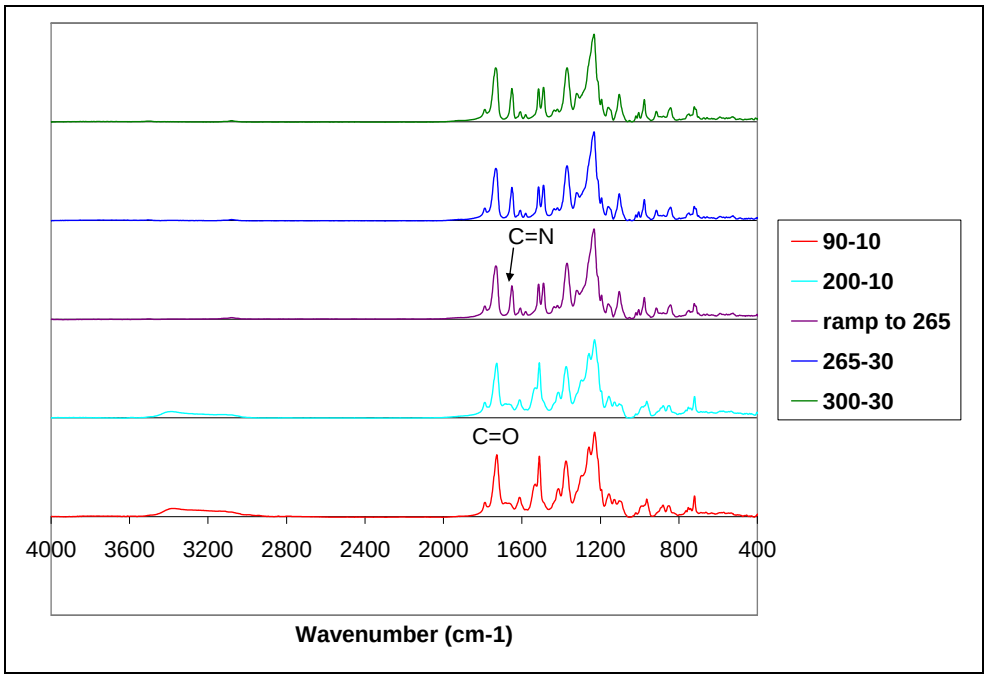

Figure 5.5 FTIR of PBOX-6FDIAC (Temperature (°C)-Time (min.))

Table 5.1 Solubility of the polymer in different solvents.

	Acetone	Methanol	DMF	GBL	PGMEA	THF	0.26N TMAH
PBOX-6FDIAC	√	X	√	√	√	√	√

5.5 Polymer Film Properties

Polymer film properties including dielectric constant (k), thermal expansion coefficient (CTE), glass transition temperature (T_g) and water absorption were examined. All film properties are shown in Table 5.2. As expected, a low value for the polymer dielectric constant was observed due to the presence of hexafluoropropane in the acid chloride. Somewhat more unexpectedly, the presence of imide carbonyl groups does not significantly increase the dielectric constant or water absorption.

Table 5.2 PBOX-6FDIAC properties

Precursor η_{inh} (dL/g)	0.59
M_n / M_w (kg/mol)	18/28.7
Cure Temperature (^oC)	265
Dielectric Constant	2.2
Water Absorption (wt%)	0.60
CTE (ppm/^oC)	74.6
T_g (^oC)	256
T_5/T_{10} (^oC)	498/514
Young's Modulus (GPa)	18.6
DR (nm/sec) 0.26N TMAH	1

The in-plane CTE and T_g were determined by thermomechanical analysis (TMA) using free standing films. From Figure 5.6, PBOX-6FDIAC is shown to have a CTE of 74.6 ppm/^{o}C and a T_g of 256 ^{o}C. The incorporation of an imide into the polymer backbone was pursued due to the high CTE and low T_g found for the polybenzoxazines in

Chapter 4. The presence of an imide helps to both lower the CTE and increase the T_g. Further improvements in the CTE in the materials would be desirable.

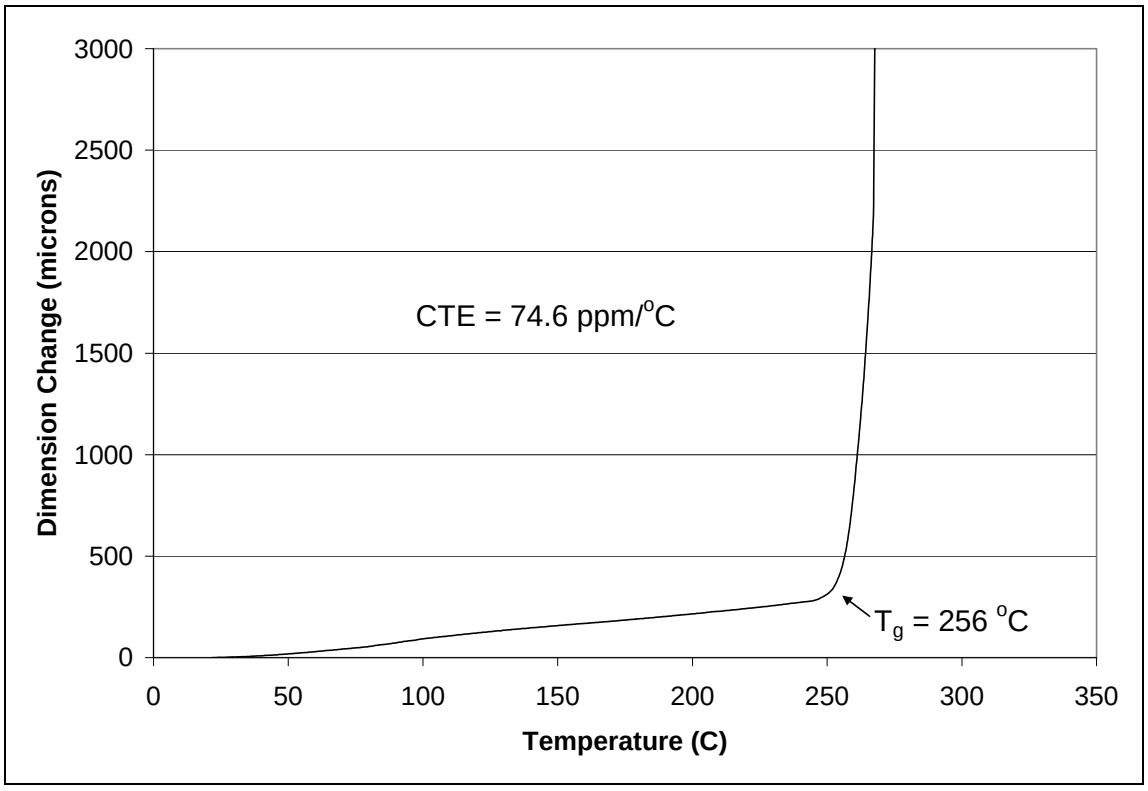

Figure 5.6 TMA data for PBOX-6FDIAC at a heating rate of 10 °C/min.

Figure 5.7 shows an example of a QCM (Quartz Crystal Microbalance) measurement for water absorption and desorption in a film of PBOX-6FDIAC cured at 265 °C for 30 min. The measured difference in QCM frequency between the dry and wet (i.e., exposed to a ~95 % humidity atmosphere) films corresponds to a water absorption value of 0.60 wt%. This value is acceptable for polymer dielectrics and considerably lower than the observed range of water absorption values for polyimides in general which typically range from approximately 1 wt% to 5 wt%.

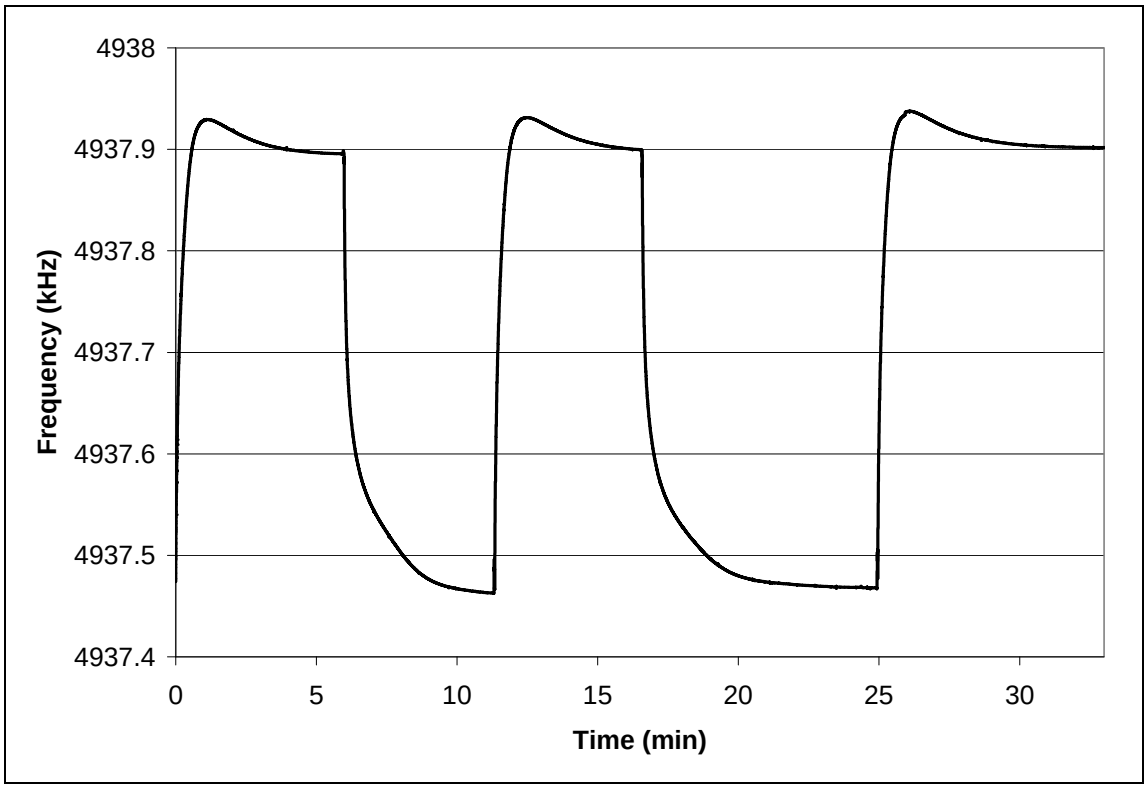

Figure 5.7 QCM measurement of PBOX-6FDIAC cured at 265 ^{o}C for 30 min.

5.6 Formulation of a Photodefinable Polybenzoxazine

Photodefinable polymer formulations were made by loading a trifunctional DNQ inhibitor into the polymers. Figure 5.8 shows a Meyerhofer plot for various loadings of the DNQ in PBOZ-6FDIAC. It is observed the difference between the dissolution rate (DR) of the unexposed and exposed formulation in 0.26N TMAH is a factor of ~100 at a loading of 20 wt% DNQ and a factor of ~400 at a loading of 30 wt% DNQ. This DR contrast is sufficient to allow for production of high resolution photopatterned structures with resolution down to the micron scale and with minimal dark loss.

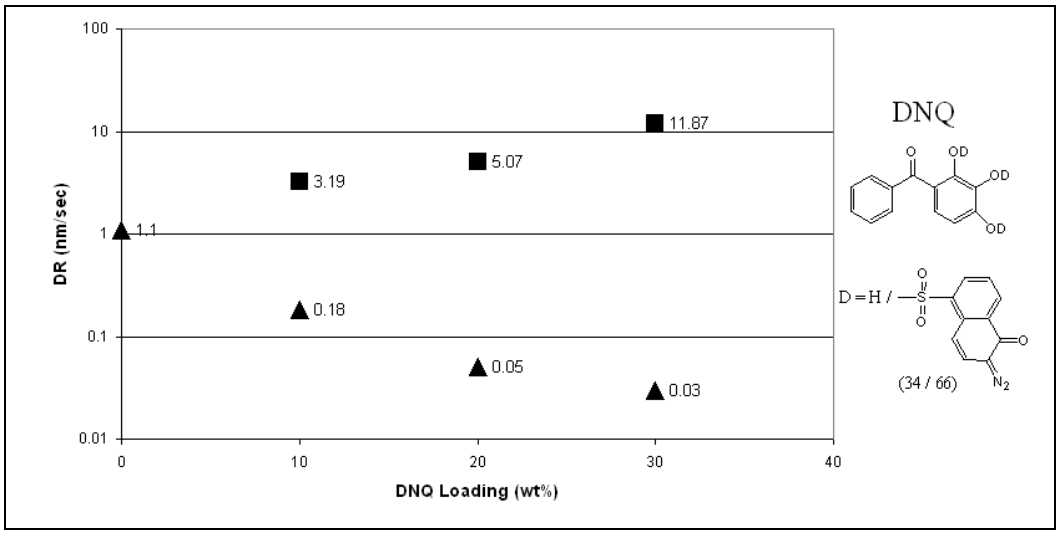

Figure 5.8 Dependence of unexposed (▲) and exposed (■, I-line at 600 mJ/cm^2) DRs onto DNQ loading for PBOX-6FDIAC

Figures 5.9 and 5.10 show SEM pictures of contact-printed images for a 500 nm PBOZ-6FDIAC film obtained from dark and bright field masks which produce dense space and line arrays, respectively. Both resulting images agreed well with mask feature sizes. Representative images are shown of some of the small scale patterns printed in the 30 wt% DNQ loaded PBOZ-6FDIAC (here a 130-μm space feature is shown). No wavy edges or distorted wavy line features were observed in the case of the PBOZ-6FDIAC material, supporting other observations that indicate that this material exhibits little or no swelling during development.

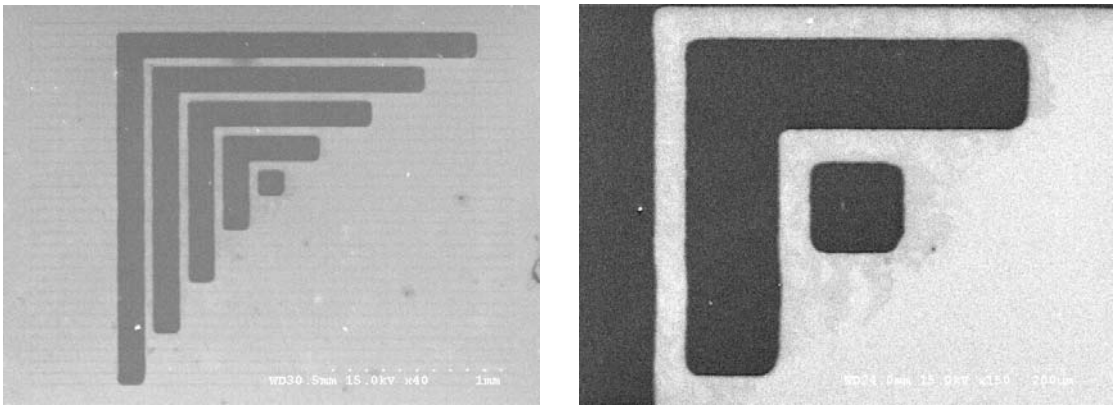

(a) (b)

Figure 5.9 SEM pictures of 30 wt% DNQ-loaded PBOX-6FDIAC at (a) 15.0 kV x40, (b) 15.0 kV x150, obtained by using a dark field mask: exposed at 600 mJ/cm^2, developed with 0.26 N TMAH for 5 min., and then cured at 265 ^{o}C for 30min.

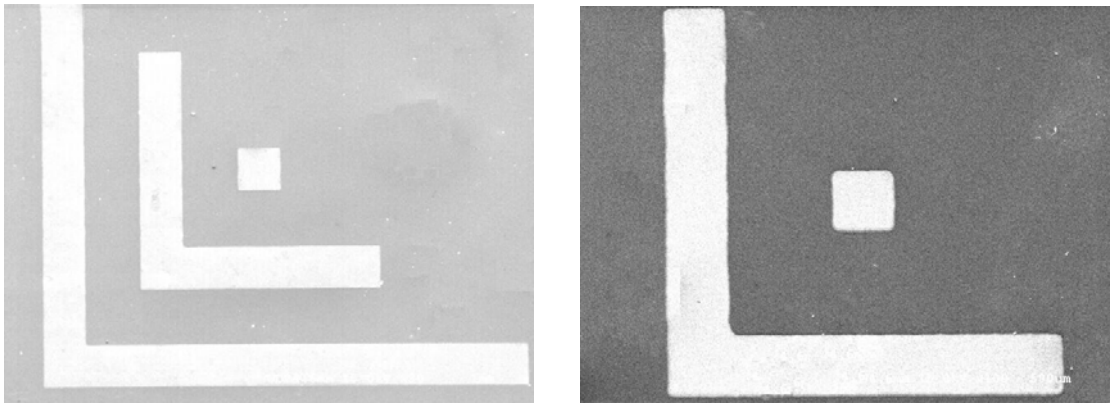

(a) (b)

Figure 5.10 SEM pictures of 30 wt% DNQ-loaded PBOX-6FDIAC at (a) 15.0 kV x30, (b) 15.0 kV x100, obtained by using a bright field mask: exposed at 600 mJ/cm^2, developed with 0.26 N TMAH for 5 min., and then cured at 265 ^{o}C for 30 min.

5.7 Experimental Section

5.7.1 Chemicals

3,3'-Bis(1-hydroxy-1-trifluoromethyl-2,2,2-trifluoroethyl)-4,4'oxydianiline and 2,2-bis(3,4-dicarboxyphenyl)hexafluoropropane dianhydride were provided by Central Glass. Co., Ltd. 4-Amino benzoic acid was purchased from Acros Organics. The DNQ inhibitor used in this work was provided by St-Jean Photochemicals Inc. The TMAH developer solution used in this work was AZ 300 MIF which was provided by AZ Electronic Materials. Other solvents and reagents were purchased from Aldrich and used as-received.

5.7.2 Preparation of 2,2-bis[N-(4-carboxyphenyl)phthalimidyl]-hexafluoropropane (6FDIA)

In a 100-mL flask, 2.497 g (5.6 mmol) of 6FDA, 1.543 g (11.3 mmol) of 4-aminobenzoic acid and 25mL of glacial acetic acid were added and stirred under nitrogen at 120 ^{o}C. After 15 min, a solution had formed. After 3.5 hrs, a white precipitate formed. The reaction was carried out for another 24 hrs. The precipitate was filtered, washed with DI water and dried at 120 ^{o}C for 3 hrs. The white powdery product was 3.580 g: yield 93.3 %; ^{1}H-NMR (Appendix A.16, DMSO-d_6) δ 8.17-8.20 (d, 2H, Ar-H), 8.07-8.10 (d, 4H, Ar-H), 7.94-7.97 (d, 2H, Ar-H), 7.75 (s, 2H, Ar-H), 7.57-7.60 (d, 4H, Ar-H), 3.38 (s, 2H, COOH) ppm.

5.7.3 Preparation of 2,2-bis[N-(4-chlorocarboxyphenyl)phthalimidyl]-hexafluoropropane (6FDIAC)

In a 100-mL flask, 1.002 g (1.5 mmol) of 6FDIA, 1 drop of pyridine and 5mL of thionyl chloride were added and stirred under nitrogen at 90 ^{o}C for 12 hrs. The mixture was cooled, filtered, washed with dry hexane and dried in a vacuum desiccator for 3 hrs. The white powdery product was 0.842 g: yield 79.9 %; ^{1}H-NMR (Appendix A.17, DMSO-d_6) δ 8.17-8.20 (d, 2H, Ar-H), 8.05-8.08 (d, 4H, Ar-H), 7.93-7.96 (d, 2H, Ar-H), 7.74 (s, 2H, Ar-H), 7.56-7.58 (d, 4H, Ar-H) ppm.

5.7.4 Preparation of PBOX-6FDIAC

In a 100-mL three-neck flask, 0.603 g (1.1 mmol) of HFA-ODA and 4.2mL of DMAc were stirred under nitrogen at r.t. When a solution was reached, the flask was lowered into an ice water bath. After the solution was cooled, 0.812 g (1.1 mmol) of 6FDIAC and 1.5mL of DMAc were added. The ice water bath was removed after one hour. Once removed, the solution viscosity appeared to slowly increase. The solution was stirred for 24 hrs. The reaction solution was poured into methanol, precipitating a polymer. The polymer was collected by filtration, and then dried under vacuum drying overnight at 100 ^{o}C. The yield was 96.2% (1.281g). An inherent viscosity (η_{inh}) was 0.59 dL/g at a concentration of 0.5 g/dL in NMP at 25 ^{o}C; ^{1}H-NMR (Appendix A.18, DMSO-d_6) δ 10.68 (br, 2H, amide-H), 10.51 (s, 2H, HFA-OH), 8.45-8.47 (d, 2H, Ar-H), 8.21-8.23 (d, 2H, Ar-H), 7.97-8.03 (2d, 6H, Ar-H), 7.77 (s, 2H, Ar-H), 7.65-7.68 (d, 4H, Ar-H), 7.36-7.39 (d, 2H, Ar-H), 7.10 (s, 2H, Ar-H) ppm; ^{19}F-NMR (Appendix B.5, DMSO-d_6) δ -63.28 (s, 6F, hexafluoroisopropylidene-F), -73.36 (s, 12F, HFA-F) ppm.

5.7.5 Lithographic Characterization

For generation of the Meyerhofer plot (see Figure 5.8) and patterned materials (see Figures 5.9, 5.10), solutions of DNQ loaded in the copolymer was made in PGMEA at 20 wt% total solids. Silicon wafers were primed with polyimide to improve adhesion of the polymer film onto the substrate. Photosensitive copolymer solutions were spin coated onto the treated Si wafers at 4000 rpm for 30 sec, then soft baked at 110 ^{o}C for 3 min. After exposure and post-exposure baking at 110 ^{o}C for 3 min, films were developed in 0.26 N TMAH for 300 sec, rinsed with water, and then cured at 265 ^{o}C for 30 min.

5.8 Summary

A novel, low dielectric photodefinable copolymer was successfully prepared. The resulting amid alcohol precursor showed good solubility in common organic solvents including acetone, THF, PGMEA, GBL, DMF and 0.26 N TMAH. The copolymer was shown to have a higher T_g and lower CTE than previous polybenzoxazines analyzed. A photosensitive composition based on the PBOX-6FDIAC polybenzoxazine precursor loaded with a trifunctional DNQ inhibitor was found to serve as an excellent positive-tone photodefinable polybenzoxazine using standard 0.26N TMAH developer. During development, it was shown that there is little or no swelling in this material. Unlike traditional dielectric polymer precursors, thermal curing is shown to be achievable in polybenzoxazines at 265 ^{o}C. Thermal curing renders the polymer insoluble in aqueous developers and produces a polymer with a low dielectric constant and low water absorption.

5.9 References

1. Hergenrother, P.M., et al., *Copolyimides from 2,3,3',4'-biphenyltetracarboxylic dianhydride and pyromellitic dianhydride with 4,4'-oxydianiline.* Polymer FIELD Full Journal Title:Polymer, 2004. **45**(16): p. 5441-5449.

2. Kuo, S.-W., et al., *Synthesis, thermal properties, and specific interactions of high Tg increase in poly(2,6-dimethyl-1,4-phenylene oxide)-block-polystyrene copolymers.* Polymer FIELD Full Journal Title:Polymer, 2005. **46**(22): p. 9348-9361.

3. Bruma, M., et al., *Synthesis and characterization of fluorinated poly(imide-amide-sulfone)s.* J. Appl. Polym. Sci. FIELD Full Journal Title:Journal of Applied Polymer Science, 1995. **56**(5): p. 527-32.

4. Bruma, M., et al., *Fluorinated poly(benzoxazole-imide)s.* Polym. Adv. Technol. FIELD Full Journal Title:Polymers for Advanced Technologies, 1994. **5**(9): p. 535-40.

5. Bruma, M., B. Schulz, and F.W. Mercer, *Synthesis and characterization of fluorinated poly(imide-pyridazine-amide)s.* Polymer FIELD Full Journal Title:Polymer, 1994. **35**(19): p. 4209-14.

6. Hamciuc, C., et al., *New fluorinated poly(imide-ether-amide)s.* High Perform. Polym. FIELD Full Journal Title:High Performance Polymers, 2000. **12**(2): p. 265-276.

7. Hamciuc, E., et al., *Fluorinated heterocyclic polyamides.* Eur. Polym. J. FIELD Full Journal Title:European Polymer Journal, 2000. **37**(2): p. 287-293.

8. Hamciuc, E., et al., *Synthesis and study of new fluorinated poly(imide-amide)s.* Macromol. Mater. Eng. FIELD Full Journal Title:Macromolecular Materials and Engineering, 2000. **283**: p. 36-40.

9. Irvin, D.J., et al., *N-methylated copoly(imide amide)s containing hexafluoroisopropylidene.* Polymer FIELD Full Journal Title:Polymer, 1996. **37**(11): p. 2227-2232.

10. Lavrenko, P., et al., *Conformational and dynamo-optical properties of fluorinated poly(p-phenylene-1,3,4-oxadiazole-imide-amide) molecules in solutions.* Polymer FIELD Full Journal Title:Polymer, 2003. **44**(10): p. 2919-2925.

11. Chang, J.-H., et al., *Two-step thermal conversion from poly(amic acid) to polybenzoxazole via polyimide: their thermal and mechanical properties.* Journal of Polymer Science, Part B: Polymer Physics, 2000. **38**(19): p. 2537-2545.

12. Chen, X., M. Anthamatten, and D.R. Harding, *Vapor deposition and curing of polybenzoxazole precursors.* Macromolecules, 2006. **39**(22): p. 7561-7565.

CHAPTER 6

PHOTODEFINABLE POLYIMIDE WITH ACID LABILE PROTECTING GROUP

6.1 Introduction

From the previous chapters, there continues to be a need for a polymer that can be photopatterned and cured under 200 ^{o}C. One method of producing such a polymer is to protect the alcohol with an acid labile protecting group. In this chapter, a combination of the novel HFA-substituted diamine monomer with a fluorinated dianhydride was used to synthesize novel thermoplastic polyimides. Dehydration of the carboxylic acid situated ortho to the amide forming an imide ring was performed in solution to remove the need to process at high temperatures once the polymer is applied. The HFA polyimide can be cast in its current state with DNQ or can be protected and subsequently deprotected with a photoacid generator (PAG) to produce a polyimide with a lower dielectric constant and water absorption. Chemically amplified polyimides have been reported in the literature [1, 2].

In contrast to the reported polymers in this thesis which cyclize at temperatures above 200 ^{o}C, the new polymers reported here can be processed at temperatures below 200 ^{o}C. This substantially improves the integration of these polymers into a wider variety of materials such as liquid crystal displays. The polyimides in this chapter exhibit good solubility in a variety of different casting solvents including THF, PGMEA, GBL, DMF, and have also shown selective solubility in 0.26 N TMAH. Characterization

of the physiochemical properties of these polyimide materials are presented including polymer structures, dielectric constants, coefficients of thermal expansion, and lithographic characteristics.

6.2 Polymer Synthesis

As shown in Figure 6.1, polymerization of 3,3'-bis(1-hydroxy-1-trifluoromethyl-2,2,2-trifluoroethyl)-4,4'oxydianiline (HFA-ODA) with 2,2-bis(3,4-dicarboxyphenyl) hexafluoropropane dianhydride (6FDA) to form poly(amic acid) **6.1** was carried out in NMP for 24 hours. Following polymerization, the temperature was increased to 200 ^{o}C for 8 hours to complete imidization of polymer **6.1** to form polyimide **6.2**. The solution was poured into a mixture of methanol and water to precipitate the product. For protection, the polymer was dissolved in THF with isopropyl chloroformate and TEA to form a salt from the generated hydrochloric acid to form an isopropoxycarbonyl (i-POC) protecting group. The reaction was run for 24 hours at room temperature. The solution was poured into methanol to precipitate polymer **6.3**.

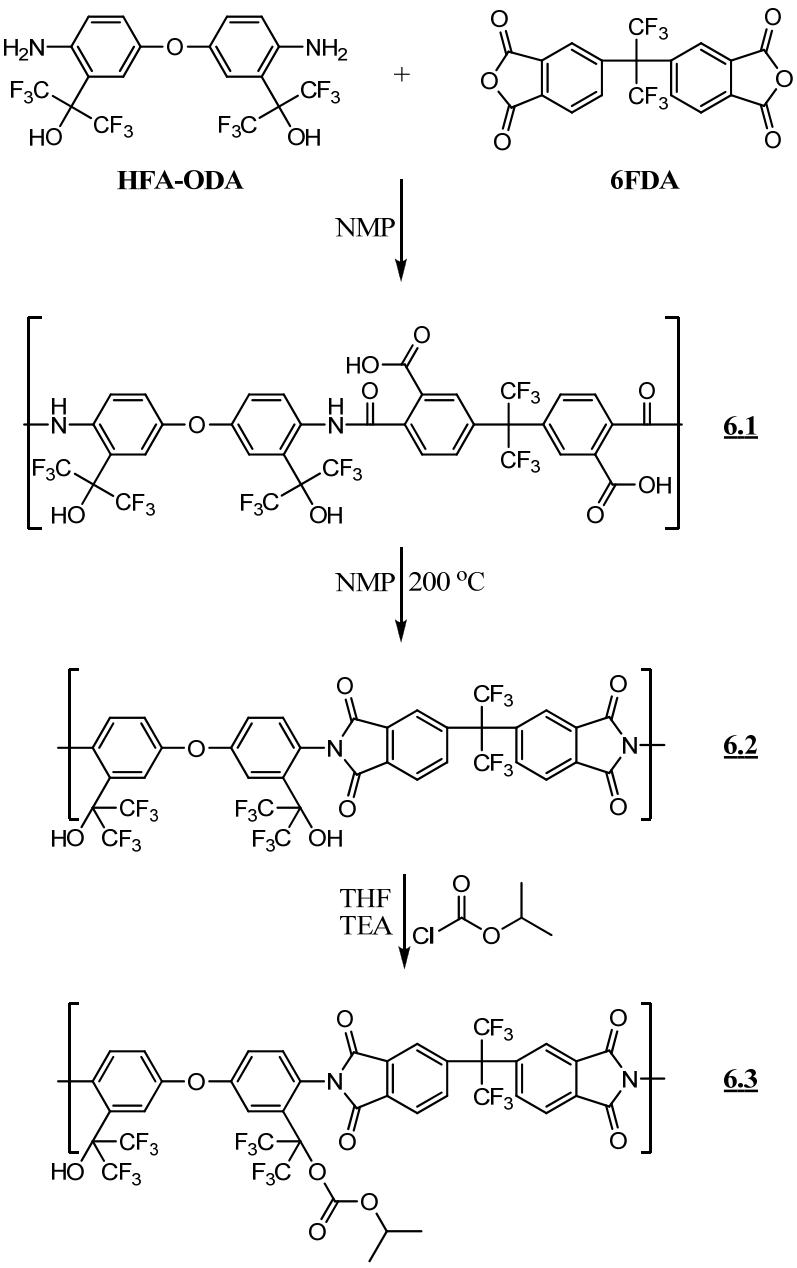

Figure 6.1 Polymerization and protection to form polymer **6.3**

6.3 Polymer Characterization

The polymer structures were characterized by NMR, FTIR, and TGA measurements. The ^{1}H-NMR and ^{19}F-NMR spectra of the resulting compounds show the desired structures (Appendices A and B). Continuous ramp TGA curves (10 ºC/min

ramp rate) are shown in Figure 6.2 for polymers **6.2** and **6.3**. Weight loss from the removal of the i-POC protecting group can be seen above 230 °C for polymer **6.3**. TGA measurements conclude polymer **6.3** lost 10 % of its weight during the first weight loss which corresponds to 50 % protection of the HFA in polymer **6.2**. This result is in agreement with the protection observed in the ^{19}F-NMR spectrum. The second weight loss above 350 °C for both polymers is from cyclization of the HFA to form a benzoxazine ring which releases carbon dioxide as illustrated in Figure 6.3. Cyclization of alcohols situated ortho to the imide ring to form polybenzoxazoles has been well documented [3-7]. In the case of polymers **6.2** and **6.3**, the polybenzoxazine formed is structurally identical to PBOX-6FDC.

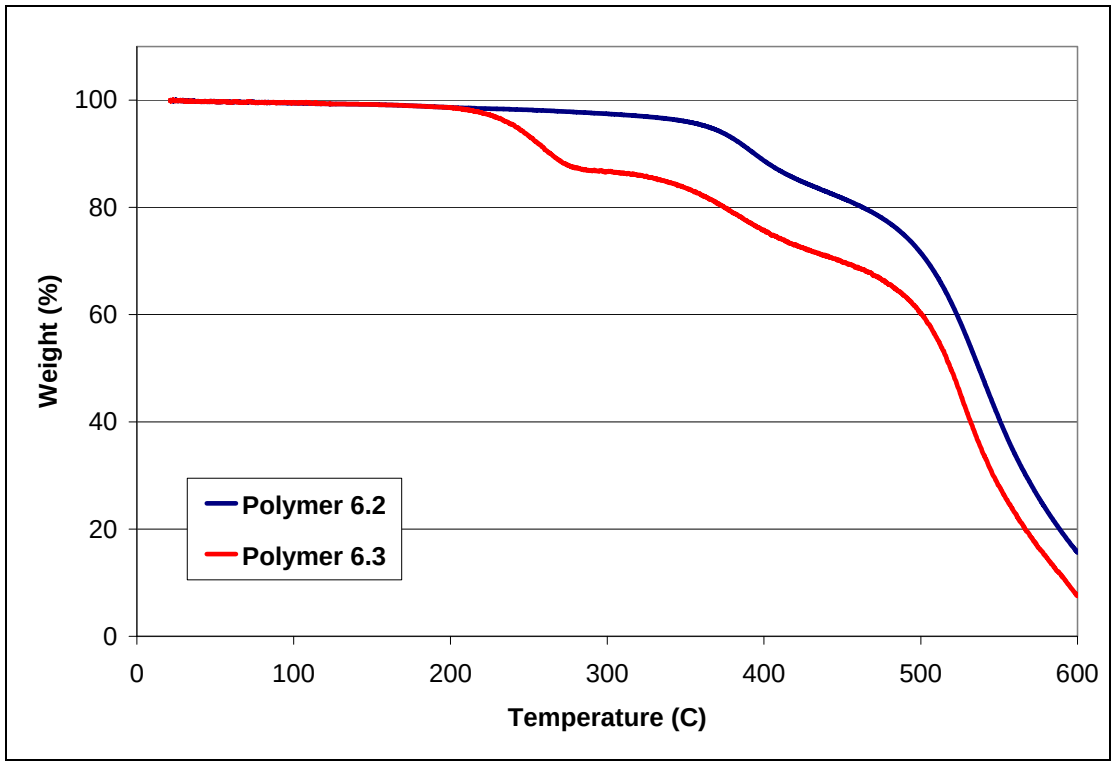

Figure 6.2 TGA curves in air at a heating rate of 10 °C/min for polymers **6.2** and **6.3**

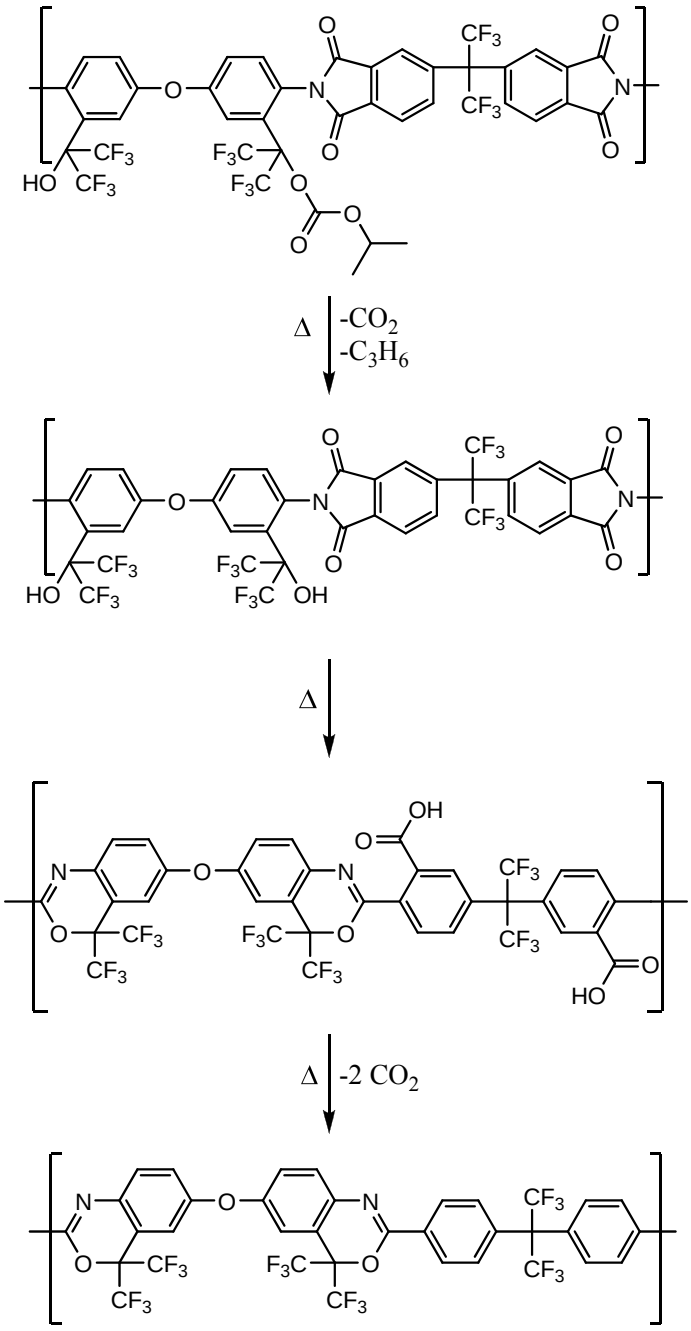

Figure 6.3 Thermal degradation of polymer **6.3** to form PBOX-6FDC

From IR analyses, a noticeable decrease in the HFA peak is observed for the protected polymer **6.3** between 3000 cm^{-1} and 3600 cm^{-1} (Figure 6.4). For polymer **6.3**, the peak at 2980 cm^{-1} is most likely alkane stretching from the isopropyl groups.

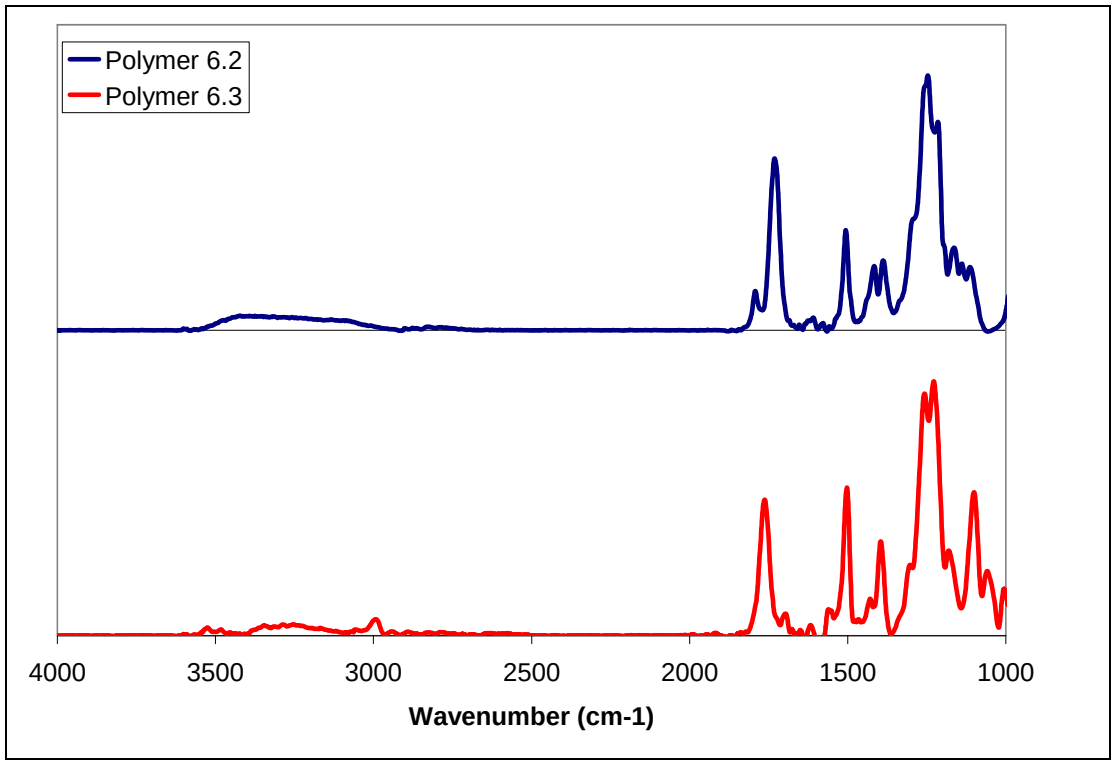

Figure 6.4 FTIR of Polyimides

Table 6.1 lists the solubility properties of the two polyimides. Although polymer **6.3** is shown to be insoluble in 0.26N TMAH, acid catalyzed deprotection of enough of the i-POC protecting groups produces a soluble polymer.

Table 6.1 Solubility of the various polybenzoxazines in different solvents.

Polymer	Acetone	Methanol	DMF	GBL	PGMEA	THF	0.26N TMAH
6.2	√	√	√	√	√	√	√
6.3	√	X	√	√	√	√	X

6.4 Polymer film properties

Polymer film properties including dielectric constant, CTE, T_g, and water absorption were examined. All film properties are shown in Table 6.2. Protection of the

HFA produces a polymer with a much lower dielectric constant. One advantage to polymer **6.3** is that along with the alcohol protection, the large fluorine presence serves to aid in producing a polymer with a desirable dielectric constant. Unfortunately, it was originally theorized that the six fluorine atoms surrounding the alcohol would serve to prevent the alcohol from increasing the dielectric constant. It was shown that removal of the HFA side group produces a polymer with a lower dielectric constant even though the fluorine content has been considerably reduced. The resulting dielectric constant in polymer **6.3** further serves to disprove the theory that hexafluoroalcohols can produce low dielectric constant polymers without protection.

Table 6.2 Polymer properties

Polymer	**6.2**	**6.3**
Precursor ηinh (dL/g)	0.17	0.16
Dielectric Constant	3.0	2.5
Water Absorption (wt %)	4.9	2.6
CTE (ppm/^{o}C)	47.4	84.5
T_g (^{o}C)	250	>220
T_5/T_{10} (^{o}C)	364/394	242/264
Young's Modulus (GPa)	8.4	6.4

The large presence of fluorine in polymer **6.2** led to a belief that it would have a lower dielectric constant. As expected, a substantial reduction in the polymer dielectric constant was observed with protection of the HFA. Based on the data collected, further protection of the HFA can produce a polymer with a lower dielectric constant.

Figure 6.5 shows the QCM measurements for polymers **6.2** and **6.3**. The measured difference in QCM frequency between the dry and wet (i.e., exposed to a ~95 % humidity atmosphere) films corresponds to a water absorption value of 4.9 wt% for polymer **6.2** and 2.6 wt% for polymer **6.3**. These values are not desirable for polymer

dielectrics but do fall in the observed range of water absorption values for polyimides in general which typically range from approximately 1 wt% to 5 wt%. By protecting 50 % of the HFA in the polymer, the water absorption was nearly cut in half. Based on the low water absorption observed for polybenzoxazines, further protection can further lower the water absorption

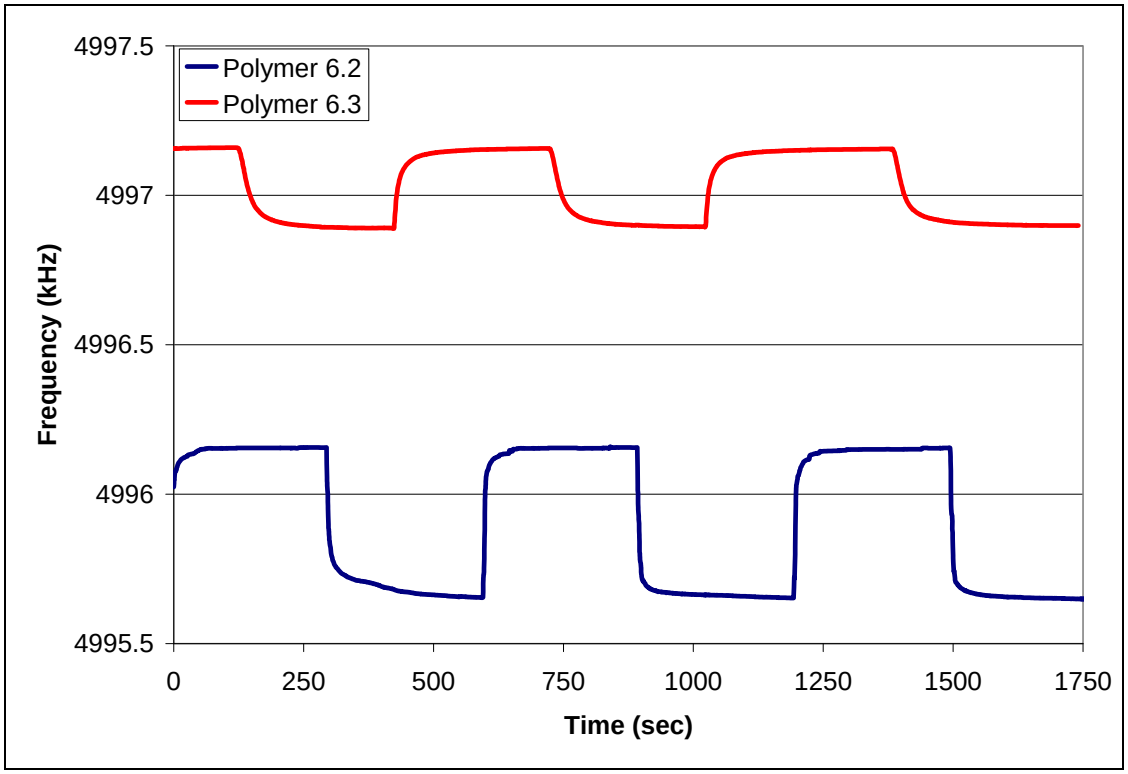

Figure 6.5 QCM measurement for polymers **6.2** and **6.3** cured at 80 ^{o}C.

Using a thermoplastic Poisson's ratio of 0.33, the through plane CTE for both polyimides was determined with results shown in Figure 6.6. Although polymer **6.3** has a CTE of 84.5 ppm/^{o}C which is typical for similarly structured polymers, polymer **6.2** has the unique characteristic of having a low CTE of 47.4 ppm/^{o}C. Thermal expansion is a unique quality in which the mismatch between layers is the issue of importance, not the

overall value. A low CTE is desired if the polymer is adjacent to silicon because of silicon's low CTE. Polyimides are known to have low CTEs because of the imide's planarization. It is reasonable to expect that the introduction of the iPOC functionality diminishes this planarization leading to a higher CTE.

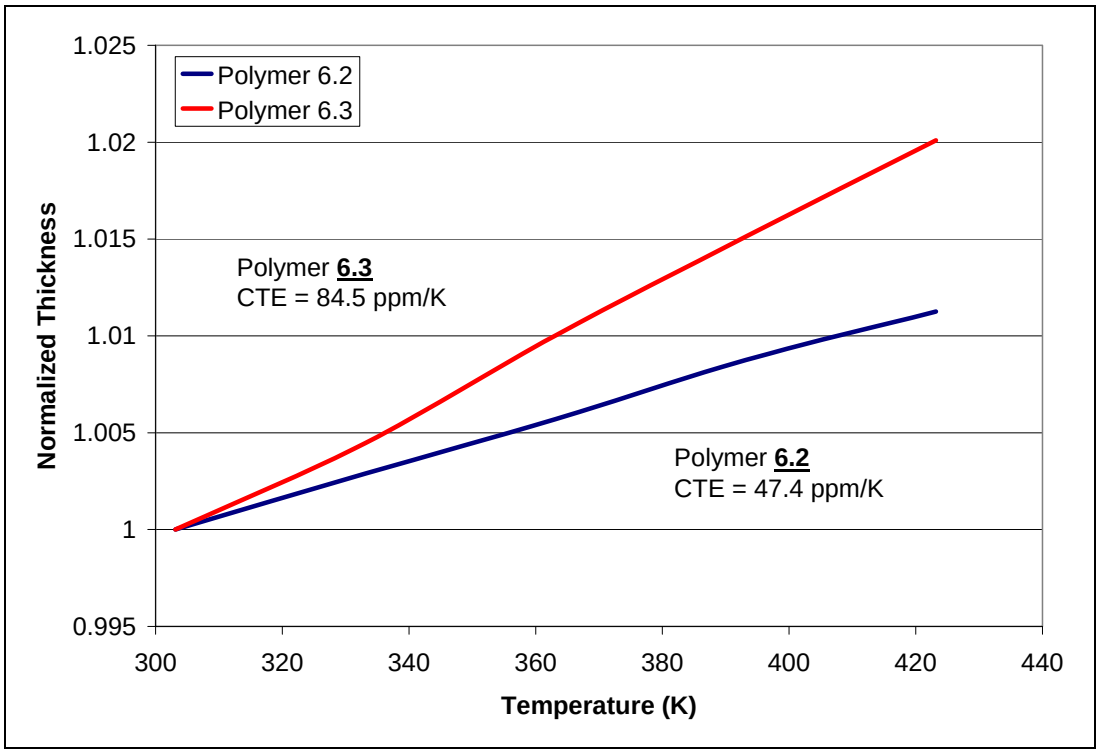

Figure 6.6 Ellipsometry data for polymers **6.2** and **6.3**

The Young's modulus of the polyimides is different from the results of the previous tests. In previous chapters, the Young's modulus was dependent on the amount of fluorine in the polymer backbone. Both polyimides reported have eighteen fluorines which match that of all polymers with fluorine in the diacid chloride or dianhydride; however, those polymers had a Young's modulus above 17 GPa. These polyimides have a Young's modulus that more resembles that of the non-fluorinated polybenzoxazines.

Both polyimides do have a high enough Young's modulus to be used in electronic packaging. In addition, the low modulus might serve to help the overall stress product to avoid cracking when stress as a result of thermal expansion is taken into consideration.

6.5 Formulation of a Photodefinable Polyimide

Photodefinable polyimide formulations were made by loading a trifunctional DNQ inhibitor into the polyimide. A film thickness of polymer **6.2** showed uniform decrease over developing time starting from the initial FT of 1.5 μm. The dissolution rate was calculated to be 17 nm/sec. Figure 6.7 shows a Meyerhofer plot for various loadings of the DNQ in polymer **6.2**. As can be seen in Figure 6.7, dissolution rates after I-line exposure dramatically changed to 120 nm/sec and 200 nm/sec for 20 wt% and 30 wt% DNQ loaded polymer **6.2**. On the other hand, unexposed rates were 10 nm/sec and 6 nm/sec which show a weak inhibition effect. It is observed the difference between the dissolution rate of the unexposed and exposed formulation in 0.26N TMAH is a factor of ~12 at a loading of 20 wt% DNQ and a factor of ~33 at a loading of 30 wt% DNQ.

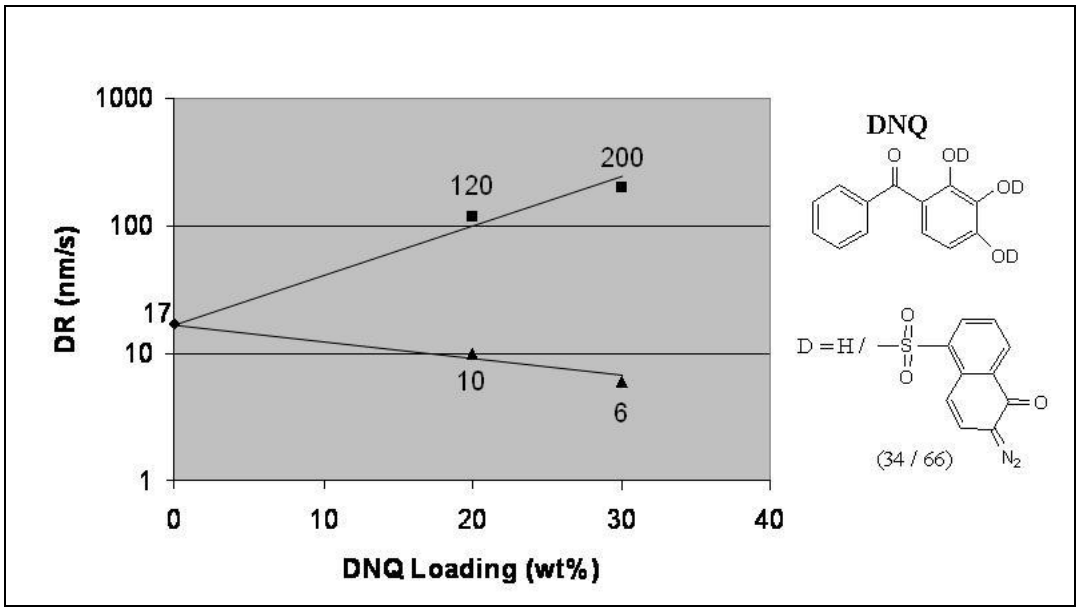

Figure 6.7 Dependence of unexposed (▲) and exposed (■, I-line at 500 mJ/cm^2) DRs on DNQ loading for polymer **6.2**

Figure 6.8 shows optical microscope pictures of contact-printed images for a micron thick film of **6.2** obtained from dark and bright field masks. Both resulting images agreed well with mask feature sizes.

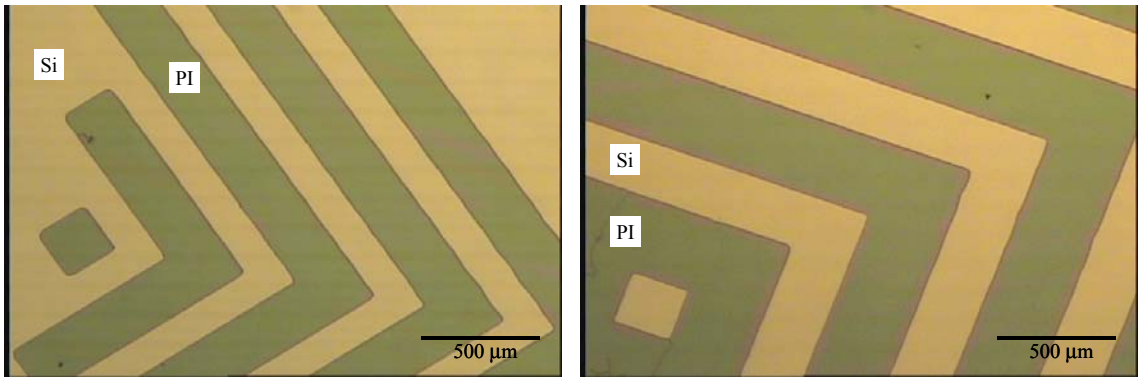

(a) (b)

Figure 6.8 Optical microscopic pictures of 20wt% THBP-loaded polymer **6.2** obtained by using (a) a bright field mask and (b) a dark field mask: exposed at 500 mJ/cm2, developed in 0.26 N TMAH for 50 sec., and then cured at 120 ^{o}C for 3 min.

Even though DNQ-loaded polymer **6.2** does not show significant contrast, a photopatterning experiment with quick development is shown in Figure 6.8. Figure 6.8 illustrates optical microscopic pictures obtained from 20wt% THBP-loaded polymer **6.2**, where both film thicknesses were measured to be 0.9 μm. These resulting thicknesses were also estimated to be 65 % of the initial FT of 1.4 μm. From Figure 6.8, there appears to be no swelling as a result of development. These pictures agree with results from the DRM.

From the point of view to decrease the dissolution rate of pure polymer, copolymerization with 2,2'-bis(trifluoromethyl)-4,4'-diaminobenzene (TFDB) was examined. Copolymerization reaction smoothly proceeded and produced polymers with a composition ratio of 45 / 55 and 70 / 30 for HFA-ODA / TFDB (Table 6.3). As expected, the dissolution rates were surely strongly dependent onto the content of HFA-OH. Photo-formulation experiments were also examined for copolyimides by means of DNQ. In contrast to polymer **6.2**, exposed dissolution rates for the copolymers increased only up to 1 nm/sec and 9 nm/sec. Absorbance spectra for polymer **6.2** loaded with 20 wt% of DNQ was investigated. The photoreaction (bleach) of DNQ was clearly detected for the spectrum after exposure at 500 mJ/cm^2 (spectrum (d)) compared to that before exposure (spectrum (b)) in Figure 6.9.

Table 6.3 Polymer dissolution properties

Polymer (HFA-ODA / TFDB)	ηinh (dL/g)	DR (nm/sec)	DR with DNQ[a]
45 / 55	0.28	0.3	- / 1
70 / 30	0.24	4.1	2 / 9
100 / 0	0.17	17	10 / 120

a) Measured for 20 wt% THBP loaded photosensitive compositions (unexposed / exposed using I-line at 500 mJ/cm^2)

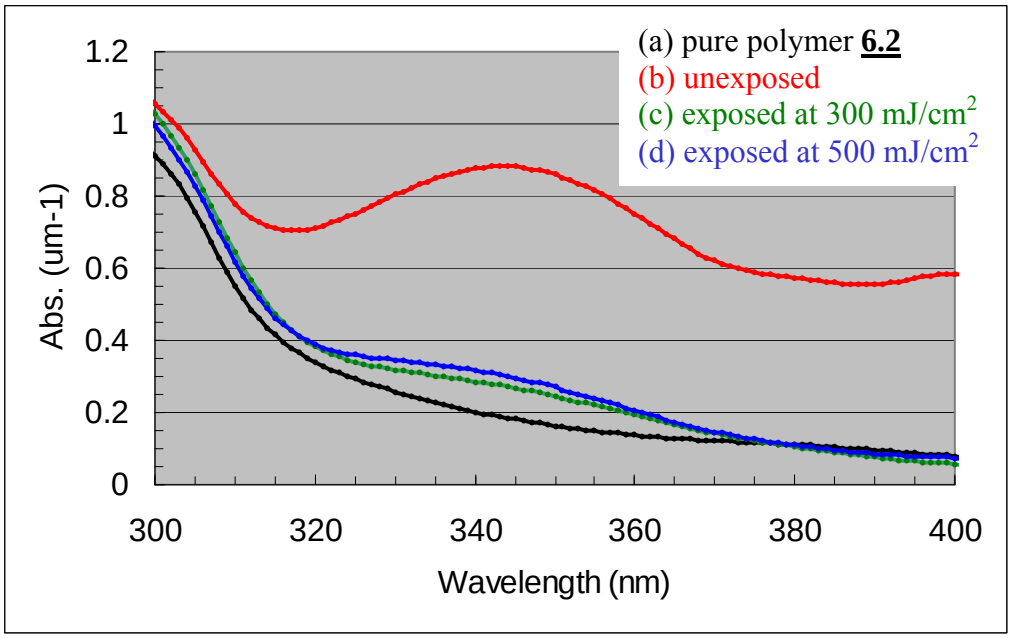

Figure 6.9 Absorbance spectra for polymer **6.2** loaded with DNQ

In order to get the dissolution contrast enough for photopatterning experiment, the protection of the hexafluoroisopropanol in polymer **6.2** with an acid labile group was examined. Methoxymethyl (MOM) protection reaction of polymer **6.2** was carried out in the presence of MOM-Cl and NaH using THF solvent. In ^{1}H-NMR spectrum, a resulting product contained a peak at 4.8 ppm assigned to methylene proton in MOM group, and another broad peak in the range of 9.5-10.2 ppm as well. The integration analysis of the methylene proton turned out to be the MOM-protection of 55 % (i.e., HFA-OH / HFA-OMOM = 45 / 55). However, this product was found to be quite soluble in 0.26 N TMAH. Both findings of good solubility in TMAH and the broad peak shown in 9.5-10.2 ppm might imply that an amic-acid structure was regenerated by opening an imide ring during the reaction.

The *tert*-butoxycarbonyl (t-BOC) protection of polymer **1** was also demonstrated with $(t\text{-}BOC)_2O$ and catalytic amount of pyridine. For ^{1}H-NMR spectrum of a resulting product, the proton from t-BOC group was clearly observed at 1.23 ppm, where the t-BOC protection was calculated to be 27-28 %. In the dissolution test of the film into 0.26 N TMAH, the film thickness decrease was observed with 2 nm/sec up to 60 sec (i.e., at the point of remaining film thickness of 450 nm) starting from an initial film thickness of 570 nm, and then the following film thickness increase (i.e., swelling) was observed up to the end (260 sec.). We confirmed the dissolution behavior of t-BOC protected polymer **6.2** was different from polymer **6.2**, although the polymer still had not sufficient t-BOC protection.

Polymer **6.2** was finally protected with i-POC. The use of i-POC was selected because it poses more thermal stability than t-BOC but can still be photochemically cleaved. This is due to the lower stability of the secondary carbocation as compared to a tertiary carbocation [8]. From ^{1}H-NMR and ^{19}F-NMR, 50 % protection has been achieved. Literature has shown this carbonate can be cleaved with a PEB as low as 130 ^oC [9]. With a PEB of 150 ^oC, a dissolution rate of 5.2 nm/sec is observed. Using a higher PEB will promote dissolution as a result of acid diffusion but the goal of this research was to make a polymer that has as low a cure temperature as possible; therefore, 150 ^oC was selected as the PEB. Triphenylsulfonium hexafluoroantimonate was loaded in polymer **6.3** (10 wt% PAG, 90 wt% **6.3**) in PGMEA at 20 wt% total solids. Silicon wafers were primed with hexamethyldisilizane. The polymer **6.3** solution was spin coated onto the treated Si wafers at 1000 rpm for 30 sec, then soft baked at 150 ^oC for 3 min. After exposure and post-exposure baking at 150 ^oC for 5 min, films were developed

in 0.26 N TMAH for 5 min, rinsed with sonicating water, and then cured at 150 ^{o}C for 3 min. Figure 6.10 shows optical microscope pictures of contact-printed images for a 750 nm thick film of **6.3** obtained from dark and bright field masks. Both resulting images agreed well with mask feature sizes.

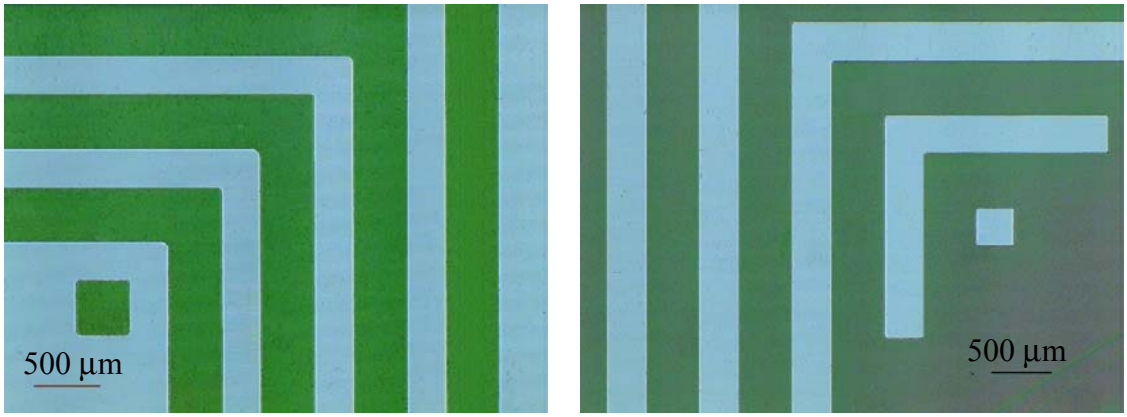

(a) (b)

Figure 6.10 Optical microscopic pictures of 10wt% PAG-loaded polymer **6.3** obtained by using (a) a bright field mask and (b) a dark field mask: exposed at 5 J/cm2, 5 min. PEB, developed with 0.26 N TMAH for 5 min., and then cured at 150 ^{o}C for 3 min.

Figure 6.10 illustrates optical microscopic pictures obtained from 10wt% PAG-loaded polymer **6.3**, where both film thicknesses were measured to be 0.75 µm. These resulting thicknesses were also estimated to be 100 % of the initial film thickness because polymer **6.3** is insoluble in developer. From Figure 6.10, there appears to be no swelling as a result of development.

6.5 Experimental Section

6.5.1 Chemicals

3,3'-Bis(1-hydroxy-1-trifluoromethyl-2,2,2-trifluoroethyl)-4,4'oxydianiline, 2,2-bis(3,4-dicarboxyphenyl) hexafluoropropane dianhydride, and 2,2'-bis(trifluoromethyl)-4,4'-diaminobenzene were provided by Central Glass. Co., Ltd. The DNQ inhibitor used in this work was provided by St-Jean Photochemicals Inc. The PAG triphenylsulfonium hexafluoroantimonate was provided by Midori Kagaku Co., Ltd. The TMAH developer solution used in this work was AZ 300 MIF which was provided by AZ Electronic Materials. Other solvents and reagents were purchased from Aldrich and used as-received.

6.5.2 Preparation of Polymer 6.2

In a 100-mL three-neck flask, 2.001 g (3.76 mmol) of HFA-ODA and 12 mL of N-methyl-2-pyrrolidone (NMP) were stirred under nitrogen at r.t. When a solution was reached, the flask was lowered into an ice water bath. After the solution was cooled, 1.668 g (3.76 mmol) of 6FDA and 3 mL of NMP were added. The solution was stirred for 24 hrs and slowly warmed to r.t. The solution was then raised to 200 ^{o}C for 8 hrs. The reaction solution was poured into 400 mL of a mixture (1:1, v/v) of methanol and water, precipitating a polymer. The polymer was collected by filtration, and then dried under vacuum drying overnight at 80 ^{o}C. The yield was 76.3 % (2.695 g). An inherent viscosity (η_{inh}) was 0.17 dL/g at a concentration of 0.5 g/dL in NMP at 30 ^{o}C; ^{1}H-NMR (Appendix A.20, DMSO-d_6) δ 8.76 (s, 2H, HFA-OH), 8.21-8.23 (d, 2H, Ar-H), 7.93 (s, 2H, Ar-H), 7.75-7.77 (d, 2H, Ar-H), 7.69-7.71 (d, 2H, Ar-H), 7.51-7.53 (d, 2H, Ar-H),

7.28 (s, 2H, Ar-H) ppm; ^{19}F-NMR (Appendix B.7, DMSO-d_6) δ -63.19 (s, 6F, hexafluoroisopropylidene-F), -73.70-73.79 (d, 12F, HFA-F) ppm.

6.5.3 Preparation of Polymer 6.3

In a 100-mL flask, 2.004 g (2.12 mmol) of polymer **6.2** and 20 mL of THF were stirred under nitrogen at r.t. When a solution was reached, 5.2 mL (1 M in toluene) of isopropyl chloroformate and 1 mL of TEA were added. The solution was stirred for 24 hrs. The reaction solution was poured into methanol, precipitating a polymer. The polymer was collected by filtration, and then dried under vacuum drying overnight at 80 ^{o}C. The yield was 91.1 % (1.992 g). An inherent viscosity (η_{inh}) was 0.16 dL/g at a concentration of 0.5 g/dL in NMP at 30 ^{o}C; ^{1}H-NMR (Appendix A.21, $CDCl_3$) δ 8.26-8.29 (d, 2H, Ar-H), 8.17-8.20 (d, 2H, Ar-H), 7.93-8.00 (d, 2H, Ar-H), 7.76 (s, 2H, Ar-H), 7.37 (s, 4H, Ar-H), 4.69-4.85 (q, 1H, Ar-H), 1.17-1.23 (d, 6H, Ar-H) ppm; ^{19}F-NMR (Appendix B.8, $CDCl_3$) δ -63.73 (s, 6F, hexafluoroisopropylidene-F), -72.12 (s, 6F, HFiPOC-F), -77.24-77.38 (d, 6F, HFA-F) ppm.

6.5.4 Lithographic Characterization

For generation of the Meyerhofer plot (see Figure 6.7) and DNQ patterned materials (see Figure 6.8), solutions of DNQ loaded in polymer **6.2** were made in PGMEA at 20 wt% total solids. Silicon wafers were primed with hexamethyldisilizane to improve adhesion of the polymer film onto the substrate. Polymer **6.2** was spin coated onto the treated Si wafers at 1000 rpm for 30 sec, then soft baked at 80 ^{o}C for 3 min. After exposure and post-exposure baking at 80 ^{o}C for 3 min, films were developed in 0.26 N TMAH for 60 sec, rinsed with water, and then cured at 120 ^{o}C for 3 min. For

generation of the PAG patterned materials (see Figure 6.10), a solution of triphenylsulfonium hexafluoroantimonate loaded in polymer **6.3** (10 wt% PAG, 90 wt% **6.3**) was made in PGMEA at 20 wt% total solids. Silicon wafers were primed with hexamethyldisilizane. The polymer **6.3** solution was spin coated onto the treated Si wafers at 1000 rpm for 30 sec, then soft baked at 150 ^{o}C for 3 min. After exposure and post-exposure baking at 150 ^{o}C for 5 min, films were developed in 0.26 N TMAH for 5 min, rinsed with sonicating water, and then cured at 150 ^{o}C for 3 min.

6.6 Summary

Novel, low dielectric photodefinable polyimides were successfully prepared. The resulting polyimides showed good solubility in common organic solvents including acetone, THF, PGMEA, GBL, DMF and 0.26 N TMAH when deprotected. One polyimide displayed a low dielectric constant while another has low thermal expansion. A photosensitive composition based on the polyimide loaded with a trifunctional DNQ inhibitor for the unprotected polyimide and PAG for the protected polyimide was found to serve as a positive-tone photodefinable polymer using standard 0.26N TMAH developer. Unlike traditional dielectric polymer precursors, thermal curing is shown to be achievable in these polyimides at temperatures below 200 ^{o}C.

6.7 References

1. Jung, M.-S., J. Hyeon-Lee, and T.-L. Choi, *A positive-working photosensitive polyimide based on thermal crosslinking and acidolytic cleavage.* J. Appl. Polym. Sci. FIELD Full Journal Title:Journal of Applied Polymer Science, 2008. **107**(4): p. 2632-2637.

2. Omote, T., K.i. Koseki, and T. Yamaoka, *Fluorine-containing photoreactive polyimide. 6. Synthesis and properties of a novel photoreactive polyimide based on photo-induced acidolysis and the kinetics for its acidolysis.* Macromolecules FIELD Full Journal Title:Macromolecules, 1990. **23**(22): p. 4788-95.

3. Chen, X., M. Anthamatten, and D.R. Harding, *Vapor deposition and curing of polybenzoxazole precursors.* Macromolecules, 2006. **39**(22): p. 7561-7565.

4. Guzman-Lucero, D. and D. Likhatchev, *Imide-to-benzoxazole rearrangement in ortho substituted poly(4-4'-diphenylene pyromellitimide)s.* Polym. Bull. (Berlin, Ger.) FIELD Full Journal Title:Polymer Bulletin (Berlin, Germany), 2002. **48**(3): p. 261-269.

5. Hsiao, S.-H. and Y.-J. Chen, *Synthesis and properties of hydroxy-containing ortho-linked poly(ether-imide)s.* High Perform. Polym. FIELD Full Journal Title:High Performance Polymers, 2000. **12**(4): p. 515-524.

6. Likhatchev, D., et al., *Soluble aromatic polyimides based on 2,2-bis(3-amino-4-hydroxyphenyl)hexafluoropropane: synthesis and properties.* J. Appl. Polym. Sci. FIELD Full Journal Title:Journal of Applied Polymer Science, 1996. **59**(4): p. 725-35.

7. Tullos, G.L., et al., *Thermal Conversion of Hydroxy-Containing Imides to Benzoxazoles: Polymer and Model Compound Study.* Macromolecules FIELD Full Journal Title:Macromolecules, 1999. **32**(11): p. 3598-3612.

8. Stewart, M.D., et al., *Acid mobility in chemically amplified photoresists.* Proc. SPIE-Int. Soc. Opt. Eng. FIELD Full Journal Title:Proceedings of SPIE-The International Society for Optical Engineering, 2002. **4690**(Pt. 2, Advances in Resist Technology and Processing XIX): p. 943-951.

9. Fahey, J., et al., *A new positive tone deep-UV photoresist based on poly(4-hydroxystyrene) and an acid labile protecting group.* Proc. SPIE-Int. Soc. Opt. Eng. FIELD Full Journal Title:Proceedings of SPIE-The International Society for Optical Engineering, 1995. **2438**(Advances in Resist Technology and Processing XII): p. 125-42.

CHAPTER 7

SUMMARY AND FUTURE WORK

7.1 Summary of Synthesized Polymers

A novel HFA-substituted aromatic polyimide **3.5** was successfully prepared. The resulting polyimide showed good solubility in common organic solvents including PGMEA, γ-GBL, THF, and methanol, and 0.26 N TMAH. It was shown that the HFA-containing side-group can be cleaved thermally and removed to produce final materials which do not contain polar hygroscopic groups and which are insoluble in TMAH. The final polyimide with the thermally cleaved side-group is shown to have a lower dielectric constant and CTE. A photosensitive composition of the polyimide loaded with a DNQ inhibitor was shown to serve as a positive-type photodefinable polyimide using I-line exposure. This ability to remove these polar groups, which provide improved solubility characteristics when compared to the pre-imidized polymer as well as the ability to develop these material in common aqueous developers, is viewed as a distinct and unique advantage to produce a final polymer with a lower dielectric constant and lower water uptake over other previously reported polyimides that have been functionalized with hydrophilic groups such as phenols. This general design strategy is currently being explored in polyimides and other related materials to produce photodefinable polymers for electronics and optoelectronics applications with improved final film properties and lower processing temperatures.

Novel photodefinable polybenzoxazines were successfully prepared. The resulting polybenzoxazine amid alcohol precursors showed good solubility in common organic solvents including acetone, methanol, THF, PGMEA, GBL, DMF and 0.26 N TMAH. A photosensitive composition based on the polybenzoxazine precursor loaded with a trifunctional DNQ inhibitor was found to serve as a positive-tone photodefinable polybenzoxazine using standard 0.26N TMAH developer. During development, it was shown that there is swelling that might limit the implementation of this material. Unlike traditional dielectric polymer precursors, thermal curing is shown to be achievable in polybenzoxazines at temperatures as low as 210 ^{o}C. Thermal curing renders the polymer insoluble in aqueous developers and produces a polymer with a dielectric constant as low as 2.0 and water absorption as low as 0.09 %.

A photodefinable imide/benzoxazine copolymer was successfully prepared. The resulting amid alcohol precursor showed good solubility in common organic solvents including acetone, THF, PGMEA, GBL, DMF and 0.26 N TMAH. A photosensitive composition based on the PBOX-6FDIAC polybenzoxazine precursor loaded with a trifunctional DNQ inhibitor was found to serve as an excellent positive-tone photodefinable polybenzoxazine using standard 0.26N TMAH developer. During development, it was shown that there is little or no swelling in this material. Thermal curing is shown to be achievable in polybenzoxazines at 265 ^{o}C. Thermal curing renders the polymer insoluble in aqueous developers and produces a polymer with a dielectric constant of 2.2 and 0.60 % water absorption.

Novel photodefinable polyimides **6.2** and **6.3** were successfully prepared. The resulting polyimides showed good solubility in common organic solvents including

acetone, THF, PGMEA, GBL, DMF and 0.26 N TMAH when deprotected. Polymer **6.3** displayed a low dielectric constant while polymer **6.2** has low thermal expansion. A photosensitive composition based on polymer **6.2** loaded with a trifunctional DNQ inhibitor for the unprotected polyimide and PAG for polymer **6.3** was found to serve as a positive-tone photodefinable polymer using standard 0.26N TMAH developer. Unlike traditional polyimides, thermal curing is shown to be achievable in these polyimides at temperatures below 200 ^{o}C.

From characterization of polymers containing the HFA-ODA diamine, several conclusions can be drawn. With the exception of the glass transition temperature for intermetallic dielectrics, the other properties examined met requirements for use as either an intermetallic dielectric or an electronic package. Polybenzoxazines displayed a low dielectric constant and low water absorption. The benzoxazine/imide copolymer has a higher T_g and lower CTE than the polybenzoxazines examined while maintaining a low dielectric constant and low water absorption. The HFA-ODA polyimide has the lowest cure temperature and CTE of all the polymers examined. Protection of that polyimide with an acid labile protecting group produced an acceptable dielectric constant with a low cure temperature and nearly cut the water absorption in half. HFA-ODA has been shown to produce a variety of photodefinable polymers with beneficial properties in low temperature electronic packaging applications.

7.2 Recommendations for Future Work

In this work, polybenzoxazines have been shown to complete curing at temperatures as low as 210 ^{o}C. Polyimides have been shown to serve as a negative-type photodefinable polymer that cyclizes at 200 ^{o}C with the use of a photobase generator [1].

This method of cyclization should be explored because of the need to create polymers that cure below 200 ^{o}C.

Although polybenzoxazines have shown excellent dielectric constants and water absorption, their T_g is below the temperature to cure to the film and the CTE falls in a range typical for polymers. A copolymer that incorporates the use of an imide along with the benzoxazine linkages has been shown to lower the CTE and raise the T_g. Unfortunately, the cure temperature for the copolymer also falls above the T_g of the final polymer structure. Literature has shown that the T_g can be increased by incorporating a hydroxyl group situated ortho to the carboxylic acid used to make polybenzoxazoles [2]. In addition to raising the T_g, the dielectric constant is shown to decrease in certain situations for reasons unknown. Attempts to make the acid chloride have failed to produce a polymer of reasonable molecular weight. One alternative to making an acid chloride that produces a polymer with a lower CTE and higher T_g is to study the effect of fractionating the polybenzoxazines that have been successfully synthesized.

Protecting polymer **6.2** has produced a polymer with a lower dielectric constant and water absorption. However, attempts to add further protection to the polymer with isopropyl chloroformate has produced a polymer that is insoluble after exposure. This is due to the limited stability of the secondary carbocation formed upon exposure and post exposure bake. Although the use of a tertiary carbocation has more stability, protection was weak and the protected polymer was still soluble. Attempts should be made using other acid labile protecting groups such as acetals.

From characterization of HFA-ODA polymers, several properties have been found that would be useful in low temperature electronic packaging applications.

Unfortunately, these advantageous properties were scattered among several different structures. The research presenting in this thesis should serve as groundwork for further optimization to produce an HFA-ODA incorporated polymer that meets all of the desired properties.

7.3 References

1. Mizouti, K., Y. Shibasaki, and M. Ueda, *Development of negative-type photosensitive semi-alicyclic polyimide using a photobase generator.* J. Photopolym. Sci. Technol. FIELD Full Journal Title:Journal of Photopolymer Science and Technology, 2007. **20**(2): p. 181-186.

2. Dang, T.D., et al., *Synthesis and characterization of fluorinated benzoxazole polymers with high Tg and low dielectric constant.* Journal of Polymer Science, Part A: Polymer Chemistry, 2000. **38**(11): p. 1991-2003.

APPENDIX A

H^1-NMR

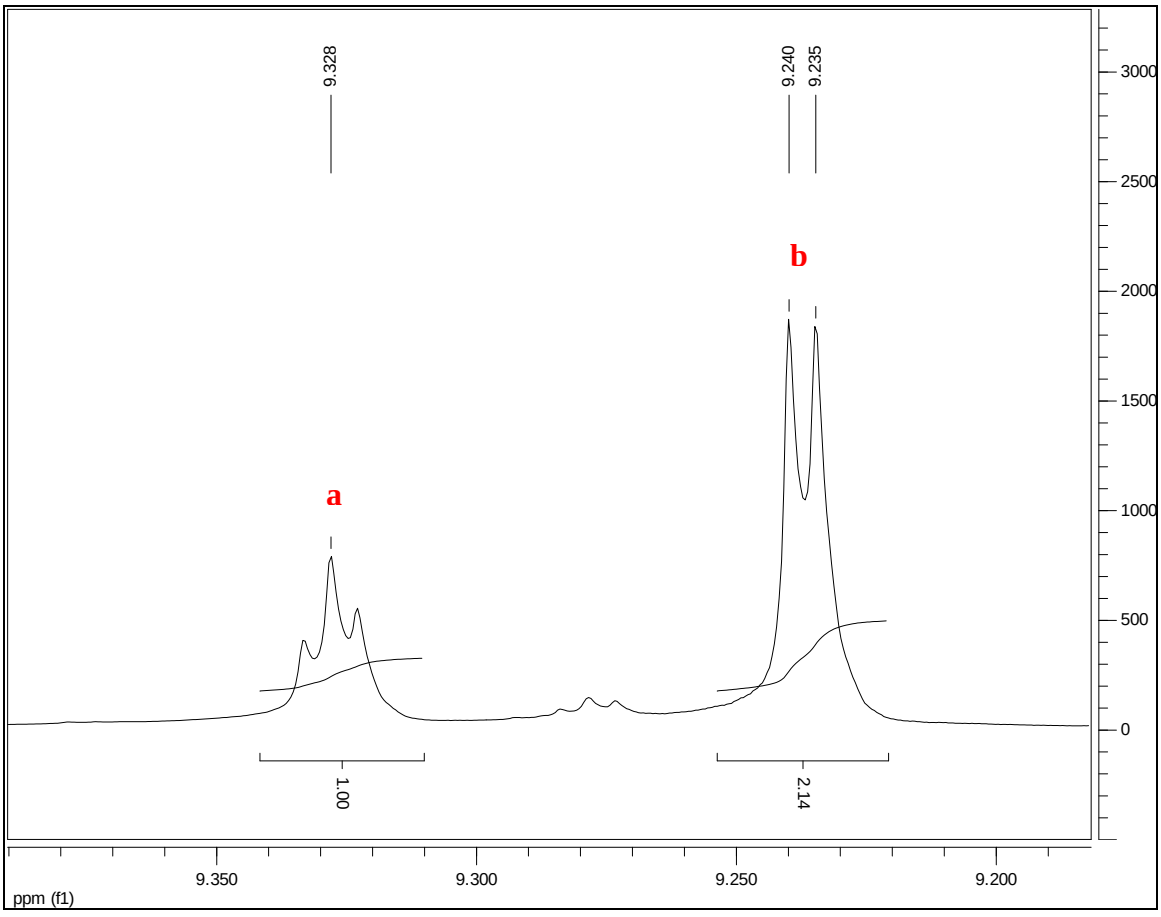

Figure A.1 3,5 Dinitrobenzoyl Chloride in $CDCl_3$

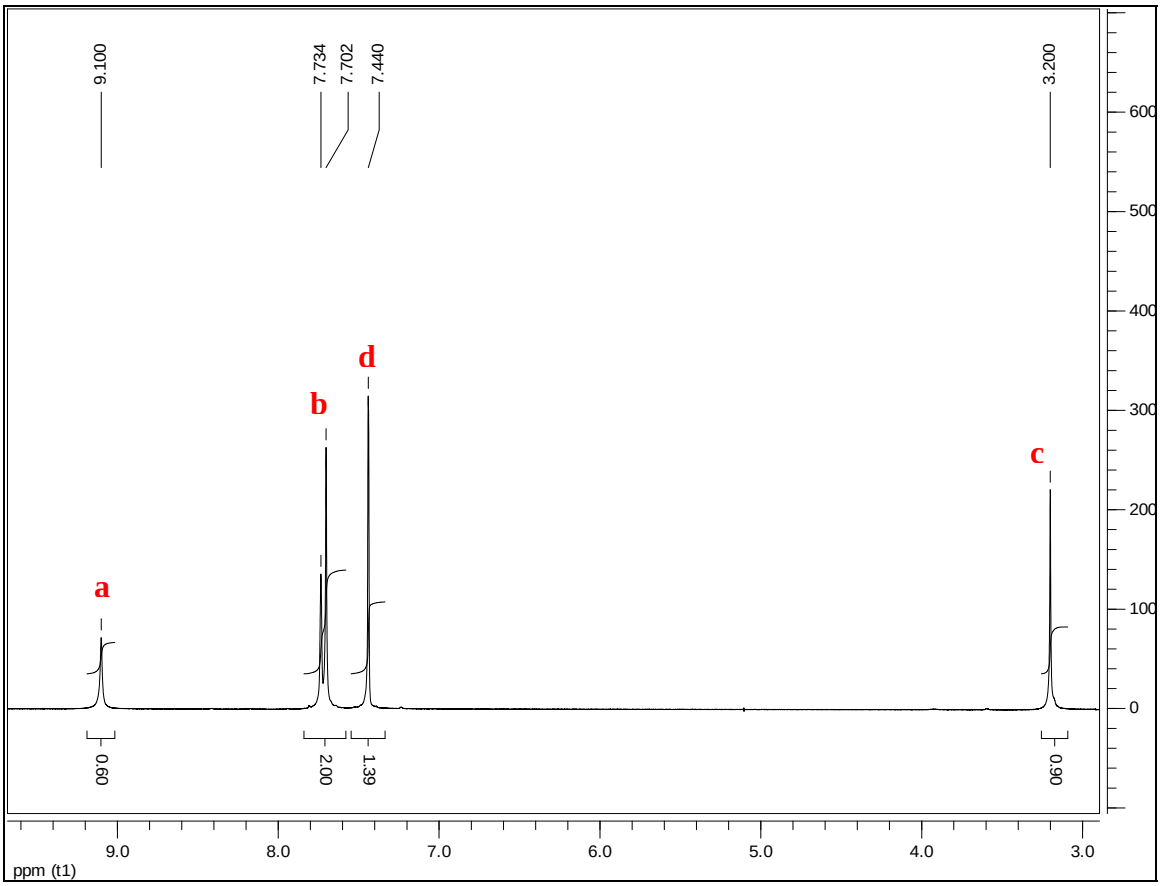

Figure A.2 Monomer **3.1** in Acetone-d_6

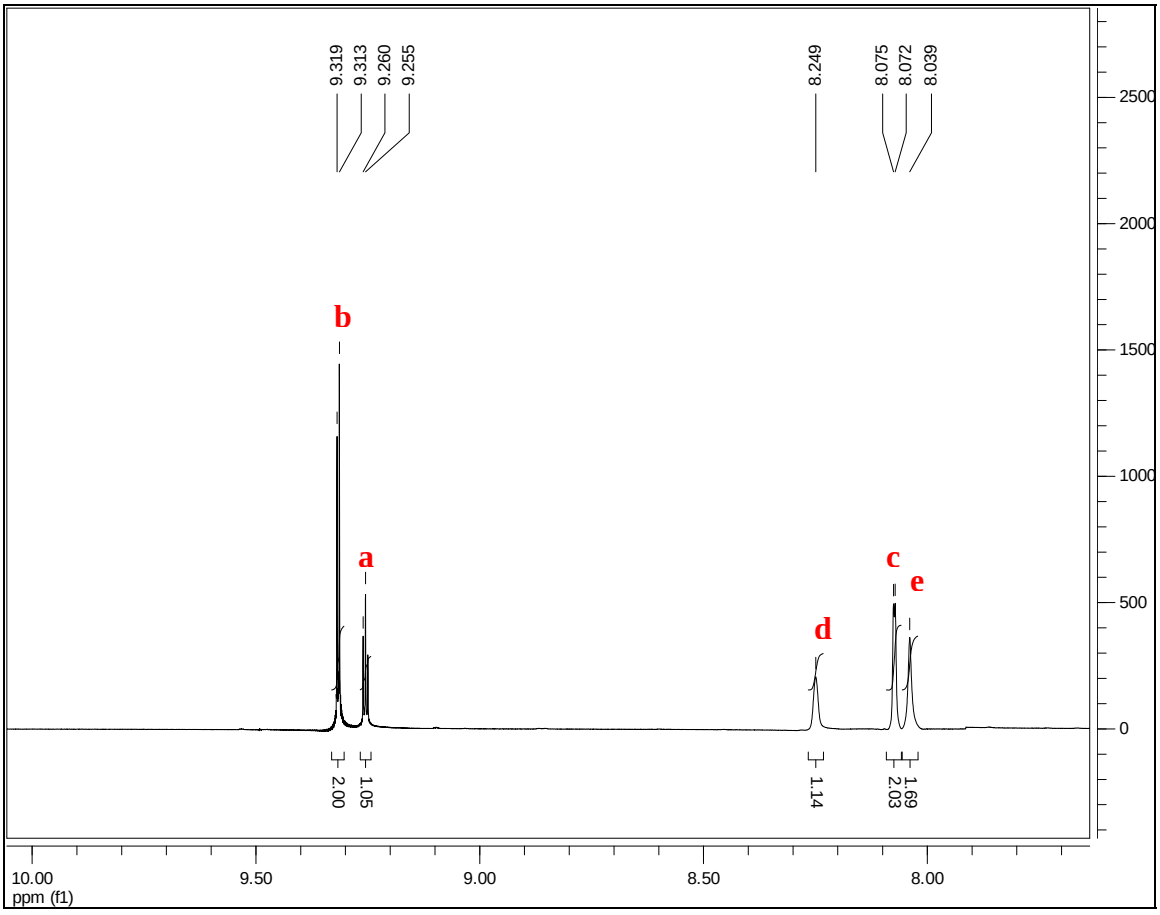

Figure A.3 Monomer **3.2** in Acetone-d_6

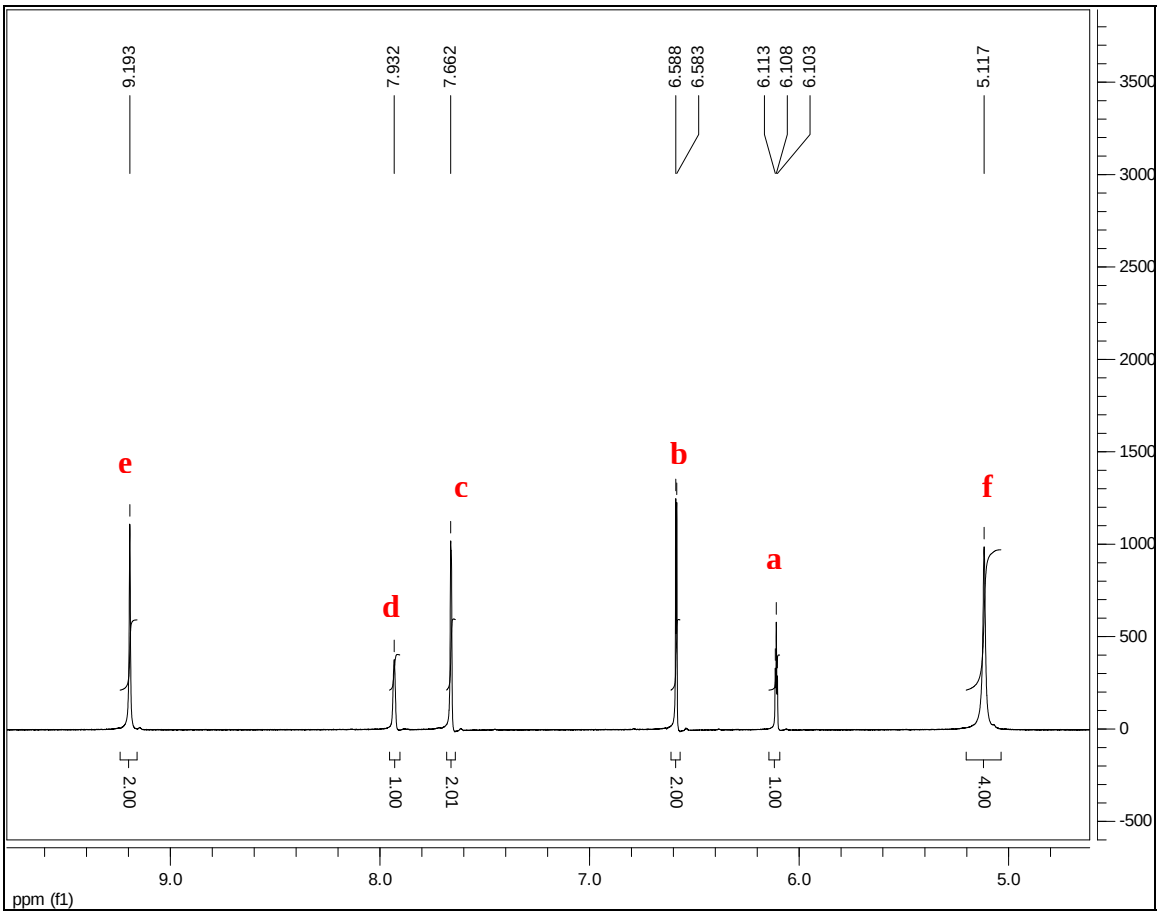

Figure A.4 Monomer **3.3** in Acetone-d_6

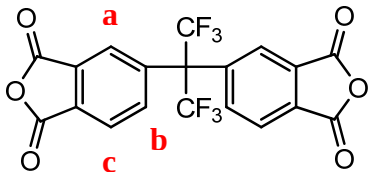

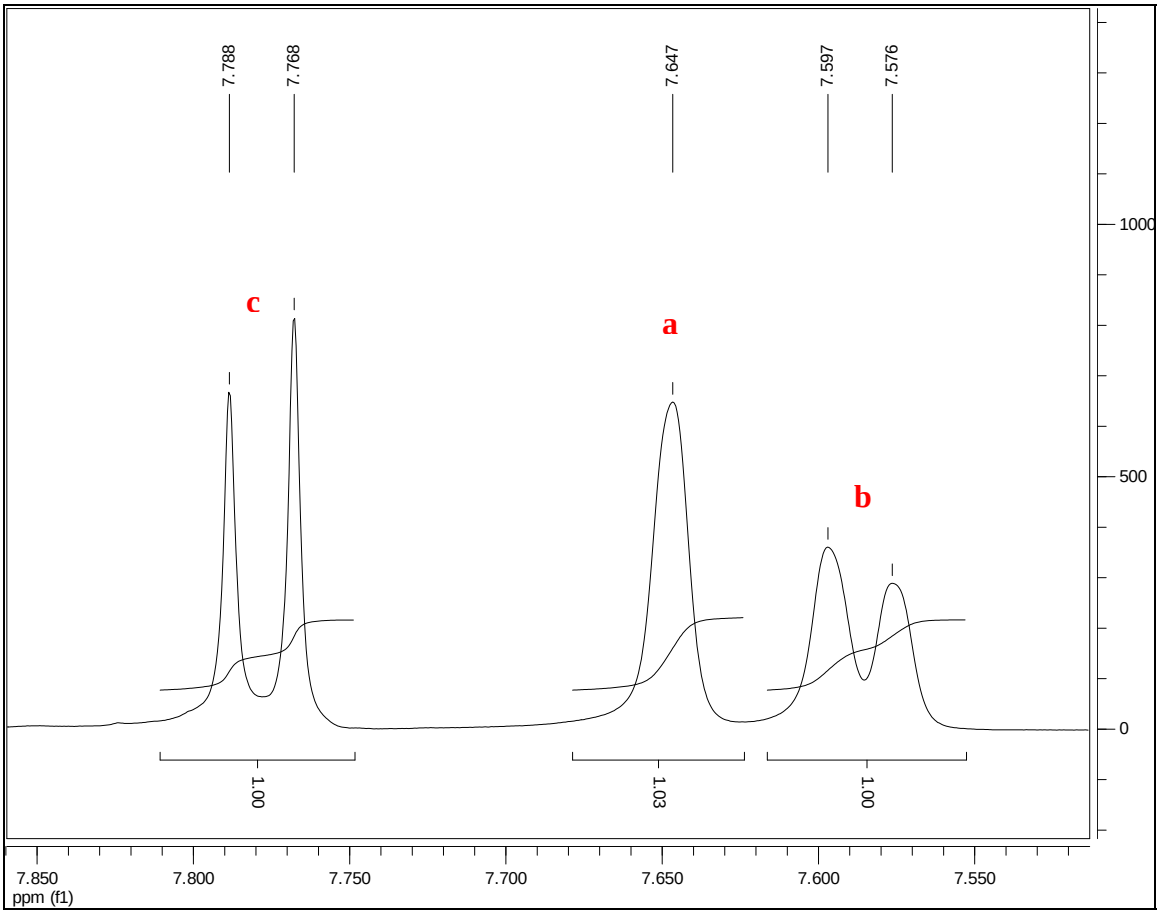

Figure A.5 6FDA in DMSO-d_6

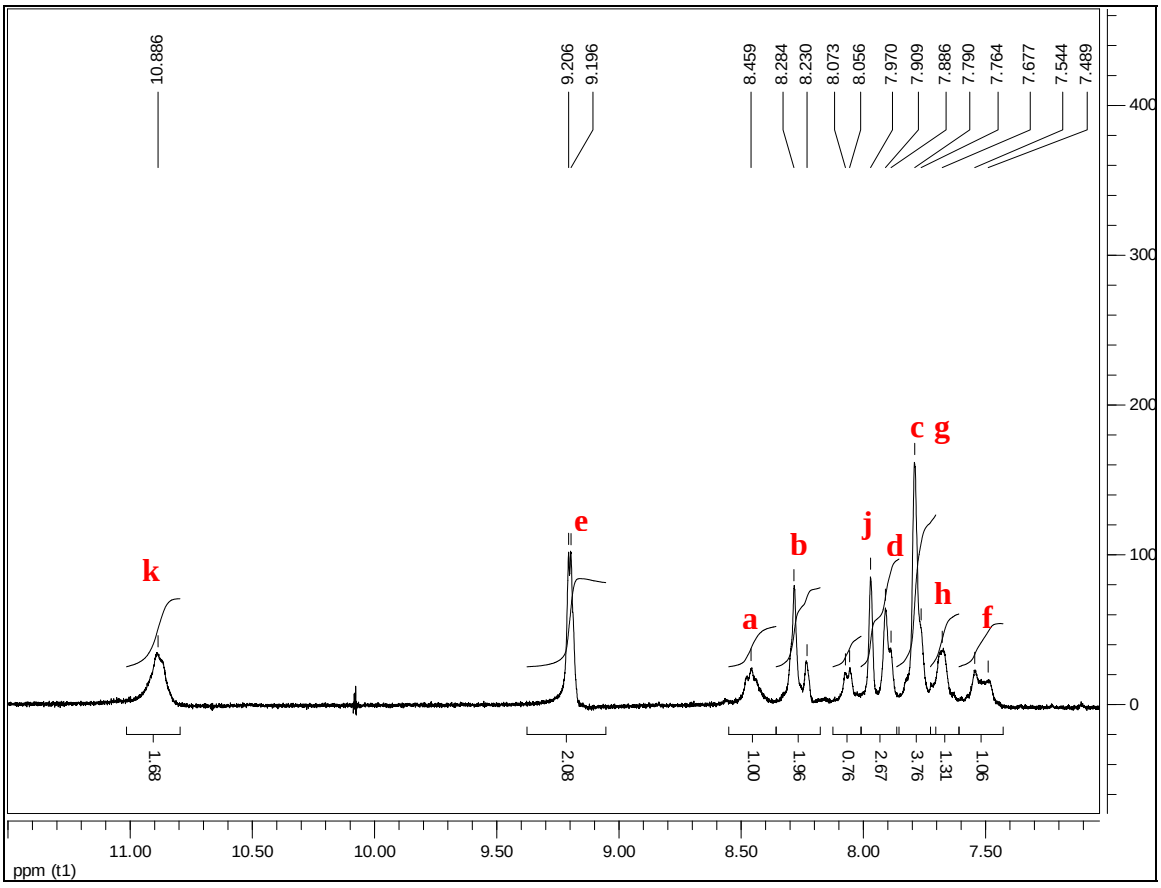

Figure A.6 Polymer **3.4** in DMSO-d_6

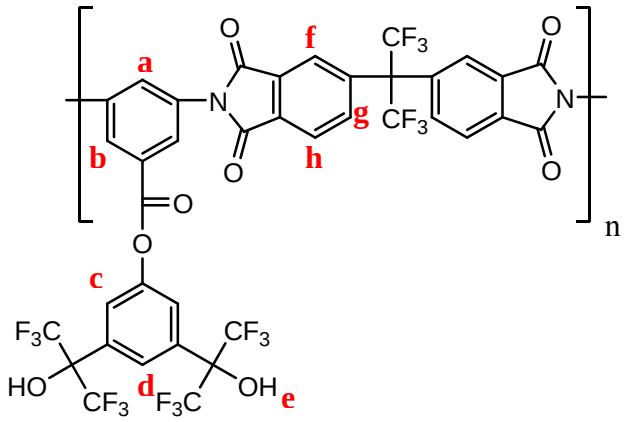

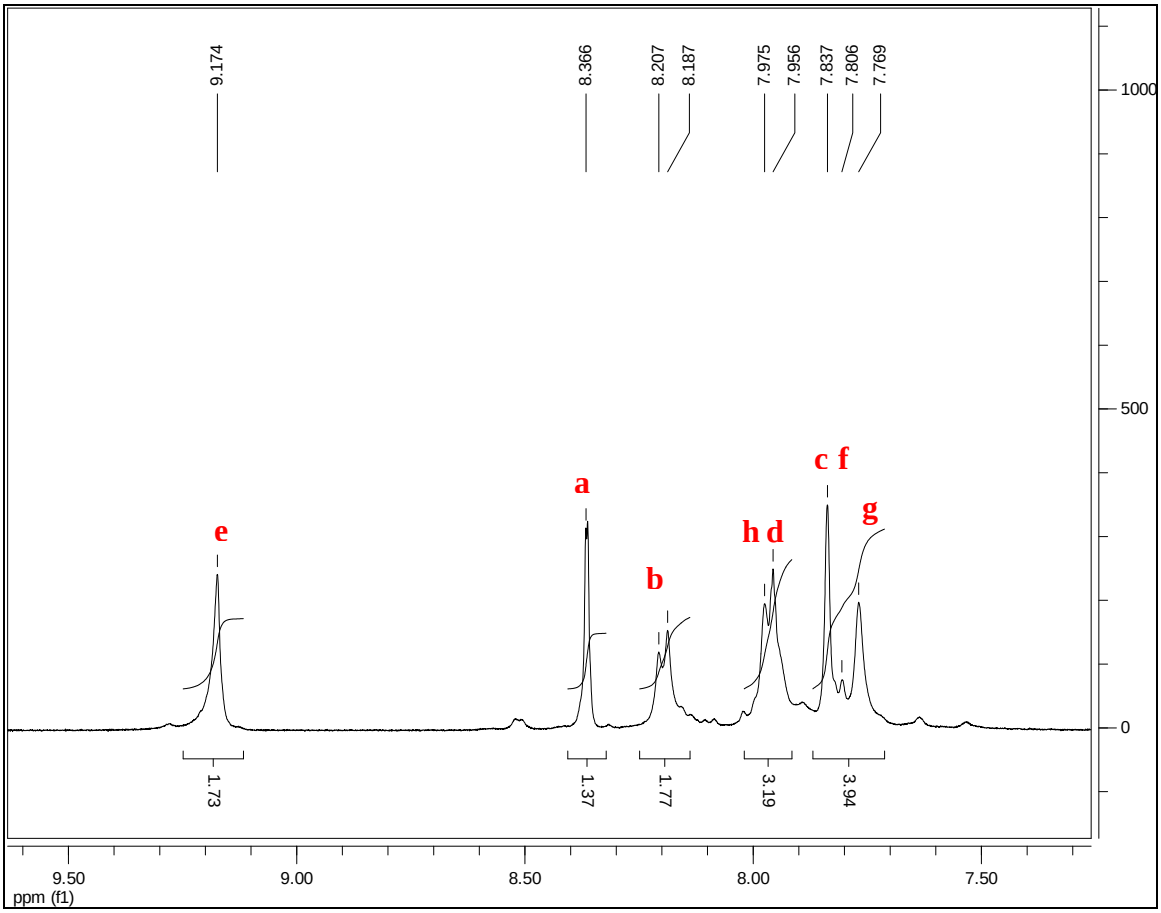

Figure A.7 Polymer **3.5** in DMSO-d_6

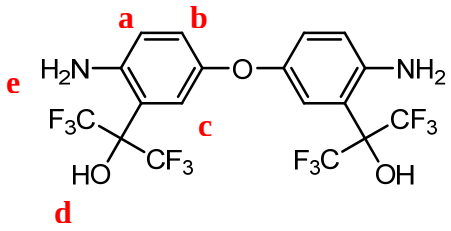

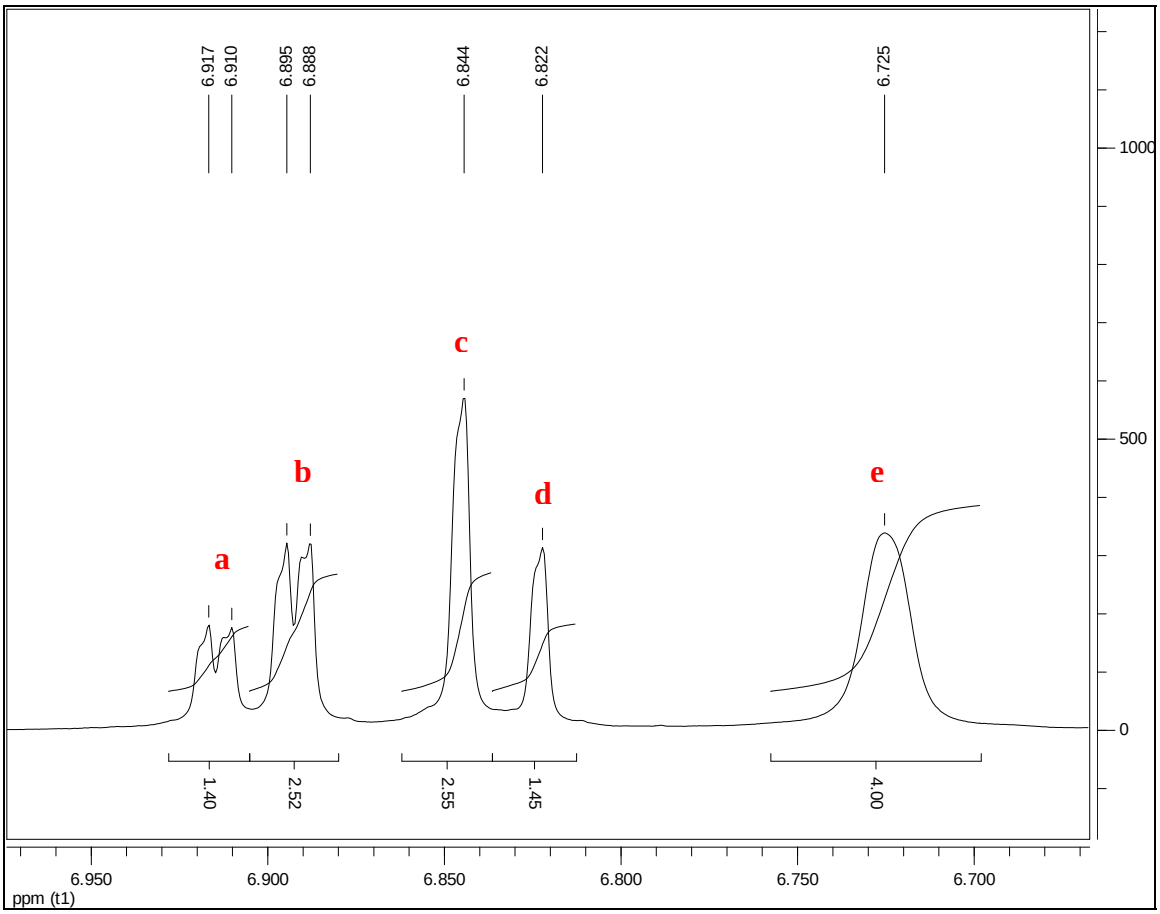

Figure A.8 HFA-ODA in DMSO-d_6

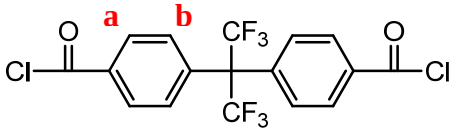

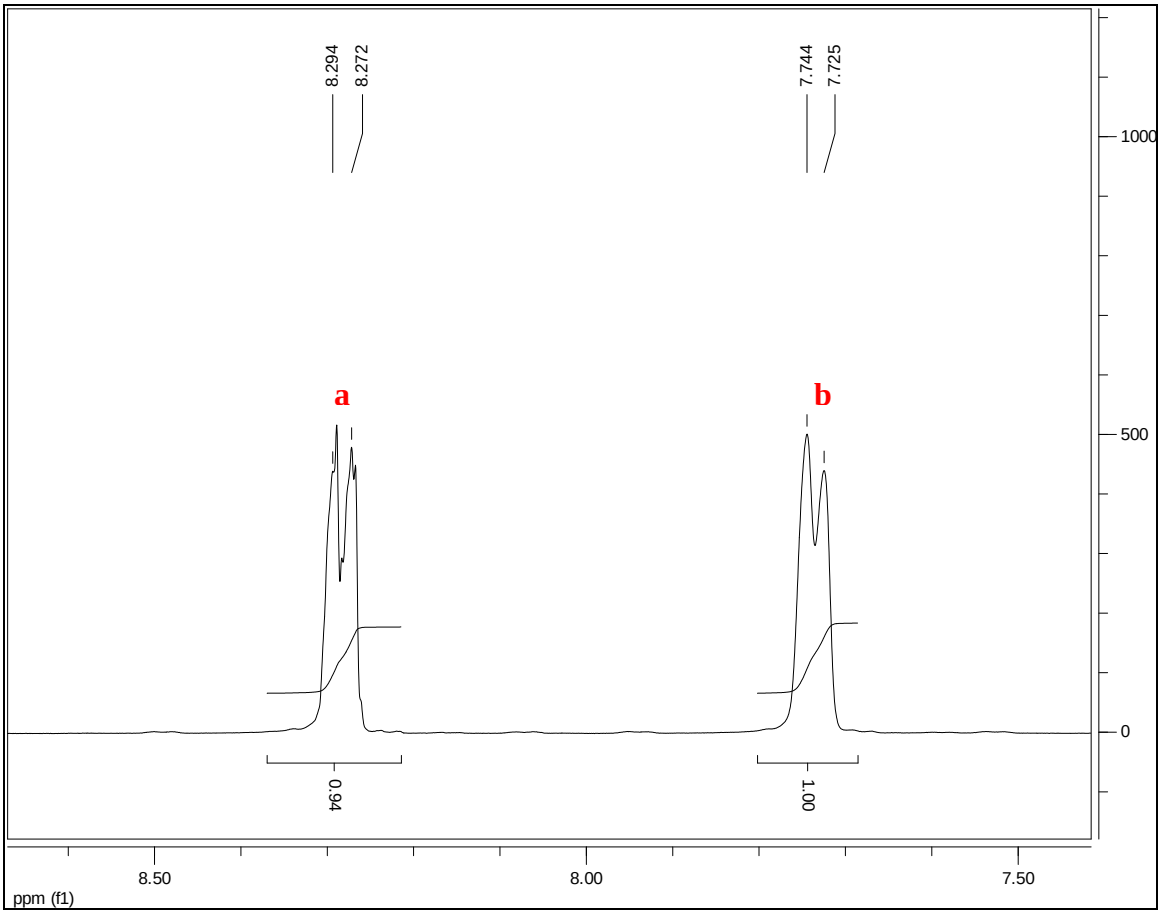

Figure A.9 6FDC in Acetone-d_6

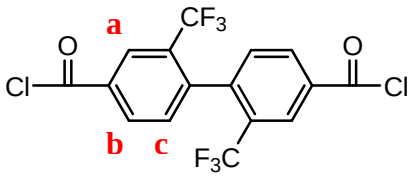

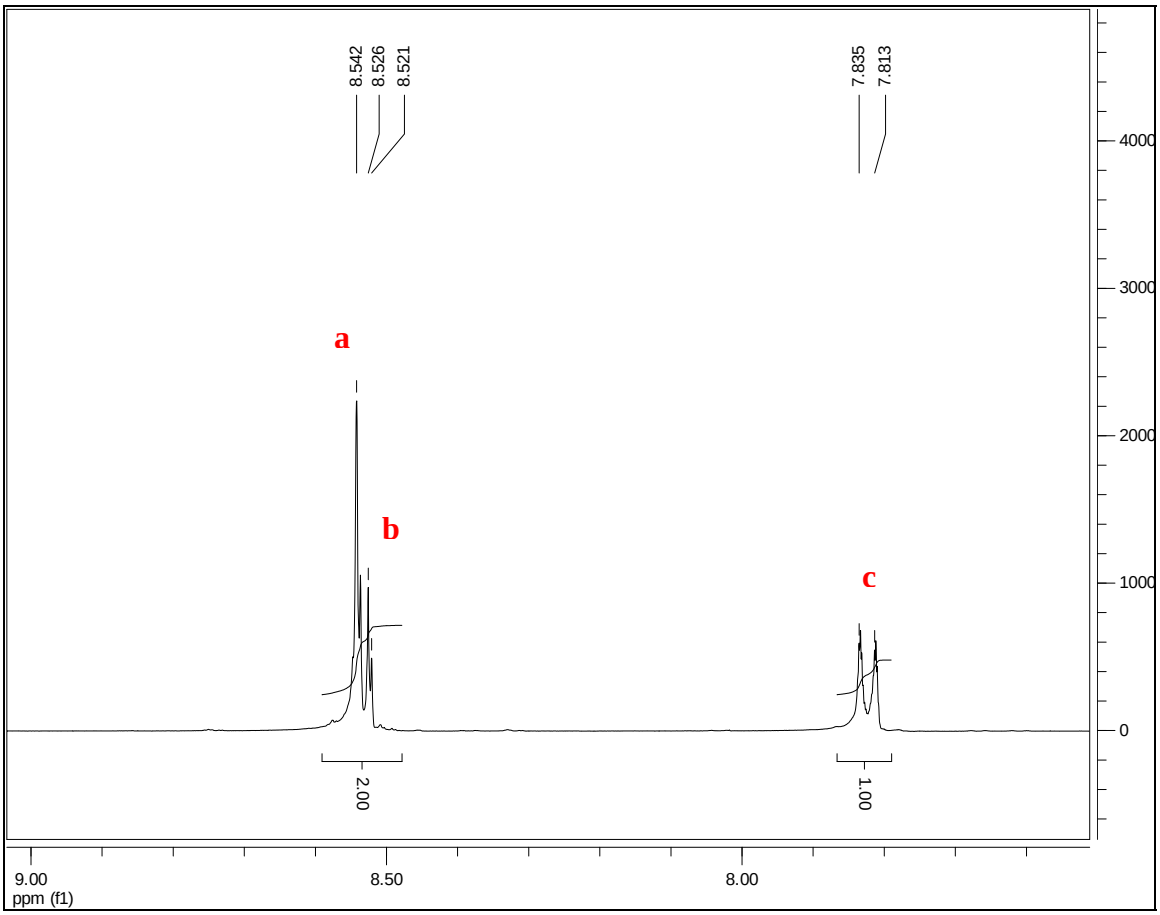

Figure A.10 6FBDC in Acetone-d_6

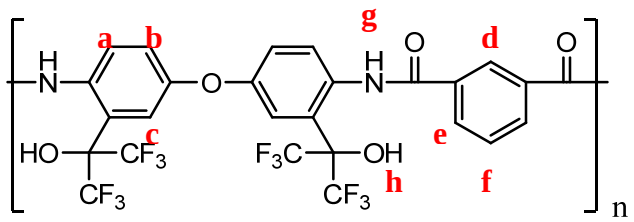

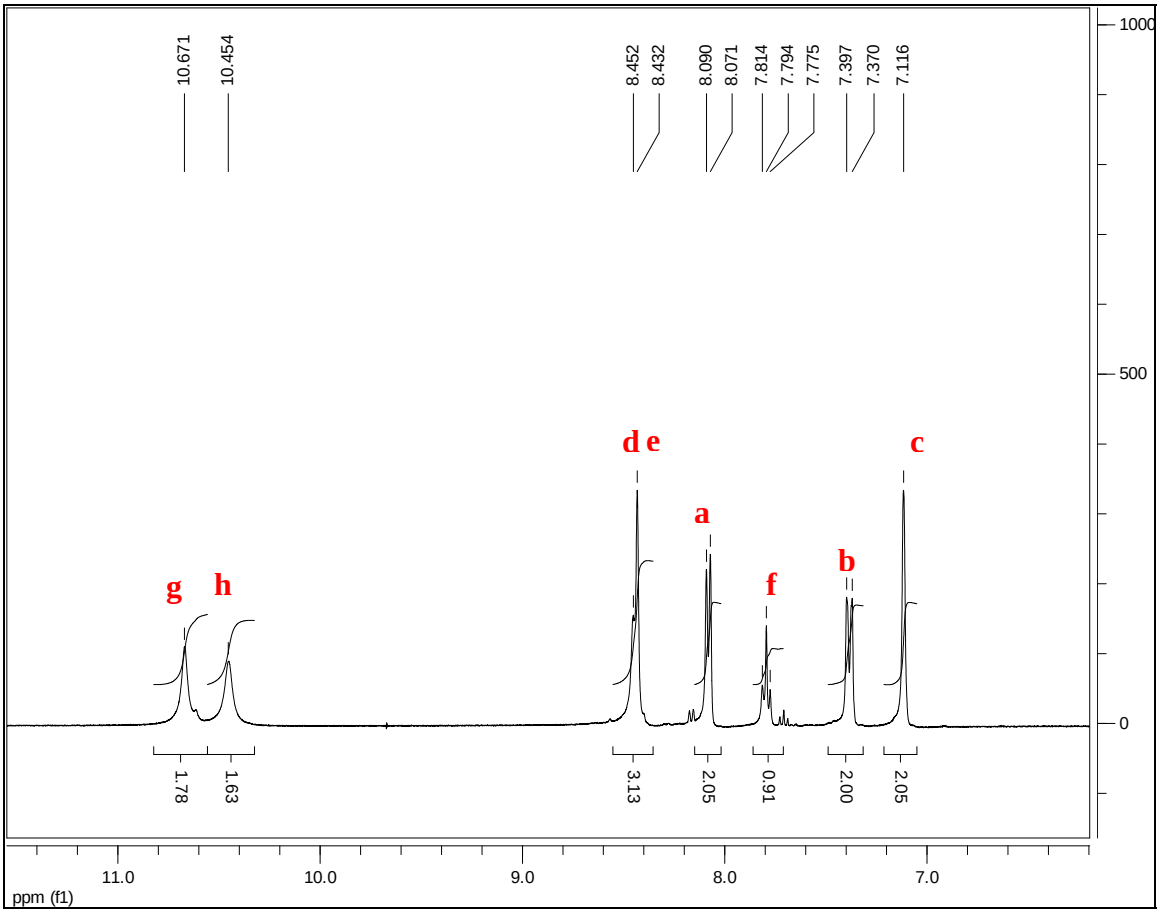

Figure A.11 PBOX-IPC in DMSO-d_6

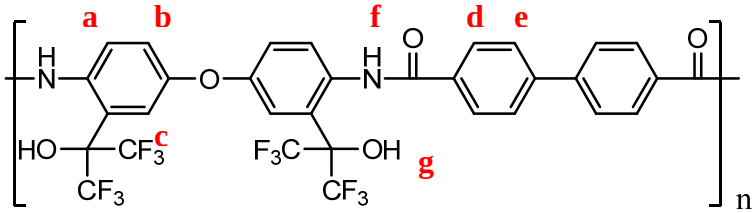

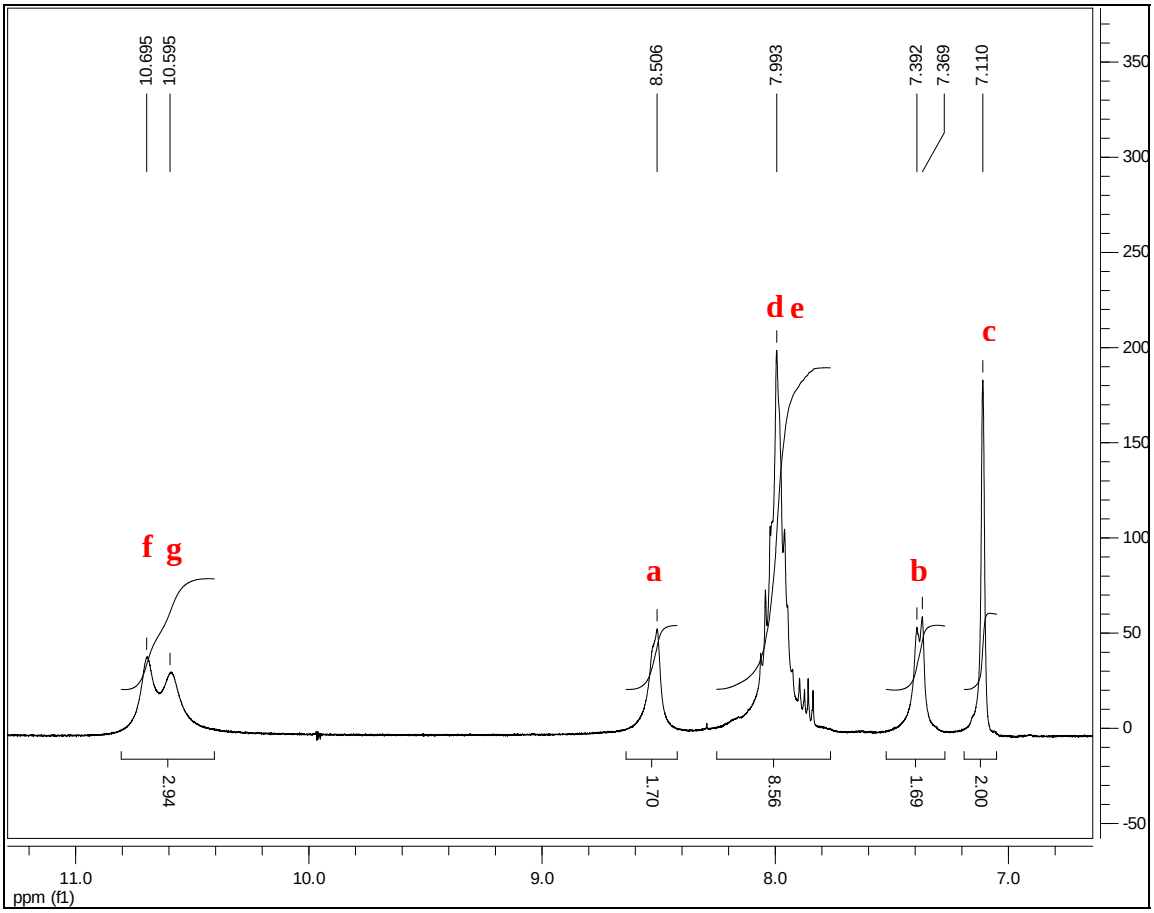

Figure A.12 PBOX-BPDC in DMSO-d_6

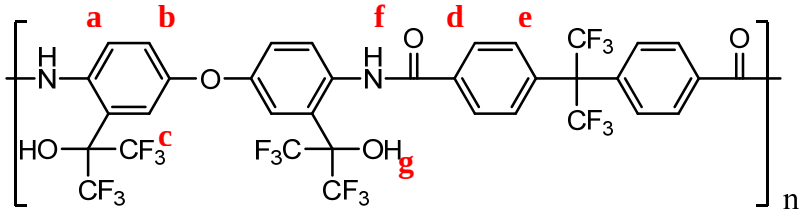

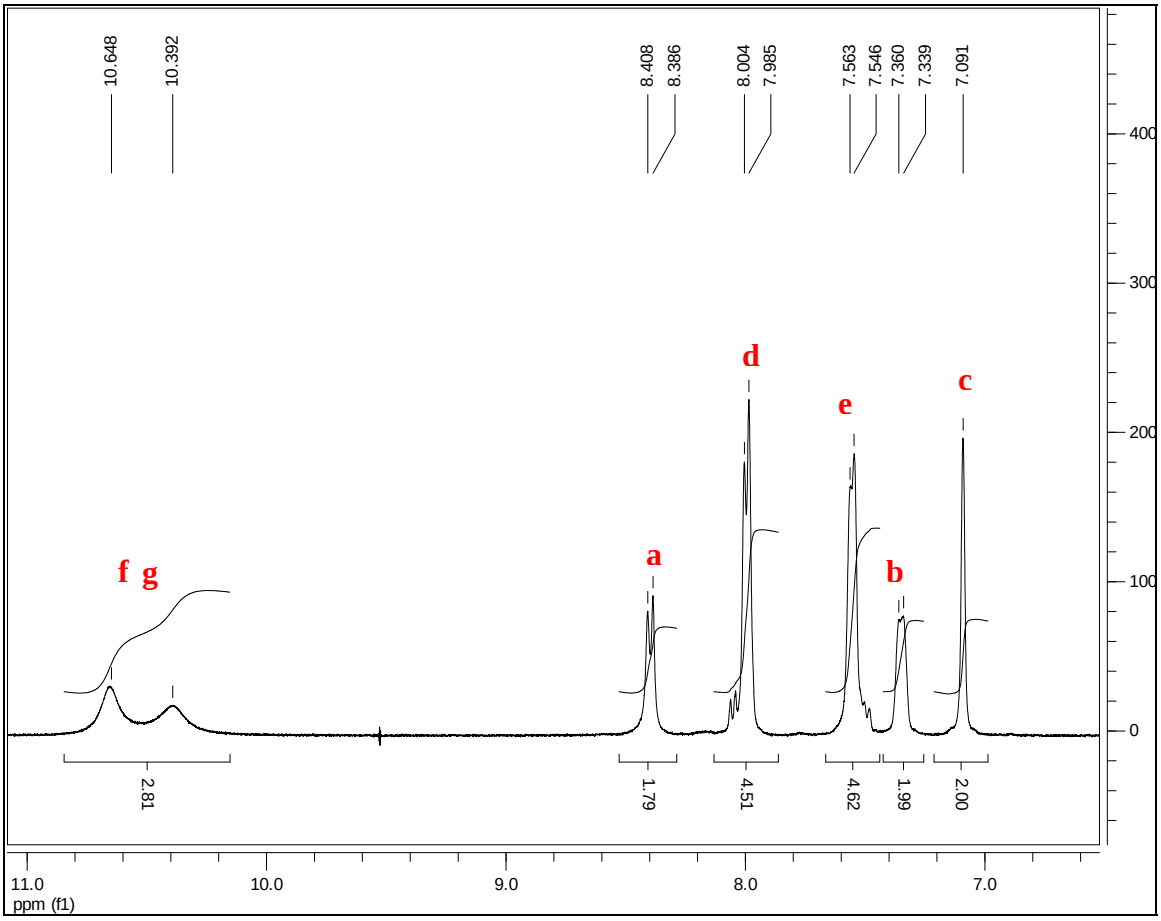

Figure A.13 PBOX-6FDC in DMSO-d_6

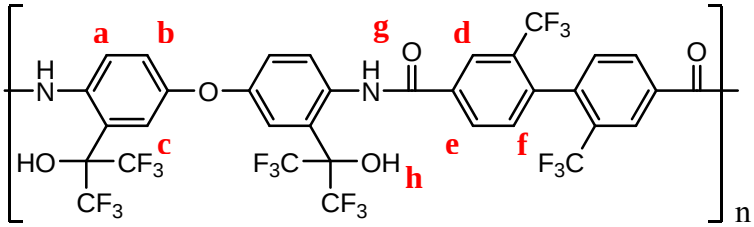

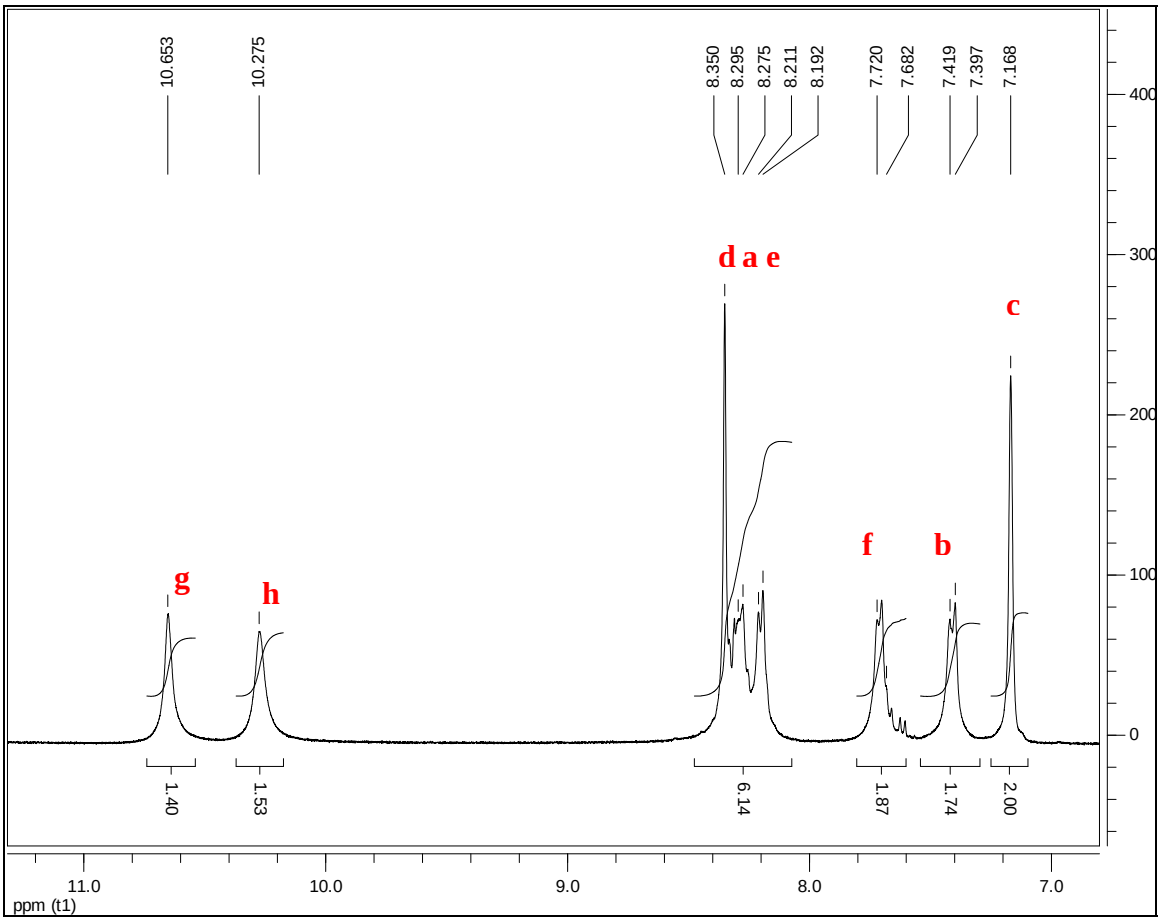

Figure A.14 PBOX-6FBDC in DMSO-d_6

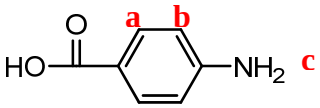

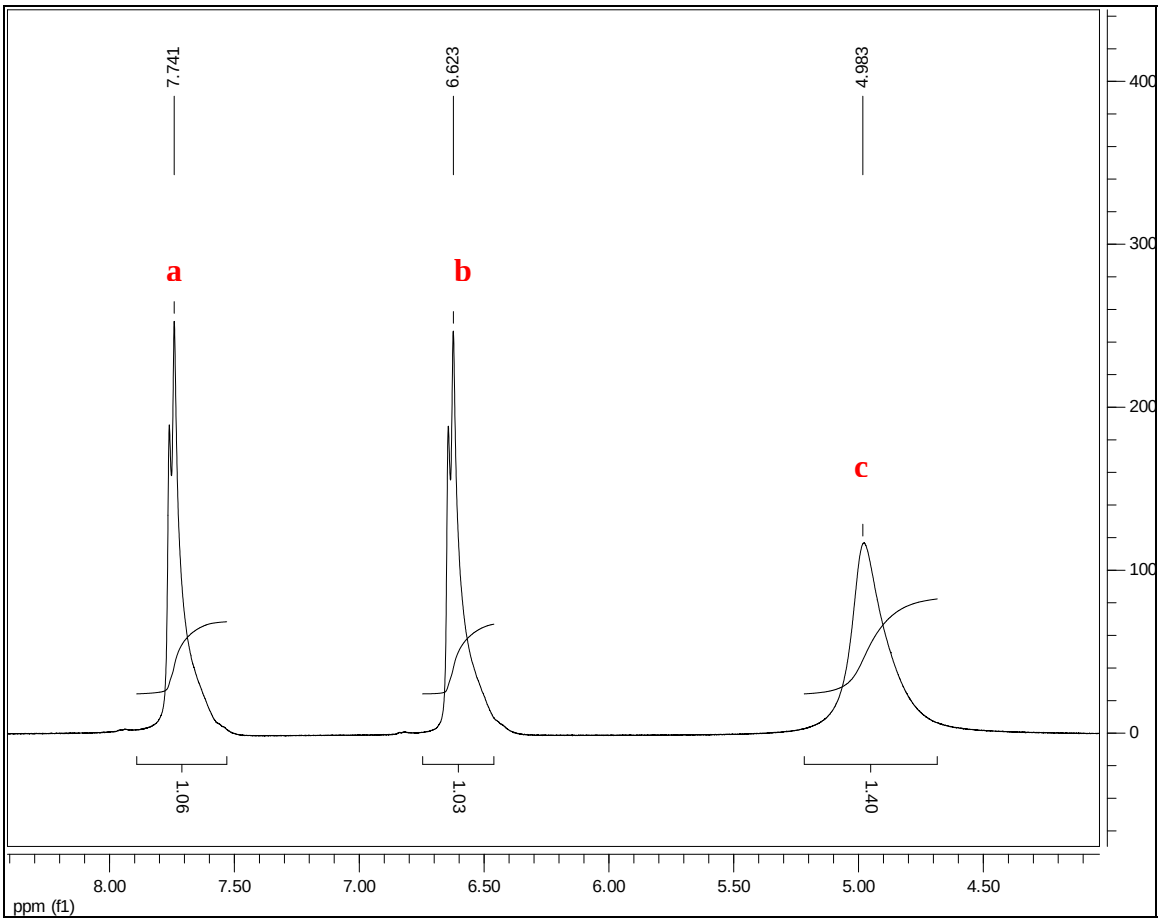

Figure A.15 4-Aminobenzoic Acid in methyl-d_3 alcohol-*d*

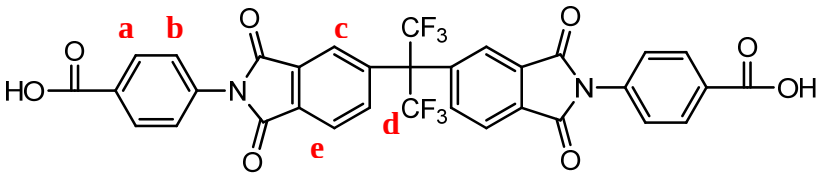

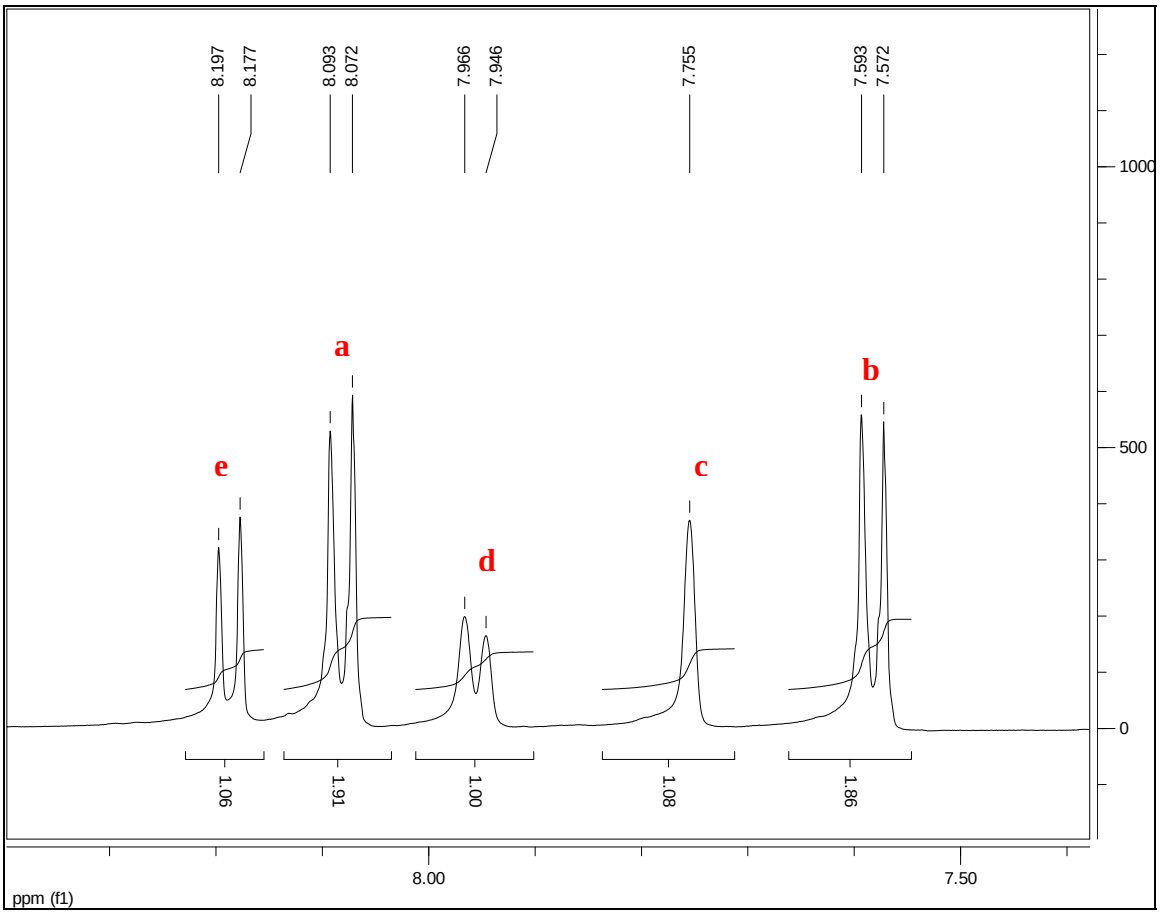

Figure A.16 6FDIA in DMSO-d_6

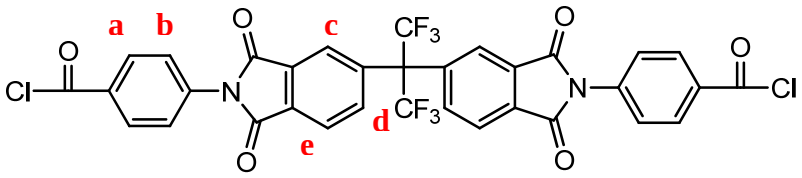

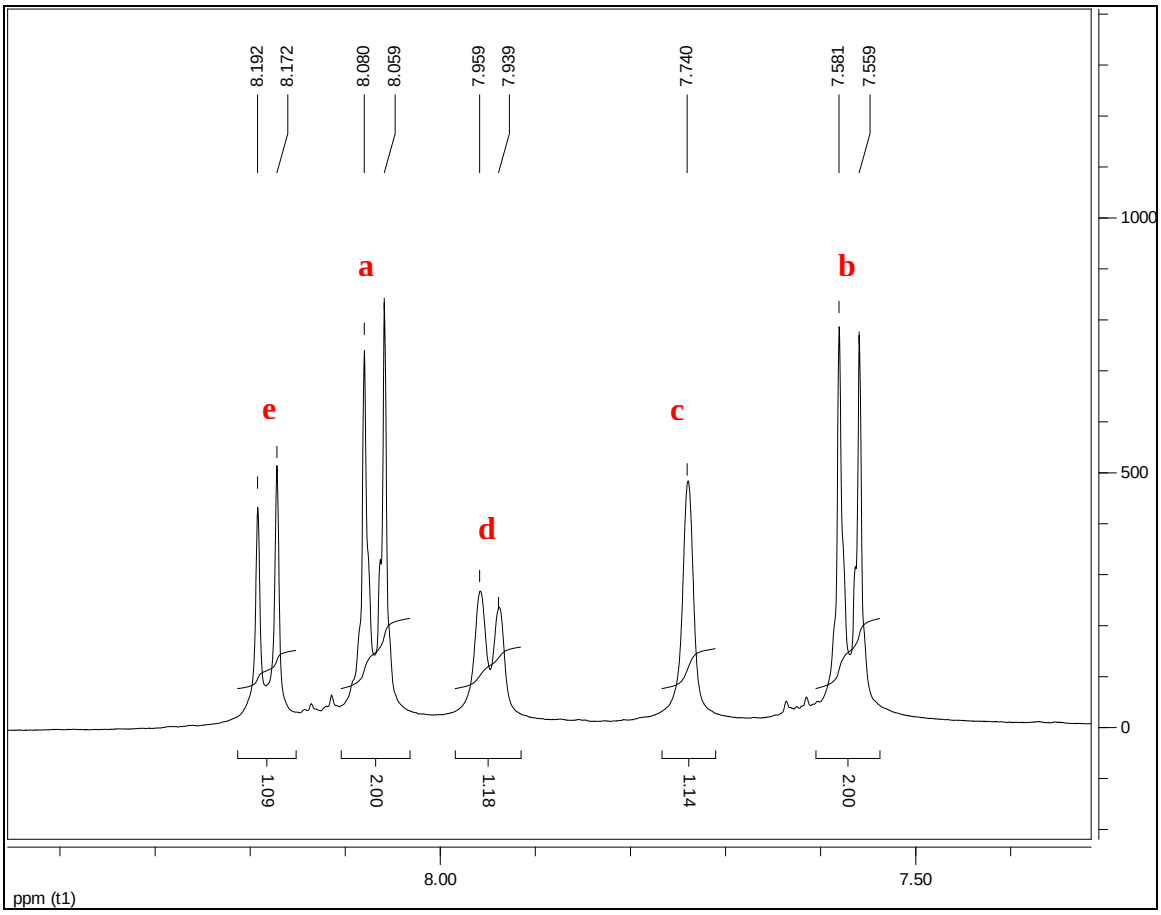

Figure A.17 6FDIAC in DMSO-d_6

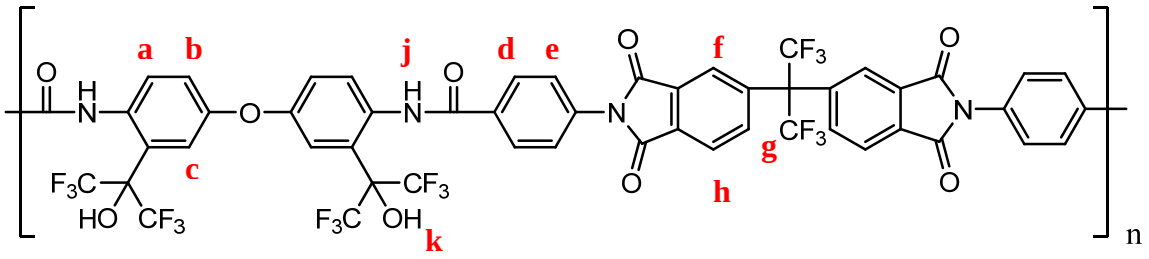

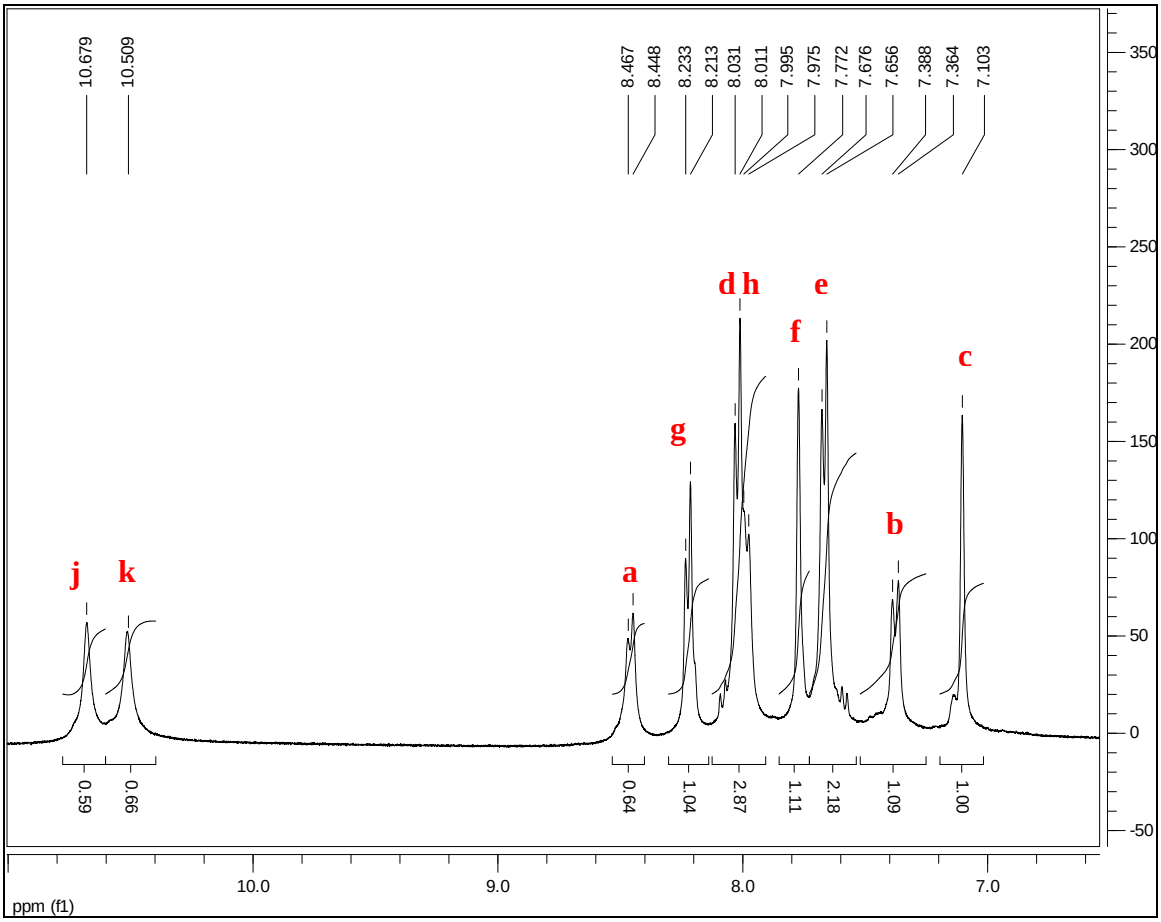

Figure A.18 PBOX-6FDIAC in DMSO-d_6

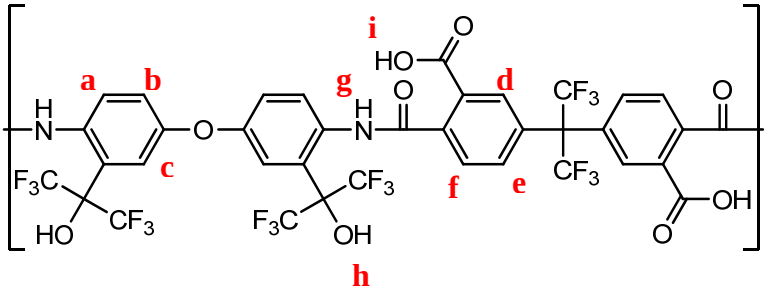

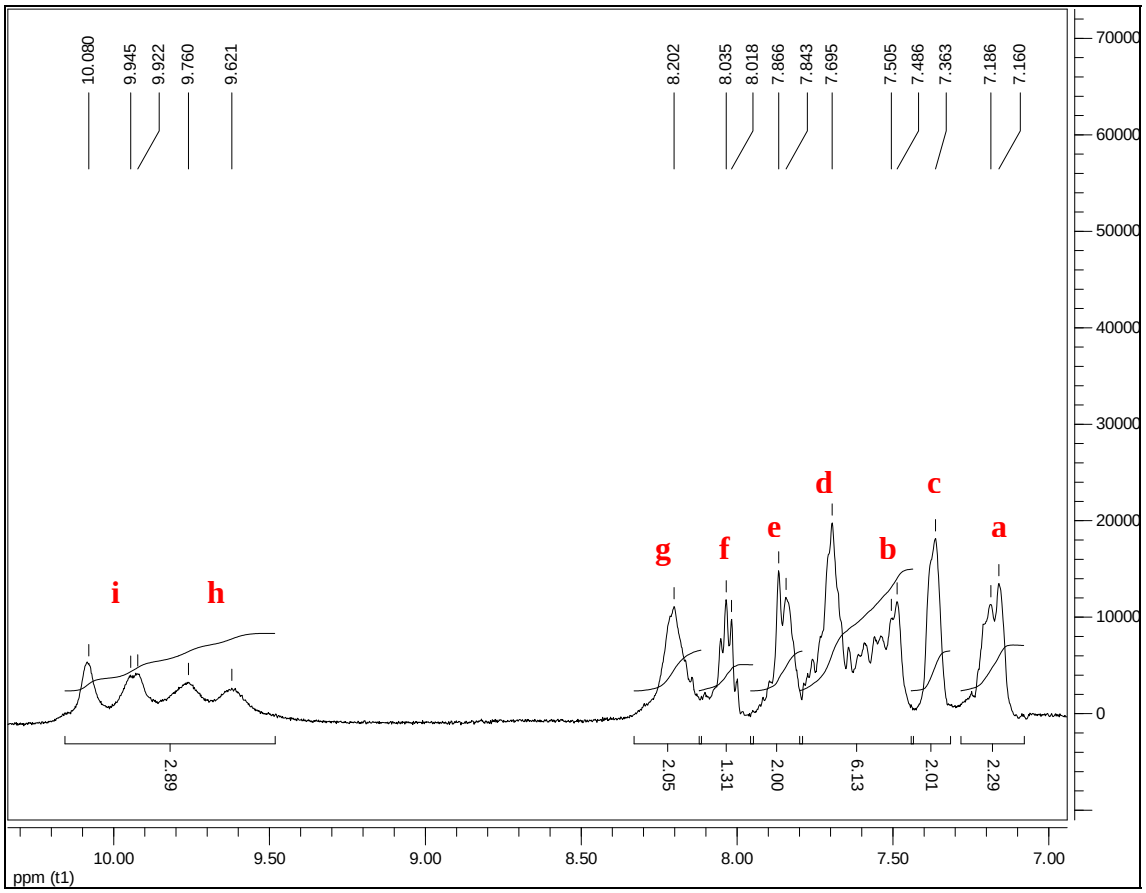

Figure A.19 Polymer **6.1** in DMSO-d_6

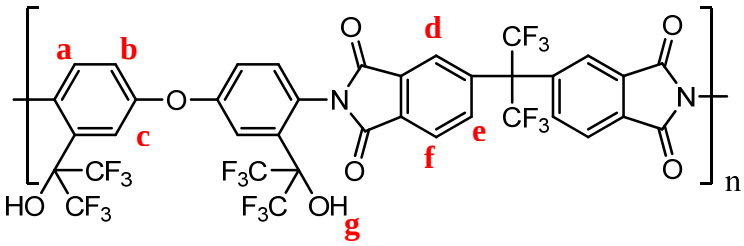

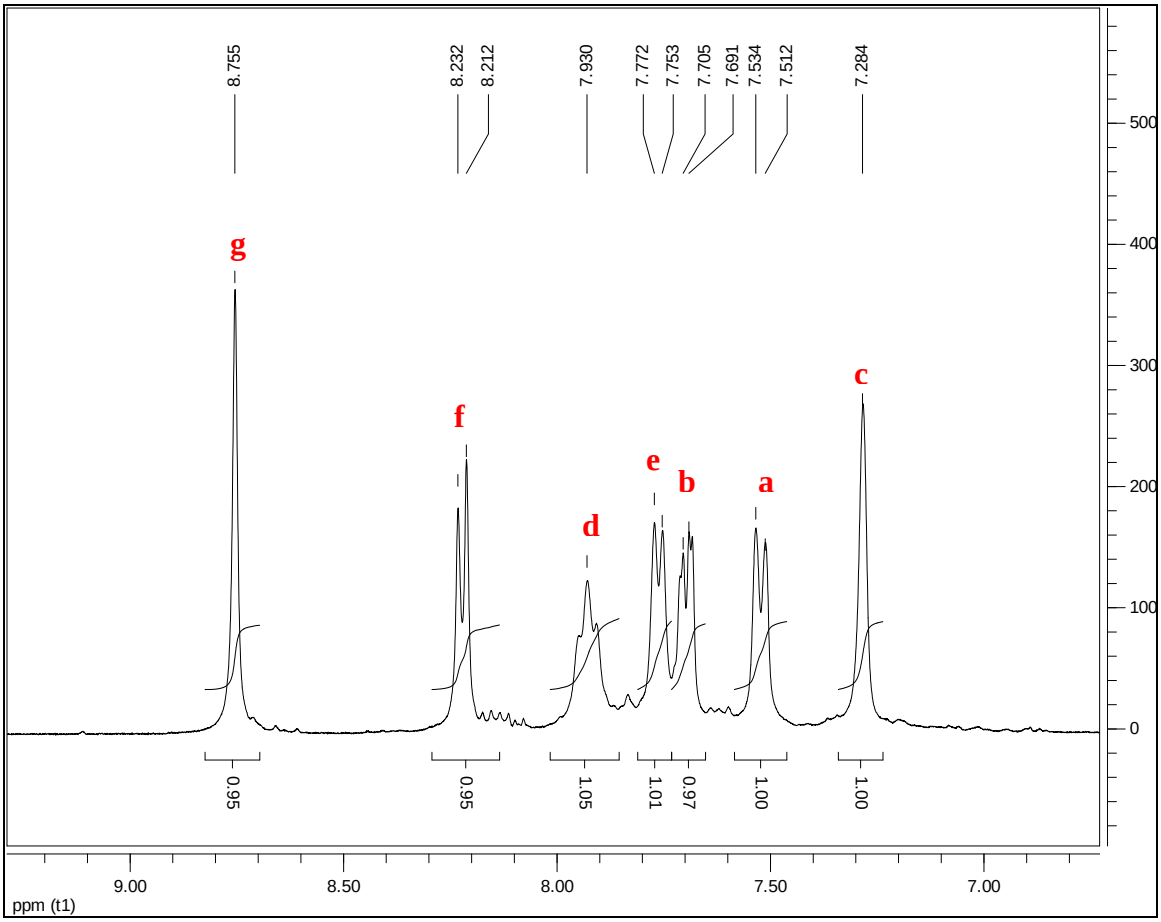

Figure A.20 Polymer **6.2** in DMSO-d_6

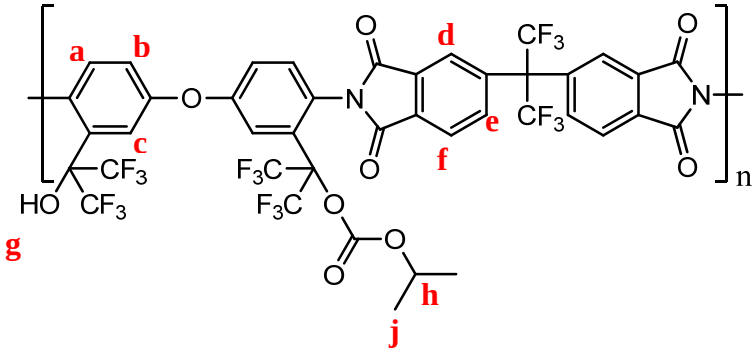

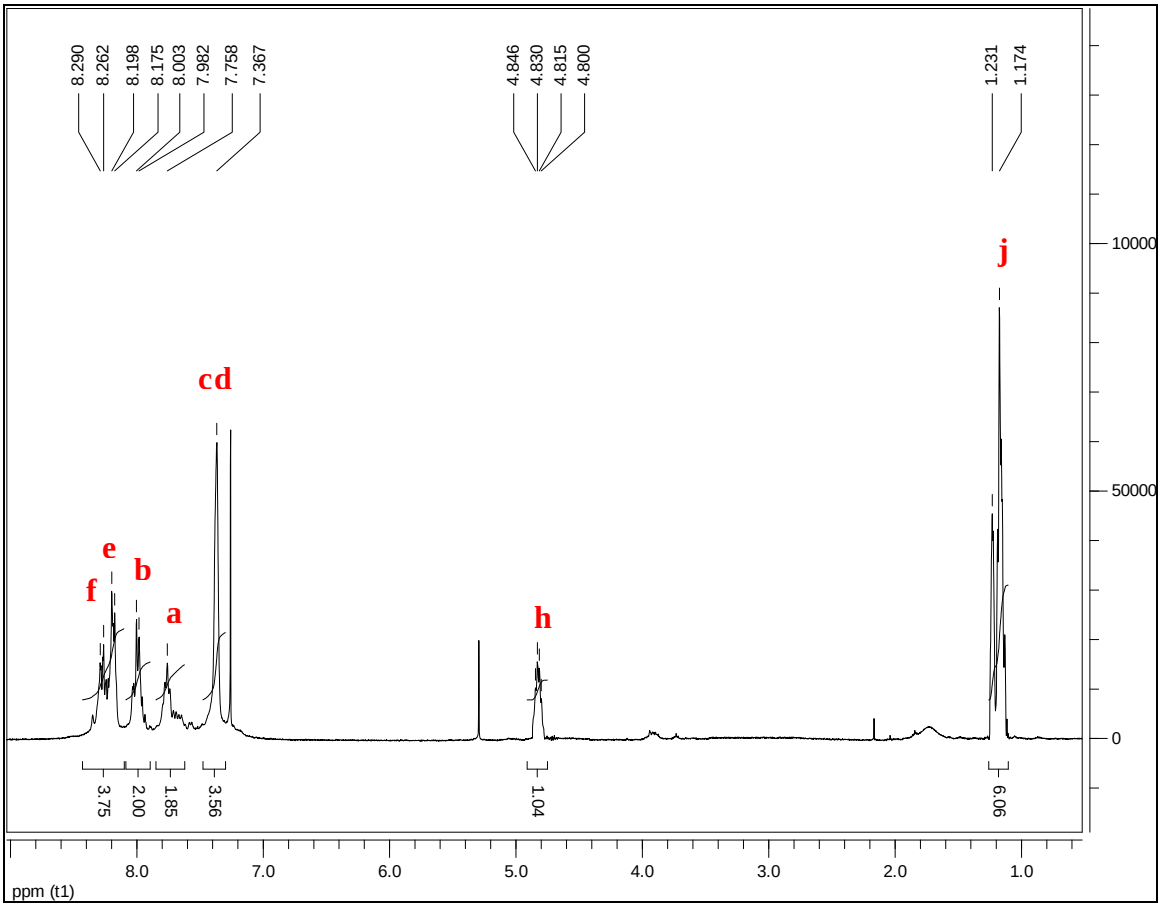

Figure A.21 Polymer **6.3** in $CDCl_3$

APPENDIX B

F^{19}-NMR

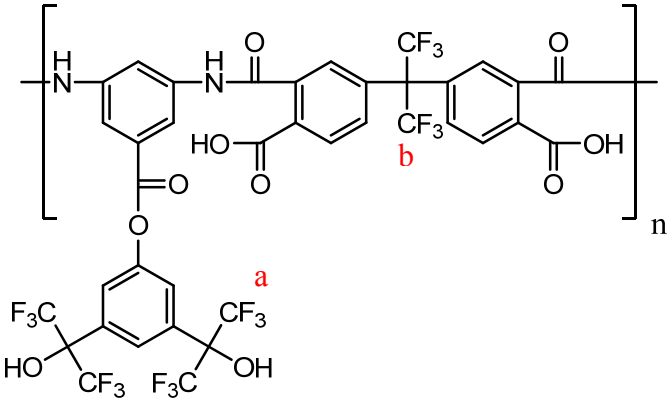

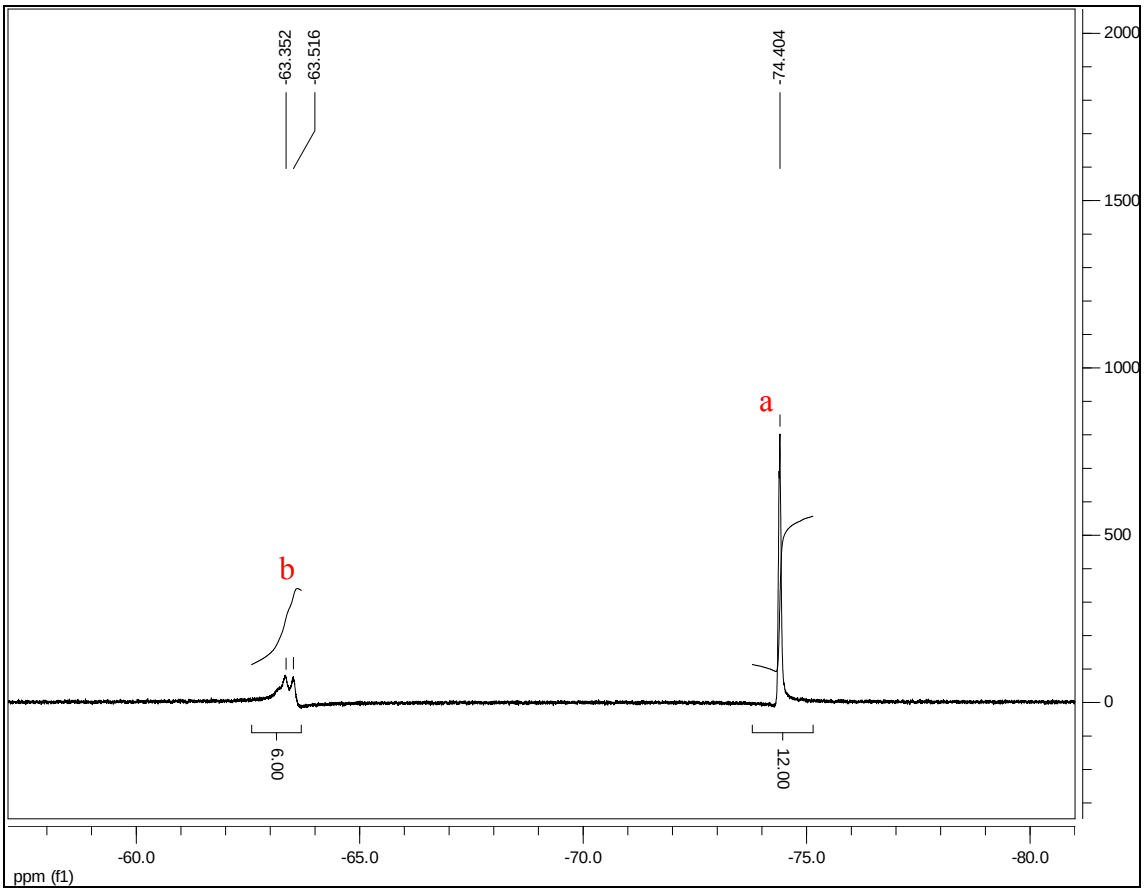

Figure B.1 Polymer **3.4** in DMSO-d_6

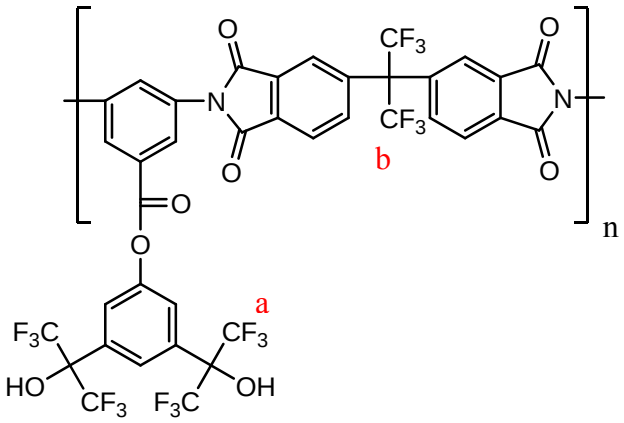

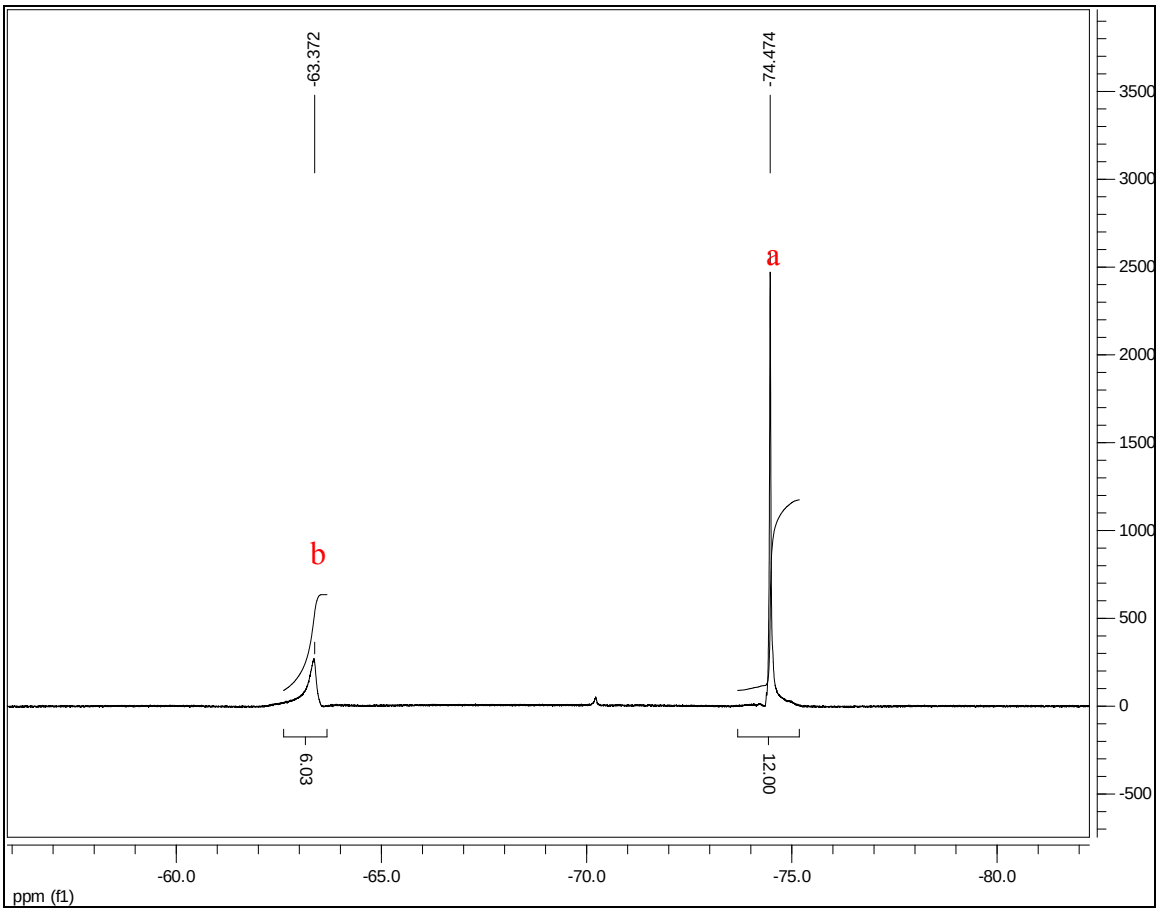

Figure B.2 Polymer **3.5** in DMSO-d_6

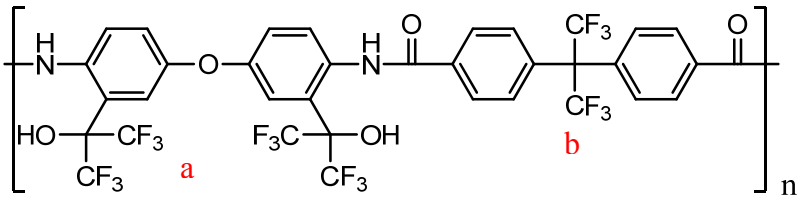

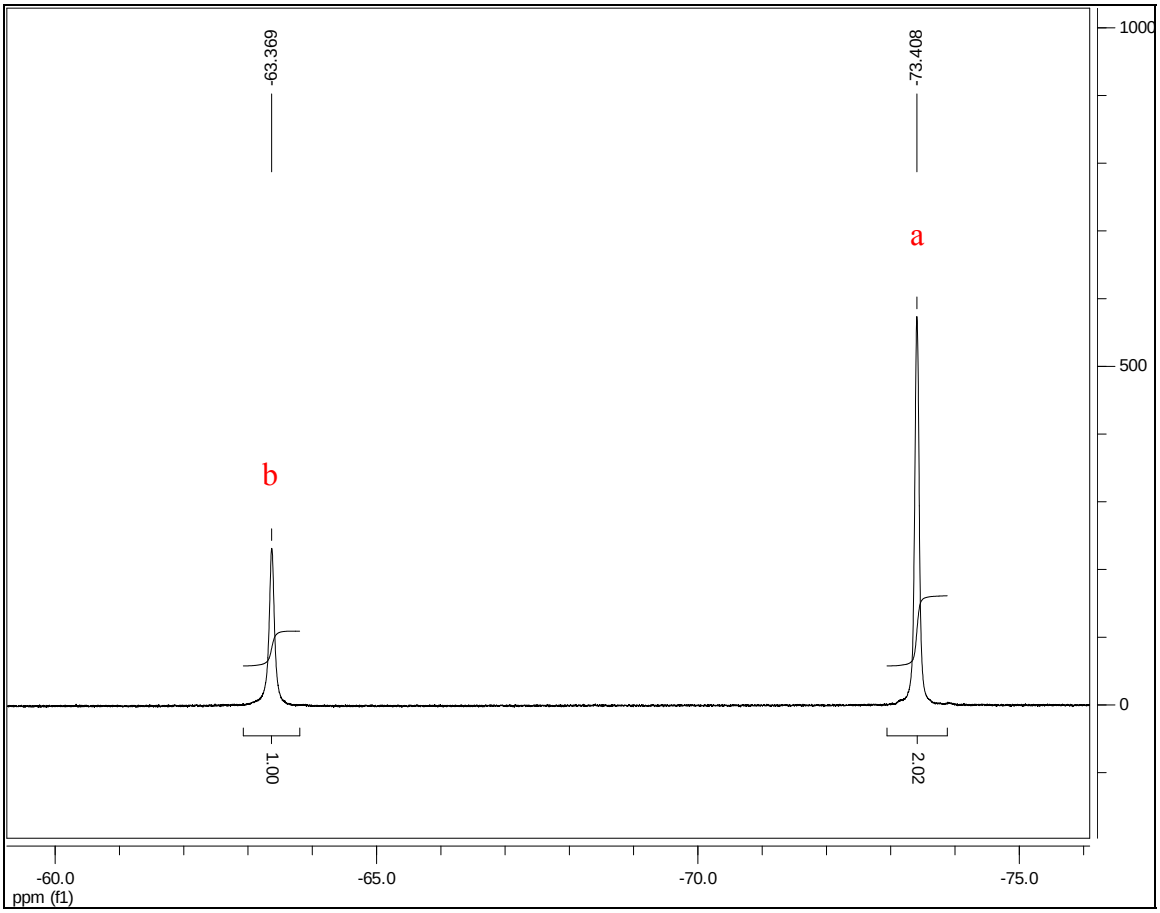

Figure B.3 PBOX-6FDC in DMSO-d_6

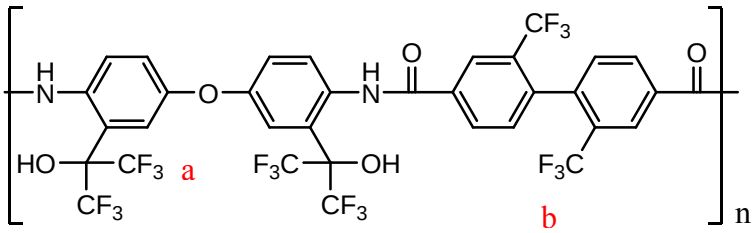

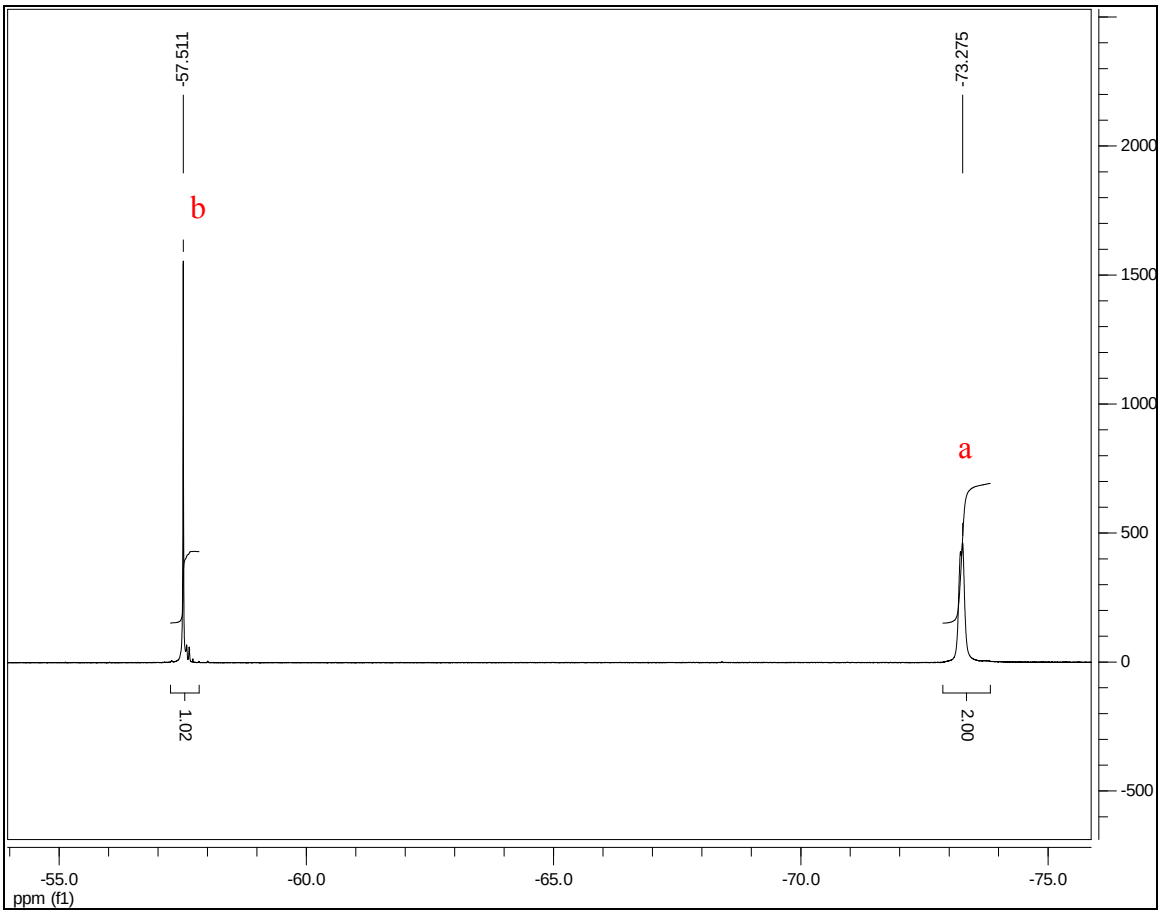

Figure B.4 PBOX-6FBDC in DMSO-d_6

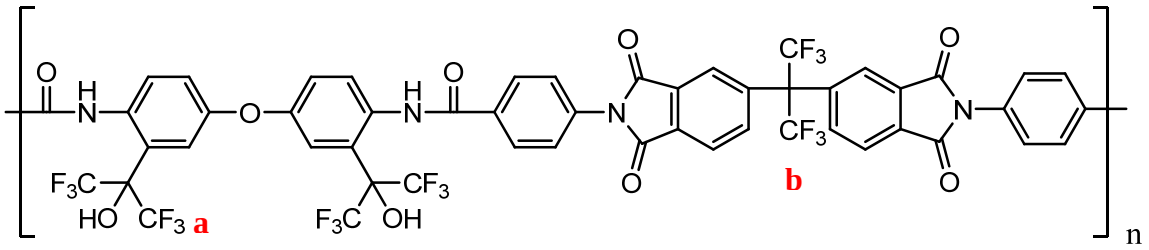

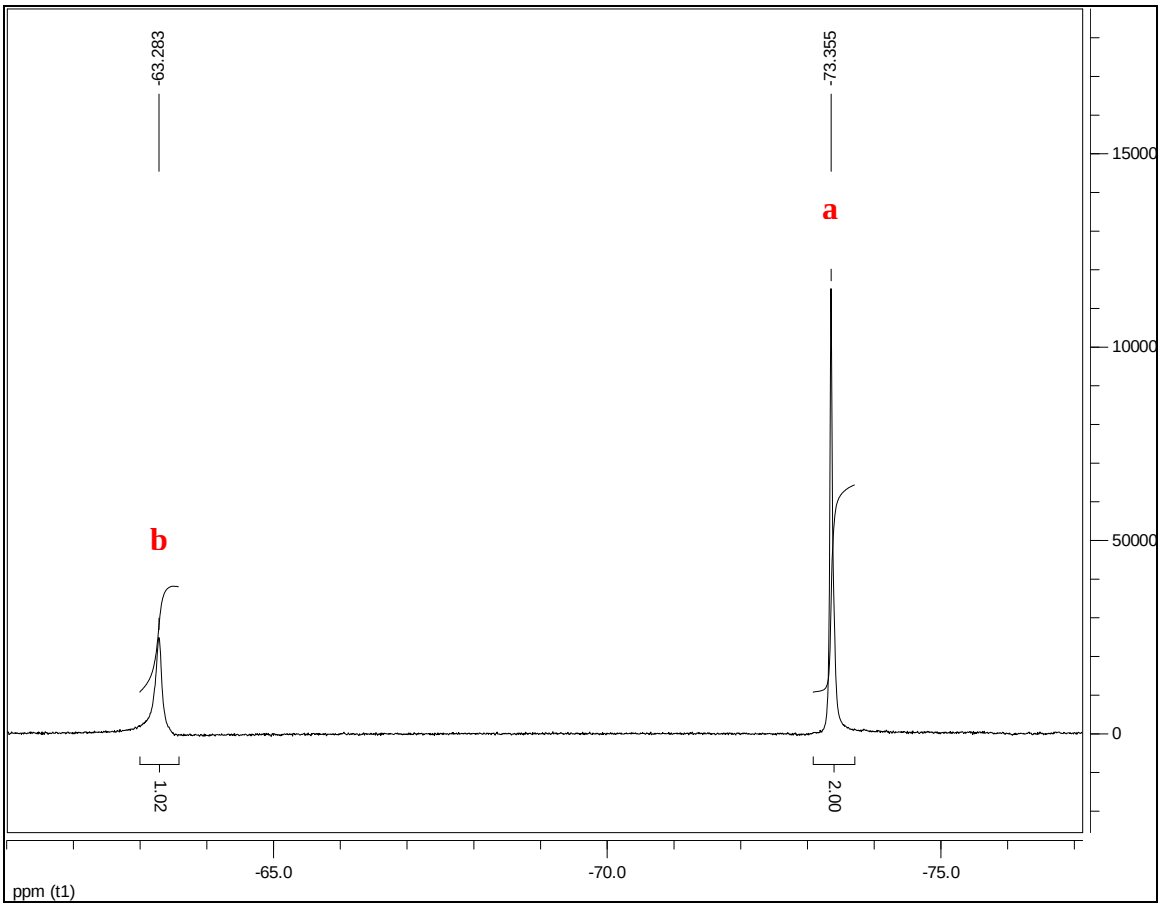

Figure B.5 PBOX-6FDIAC in DMSO-d_6

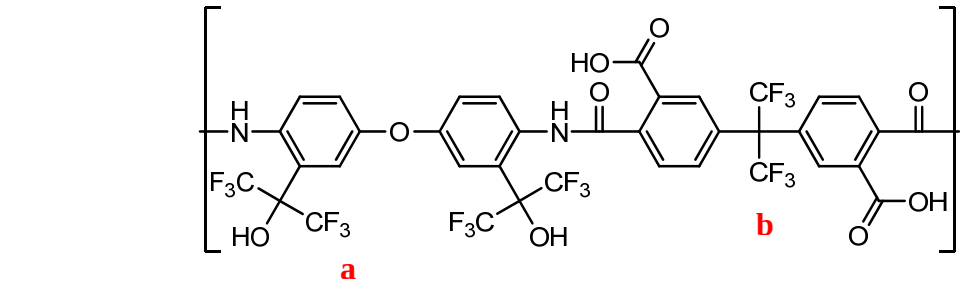

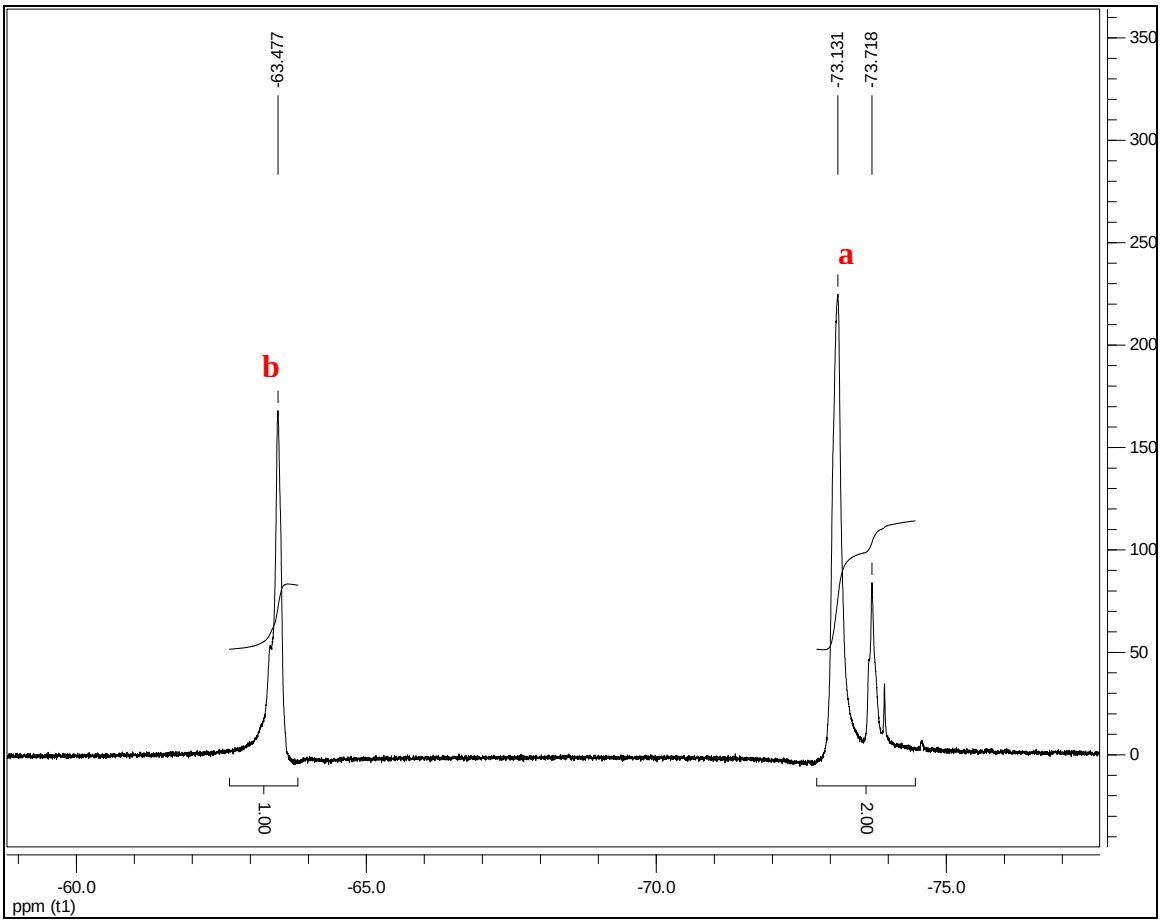

Figure B.6 Polymer **6.1** in DMSO-d_6

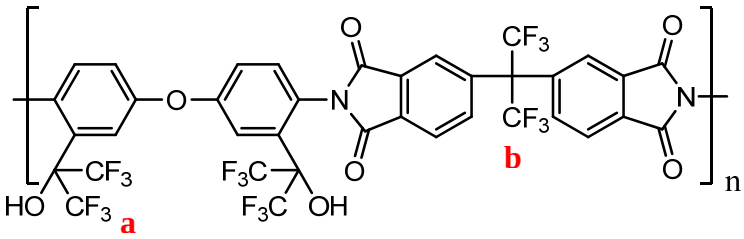

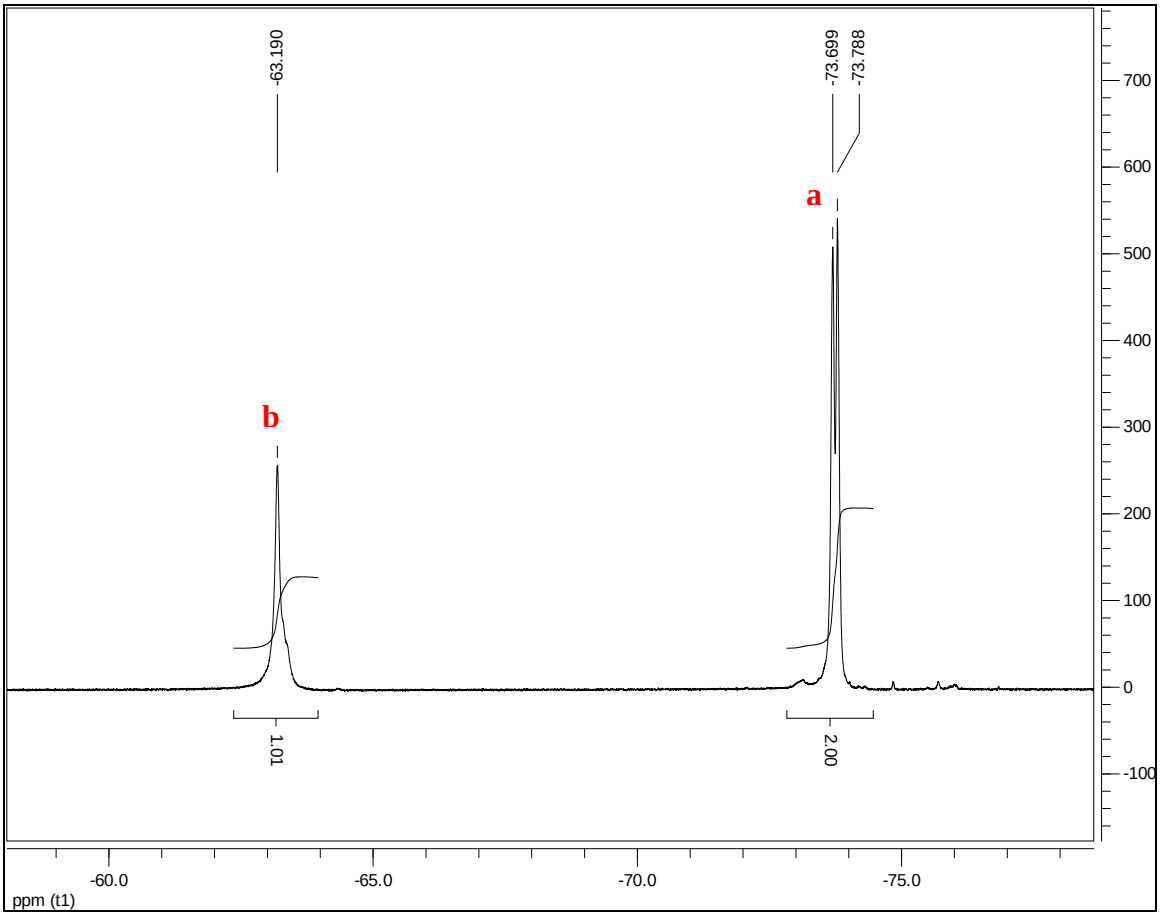

Figure B.7 Polymer **6.2** in DMSO-d_6

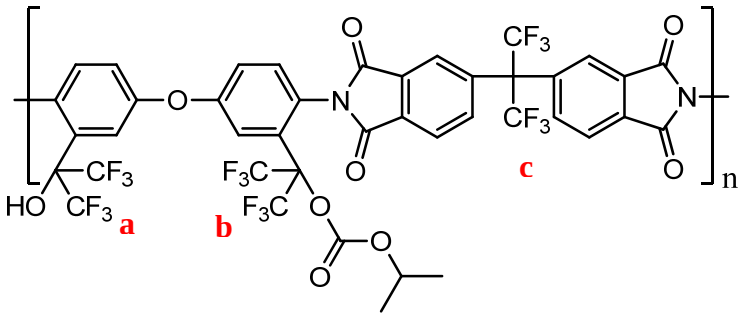

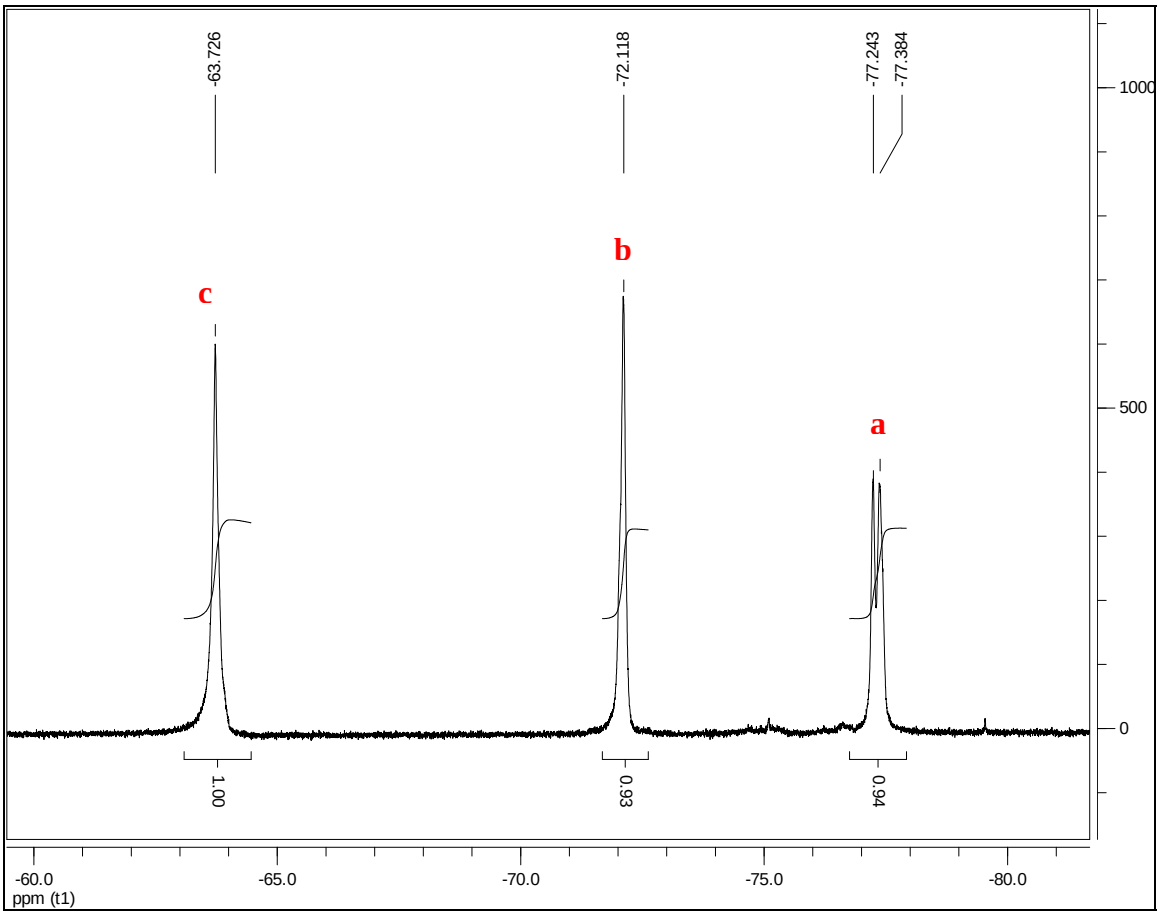

Figure B.8 Polymer **6.3** in $CDCl_3$

APPENDIX C

GPC

Table C.1 Polystyrene Standards

Molecular Weight (g/mol)	Retention Time (min)
215000	16.401
72200	17.714
30300	19.191
13100	20.619
2850	23.663
1260	25.35

Table C.2 Polymer Molecular Weights

Polymer	M_n (g/mol)	M_w (g/mol)	PDI
3.5	21,550	58,393	2.71
PBOX-IPC	9,855	20,140	2.04
PBOX-BPDC	29,589	73,521	2.49
PBOX-6FDC	22,824	46,436	2.04
PBOX-6FBDC	33,830	78.288	2.31
PBOX-6FDIAC	18,032	28,699	1.59
6.2	6,700	21,056	3.05
6.3	18,385	54,591	2.97

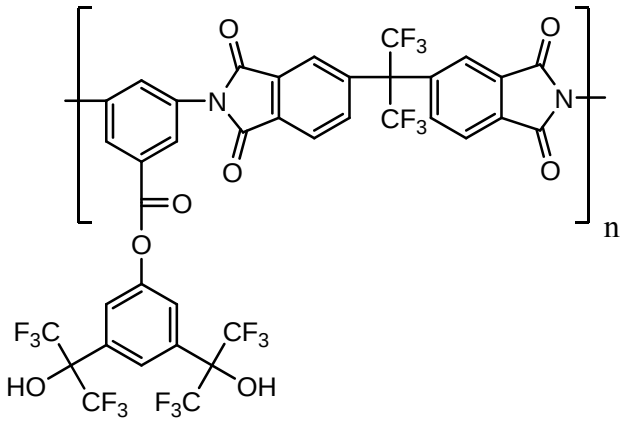

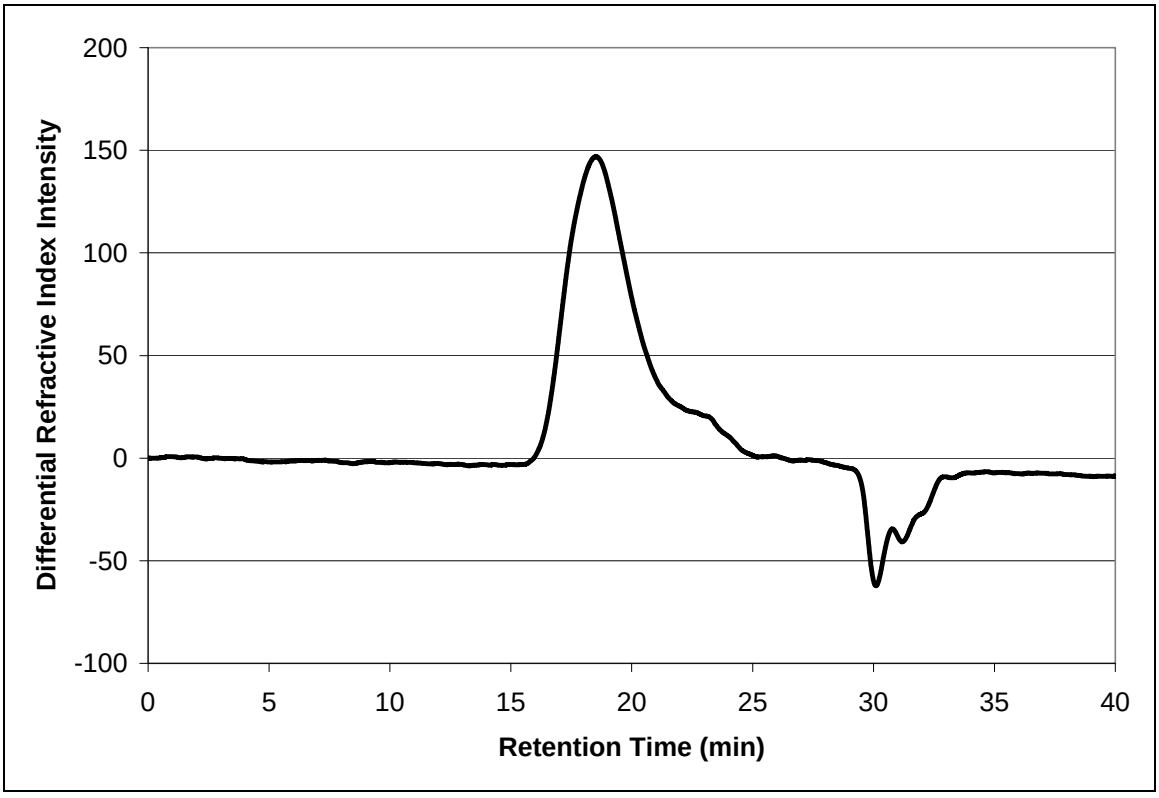

Figure C.1 Polymer **3.5** in THF

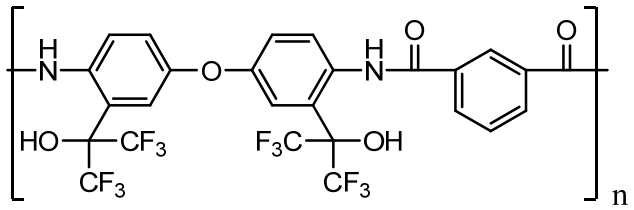

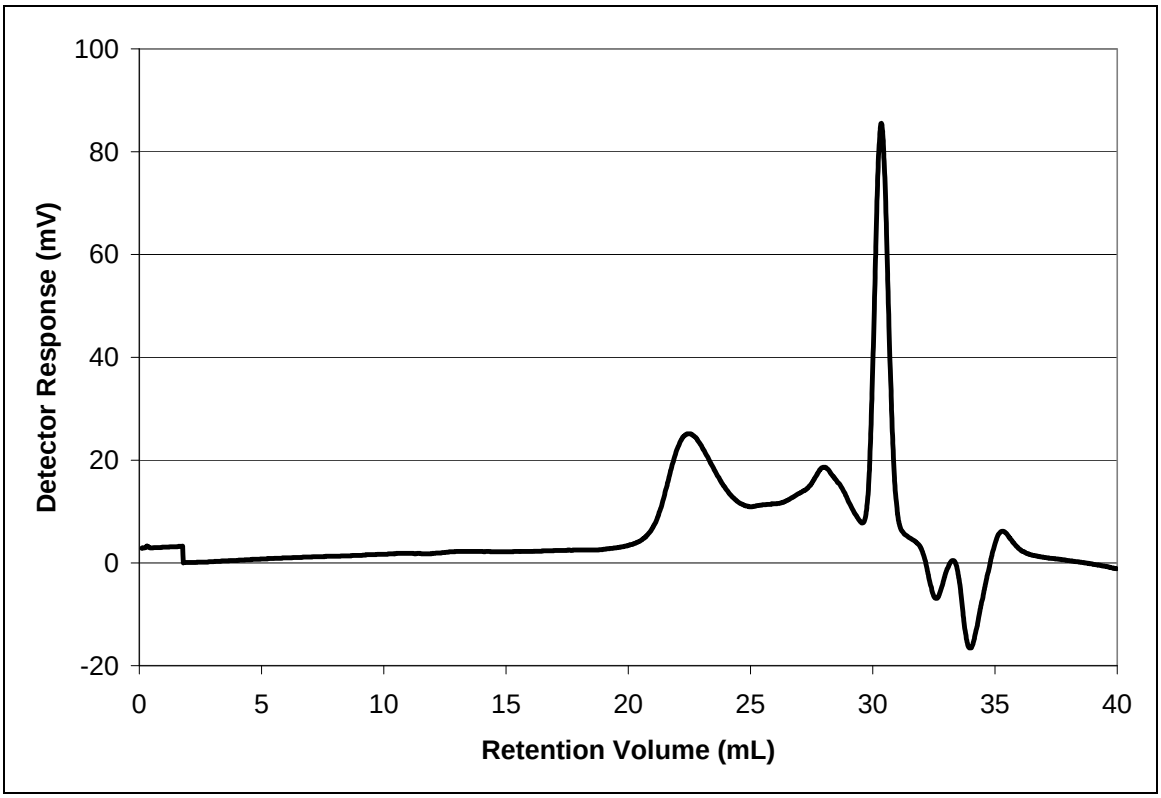

Figure C.2 PBOX-IPC in THF

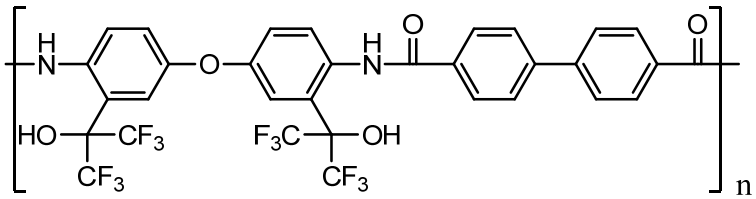

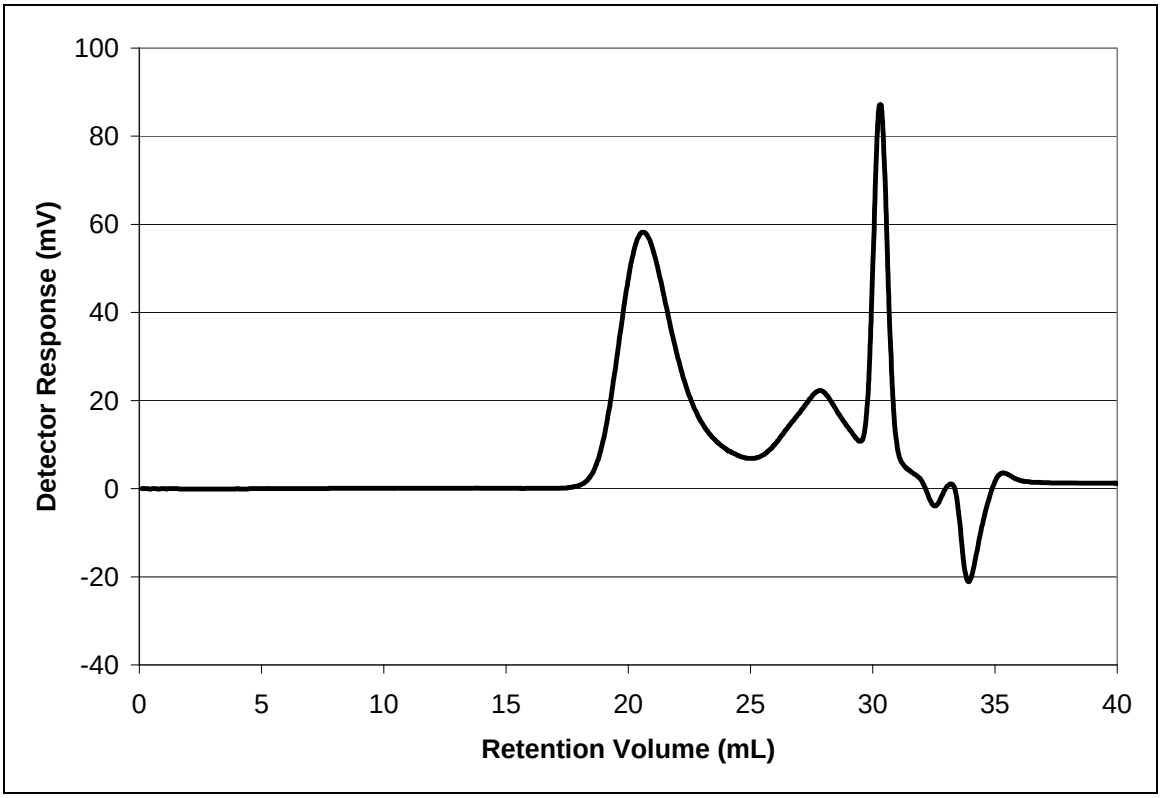

Figure C.3 PBOX-BPDC in THF

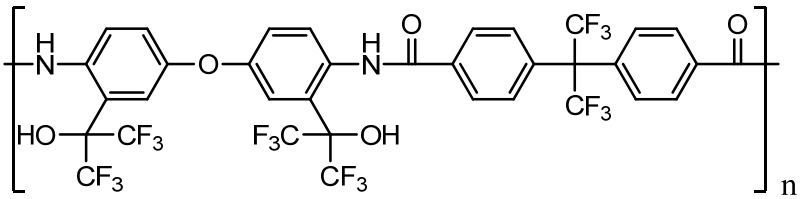

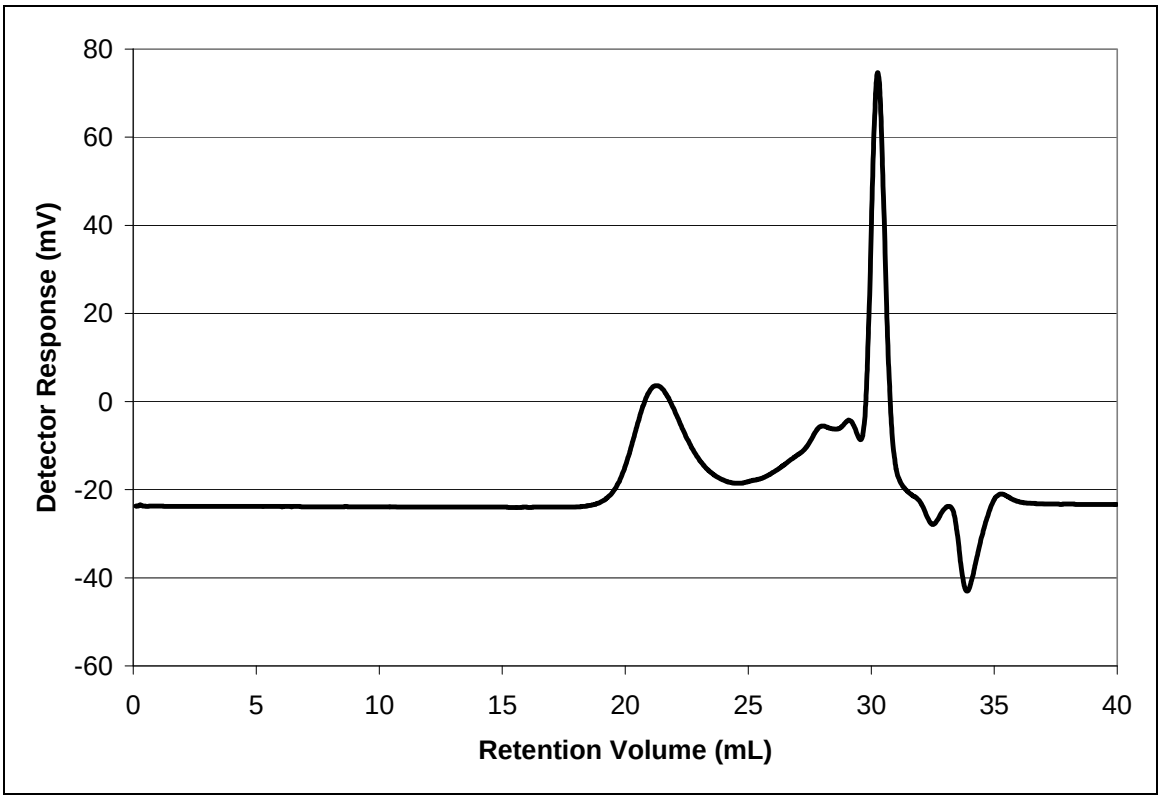

Figure C.4 PBOX-6FDC in THF

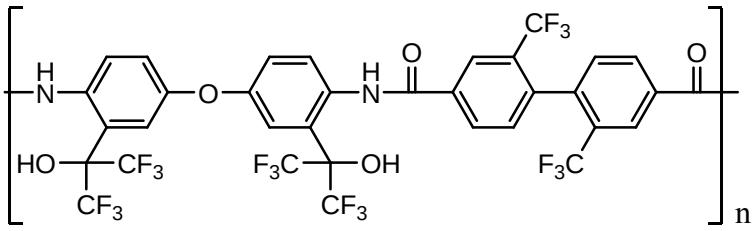

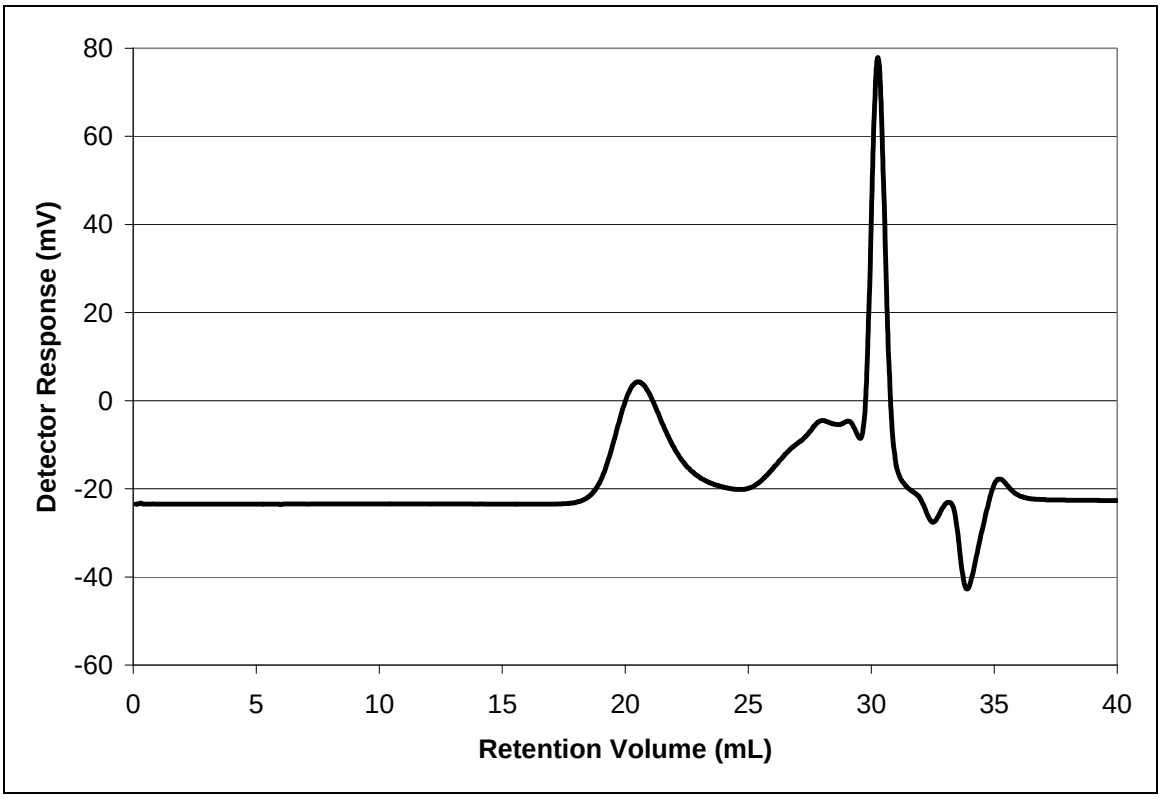

Figure C.5 PBOX-6FBDC in THF

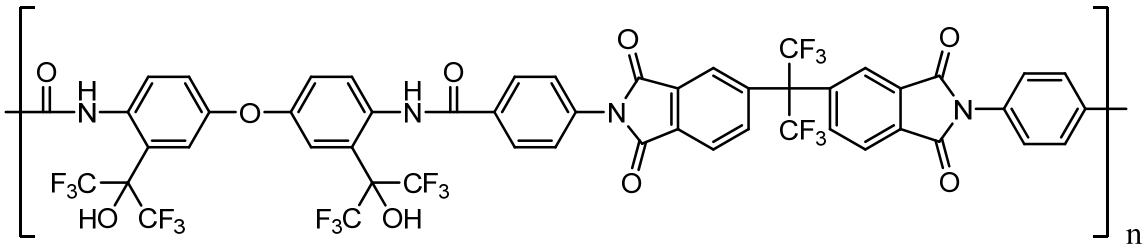

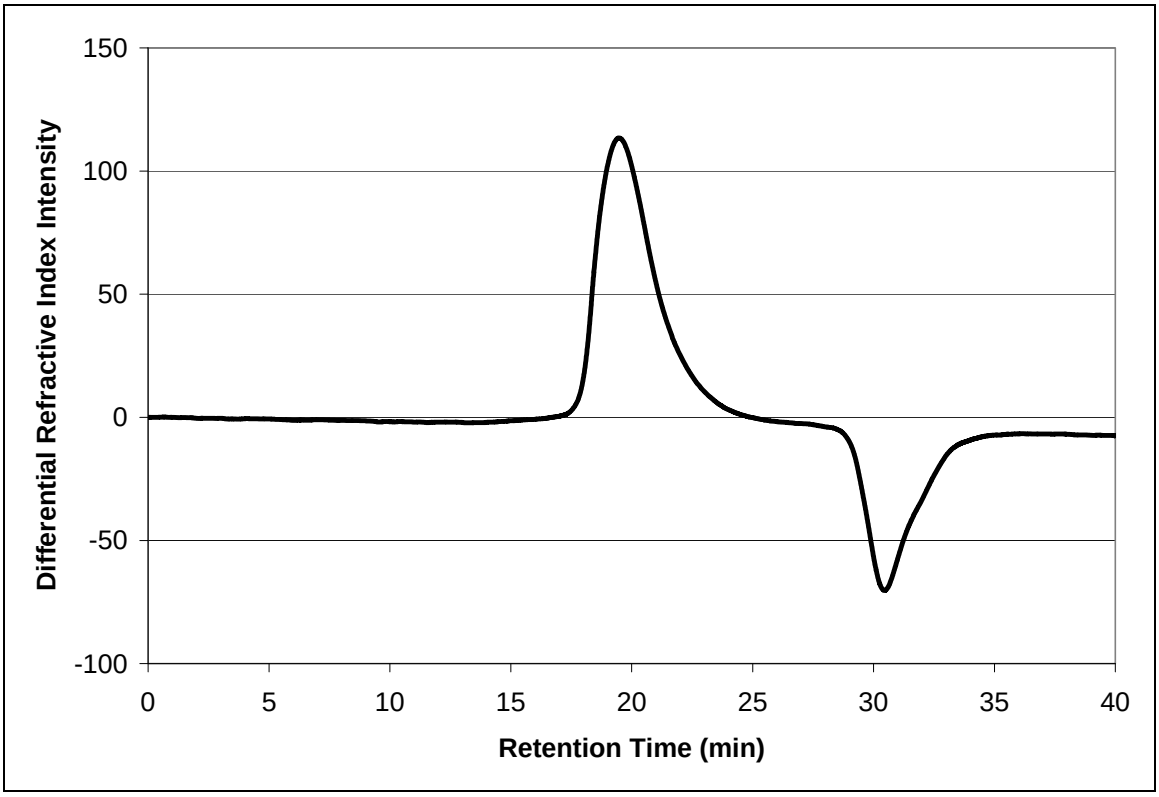

Figure C.6 PBOX-6FDIAC in THF

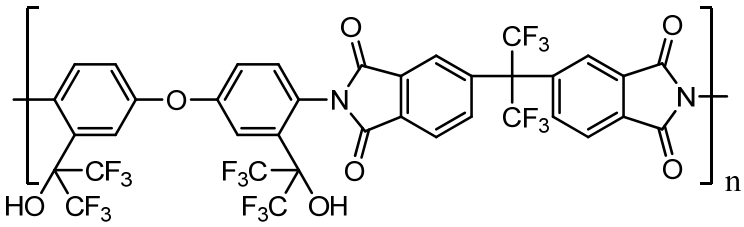

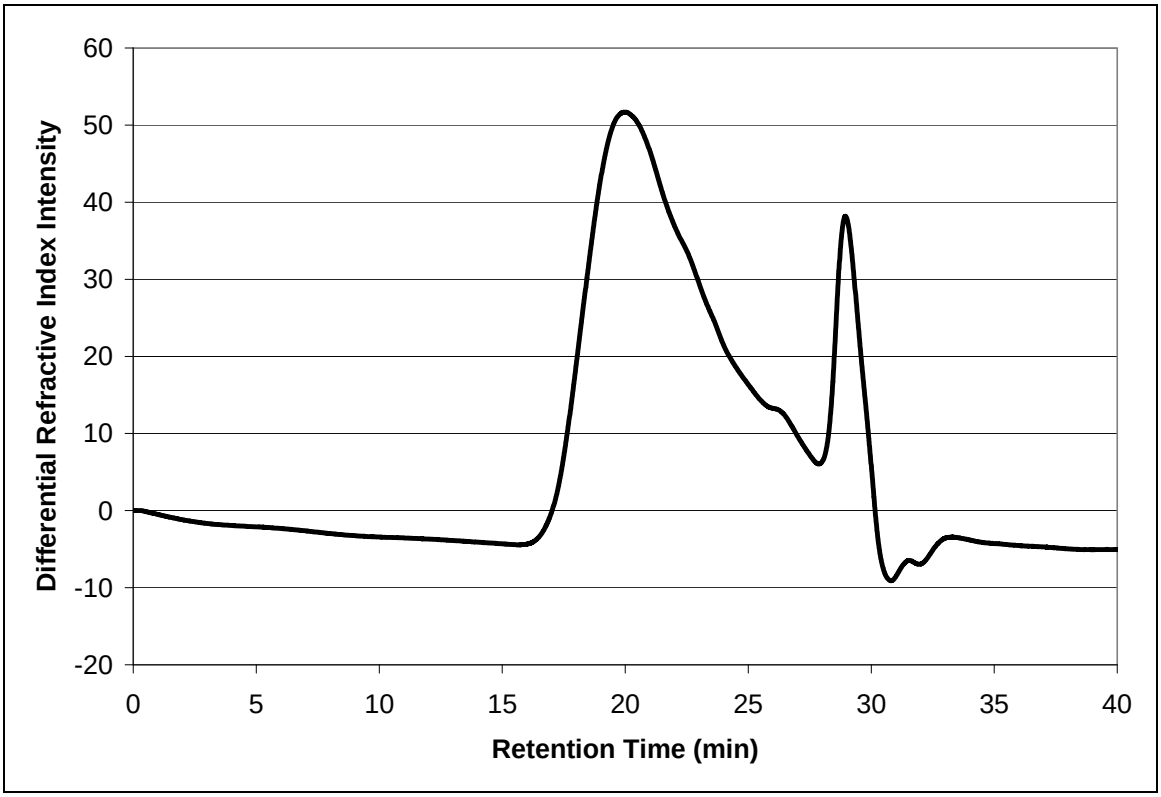

Figure C.7 Polymer **6.2** in THF

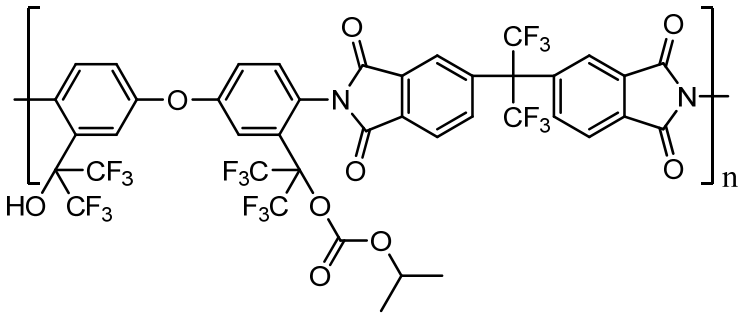

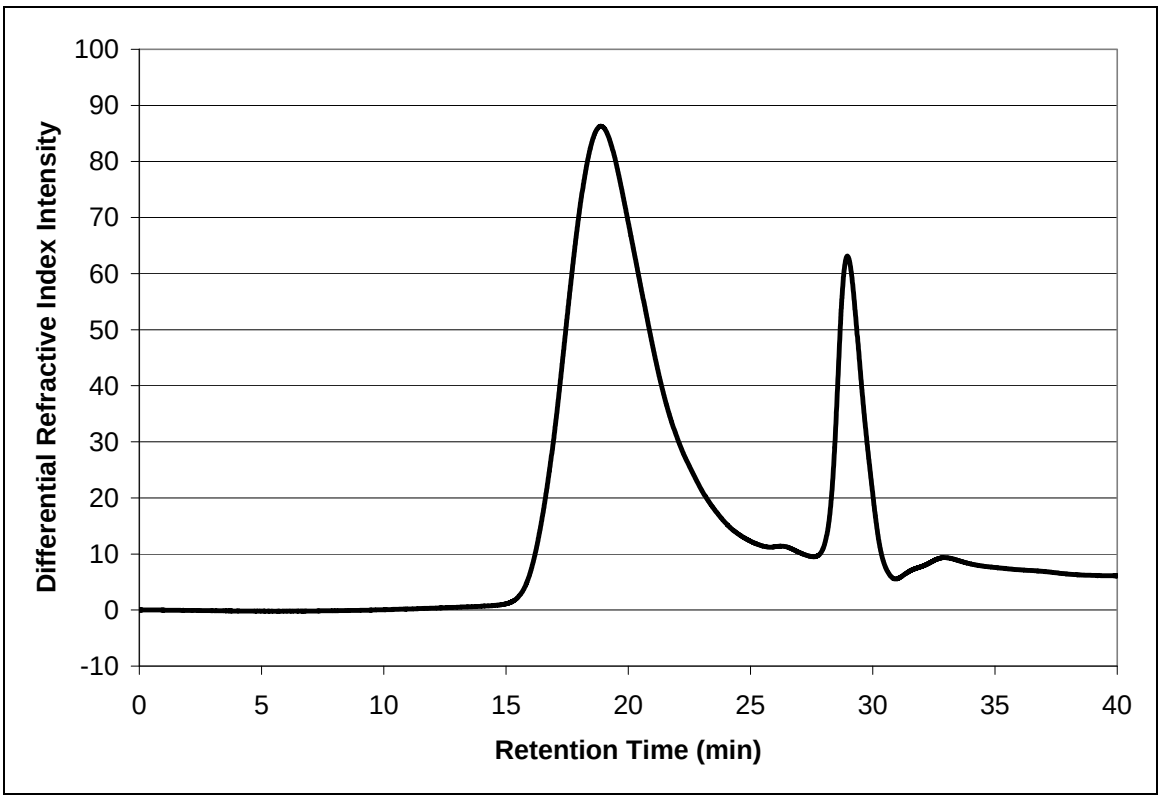

Figure C.8 Polymer **6.3** in THF

APPENDIX D

EXPERIMENTAL VALUES WITH CONFIDENCE INTERVALS

D.1 Dielectric Constant

$$k = 2C_{meas}\delta/\varepsilon_o A$$

C_{meas} = capacitance measured on the probe station

k = dielectric constant

δ = film thickness

A = capacitor area ($3.14*10^{-6}$ m^2)

ε_o = permittivity of air ($8.854*10^{-12}$ F/m)

Table D.1 Dielectric Measurements at 1 MHz

Polymer	Thickness (nm)	Average C_{meas} (pF)	Dielectric Constant	95 % Confidence
3.5 Before Side Group Cleavage	1755	25.38	3.20	0.01
3.5 After Side Group Cleavage	775	47.03	2.62	0.02
PBOX-IPC	2191	15.96	2.51	0.04
PBOX-BPDC	1848	19.79	2.63	0.03
PBOX-6FDC	2450	11.61	2.04	0.02
PBOX-6FBDC	2258	13.69	2.22	0.04
PBOX-6FDIAC	2790	11.14	2.23	0.03
6.2	1630	25.98	3.04	0.05
6.3	2616	13.23	2.49	0.04

D.2 Water Absorption

$$\text{Water Absorption} = \frac{(\text{Dry Frequency} - \text{Wet Frequency})}{(\text{Blank Frequency} - \text{Dry Frequency})}$$

Dry Frequency = quartz crystal frequency under nitrogen

Wet Frequency = quartz crystal frequency under 98 % relative humidity

Blank Frequency = quartz crystal frequency with no film

Table D.2 Water Absorption Measurements

Polymer	Average Wet Frequency (Hz)	Average Dry Frequency (Hz)	Blank Frequency (Hz)	Water Absorption (%)	95 % Confidence (%)
3.5	5002180	5002261	5004127	4.13	0.14
PBOX-IPC	5004276	5004285	5006592	0.38	0.02
PBOX-BPDC	5008128	5008140	5010984	0.42	0.03
PBOX-6FDC	4998968	4998978	5011093	0.09	0.01
PBOX-6FBDC	4999065	4999074	5006574	0.12	0.01
PBOX-6FDIAC	4937461	4937899	5011019	0.60	0.01
6.2	4995650	4996155	5006511	4.87	0.15
6.3	4996897	4997156	5006996	2.64	0.10

D.3 Coefficient of Thermal Expansion

D.3.1 Ellipsometer

$$CTE_{constrained} = (dThickness/dT)/(average\ thickness)$$

$$CTE_{unconstrained} = CTE_{constrained}*((1-\nu)/(1+\nu))$$

dThickness/*dT* = slope

ν = Poisson's ratio (0.33)

Table D.3.1 Ellipsometer Measurements

Polymer	Average Thickness (nm)	Slope (nm/K)	CTE (ppm/K)	95 % Confidence (ppm/K)
3.5 Before Side Group Cleavage	202.28	0.032	79.84	5.65
3.5 After Side Group Cleavage (Initial Heating)	136.62	0.010	36.80	5.31
3.5 After Side Group Cleavage (Repeated Heating)	136.04	0.016	59.62	7.18
PBOX-IPC	260.75	0.045	87.21	7.68
PBOX-IPC (ν = 0.3375)	260.75	0.045	85.74[a]	7.55
6.2	243.82	0.041	84.51	7.89
6.3	859.09	0.081	47.40	4.16

a) Identical to in-plane CTE from TMA

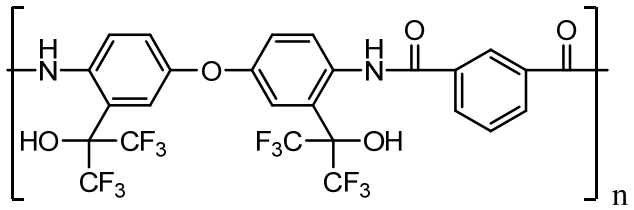

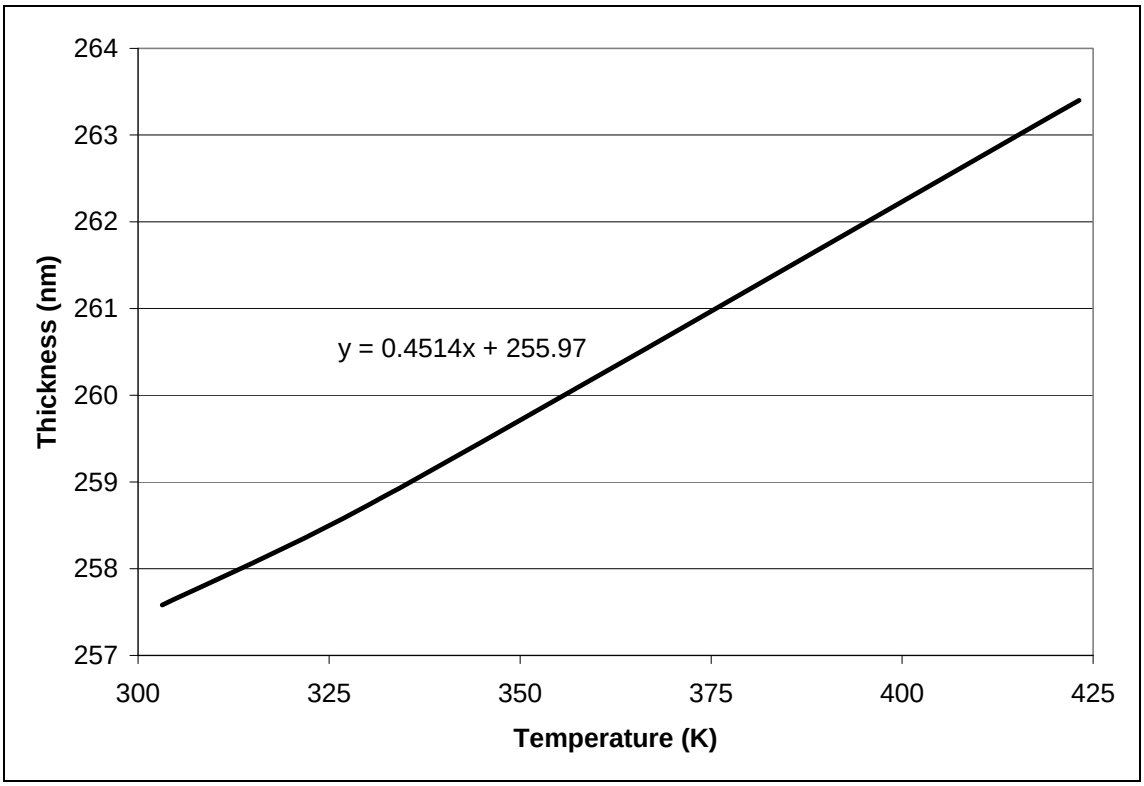

Figure D.3.1 CTE for PBOX-IPC

D.3.2 Thermal Mechanical Analysis

$$CTE = \text{slope/sample length}$$

Table D.3.2 TMA Measurements

Polymer	Sample length (mm)	Slope (μm/K)	Slope Error (μm/K)	CTE (ppm/K)	95 % Confidence (ppm/K)
PBOX-IPC	24.7887	2.125	0.000696	85.74	0.055
PBOX-BPDC	11.9509	1.075	0.000993	89.93	0.16
PBOX-6FDC	12.0514	0.982	0.00172	81.49	0.28
PBOX-6FBDC	12.2216	1.030	0.00359	84.31	0.58
PBOX-6FDIAC	16.3868	1.223	0.00295	74.61	0.35

D.4 Young's Modulus

D.4.1 Atomic Force Microscopy

$$z - z_0 = d - d_0 + \sqrt{\frac{k(d - d_0)}{(2/\pi)[E(1 - \nu^2)]\tan(\alpha)}}$$

d_0 = zero deflection (nm)

z_0 = contact point (nm)

k = cantilever spring constant (60 mN/m)

α = half-opening angle (10°)

Table D.4.1 AFM Measurements

Polymer	Slope	d_0 (nm)	$E/(1-\nu^2)$ (GPa)	95 % Confidence (GPa)
3.5 Before Side Group Cleavage	-0.9897	-282.026	23.27	5.09
3.5 After Side Group Cleavage	-0.9763	-247.095	5.93	1.96
PBOX-IPC	-0.9818	-206	6.03	0.68
PBOX-BPDC	-0.9826	-1130.71	4.34	2.58
PBOX-6FDC	-0.9885	-296.277	17.56	1.17
PBOX-6FBDC	-0.9854	-205.531	22.97	2.87

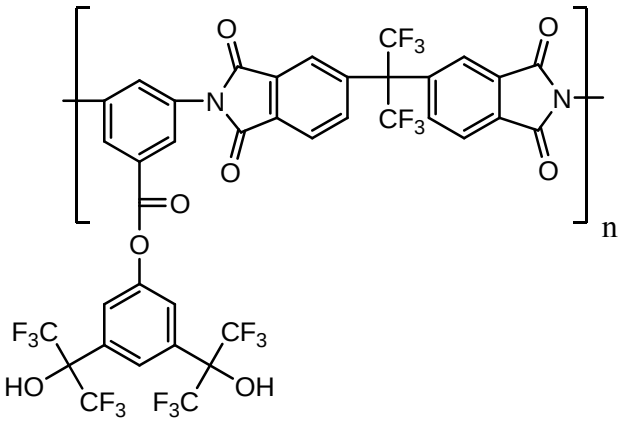

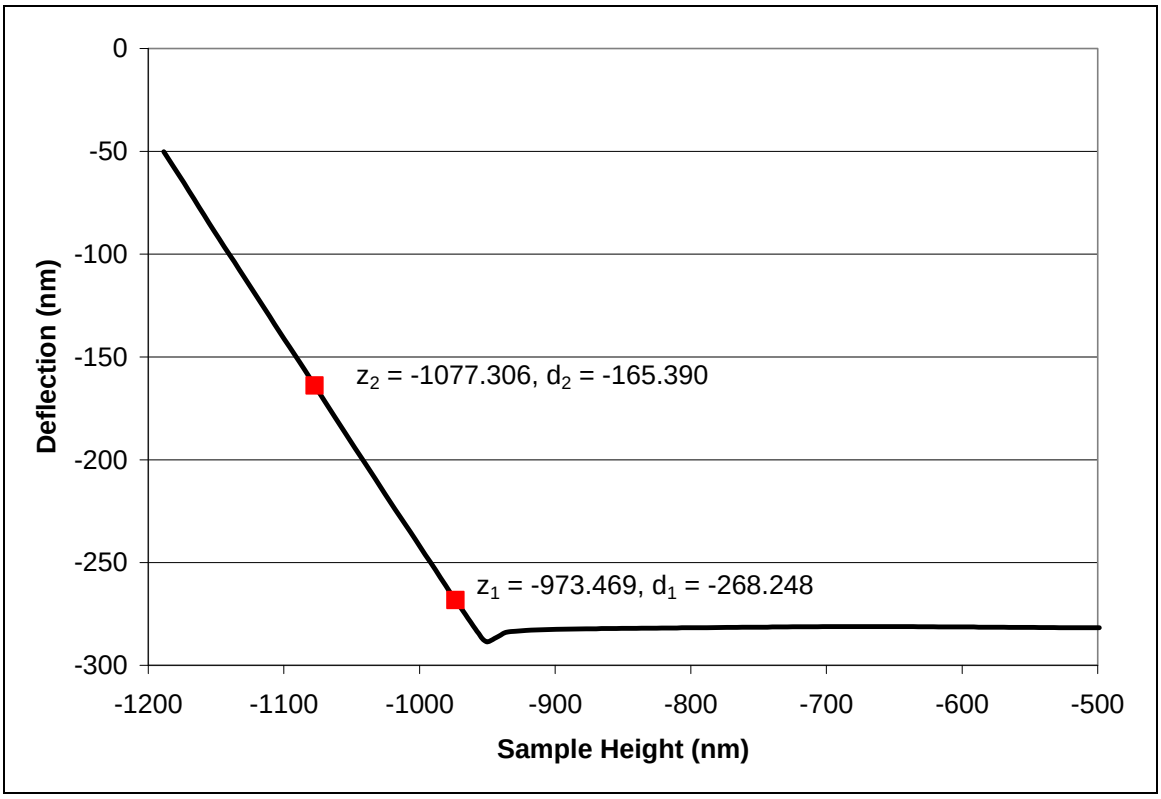

Figure D.4.1 AFM for Polymer **3.5**

D.4.2 Nanoindentation

$$E/(1-\nu^2) = \{(1/E_r) - [(1-\nu_i^2)/E_i]\}^{-1}$$

E_r = Sample Reduced Modulus (GPa)

E = Sample Young's Modulus (GPa)

ν = Sample Poisson's Ratio

E_i = indenter Young's Modulus (1140 GPa)

ν_i = indenter Poisson's Ratio (0.07)

Table D.4.2 Nanoindentation Results

Polymer	Reduced Modulus (GPa)	$E/(1-\nu^2)$ (GPa)	95 % Confidence (GPa)
3.5 Before Side Group Cleavage	22.36	22.81	0.78
PBOX-6FDIAC	18.32	18.62	0.31
6.2	8.37	8.44	1.80
6.3	6.40	6.44	1.73

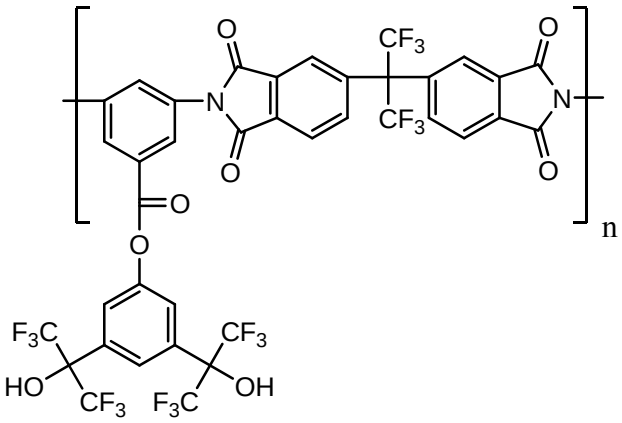

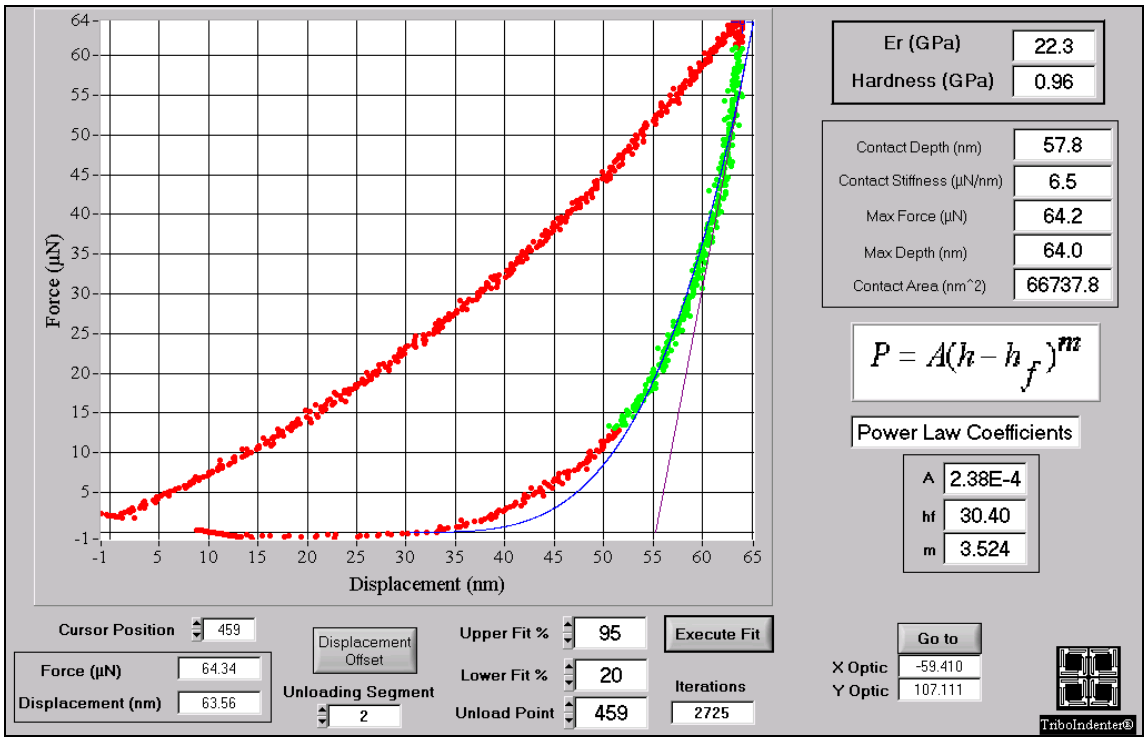

Figure D.4.2 Nanoindentation for Polymer **3.5**

BIBLIOGRAPHY

Agrawal, A. and C. L. Henderson (2003). "Investigation of surface inhibition and its effects on the lithographic performance of polysulfone-novolak electron-beam resists." Proc. SPIE-Int. Soc. Opt. Eng. FIELD Full Journal Title:Proceedings of SPIE-The International Society for Optical Engineering **5039**(Pt. 2, Advances in Resist Technology and Processing XX): 1019-1030.

Akimoto, S., M. Jikei, et al. (2000). "A novel photosensitive polyimide: a polyimide containing the hydroxytriphenylamine structure with diazonaphthoquinone." High Perform. Polym. FIELD Full Journal Title:High Performance Polymers **12**(1): 177-184.

Ando, S. and M. Yoshida (2003). Synthesis and Optical Properties of Rod-Like Fluorinated Polyimides Having High Charge-Transfer Interactions. Proc. 6th European Conf. Polyimides & High Performance Polymers.

Bae, Y. C., K. Douki, et al. (2002). "Tailoring transparency of imageable fluoropolymers at 157 nm by incorporation of hexafluoroisopropyl alcohol to photoresist backbones." Chem. Mater. FIELD Full Journal Title:Chemistry of Materials **14**(3): 1306-1313.

Bai, Y., P. Chiniwalla, et al. (2004). "Photosensitive polynorbornene based dielectric. I. Structure-property relationships." Journal of Applied Polymer Science **91**(5): 3023-3030.

Barrett, C. R. (1997). The Solid-State Century. Scientific American, Special Issue**:** 56-61.

Beckham, H. W. (2000). Spectroscopy. Atlanta, GA, Georgia Institute of Technology.

Bhushan, B., J. C. Wyant, et al. (1985). "Measurement of surface topography of magnetic tapes by Mirau interferometry." Applied Optics **24**(10): 1489-1497.

Bruma, M., F. Mercer, et al. (1995). "Synthesis and characterization of fluorinated poly(imide-amide-sulfone)s." J. Appl. Polym. Sci. FIELD Full Journal Title:Journal of Applied Polymer Science **56**(5): 527-32.

Bruma, M., F. Mercer, et al. (1994). "Fluorinated poly(benzoxazole-imide)s." Polym. Adv. Technol. FIELD Full Journal Title:Polymers for Advanced Technologies **5**(9): 535-40.

Bruma, M., B. Schulz, et al. (1994). "Synthesis and characterization of fluorinated poly(imide-pyridazine-amide)s." Polymer FIELD Full Journal Title:Polymer **35**(19): 4209-14.

Chang, J.-H., D.-K. Park, et al. (2001). "Montmorillonite-based nanocomposites of polybenzoxazole: synthesis and characterization (Part 1)." Journal of Polymer Science, Part B: Polymer Physics **39**(5): 471-476.

Chang, J.-H., K. M. Park, et al. (2000). "Two-step thermal conversion from poly(amic acid) to polybenzoxazole via polyimide: their thermal and mechanical properties." Journal of Polymer Science, Part B: Polymer Physics **38**(19): 2537-2545.

Chen, X., M. Anthamatten, et al. (2006). "Vapor deposition and curing of polybenzoxazole precursors." Macromolecules **39**(22): 7561-7565.

Chiba, T., R. J. Hung, et al. (2000). "Resist (157 nm) materials: a progress report." J. Photopolym. Sci. Technol. FIELD Full Journal Title:Journal of Photopolymer Science and Technology **13**(4): 657-664.

Choi, K. H., J. C. Jung, et al. (2005). "New base-soluble positive-working photosensitive polyimides having o-nitrobenzyl ester group." Polymers for Advanced Technologies **16**(5): 387-392.

Choi, S. M., K. J. Kim, et al. (2005). "Synthesis and characterization of negative-type photosensitive polyimides based on cyclobutane-1,2,3,4-tetracarboxylic dianhydride." Journal of Applied Polymer Science **96**(6): 2300-2308.

Clarke, M. E. (2001). Introducing Low-k Dielectrics into Semiconductor Processing, Mykrolis**:** 1-20.

Dammel, R. R. Diazonaphthoquinone-Based Resists. SPIE Short Course SC104.

Dammel, R. R., R. Sakamuri, et al. (2001). "New resin systems for 157 nm lithography." J. Photopolym. Sci. Technol. FIELD Full Journal Title:Journal of Photopolymer Science and Technology **14**(4): 603-612.

Dang, T. D., F. E. Arnold, et al. (2001). "Low Dielectric Constant Polymers Developed for High-Speed Integrated Circuits." from http://www.afrlhorizons.com/Briefs/June01/ML0016.html. Accessed June 3, 2004.

Dang, T. D., P. T. Mather, et al. (2000). "Synthesis and characterization of fluorinated benzoxazole polymers with high Tg and low dielectric constant." Journal of Polymer Science, Part A: Polymer Chemistry **38**(11): 1991-2003.

Domke, J. and M. Radmacher (1998). "Measuring the Elastic Properties of Thin Polymer Films with the Atomic Force Microscope." Langmuir **14**(12): 3320-3325.

Ebara, K., Y. Shibasaki, et al. (2003). New synthetic route for positive photoresist based on poly(benzoxazole) precursor from diphenyl isophthalate and bis(o-aminophenol). RadTech Asia.

Fahey, J., W. Conley, et al. (1995). "A new positive tone deep-UV photoresist based on poly(4-hydroxystyrene) and an acid labile protecting group." Proc. SPIE-Int. Soc. Opt. Eng. FIELD Full Journal Title:Proceedings of SPIE-The International Society for Optical Engineering **2438**(Advances in Resist Technology and Processing XII): 125-42.

Farona, M. F. (1996). "Benzocyclobutenes in polymer chemistry." Progress in Polymer Science **21**(3): 505-555.

Foster, R. (1995). "Photoimageable BCB technology lowers costs for MCMs." Solid State Technology **38**(6): 125-6,128,130.

Fujita, Y. and M. Tomikawa (2001). Positive photoimaging polybenzoxazole precursor compositions containing o-quinonediazide derivatives. Application: JP, (Toray Industries, Inc., Japan). 12 pp.

Guzman-Lucero, D. and D. Likhatchev (2002). "Imide-to-benzoxazole rearrangement in ortho substituted poly(4-4'-diphenylene pyromellitimide)s." Polym. Bull. (Berlin, Ger.) FIELD Full Journal Title:Polymer Bulletin (Berlin, Germany) **48**(3): 261-269.

Hall, S. and C. C. Schuckert (1999). "Single mask wafer overcoat process using photodefinable polyimide." Solid State Technology **42**(10): 95-96.

Hamciuc, C., E. Hamciuc, et al. (2000). "New fluorinated poly(imide-ether-amide)s." High Perform. Polym. FIELD Full Journal Title:High Performance Polymers **12**(2): 265-276.

Hamciuc, E., C. Hamciuc, et al. (2000). "Fluorinated heterocyclic polyamides." Eur. Polym. J. FIELD Full Journal Title:European Polymer Journal **37**(2): 287-293.

Hamciuc, E., C. Hamciuc, et al. (2000). "Synthesis and study of new fluorinated poly(imide-amide)s." Macromol. Mater. Eng. FIELD Full Journal Title:Macromolecular Materials and Engineering **283**: 36-40.

Hasegawa, T. and K. Maeda (2005). Polybenzoxazoles with low linear thermal expansion coefficient, their precursors, coating solutions containing them, their films, and their manufacture. Application: JP, (Central Glass Co., Ltd., Japan). 14 pp.

Henderson, C. L. (1998). Advances in Photoresist Characterization and Lithography Simulation, University of Texas at Austin. **Ph.D.**

Hergenrother, P. M., K. A. Watson, et al. (2004). "Copolyimides from 2,3,3',4'-biphenyltetracarboxylic dianhydride and pyromellitic dianhydride with 4,4'-oxydianiline." Polymer FIELD Full Journal Title:Polymer **45**(16): 5441-5449.

Hinsberg, W. D., F. A. Houle, et al. (2001). "Chemical and physical aspects of the post-exposure baking process used for positive-tone chemically amplified resists." IBM Journal of Research and Development **45**(5): 667-681.

Hoskins, T. P. J. (2005). Characterization of Sustituted Polynorbornenes for Advanced Lithography, Georgia Institute of Technology**:** 223.

Hsia, C. C. (2006). "The quest of porous ELK materials for high performance logic technologies." Microelectron. Eng. FIELD Full Journal Title:Microelectronic Engineering **83**(11-12): 2055-2058.

Hsiao, S.-H. and Y.-J. Chen (2000). "Synthesis and properties of hydroxy-containing ortho-linked poly(ether-imide)s." High Perform. Polym. FIELD Full Journal Title:High Performance Polymers **12**(4): 515-524.

Hsu, S. L.-C. and W.-C. Chen (2002). "A Novel Positive Photosensitive Polybenzoxazole Precursor for Microelectronic Applications." Polymer **43**(25): 6743-6750.

Hsu, S. L.-C., W.-C. Chen, et al. (2003). "A novel positive photosensitive polybenzoxazole based on a tetrahydropyranyl (THP) protected polyhydroxyamide." Polymer Bulletin (Berlin, Germany) **50**(5-6): 295-302.

Hsu, S. L.-C., P.-I. Lee, et al. (2002). "Synthesis and characterization of a positive-working, aqueous-base-developable photosensitive polyimide precursor." Journal of Applied Polymer Science **86**(2): 352-358.

Huang, X. and A. A. Pelegri (2003). "Nanoindentation Measurements on Low- kPorous Silica Thin Films Spin Coated on Silicon Substrates." Journal of Engineering Materials and Technology **125**: 361-367.

Irvin, D. J., P. E. Cassidy, et al. (1996). "N-methylated copoly(imide amide)s containing hexafluoroisopropylidene." Polymer FIELD Full Journal Title:Polymer **37**(11): 2227-2232.

Ito, H., N. Seehof, et al. (1997). "Synthesis and preliminary evaluation of substituted poly(norbornene sulfones) for 193 nm lithography." Polym. Mater. Sci. Eng. FIELD Full Journal Title:Polymeric Materials Science and Engineering **77**: 449-450.

Ito, H., H. D. Truong, et al. (2004). "Fluoropolymer resists: Fundamentals and lithographic evaluation." J. Photopolym. Sci. Technol. FIELD Full Journal Title:Journal of Photopolymer Science and Technology **17**(4): 609-620.

Ito, H., G. M. Wallraff, et al. (2001). "Polymer design for 157-nm chemically amplified resists." Proc. SPIE-Int. Soc. Opt. Eng. FIELD Full Journal Title:Proceedings of SPIE-The International Society for Optical Engineering **4345**(Pt. 1, Advances in Resist Technology and Processing XVIII): 273-284.

Ito, H., G. M. Wallraff, et al. (2001). "Development of 157 nm positive resists." J. Vac. Sci. Technol., B FIELD Full Journal Title:Journal of Vacuum Science & Technology, B: Microelectronics and Nanometer Structures **19**(6): 2678-2684.

Jakubek, V., X.-Q. Liu, et al. (2003). "Strategies for high transparency acrylate resists for 157 nm lithography." J. Photopolym. Sci. Technol. FIELD Full Journal Title:Journal of Photopolymer Science and Technology **16**(4): 573-580.

Jung, M.-S., J. Hyeon-Lee, et al. (2008). "A positive-working photosensitive polyimide based on thermal crosslinking and acidolytic cleavage." J. Appl. Polym. Sci. FIELD Full Journal Title:Journal of Applied Polymer Science **107**(4): 2632-2637.

Kahle, O., U. Wielsch, et al. (1998). "Glass transition temperature and thermal expansion behavior of polymer films investigated by variable temperature spectroscopic ellipsometry." Thin Solid Films **313-314**: 803-807.

Kim, J.-H. and J. K. Lee (2001). "Hydroxy-substituted polyenaminonitrile as a soluble precursor for rigid-rod polybenzoxazole." Bulletin of the Korean Chemical Society **22**(9): 999-1004.

Kirchhoff, R. A. and K. J. Bruza (1994). "Polymers from benzocyclobutenes." Advances in Polymer Science **117**(High Performance Polymers): 1-66.

Kuo, S.-W., C.-F. Huang, et al. (2005). "Synthesis, thermal properties, and specific interactions of high Tg increase in poly(2,6-dimethyl-1,4-phenylene oxide)-block-polystyrene copolymers." Polymer FIELD Full Journal Title:Polymer **46**(22): 9348-9361.

Lavrenko, P., O. Okatova, et al. (2003). "Conformational and dynamo-optical properties of fluorinated poly(p-phenylene-1,3,4-oxadiazole-imide-amide) molecules in solutions." Polymer FIELD Full Journal Title:Polymer **44**(10): 2919-2925.

Lee, J. K., J.-H. Kim, et al. (2003). "Synthesis and characterization of fluorine-containing polybenzoxazoles by high-temperature direct polycondensation." Bulletin of the Korean Chemical Society **24**(7): 1029-1031.

Li, W., P. R. Varanasi, et al. (2003). "Rational design in cyclic olefin resists for sub-100-nm lithography." Proc. SPIE-Int. Soc. Opt. Eng. FIELD Full Journal Title:Proceedings of SPIE-The International Society for Optical Engineering **5039**(Pt. 1, Advances in Resist Technology and Processing XX): 61-69.

Likhatchev, D., C. Gutierrez-Wing, et al. (1996). "Soluble aromatic polyimides based on 2,2-bis(3-amino-4-hydroxyphenyl)hexafluoropropane: synthesis and properties." J. Appl. Polym. Sci. FIELD Full Journal Title:Journal of Applied Polymer Science **59**(4): 725-35.

Maeda, K., N. Moroi, et al. (2000). Fluorinated polybenzoxazoles with low dielectric constant and thermal expansion, and their precursors. Application: JP, (Central Glass Co., Ltd., Japan). 8 pp.

Maier, G. (2001). "Low dielectric constant polymers for microelectronics." Progress in Polymer Science **26**(1): 3-65.

Mizouti, K., Y. Shibasaki, et al. (2007). "Development of negative-type photosensitive semi-alicyclic polyimide using a photobase generator." J. Photopolym. Sci. Technol. FIELD Full Journal Title:Journal of Photopolymer Science and Technology **20**(2): 181-186.

Moore, T. M., C. D. Hartfield, et al. (2001). "Mechanical characterization of low-K dielectric materials." AIP Conf. Proc. FIELD Full Journal Title:AIP Conference Proceedings **550**(Characterization and Metrology for ULSI Technology): 431-439.

Nakayama, T., A. Mochizuki, et al. (1996). "New positive-type photosensitive polyimide: poly(hydroxyimide) with diazonaphthoquinone." React. Funct. Polym. FIELD Full Journal Title:Reactive & Functional Polymers **30**(1-3): 109-115.

Oba, M. (1996). "Effect of curing accelerators on thermal imidization of polyamic acids at low temperature." Journal of Polymer Science, Part A: Polymer Chemistry **34**(4): 651-58.

Ogata, T., S. Matsumaru, et al. (2003). "Effects of protecting group of fluoroalcohol on lithographic performance." J. Photopolym. Sci. Technol. FIELD Full Journal Title:Journal of Photopolymer Science and Technology **16**(5): 707-712.

Oishi, Y., S. Onodera, et al. (2003). "Synthesis of fluorine-containing wholly alicyclic polyimides by in situ silylation method." Journal of Photopolymer Science and Technology **16**(2): 263-266.

Omote, T., K. i. Koseki, et al. (1990). "Fluorine-containing photoreactive polyimide. 6. Synthesis and properties of a novel photoreactive polyimide based on photo-induced acidolysis and the kinetics for its acidolysis." Macromolecules FIELD Full Journal Title:Macromolecules **23**(22): 4788-95.

Oyama, T., Y. Kawakami, et al. (2003). Novel Principle For Preparing Photosensitive Engineering Plastics: Reaction Development Patterning (RDP). RadTech Asia.

Przybilla, K. J., H. Roeschert, et al. (1992). "Hexafluoroacetone in resist chemistry." Adv. Mater. (Weinheim, Fed. Repub. Ger.) FIELD Full Journal Title:Advanced Materials (Weinheim, Germany) **4**(3): 239-42.

Pyo, S., H. Son, et al. (2005). "Low-temperature processable inherently photosensitive polyimide as a gate insulator for organic thin-film transistors." Applied Physics Letters **86**(13): 133508/1-133508/3.

Qian, Z. G., Z. Z. Pang, et al. (2002). "Photoimageable polyimides derived from a,a-(4-amino-3,5-dimethylphenyl)phenylmethane and aromatic dianhydride." Journal of Polymer Science, Part A: Polymer Chemistry **40**(17): 3012-3020.

Robinson, J. D. and B. Humphreys (2003). "Plasma etch optimization of a photo-sensitive benzocyclobutene (BCB) planarisation layer for photonic integrated circuit manufacturing." Proceedings of SPIE-The International Society for Optical Engineering **5260**(Applications of Photonic Technology 6): 411-417.

Rosen, S. L. (1993). Fundamental Principles of Polymeric Materials. New York, NY, John Wiley & Sons, Inc.

Sasaki, T., Y. Takebe, et al. (2004). "A new monocyclic fluoropolymer for 157-nm photoresists." J. Photopolym. Sci. Technol. FIELD Full Journal Title:Journal of Photopolymer Science and Technology **17**(4): 639-644.

Shamiryan, D., T. Abell, et al. (2004). "Low-k dielectric materials." Materials Today (Oxford, United Kingdom) **7**(1): 34-39.

Shi, F. F., L. A. Schneggenburger, et al. (1997). "New photoimageable dielectric insulating copolyester thin films: synthesis and characterization." Journal of Applied Polymer Science **63**(9): 1199-1211.

Simpson, J., Z. Ounaies, et al. (1997). "Polarization and piezoelectric properties of a nitrile substituted polyimide." Materials Research Society Symposium Proceedings **459**(Materials for Smart Systems II): 59-64.

Simpson, J. O. and A. K. St. Clair (1997). "Fundamental insight on developing low dielectric constant polyimides." Thin Solid Films **308-309**: 480-485.

Skoog, D. A. and J. J. Leary (1992). Principles of Instrumental Analysis. San Diego, CA, Saunders College Publishing, A Harcourt Brace Javanovich College Publisher.

Smith, B. C. (1996). Fundamentals of Fourier Transform Infrared Spectroscopy, CRC Press.

So, Y.-H., J. P. Heeschen, et al. (1995). "A mechanistic study of polybenzoxazole formation with model compounds." Macromolecules **28**(21): 7289-90.

Stewart, M. D., D. J. Becker, et al. (2002). "Acid mobility in chemically amplified photoresists." Proc. SPIE-Int. Soc. Opt. Eng. FIELD Full Journal Title:Proceedings of SPIE-The International Society for Optical Engineering **4690**(Pt. 2, Advances in Resist Technology and Processing XIX): 943-951.

Thompson, L. F., C. G. Willson, et al. (1994). Introduction to microlithography. Washington, DC, American Chemical Society.

Toyokawa, F., Y. Shibasaki, et al. (2005). "A novel low temperature curable photosensitive polybenzoxazole." Polymer Journal (Tokyo, Japan) **37**(7): 517-521.

Treichel, H., G. Ruhl, et al. (1998). "Low dielectric constant materials for interlayer dielectric." Microelectronic Engineering **40**(1): 1-19.

Tsutomu Takeichi, T. A., Rachib Zeidam (2001). "Preparation and Properties of Polybenzoxazine/Poly(imidesiloxane) Alloys: In Situ Ring-Opening Polymerization of Benzoxazine in the Presence of Soluble Poly(imide-siloxane)s." Journal of Polymer Science: Part A: Polymer Chemistry **29**: 2633-2641.

Tsutomu Takeichia, Y. G., Sarawut Rimdusit (2005). "Performance improvement of polybenzoxazine by alloying with polyimide: effect of preparation method on the properties." Polymer **46**: 4909–4916.

Tullos, G. L., J. M. Powers, et al. (1999). "Thermal Conversion of Hydroxy-Containing Imides to Benzoxazoles: Polymer and Model Compound Study." Macromolecules FIELD Full Journal Title:Macromolecules **32**(11): 3598-3612.

Tummala, R. R. (2001). "Fundamentals of microsystems packaging."

Vogt, B. D., E. K. Lin, et al. (2004). "Effect of Film Thickness on the Validity of the Sauerbrey Equation for Hydrated Polyelectrolyte Films." Journal of Physical Chemistry B **108**(34): 12685-12690.

Wang, T. H., S. M. Ho, et al. (1993). "Temperature effect on polyimide/copper interface." Journal of Applied Polymer Science **47**(6): 1057-64.

Yamanaka, K., M. Romeo, et al. (2006). "Novel low-dielectric constant photodefinable polyimides for low-temperature polymer processing." Proc. SPIE-Int. Soc. Opt. Eng. FIELD Full Journal Title:Proceedings of SPIE-The International Society for Optical Engineering **6153**(Pt. 1, Advances in Resist Technology and Processing XXIII): 61531H/1-61531H/11.

Yamaoka, T., N. Nakajima, et al. (1990). "A study of novel heat-resistant polymers: preparation of photosensitive fluorinated polybenzoxazole precursors and physical properties of polybenzoxazoles derived from the precursors." Journal of Polymer Science, Part A: Polymer Chemistry **28**(9): 2517-32.

Yamashita, T., T. Ishikawa, et al. (2005). "Synthesis of fluorinated materials for 193 nm immersion lithography and 157 nm lithography." J. Photopolym. Sci. Technol. FIELD Full Journal Title:Journal of Photopolymer Science and Technology **18**(5): 631-639.

Yan, Z. and A. Reiser (1998). "Effect of Hydrogen Acceptors on pKa of Phenolic Resins: Link to Dissolution Inhibition." Macromolecules **31**(22): 7723-7727.

Yi-Che Su, F.-C. C. (2003). "Synthesis and characterization of fluorinated polybenzoxazine material with low dielectric constant." Polymer **44**: 7989–7996.

Yi-Che Su, W.-C. C., Feng-Chih Chang (2004). "Investigation of the Thermal Properties of Novel Adamantane-Modified Polybenzoxazine." Journal of Applied Polymer Science **94**: 932-940.

Ying-Ling Liu, J.-M. Y., Ching-I Chou (2004). "Preparation and Properties of Novel Benzoxazine and Polybenzoxazine with Maleimide Groups." Journal of Polymer Science: Part A: Polymer Chemistry **42**: 5954-5963.

Zhang, J.-Y. and I. W. Boyd (1998). "UV light-induced deposition of low dielectric constant organic polymer for interlayer dielectrics." Optical Materials (Amsterdam) **9**(1-4): 251-254.

VITA

MICHAEL JOSEPH ROMEO was born in Fort Worth, Texas. He is the son of Frank and Florence Romeo. After graduating from W.E. Boswell High School in Saginaw, Texas, in 1998, he attended the University of Texas at Austin, receiving a B.S. in Chemical Engineering in December of 2002. He began pursuing his Ph.D. in Chemical Engineering at the Georgia Institute of Technology in Atlanta, Georgia in the Fall of 2003.

Michael is a member of the National Society of Professional Engineers, the American Chemical Society, the National Society of Collegiate Scholars, and SPIE – the International Society for Optical Engineering.